TARGETING TAXANE-PLATIN RESISTANT NON-SMALL CELL LUNG CANCERS

WITH JUMONJI C HISTONE LYSINE DEMETHYLASE INHIBITORS

APPROVED BY SUPERVISORY COMMITTEE

John D. Minna, M.D. (Mentor)

Elisabeth D. Martinez, Ph.D. (Mentor)

Ralf Kittler, Ph.D. (Chair)

Jerry W. Shay, Ph.D.

Michael Roth, Ph.D.

Dedicated to

My parents Manik and Prafulla Dalvi
My sister Vaishnavi Dalvi
And my husband Aditya Paranjape

TARGETING TAXANE-PLATIN RESISTANT NON-SMALL CELL LUNG CANCERS WITH JUMONJI C HISTONE LYSINE DEMETHYLASE INHIBITORS

by

MAITHILI PRAFULLA DALVI

DISSERTATION

Presented to the Faculty of the Graduate School of Biomedical Sciences

The University of Texas Southwestern Medical Center at Dallas

In Partial Fulfillment of the Requirements

For the Degree of

DOCTOR OF PHILOSOPHY

The University of Texas Southwestern Medical Center

Dallas, Texas

December, 2015

ACKNOWLEDGMENTS

I would like to express my sincere and unconditional gratitude to the many people who have made my research training possible, including my mentors, colleagues, friends and family.

First and foremost, I am deeply thankful to my mentors Dr. John D. Minna and Dr. Elisabeth D. Martinez. I value their advice and guidance, and feel greatly honored to have worked with them during this important phase of my research career. Dr. Minna has been my role model as an outstanding researcher, ever since I joined his lab five years ago. His expansive knowledge and continued eagerness to know more, amazes me and inspires me to do the same. I acknowledge the time and resources that he has invested in my training, while also exposing me to an esteemed network of research scientists and collaborators through conferences and institutional visits. I am grateful to Dr. Martinez for mentoring me during this last, crucial year of my Ph.D. training. I acknowledge her guidance in my dissertation work and especially, during manuscript submission. I also thank her for giving me the opportunity to hone my scientific writing skills while working on a review.

Along with having great mentors, I had the privilege of having excellent thesis committee members who are well-renowned in their own specialized fields of research ─ Drs. Jerry Shay, Michael Roth and Ralf Kittler. Their varied research expertise and scientific opinions have added new flavors to my dissertation research and have played an important role in giving it a proper direction. I thank Dr. Shay for his constant inspiration and support. I am grateful to Dr. Roth for motivating me to set research goals and timelines, and for patiently reading the draft of my manuscript. I thank Dr. Kittler for his scientific advice and resources, while helping me to incorporate a new technique in my thesis research.

In addition to having such role models to look up to, it is equally important to have peers who learn with you and share some of the same experiences that you do. For this reason and many more, I am thankful to my colleagues, including fellow graduate students in the lab - Suzie, Patrick, Ryan, Dhruba and Alex. I am thankful to Paul for his help in completing an important experiment in my project. I am also grateful to the various postdoctoral researchers and research scientists in both Minna and Martinez labs. Lei and Juan have both been very helpful while carrying out another key experiment in my research project. I am very grateful to Mike, Amit, Buddy, Boning and Luc, the senior members in our lab with varied expertise in different aspects of lung cancer research. I thank Dr. Michael Peyton for his excellent advice on various matters and for being kind enough to read my manuscript draft. Our lab manager, Dr. Brenda Timmons, has been really patient and generous with lab issues and otherwise. Hyunsil, Shanshan, Long Shan, Sam, Anh and Krista have all been a great company. I am also thankful to lab alumni - James, Jill, Misty, Chunli, Chris, Robin, Rachel, Rebecca and Subodh for their support.

Outside of the Minna and Martinez labs, I am thankful to everyone in the Hamon Center and at UT Southwestern. I thank Dr. Gazdar for examining my histology slides. I thank Rahul Kollipara, Tae Hyun Hwang, Rui Zhong, Yunyun Zhou and Yang Xie for their help in biostatistics. I acknowledge the wisdom of the faculty members of Cancer Biology Program for their critical evaluations of my research. I feel honored to have been an HHMI Med-into-Grad Fellow as a part of the Mechanisms of Disease, MoD track. I am thankful to Dr. Helen Yin and to Drs. Robert Toto, Joan Schiller and David Gerber for allowing me to shadow them in their clinic. Such exposure has been valuable in shaping me to be a good translational researcher. Research collaborators at various institutions outside UT Southwestern have also been

instrumental in advancing my thesis research. I am grateful to Drs. Ignacio Wistuba, Carmen Behrens, and the various surgeons and pathologists at MD Anderson Cancer Center, without whom we would not have had access to valuable patient datasets.

During my past few years in the UT Southwestern Graduate School, the friends that I made have kept me smiling through the various ups and downs of student life. They have all been like a 'new home', when I moved here thousands of miles away from my family in India.

Last but not the least, I express my heartfelt gratitude to my family for believing in me and my abilities. My parents, Drs. Prafulla and Manik Dalvi have been instrumental in my decision to be a scientist and in aiming for outstanding research. As doctors, they have been deeply concerned about their patients, and that has greatly influenced me in deciding to pursue cancer research. It is their zeal and passion in the medical profession that I sometimes see myself mirroring in my own work. I feel lucky to have such ambitious, inspirational, thoughtful and caring parents. My acknowledgements would be incomplete if I did not emphasize how great of a sister Vaishnavi has been to me. Growing up with a talented and committed sister like her has inspired me to reach beyond my limits and aim for the best. Finally, I am grateful for the recent new addition to my family, my husband Aditya. Aditya is a very talented person and brings with him so many great qualities that I wish to emulate in my own work. I am also thankful to have such wonderful parents-in-law, Geeta and Shreenivas Paranjape who support our endeavors. I feel lucky to have been blessed with a wonderful family, friends, colleagues and acquaintances that inspire me to be a better person every day, both personally and academically.

TARGETING TAXANE-PLATIN RESISTANT NON-SMALL CELL LUNG CANCERS WITH JUMONJI C HISTONE LYSINE DEMETHYLASE INHIBITORS

MAITHILI PRAFULLA DALVI, Ph.D.

The University of Texas Southwestern Medical Center at Dallas, 2015

Supervising Professors: John D. Minna, M.D. and Elisabeth D. Martinez, Ph.D.

Taxane-platin doublet therapy provides benefit as front-line chemotherapy in advanced and localized non-small cell lung cancer (NSCLC); however the majority of patients relapse with drug resistant tumors. Novel therapies for targeting drug refractory NSCLC tumors are urgently needed. The goals of this dissertation project were to establish pre-clinical models of NSCLC resistance to standard chemotherapy, identify clinically relevant resistance mechanisms, and develop new rational pharmacologic approaches for overcoming taxane-platin drug resistance in lung cancer.

Pre-clinical resistance models were established by treating chemo-sensitive human NSCLC cell lines with increasing cycles of paclitaxel + carboplatin therapy, given in clinically relevant dose ratios. Progression of resistance was monitored by comparing drug response phenotypes, and by investigating genome-wide mRNA expression profiling. Xenografts of parental cells and resistant variants were developed to identify differential gene expression changes *in vivo*. Pre-clinical mRNA expression signature for taxane + platin resistance was developed and evaluated on a molecularly and clinically annotated dataset of 65 neoadjuvant treated NSCLC patient tumors, to identify therapeutic targets.

NSCLC cell lines NCI-H1299 and NCI-H1355 treated for 16-18 cycles with paclitaxel + carboplatin showed progressive increases in drug resistance, eventually achieving >50 fold shift in IC_{50}. Resistant tumors showed reduced response to taxane-platin chemotherapy *in vivo*. Resistant cell line variants expressed multi-drug resistance transporter and exhibited cross-resistance to several chemotherapies. But, resistance was partially reversible upon drug-free culturing, suggesting transient mechanisms. To systematically identify gene expression changes associated with drug resistance, a linear regression model was fitted on microarray datasets of progressively resistant H1299 and H1355 variants. Overlap between cell line models and *in vivo* xenograft expression yielded a 35-gene resistance signature. This pre-clinical resistance signature clustered the cohort of 65 neoadjuvant treated NSCLC patients into two distinct groups that showed significant differences in cancer recurrence-free survival. Cox multivariate regression identified the JumonjiC histone lysine demethylase *KDM3B* as the most significant contributor to poor recurrence-free prognosis. Taxane-platin resistant cell line variants showed up-regulation of several JumonjiC histone lysine demethylases and exhibited globally reduced levels of histone H3K27 trimethylation. Resistant variants showed increased sensitivity to

JumonjiC demethylase inhibitors, JIB-04 and GSK-J4, *in vitro* and *in vivo*. JumonjiC inhibitors synergistically inhibited colony formation from paclitaxel + carboplatin resistant variants, and also prevented the emergence of drug-tolerant clones from chemo-sensitive, parental cell lines. In conclusion, these studies reveal up-regulation of JumonjiC lysine demethylases during the development of drug resistance and define JumonjiC demethylase inhibitors as a new therapeutic approach for overcoming taxane-platin drug resistance in NSCLCs.

TABLE OF CONTENTS

PRIOR PUBLICATIONS

Dalvi MP, Zhong R, Wang L, Bayo J, Yenerall P, Kollipara RK, Zhou Y, Timmons B, Levonyak N, Rodriguez-Canales J, Behrens C, Mino B, Villalobos P, Suraokar M, Pataer A, Swisher SG, Kalhor N, Heymach JV, Coombes K, Xie Y, Girard L, Gazdar AF, Kittler R, Wistuba II, Martinez ED, Minna JD. Targeting Taxane-Platin Resistant Lung Cancers with JumonjiC Lysine Demethylase Inhibitors. 2015 (Submitted)

Bayo J*, **Dalvi MP***, Martinez ED. Successful strategies in the discovery of small-molecule epigenetic modulators with anticancer potential. *Future Med. Chem.* 2015 Oct; 7(16): 2243-61. (*Co-First authors)

Sato M, Larsen JE, Lee W, Sun H, Shames DS, **Dalvi MP**, Ramirez RD, Tang H, DiMaio JM, Gao B, Xie Y, Wistuba II, Gazdar AF, Shay JW, Minna JD. Human lung epithelial cells progressed to malignancy through specific oncogenic manipulations. *Mol Cancer Res.* 2013 Jun; 11(6):638-50.

Phadnis SM, Joglekar MV, **Dalvi MP**, Muthyala S, Nair PD, Ghaskadbi SM, Bhonde RR, Hardikar AA. Human bone marrow-derived mesenchymal cells differentiate and mature into endocrine pancreatic lineage in vivo. *Cytotherapy* 2011 Mar; 13(3):279-93.

Dalvi MP, Umrani MR, Joglekar MV, Hardikar AA. Human pancreatic islet progenitor cells demonstrate phenotypic plasticity in vitro. *J Biosci.* 2009 Oct; 34(4):523-8.

LIST OF FIGURES AND TABLES

LIST OF ABBREVIATIONS

AC – adenocarcinoma

ABCB1 – ATP-binding cassette, sub-family B, member 1

ANOVA – analysis of variance

APC – allophycocyanin

CARB – carboplatin

ChIP-Seq – chromatin immunoprecipitation and sequencing

CSC – cancer stem cell

DMSO – dimethyl sulfoxide

EMT – epithelial to mesenchymal transition

EPCAM – epithelial cell adhesion molecule

FBS – fetal bovine serum

FITC – fluorescein isothiocyanate

GAPDH – glyceraldehyde 3-phosphate dehydrogenase

GSEA – gene set enrichment analysis

H3K4 – histone 3 lysine 4

H3K9 – histone 3 lysine 9

H3K27 – histone 3 lysine 27

H&E – hematoxylin and eosin staining

HSP90 – heat shock protein 90

IACUC – institutional animal care and use committees

IC_{50} – inhibitory concentration that kills 50% of the population

IHC – immunohistochemistry

i.p. – intraperitoneal injection

JmjC – Jumonji C

KDM – lysine demethylase

LCC – large cell carcinoma

MDR – multi-drug resistance

MTS – 3-(4,5-dimethylthiazol-2-yl)-5-(3-carboxymethoxyphenyl)-2-(4-sulfophenyl)-2H-tetrazolium

NOD/SCID – non-obese diabetic severe combined immunodeficiency mouse

NSCLC – non-small cell lung cancer

PAC – paclitaxel

PI – propidium iodide

PBS – phosphate buffered saline

PTM – post-translational modification

qRT-PCR – quantitative real-time polymerase chain reaction

RPMI – Roswell Park Memorial Institute medium

s.c. – subcutaneous injection

SCC – squamous cell carcinoma

siRNA – short-interfering ribonucleic acid

TMA – tissue microarray

TSS – transcription start site

CHAPTER ONE

DRUG RESISTANCE IN LUNG CANCER

1.1 Lung Cancer

Lung cancer is the leading cause of cancer-related deaths in U.S.A. accounting for 27% of all cancer deaths (American Cancer Society 2015; Howlader N, 1975-2012). While the most common cancers are prostate cancer in men and breast cancer in women, lung cancer remains the second most common cancer, accounting for about 13% of all new cancer cases. The chance of a man developing lung cancer in his lifetime is 1 in 13 and for a woman, the risk is about 1 in 16. Though the risk is higher in smokers, the above ratios include both smokers and non-smokers. Lung cancer in non-smokers can be caused by occupational or environmental exposure to secondhand smoke, radon gas, air pollution, radiation, asbestos, diesel exhaust, metals and organic chemicals. Risk factors associated with genetic mutations also play a role. It is estimated that about 221,200 new cases of lung cancer will be diagnosed in 2015 in U.S.A. (American Cancer Society 2015).

More than 50% of lung cancers are diagnosed at an advanced stage, due to lack of early signs or symptoms. The TNM (tumor size, nodes and metastasis) staging system accepted by the Union for International Cancer Control (UICC) and the American Joint Committee on Cancer (AJCC) is widely used for describing the size, extent and degree of cancer spread. Stages I, II, III, or IV are also designated, with stage I being early, and stage IV being the most advanced

disease. The five-year survival rate for advanced stage lung cancer is only 4% (American Cancer Society 2015).

Lung cancer is classified into small cell lung cancer (SCLC) with 15% of the cases reporting this type whereas 85% of the diagnosed cases are non-small cell lung cancer (NSCLC). SCLC is primarily associated with smoking and is characterized by tumor cells that typically express neuroendocrine markers. NSCLC consists of three histologically distinct subtypes called as squamous cell carcinomas (SCC), adenocarcinomas (AC), and large cell carcinomas (LCC). Treatment options vary depending upon the type of lung cancer.

1.2 Standard Chemotherapies

Lung cancer therapy is determined based on cancer stage, type and molecular characteristics. Treatment options include surgery, radiation, chemotherapy or targeted therapies. Surgery is the treatment of choice for early stage or localized NSCLC. Chemotherapy is an important component of treatment for all stages of lung cancer, including patients with early stage resectable tumors as well those with metastatic, unresectable disease. For resectable tumors, neoadjuvant chemotherapy may be administered to shrink the tumor prior to surgery. After surgery, adjuvant chemotherapy and maintenance therapy may be given. For more advanced stage NSCLC, chemotherapy or radiation therapy is recommended. In cases where the genetic driver mutations are known, such as EGFR, targeted therapy is used. For all other lung cancers where molecular drivers are unknown, standard platin-based doublet chemotherapy is commonly administered.

Platin-based combination chemotherapy is the mainstay of lung cancer treatment. Platinum analogs (carboplatin, cisplatin) are commonly combined with anti-mitotic drugs such as taxanes (paclitaxel, docetaxel) or vinca alkaloids (vinorelbine). Anti-metabolites that affect cells in the S phase (gemcitabine, pemetrexed) or topoisomerase inhibitors that are G2 phase specific agents (topotecan, etoposide) may also be used. Anthracyclines (doxorubicin, daunorubicin) act independent of the cell cycle phase. Some of these commonly used chemotherapies have been reviewed further below.

Platinum-based drugs are classified as 'alkylating-like' due to their ability to form DNA adducts. Cisplatin/ Cis-Diamminechloroplatinum (CDDP) compound consists of two labile chloro and two stable amine ligands in a cis configuration (Seve and Dumontet, 2005). Following administration, one of the chloride ligands is displaced by water molecule. This aquation process converts the neutral compound into a reactive form that allows the platinum atom to access the DNA bases more easily. Cross-linking of DNA by cisplatin then triggers cellular apoptotic pathways. Carboplatin has a more stable bidentate cyclobutanedicarboxylate ligand instead of the chloro ligands. This slows down the aquation reaction, thereby reducing drug potency but at the same time decreasing overall toxicity. The inclusion of platinum agents in chemotherapeutic regimens, ever since the 1980s, has greatly improved response rate and has been considered a significant milestone in progressing towards effective therapy for lung cancer.

Taxanes and Vinca alkaloids are third generation cytotoxic agents that later became available in the 1990s and have been considered as another significant breakthrough in lung cancer therapy (Klastersky and Awada, 2012). Combination of these new agents with platin drugs has significantly improved overall patient survival. Taxanes are used as both neoadjuvant

and adjuvant chemotherapy for NSCLC. Paclitaxel, isolated from the bark of the Pacific yew, *Taxus brevifolia*, and docetaxel, a semi-synthetic analogue derived from the needles of the European yew tree, both show potent anti-tumor activity. Due to its higher potency than paclitaxel, docetaxel has also been approved as a second-line treatment for patients treated with prior paclitaxel-platin first-line chemotherapy (Rigas, 2004). Taxanes act as anti-tubulin agents by interfering with the functioning of the mitotic spindle, thereby blocking cells at the metaphase-anaphase junction of mitosis. Unlike vinca alkaloids (vinorelbine/ navelbine) which are microtubule-depolymerizing agents, taxanes enhance the polymerization of microtubules, resulting in microtubule stabilization. Electron crystal structure has revealed that paclitaxel binds to the β-subunit in the inner surface of microtubule. In addition, both vinca alkaloids and taxanes are known to affect spindle-microtubule dynamics by suppressing spindle treadmilling and dynamic instability (Jordan and Wilson, 2004; Seve and Dumontet, 2005). This mitotic block ultimately results in induction of apoptosis.

Anthracyclines, on the other hand, act via DNA intercalation. Doxorubicin is an anthracycline antibiotic, closely related to the natural compound daunomycin, isolated from the fungus *Steptococcus peucetius*. It exerts its anti-tumor activity by inhibiting the progression of topoisomerase II, thereby causing DNA double-strand breaks. This triggers activation of DNA damage response (DDR) signaling, subsequently leading to apoptosis. In addition, anthracyclines have recently been shown to promote histone eviction from open chromatin that results in epigenetic changes, deregulation of the transcriptome and apoptosis (Pang et al., 2013).

Other topoisomerase inhibitors such as etoposide also cause transient DNA double-strand break formation and stabilization of the topoisomerase II complex whereas irinotecan, a

semisynthetic analogue of camptothecin, is a topoisomerase I inhibitor. By interacting with the Topo I-DNA complexes, irinotecan causes an irreversible arrest of the replication fork, DNA damage signaling and apoptosis.

Gemcitabine (2', 2'-difluorodeoxycytidine, dFdC) is a deoxycytidine analogue in which the two hydrogens atoms in the 2' position of the deoxyribose sugar are substituted with fluorine atoms. Upon entering the cell, dFdC is phosphorylated to dFd-CMP, dFd-CDP and finally dFd-CTP, which gets incorporated into DNA during replication. After an additional natural nucleoside is added to the DNA chain, gemcitabine is masked and this prevents DNA repair. DNA polymerases are then unable to proceed and this ultimately results in masked DNA chain termination. Gemcitabine is also known to inhibit ribonucleotide reductase (RR) enzyme, thereby decreasing deoxyribonucleotide pools necessary for DNA synthesis (Mini et al., 2006).

Pemetrexed is a new generation anti-folate antimetabolite. It is a structural analogue of folic acid and other antimetabolite compounds such as methotrexate. Unlike its precursor methotrexate which selectively targets a single enzyme, pemetrexed acts by disrupting many folate-dependent metabolic processes (Rollins and Lindley, 2005). Within the cells, pemetrexed is converted to a pentaglutamated form that increases its potency. Pemetrexed inhibits three different enzymes required for purine and pyrimidine synthesis—thymidylate synthase (TS), dihydrofolate reductase (DHFR), and glycinamide ribonucleotide formyltransferase (GARFT). Without the formation of precursor purine and pyrimidine nucleotides, DNA and RNA synthesis are affected, leading to apoptosis.

1.3 Clinical Drug Resistance and Cancer Relapse

Despite significant advances in lung cancer chemotherapy, the overall five-year survival rate for non-small cell lung cancer (NSCLC) patients is only 21% (American Cancer Society 2015). Response to chemotherapy is graded as complete response (complete disappearance of signs and symptoms for at least 1 month), partial response (>50% reduction in tumor mass and no new lesions), stable disease (no significant change in tumor size) and progressive disease (more than 25% increase in tumor mass). Even in cases where complete response is achieved after surgery and/or chemotherapy, a significant fraction of NSCLC patients develop cancer recurrence, amounting to anywhere between 30% to 75% of cases depending on the pathological stage of the tumors evaluated in multiple retrospective studies (Sugimura et al., 2007).

Cancer relapse after chemotherapy poses a major obstacle for lung cancer treatment. Patients in which the disease was early stage and confined only to the chest have also shown recurrence following treatment. In a retrospective study that analyzed recurrence rates in NSCLC patients that had undergone complete resection (R0) following neoadjuvant chemotherapy, recurrence was reported in as high as 68% of these patients, with 19% of these exhibiting recurrence at both locoregional and distant sites (Martin et al., 2002).

More often, recurrent tumors present as a drug resistant disease, refractory to further standard treatment. A retrospective study was conducted to evaluate recurrent, advanced-stage IIIB or IV NSCLC patients who had received third- or fourth-line chemotherapy after two prior platinum-taxane chemotherapy regimens (Massarelli et al., 2003). Prior regimens had failed because the disease had progressed within 90 days of chemotherapy or the patient had experienced unacceptable toxicity. Analysis revealed that the response rates decreased with each

line of treatment: first line, 20.9%; second line, 16.3%; third line, 2.3%; and fourth line, 0%. The overall disease control rate decreased significantly with each subsequent line of chemotherapy, suggesting development of drug resistance in these tumors.

Chemotherapy resistance to standard doublets—carboplatin and paclitaxel, cisplatin and navelbine, cisplatin and docetaxel, and cisplatin and gemcitabine, was evaluated in 4571 fresh NSCLC tumor surgical biopsy specimens from 409 institutions, using *in vitro* tumor cultures in an extreme drug resistance assay (d'Amato et al., 2007). Response to chemotherapy was graded as extreme drug resistance (1 SD above the median chemotherapy resistance), intermediate drug resistance (between the median and extreme drug resistance) and low drug resistance (1 SD below the median). Extreme or intermediate drug resistance to at least one drug in the chemotherapy combination was seen in 74% of the cases to carboplatin-paclitaxel, in 68% to cisplatin-navelbline, in 88% to cisplatin-gemcitabine, and in 68% to cisplatin-docetaxel. Despite current advances in lung cancer treatment, there is still an unmet clinical need to identify effective therapies for such drug refractory tumors.

1.4 Traditional Drug Resistance Mechanisms

Lack of response to chemotherapy could be attributed to either patient-derived variables or cellular resistance mechanisms. Patient-derived factors include poor absorption or rapid excretion of the drug resulting in low serum levels, high drug-associated toxicity resulting in a need to reduce doses to a suboptimal level, poor drug delivery, or low tissue penetration as is the case with brain metastases that are protected by the blood-brain barrier (Gottesman, 2002).

Tumor cells may be intrinsically resistant to chemotherapy or may acquire genetic or epigenetic alterations contributing to drug resistance. Rare, resistant subpopulation of cells may pre-exist in the tumor population and survive by positive selection under drug pressure, or alternatively resistance might be established as a direct consequence of drug exposure through acquisition of new alterations. Finally, alterations in the tumor stroma or microenvironment may also affect response to chemotherapy.

The field of chemo-resistance in not new and involves more than 50 years of extensive research. In as early as the 1960's, R.W. Brockman (Brockman, 1963) in his book chapter mentioned that resistant cells differ from their sensitive counterparts at various levels – differences in enzyme dynamics, decreased cell permeability to drugs, molecular modifications, and altered drug metabolism. Many of these mechanisms were extensively studied by various researchers over the next few years. Mechanisms involving loss of a cell surface drug transporter, mutation of drug target, or drug-specific metabolism generally resulted in resistance to only the drug in question and its immediate analogs, as with resistance to antifolates (Gottesman, 2002). In such cases, use of combination therapy yielded improved responses. But more often than not, patient tumors not only showed increased resistance to the primary chemotherapy that they were exposed to but also exhibited cross-resistance to several other drugs. Cancer cells can show cross-resistance to drugs by either altering membrane lipids, reducing drug uptake, increasing drug efflux from the cells, activation of coordinately regulated detoxification systems or defective apoptotic pathways (Gottesman, 2002). Multi-drug resistance (MDR) and multi-factorial drug resistance caused due to tumor heterogeneity have been focus of extensive research. Research in the past decade has also shed light on the involvement of

epithelial-to-mesenchymal phenotypic switching, cancer stem cells and more recently, epigenetic alterations in drug resistance (discussed in subsequent sections).

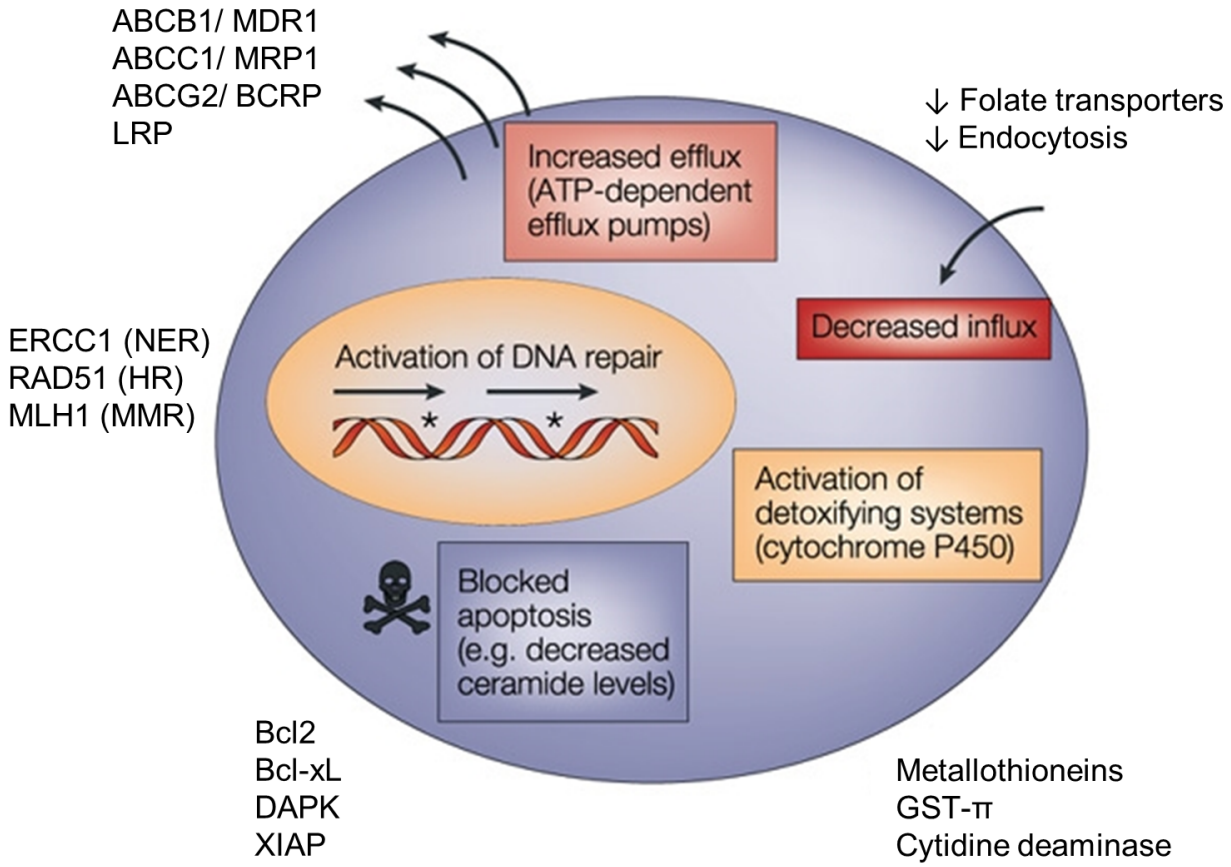

Figure 1.1 Cellular Drug Resistance Mechanisms
Cancer cells can become resistant to chemotherapeutic drugs by several mechanisms ─ (a) increasing drug efflux through ATP-dependent transporters, (b) reducing drug influx, (c) activation of detoxifying pathways, (d) activation of DNA damage repair pathways, or (e) disruption of apoptotic pathways.
Modified from Gottesman, Fojo and Bates, Nature Reviews 2002

1.4.1 Increased Drug Efflux

Classical multi-drug resistance is mediated by the expression of one or more of the energy-dependent drug transporters that exhibit broad substrate specificity. One of the most commonly described drug efflux pumps ever since the 1980s (Kartner et al., 1983a; Kartner et al., 1983b), is known as P-glycoprotein (P-gp). This transporter is a product of the *ABCB1* or *MDR1* gene, which belongs to the family of 48 known ATP-binding cassette (ABC) transporters that share sequence and structural homology. ABC genes are divided into seven different sub-families (ABCA-ABCG), based on their sequence homology and domain organization, with three widely known transporters belonging to the ABCB, ABCC and ABCG subfamilies.

The most widely studied transporter, ABCB1/P-gp/MDR1, is a 170 kDa phosphoglycoprotein that consists of two ATP-binding cassettes and two transmembrane regions with six transmembrane domains each (Chen et al., 1986). Upon substrate binding, one of the ATP binding domains is activated, ATP is hydrolyzed and a conformational change occurs within the transporter that releases the substrate into extracellular space. Hydrolysis of a second molecule of ATP restores the transporter to its original state so that it can repeat its cycle of substrate binding and release (Sauna and Ambudkar, 2000). P-glycoprotein or MDR1 is normally located in the intestines, liver, kidney and blood-brain barrier, with neutral and cationic organic compounds as its substrates. It can also bind to chemotherapeutic drugs such as doxorubicin, daunorubicin, vinblastine, vincristine and taxol, as well as other pharmaceuticals including antiarrhythmics, antihistamines, cholesterol reducing statins and HIV protease inhibitors (Gottesman, 2002). P-gp is widely expressed in many human cancers, with high *MDR1* RNA expression detected in colon, kidney, liver, pancreatic cancers and certain NSCLCs.

Additionally, cancers that had relapsed after therapy, such as breast cancer, neuroblastoma and non-Hodgkin's lymphoma, also showed elevated MDR1 expression (Goldstein et al., 1989). Some studies have shown increased *MDR1* mRNA expression in lung cancer patient samples (Young et al., 1999), whereas some others have also reported the absence of MDR1 expression (Lai et al., 1989; Oka et al., 1997). In case of acute myelogenous leukemia (AML), about one-third of the patients at diagnosis and more than 50% of the patients at relapse showed MDR1 expression (Gottesman et al., 2002).

Apart from ABCB1 transporter, the ABCB family also comprises of ABCB11, also known as sister of P-gp/ SPGP (Childs et al., 1998) and ABCB4/ MDR3 (Smith et al., 2000), both of which have been implicated in cancer drug resistance, the former particularly to paclitaxel resistance and the latter to several others including digoxin and vinblastine.

After the discovery of MDR1, researchers cloned another ABC transporter called MRP1 (multidrug resistance associated protein 1; ABCC1), using a resistant lung cancer cell line (Cole et al., 1992). ABCC family members also have two transmembrane regions and two ATP-binding domains that form the core transporter. However, unlike ABCB members, these transporters have an additional domain. ABCC1, ABCC2, ABCC3, ABCC6 and ABCC10 have an amino (N)-terminal membrane bound region connected to the core by a cytoplasmic linker. The other four members ABCC4, 5, 11 and 12 also have the linker region but without the (N)-terminal region. ABCC1/ MRP1 transporter is widely expressed in many human tissues and cancers and transports organic anionic compounds, including drugs that have been modified by glutathione conjugation, glucosylation, sulfation and glucuronylation. MRP1 was found to be overexpressed in leukemia, esophageal carcinomas and non-small cell lung cancers (Gottesman

et al., 2002). Other than the more common ABCC1 (MRP1) transporter, ABCC2, 3, 6 and 10 (MRP2, 3, 6, 7) have also been implicated in drug resistance. Cells selected in cisplatin, arsenic or N-nitro-camptothecin show increased ABCC2/ MRP2 expression (Annereau et al., 2004; Liedert et al., 2003; Liu et al., 2001).

Another ABC transporter shown to efflux anticancer drugs is the ABCG2 transporter, also known as MXR/ BCRP/ ABC-P (Allikmets et al., 1998; Doyle et al., 1998). Unlike MDR1 and MRP1, members of the ABCG subfamily have only one transmembrane region and one ATP binding cassette as the core, which dimerizes to generate the full transporter. Normally expressed in the placenta, liver, breast and intestine, MXR is also overexpressed in cancer cells selected for anthracycline and mitoxantrone resistance. Additionally, MXR transporter has been shown to be involved in efflux of methotrexate, 7-ethyl-10-hydroxycamptothecin (SN-38) and some tyrosine kinase inhibitors (Kawabata et al., 2001; Ozvegy-Laczka et al., 2005; Zhao and Goldman, 2003).

Knowing the complexity of ABC transporter-mediated drug resistance, a research group performed drug screen on 60 diverse cancer cell lines from the NCI-60 panel, to correlate the drug response to 48 known ABC transporter genes and identify candidate substrates for these transporters. About 1400 candidate anti-cancer compounds were evaluated. Several of the 48 ABC transporters were found to be associated with resistance against different candidate anti-cancer drugs in the screen (Szakacs et al., 2004). Additionally, some compounds whose activity was potentiated by MDR1 expression were also discovered and could serve as potential lead compounds against drug resistant cancers.

Apart from the ABC family members, other transporters such as the LRP (lung resistance protein) have also been implicated in drug resistance. LRP is a major vault protein found in the

cytoplasm and on nuclear membrane. It has been suggested that LRP might confer drug resistance by re-distributing drugs away from their intracellular targets. LRP has been found to be overexpressed in certain tumors (Gottesman et al., 2002).

Additionally, in case of cisplatin resistance, it has been proposed that a glutathione-S-X (GS-X) pump actively effluxes the glutathione-S-platinum (GS-Pt) complex in an ATP-dependent manner. This was inferred from the observed competitive inhibition of GS-X pump by GS-Pt complex and antagonist of leukotriene C4 which is a natural substrate of the pump (Seve and Dumontet, 2005).

1.4.2 Decreased Drug Uptake

Drugs can enter cells in various ways, the three major ones being diffusion across plasma membrane, piggy-backing on transporters and endocytosis (Gottesman et al., 2002). Alterations in these uptake mechanisms have been shown to cause resistance to chemotherapeutic agents.

Anti-folate analogues such as methotrexate depend on folate transporters for their uptake, the major one being an 85 kDa membrane glycoprotein called the reduced folate carrier (RFC). Mutations that result in reduced expression of folate transporters decrease cellular uptake of methotrexate, thereby minimizing the toxicity on cells. Decreased RFC expression has been reported to cause methotrexate resistance in osteosarcoma and breast cancer cell lines, as well as poor chemotherapy response in osteosarcoma and leukemia patient tumors (Redmond et al., 2008).

Anti-cancer agents such as immunotoxins are internalized by receptor mediated endocytosis. Mutations that cause defects in the cellular endocytotic machinery have been shown to result in reduced uptake of immunotoxins (Gottesman, 2002).

The exact mechanism by which cisplatin is taken up by cells has not been established and is a subject of controversy. It was proposed that approximately one-half of cisplatin uptake takes place by passive diffusion and the other half occurs by facilitated diffusion through a pump (Gately and Howell, 1993). Another study indicated that cellular cisplatin accumulation is dependent on cell membrane potential, based on the observation that sodium-potassium ATPase inhibitor ouabain inhibited drug uptake. Researchers have demonstrated that cisplatin resistant cancer cells that showed reduced drug accumulation and cross-resistance to methotrexate, heavy metals and some nucleoside analogs, exhibited reduced plasma membrane receptors and transporters as well as reduced endocytosis (Shen et al., 1998).

1.4.3 Drug Metabolism

Chemotherapy resistance may also be mediated by drug metabolism via metallothioneins (MT) and glutathione metabolism-related enzymes. Metallothioneins are stress response proteins that help in the cellular detoxification of heavy metals. Clinical studies showed that tumors from patients who had received prior cisplatin chemotherapy showed significantly higher expression of MT than untreated patient tumors (Matsumoto et al., 1997). Increased MT expression was found in cisplatin resistant cancer cells *in vitro* and further, transfection studies revealed that MT

transfected cells were resistant to cisplatin, melphalan, chlorambucil and low levels of doxorubicin (Seve and Dumontet, 2005).

Glutathione S-transferases (GST) play a critical role in drug detoxification and have also been implicated in cisplatin resistance. Cisplatin is known to be inactivated by conjugation with glutathione (GSH) via a reaction catalyzed by glutathione S-transferase. GST-π was reported as the predominant isoenzyme among the three classes of GST in NSCLC tumors, with significantly higher enzyme expression in tumors compared to normal lung tissues (Howie et al., 1990). Studies have indicated that cellular GST-π levels in lung cancer cell lines predict response to cisplatin (Seve and Dumontet, 2005). Immunohistochemical examination of NSCLC patient tumors who had received cisplatin-based chemotherapy also revealed that GST-π expression significantly correlated with lower response rates (Bai et al., 1996).

Gemcitabine has also been shown to be metabolized into an inactive form, thereby resulting in cellular drug resistance. Within the cells, gemcitabine can be converted into an inactive metabolite via deamination by cytidine deaminase (CDD) into 2',2'- difluoro-2'-deoxyuridine (dFd-U). Alternatively, dephosphorylation of dFd-CMP by 5'nucleotidase (5'NT) can also result in inactivation (Seve and Dumontet, 2005). Thus, increased CDD or 5'-NT activities have been suggested to cause resistance to gemcitabine.

5-fluorouracil (5-FU) is a fluoropyrimidine antimetabolite that can be inactivated by the pyrimidine catabolism enzyme dihydropyrimidine dehydrogenase (DPD), which is mainly expressed in the liver. However certain tumors may overexpress DPD, leading to 5-FU resistance. Increased expression of DPD has been reported in 5-FU resistant lung cancer cell

lines (Redmond et al., 2008). DPD expression was also shown to correlate with 5-FU response in colorectal cancer patients (Salonga et al., 2000).

Irinotecan resistance also involves metabolism of the chemotherapeutic agent into an inactive form. Normally, inside the cells, irinotecan side-chain is cleaved enzymatically by carboxylesterase to 7-ethyl-10-hydroxycamptothecin (SN-38), which is the potent, active form of the drug. Decreased carboxylesterase enzyme expression can lower irinotecan drug activation and has been correlated with resistance in colorectal cancer and non-small cell lung cancers (Redmond et al., 2008). Alternatively, the active metabolite SN-38 may get deactivated via conjugation by the uridine diphosphate glucuronosyltransferase isoform 1A1 (UGT1A1). UGT1A1 genetic polymorphisms may thus also play a role in conferring irinotecan resistance (Seve and Dumontet, 2005).

1.4.4 Enhanced DNA Damage Repair

Chemotherapeutic agents such as platinum analogs and topoisomerase inhibitors act by damaging the DNA either directly or indirectly. Cisplatin acts by intercalating with DNA, leading to the formation of DNA adducts. One of the cisplatin resistance mechanisms, mediated by glutathione (GSH), involves prevention of formation of cisplatin-DNA adducts (Seve and Dumontet, 2005). Additionally, GSH is necessary for the synthesis of DNA precursors, deoxyribonucleotide triphosphates, and indirectly affects DNA repair. Under normal steady-state conditions, most GSH in the cells exists in the reduced form. Glutathione peroxidase (GPX) catalyzes the oxidation of reduced GSH and, in this process effectively scavenges the cytotoxic

oxygen radicals or lipid peroxides induced by chemotherapy, thereby preventing DNA damage. Immunohistochemical studies of GPX and glutathione reductase in previously untreated NSCLC have revealed an inverse relationship between enzyme expression and cisplatin sensitivity (Ogawa et al., 1993).

Removal of adducts from genomic DNA is facilitated by a DNA repair pathway called nucleotide excision repair (NER). There are two types of NER: transcription-coupled repair (TCR) and global genomic repair (GGR) (Seve and Dumontet, 2005). TCR repairs lesions that block transcription, whereas GGR repairs the lesions in both transcribed and non-transcribed DNA strands. Two different sets of proteins are involved in recognition of DNA damage in TCR and GGR. In the TCR pathway, RNA polymerase II senses cisplatin induced DNA damage and two transcription-coupled repair-specific factors, CSA and CSB (Cockayne Syndrome A and B) activate the NER machinery. In case of GGR, DNA-damage binding (DDB) protein and XPC-Rad23B complexes bind to the DNA lesion caused by chemotherapy. Both the pathways converge in terms of dual excision. The basal transcription factor (TFIIH) and XPG then lead to excision. The two helicases that comprise the TFIIH, called as XPB and XPD, open a 30 bp-long DNA segment around the lesion. XPG and XPF/excision repair cross complementing 1 (ERCC1) then excise the DNA strand containing the damaged bases. The damaged DNA strand 3' from the lesion is cleaved by XPG, and XPF/ERCC1 cleaves the damaged strand 5' from the lesion. The gap is filled in by DNA polymerases and ligases. Studies have shown that cisplatin resistant tumors have an intact NER system that repairs the DNA, when compared to the sensitive tumors with defective NER machinery. In cell line models, cisplatin-resistant ovarian cancer cells were found to overexpress several NER members including ERCC1, XPA, XPB, XPC and XPG (Redmond et al., 2008). In clinical studies, high ERCC1 levels correlated with poor response to

platinum based combination chemotherapy in gastric cancers (Redmond et al., 2008). In studies evaluating advanced NSCLCs treated with gemcitabine and cisplatin, low ERCC1 expression in tumors correlated with better median overall patient survival time (Lord et al., 2002). In docetaxel-cisplatin treated stage IV NSCLC patients that were examined for ERCC1 single nucleotide polymorphisms, patients homozygous for the ERCC1 118 C allele showed better overall survival (Isla et al., 2004).

Other DNA repair pathways such as homologous recombination (HR) and non-homologous end joining (NHEJ) are also involved in conferring resistance to chemotherapy. In HR, binding of proteins such as RAD51, RAD52, BRCA1, p53 and ATM at the site of DNA break initiates the synthesis of new DNA strands. Increased RAD51 expression and HR activity have been shown to result in resistance of small cell lung cancer (SCLC) cell lines to the topoisomerase II inhibitor etoposide (Hansen et al., 2003). NHEJ, on the other hand, depends on binding of the Ku70-Ku80 heterodimer at both ends of the DNA break, followed by the recruitment of DNA-PK, and joining of DNA ends by DNA ligase. Increased NHEJ activity has been reported in the resistance of human chronic lymphocytic leukemia (CLL) to chemotherapy (Deriano et al., 2005).

Mismatch repair (MMR) may also be involved in cisplatin resistance. Cisplatin treated cell lines frequently acquire mismatch repair defects and exhibit mutations in the hMLH1 genes. MMR defects have also been reported in resistance to 6-thioguanine and 5-fluorouracil (Redmond et al., 2008). However, results from some clinical studies exploring associations between expression of mismatch repair genes and overall patient survival, have been conflicting.

1.4.5 Evasion of Cell Death

Evasion of apoptosis has been linked to cellular resistance to several chemotherapeutic agents. Apoptosis can be induced either through the intrinsic mitochondrial pathway or the extrinsic death-receptor mediated pathway. The intrinsic pathway is mediated by the Bcl-2 protein family which comprises of pro-apoptotic proteins such as Bax, Bak, Bad and Bid, as well as anti-apoptotic proteins such as Bcl-2 and Bcl-xL. The extrinsic pathway, on the other hand, involves the tumor necrosis factor (TNF) receptor superfamily.

Paclitaxel has been shown to modulate expression of Bcl-xL as well as Bcl2 (Seve and Dumontet, 2005). Overexpression of Bcl2 has also been correlated with increased cisplatin resistance. Mutations resulting in loss of p53 function have been reported to cause increased Bcl-xL levels and resistance to gemcitabine (Seve and Dumontet, 2005). Increased Bcl-xL protein in ovarian cancer cells was found to cause resistance to multiple chemotherapies such as cisplatin, paclitaxel, topotecan and gemcitabine (Williams et al., 2005). In clinical specimens, elevated Bcl-xL mRNA correlated with poor prognosis in NSCLC patients treated with chemotherapy (Karczmarek-Borowska et al., 2006).

Alterations in the proteins comprising the extrinsic apoptotic pathway, such as decoy receptors and FADD (Fas associated death domain) can result in resistance to TRAIL (TNF related apoptosis-inducing ligand) as well as chemotherapy. Low FADD expression corresponds to chemoresistance and poor clinical outcome in acute myeloid leukemia (AML) patients (Tourneur et al., 2004).

Death-associated protein (DAP) kinase is a pro-apoptotic serine/threonine kinase that is involved in ligand-induced apoptosis as well as autophagy. Hypermethylation of the DAPK promoter results in aberrant gene silencing and negatively affects the apoptotic pathway. A clinical study reported DAPK hypermethylation in ~40% of resected stage I NSCLC patient tumors, and this was associated with poor five-year survival rate in these early-stage patients (Tang et al., 2000).

Cancer cells can evade apoptosis via expression of the inhibitors of apoptosis (IAP) family of proteins. These proteins including the cIAP1, cIAP2, and X-chromosome–encoded IAP (XIAP), can bind to caspases-3, -7 and -9 and inhibit apoptosis. IAPs are normally inhibited by the second mitochondrial activator of caspases (SMAC). Increased cIAP2 and XIAP expression have been linked to pancreatic cancer cell resistance to 5-FU, cisplatin, doxorubicin and paclitaxel (Lopes et al., 2007). Studies in our laboratory have shown that inhibition of IAPs by a SMAC mimetic JP1201 resulted in sensitization of NSCLCs to doxorubicin, erlotinib, gemcitabine, paclitaxel, vinorelbine and paclitaxel/carboplatin combination chemotherapy (Greer et al., 2011).

Pro-survival pathways such as EGFR signaling, PI3K/Akt signaling or NF-kB pathway may be activated by cancer cells in response to chemotherapeutic stress, thereby leading to drug resistance. HER2 (ErbB2) expression has been implicated in breast cancer resistance to platinum agents, paclitaxel and 5-FU (Redmond et al., 2008). Inhibition of pro-survival PI3K/Akt signaling improved the effectiveness of paclitaxel in ovarian, lung and esophageal cancer cells (Redmond et al., 2008). The transcription factor NF-kB has been shown to be involved in

suppression of the apoptotic cascade induced by tumor necrosis factor-alpha (TNF-a), oncogenic Ras, and chemotherapy agents, such as irinotecan (Seve and Dumontet, 2005).

1.4.6 Mutation in Direct Drug Target

Cancer cells continually evolve in response to stress and accumulate mutations that help them survive the drug-induced insults. Mutations in genes that code for the key protein that interacts with the chemotherapeutic agent, are more likely to result in resistance against that specific drug or family of drugs. Such genomic mutations have been shown to be involved in conferring resistance to both standard as well as targeted therapies.

Since taxanes act by stabilizing microtubule polymerization, tubulin mutations that counteract this stabilizing effect, along with expression of endogenous microtubule-depolymerizing factors, have been shown to promote the development of drug resistance (Jordan and Wilson, 2004). In a NSCLC cell line model, paclitaxel resistant A549 cells were found to overexpress the active form of the microtubule destabilizing protein stathmin and the inactive form of the putative microtubule-stabilizing protein MAP4. In addition, these cells overexpressed the βIII-tubulin isotype and had a heterozygous point mutation in α-tubulin, in the region that is important for interaction with MAP4 and stathmin (Martello et al., 2003). As a result, these resistant cells exhibited faster microtubule dynamics than sensitive cells. Examination of stage IIIB/ IV NSCLC patients has also revealed that those who had mutations in the β-tubulin gene responded poorly to paclitaxel treatment (Burkhart et al., 2001).

Activating somatic mutations in the epidermal growth factor receptor (EGFR) kinase gene are a unique feature of a sub-class of NSCLCs and have been exploited in designing EGFR targeted therapy. The most predominant EGFR mutations involve in-frame deletions around the conserved LREA motif of exon 19 (that translates to amino acid residues 747−750) and a point mutation (L858R) in exon 21 (Denis et al., 2015). EGFR-mutated cells are oncogene addicted and depend upon EGFR for their survival. EGFR tyrosine kinase inhibitors (TKI) such as erlotinib and gefitinib are thus commonly used for treatment of EFGR-mutated lung cancers. Though tumors initially respond well to these targeted agents, a significant fraction of them eventually acquire secondary mutations that confer resistance to these drugs. The secondary T790M mutation in exon 20 occurs in ~50% of EGFR-mutated patient tumors and is primarily responsible for EGFR TKI resistance (Denis et al., 2015). Threonine 790 is the gatekeeper residue in EGFR and an important determinant of inhibitor specificity. Substitution of this residue with a methionine causes steric interference that affects binding of TKIs (Denis et al., 2015). A small fraction of patients may acquire D761Y, L747S or T854A EGFR mutations. Acquired amplification of MET has been identified in ~20% of erlotinib/ gefitinib resistant tumors (Nguyen et al., 2009). HER2 amplification, PIK3CA mutations or BRAF mutations have also been found in a minor subset of resistant tumors (Stewart et al., 2015).

1.4.7 Epithelial to Mesenchymal Transition

Phenotypic switching of cancer cells between epithelial and mesenchymal states is responsible not only for conferring these cells with increased migration capacity and metastatic ability, but also resistance to certain chemotherapeutic agents. Cells may utilize their ability to undergo epithelial-to-mesenchymal transition (EMT) to escape getting killed by drugs that selectively target the epithelial state.

EMT has been reported in the acquisition of resistance to standard chemotherapeutic agents such as paclitaxel and platinum agents. Paclitaxel resistant-epithelial ovarian carcinoma (EOC) cells displayed EMT-like phenotypic changes such as spindle-shaped morphology and enhanced pseudopodia formation (Kajiyama et al., 2007). Resistant cells showed decreased E-cadherin expression, increased expression of mesenchymal markers like vimentin, fibronectin and smooth-muscle actin, elevated expression of EMT-regulatory factors such as Snail and Twist, and enhanced migratory potential. Such EMT-related morphological and molecular changes were also seen in colorectal cancer cells resistant to oxaliplatin (Yang et al., 2006). Epithelial ovarian cancer cells resistant to cisplatin and taxol were found to overexpress vimentin and N-cadherin, transcription factors Snail, Slug and Twist, as well as the endothelin-1 /endothelin A receptor (ET-1/ET(A)R) axis which was shown to regulate this EMT phenotype and chemotherapy resistance (Rosano et al., 2011). 5-Fluorouracil resistant breast cancer and colorectal cancer cells also exhibited EMT-like changes (Kim et al., 2015; Zhang et al., 2012a).

Gene signature representing EMT has been associated with resistance of NSCLC cell lines to the EGFR tyrosine kinase inhibitor erlotinib (Yauch et al., 2005). Specifically, NSCLCs with acquired erlotinib resistance overexpressed the mesenchymal marker, AXL (Zhang et al.,

2012b). In a subsequent study, another 76-gene EMT signature predicted resistance to EGFR and PI3K/Akt inhibitors and identified AXL as a potential therapeutic target for overcoming EGFR inhibitor resistance (Byers et al., 2013). Further, a retrospective clinical study on stage IV or recurrent NSCLC patients that had received gefitinib or erlotinib targeted therapy, confirmed that epithelial phenotype was associated with a significantly higher response rate, as well as better progression-free and overall survival, compared to the patients whose tumors expressed EMT or mesenchymal markers (Ren et al., 2014).

Similarly, EMT has also been linked to resistance to other targeted agents such as the HER2 inhibitor trastuzumab (Herceptin). SLUG/SNAIL2-positive basal/HER2+ cell lines were found to be intrinsically resistant to trastuzumab (Oliveras-Ferraros et al., 2012). Knockdown of SLUG/SNAIL2 induced mesenchymal-to-epithelial transition (MET) and restored drug sensitivity in these cells. Extending to other targeted therapies, MED12, a component of the transcriptional MEDIATOR complex that is mutated in cancers, was found to be a determinant of response to multiple drugs including the ALK, EGFR, MEK and BRAF inhibitors (Huang et al., 2012). MED12 loss-of-function mutations in cancer are responsible for activation of TGF-βR signaling that induces an EMT switch. The authors showed that inhibition of TGF-βR signaling restored chemotherapy sensitivity in drug resistant MED12 knockdown cells

1.4.8 Cancer Stem Cells in Drug Resistance

In the past decade, several studies have proposed the existence of highly tumorigenic, cancer-initiating cells or cancer stem cells. Cancer stem cells (CSC) are defined as a rare subpopulation of cells that are capable of self-renewal as well as asymmetric division into non-CSC progeny cells that constitute the bulk of the tumor. Similar to normal stem cells, CSCs exhibit increased expression of the ATP-binding cassette (ABC) family of transporters, particularly ABCG2/ BCRP1. These cells can thus be sorted from the rest of the tumor population on the basis of exclusion of Hoechst dye, giving them a peculiar 'side population' phenotype on the flow cytometry profile. Side population (SP) cells have been identified in neuroblastoma, breast cancer, lung cancer, and glioblastoma cell lines (Hirschmann-Jax et al., 2004). Studies have revealed that SP cells have greater tumor-initiating capacity as well as increased potential for invasiveness. These cells also showed increased expression of human telomerase reverse transcriptase (hTERT), indicative of unlimited proliferative potential, and decreased expression of the DNA replication protein, minichromosome maintenance 7 (MCM7), suggesting that these cells existed in a G(0) quiescent state (Ho et al., 2007). Further, cancer stem cells have also been characterized by the expression of specific markers such as $CD133^+$ in brain, colorectal, pancreatic, hepatocellular, breast and lung cancers, $EpCAM^+$ in pancreatic, colon and hepatocellular carcinomas, $CD34^+$ in hematological cancers, $CD44^+/CD24^-$ in breast cancers and ALDH activity in breast, colon, head and neck, liver, pancreatic cancers and non-small cell lung cancers (Islam et al., 2015).

Cancer stem cells have been shown to be intrinsically resistant to chemotherapy due to their ABC transporter expression, relative quiescence as well as enhanced DNA repair capacity.

Rare, tumor stem cells are said to survive chemotherapy treatments in patients and exist in a state of dormancy, sometimes for several years, until cancer relapse. Quiescent stem cells were shown to persist in chronic myelogenous leukemia (CML) cells following treatment with the BCR/ABL tyrosine kinase inhibitor imatinib (Bhatia et al., 2003). Even recurrent glioblastoma (GBM) tissues showed higher CD133 expression compared to primary tumors. Further, $CD133^+$ cells from primary cultured cell lines established from GBM patients showed higher levels of ABCG2/ BCRP1, MGMT and several anti-apoptotic genes. Consequently, these cells were found to be resistant to chemotherapeutic agents such as temozolomide, carboplatin, paclitaxel and etoposide, compared to $CD133^-$ cells (Liu et al., 2006). Cisplatin treatment of lung cancer cells resulted in enrichment of $CD133^+$ subpopulation of cells, both in A549 cell line and primary lung tumor xenografts (Bertolini et al., 2009). The same study reported that $CD133^+$ NSCLC patients treated with platinum-containing regimens showed shorter progression-free survival time. NSCLC stem-like cells derived from tumor sphere forming assays also showed higher expression of CD133, CD44, SOX2 and OCT4 stem cell genes, and elevated expression of several drug resistance proteins such as lung resistance-related protein (LRP), glutathione-S-transferase-π (GST-π) and multidrug resistance protein-1 (MRP1) (Sun et al., 2015). Retrospective examination of previously untreated NSCLC patient tumors by immunohistochemistry found a significant association between CD133 expression and resistance-related proteins such as glutathione-S-transferase (GST), thymidylate synthase (TS), catalase, O6-methylguanine-DNA methyltransferase (MGMT) and p170 (P-glycoprotein/ MDR) (Salnikov et al., 2010).

Key stem cell pathways such as the Notch, Wnt/β-catenin, TGF-β and Hedgehog signaling, have been reported to be determinants of chemoresistance in the cancer stem cell subpopulation. Thus, pharmacological intervention of these pathways has proven useful in

enhancing tumor response from standard chemotherapeutic drugs. $CD133^+$ glioma cells showed upregulation of Notch and Sonic hedgehog (SHH) pathways upon exposure to temozolomide (TMZ) and pharmacological antagonism of these signaling pathways with GSI-1 and cyclopamine was able to enhance the therapeutic efficacy of TMZ (Ulasov et al., 2011). Treatment of lung cancer cells with cisplatin led to enrichment of $CD133^+$ cells which were regulated by the Notch pathway. Pre-treatment of these cell lines with the gamma-secretase inhibitor, DAPT, significantly reduced the enrichment of CD133+ cells and increased the sensitivity to doxorubicin and paclitaxel (Liu et al., 2013). Genetic inactivation or pharmacological inhibition of β-catenin (Wnt pathway) abrogated CML stem cells and synergized with imatinib to delay disease recurrence (Heidel et al., 2012).

Activation of pro-survival pathways such as the PI3K/Akt, JAK/STAT and several others, may also contribute to the selective survival of CSCs and the resulting chemotherapy resistance. SP cells from breast cancer cell line showed alterations in phosphatidylinositol 3-kinase (PI3K)/mammalian target of rapamycin (mTOR), signal transduction and activator of transcription (STAT3), and phosphatase and tensin homolog (PTEN) pathways that were required for CSC maintenance (Zhou et al., 2007). In another study, CD44+/CD24−/CD45− CSCs from primary ERα-positive breast cancer showed activation of PI3K pathway (Hardt et al., 2012). Studies in our laboratory have demonstrated that $ALDH^+$ CSCs from non-small cell lung cancers showed STAT3 activation in ALDH1A3 expressing cells, and genetic or pharmacological inhibitor of STAT3 or its upstream regulator EZH2 diminished this $ALDH^+$ subpopulation (Shao et al., 2014). $ALDH^+$ chemoresistant cell subpopulation from malignant pleural mesothelioma (MPM) that survived pemetrexed + cisplatin treatment were also enriched for the ALDH1A3 isoform and survival of these cells was dependent on the STAT3-

NFkB/DDIT3/CEBPβ axis (Canino et al., 2015). $CD133^+$ hepatocellular carcinoma (HCC) cells exhibited increased resistance to doxorubicin and 5-fluorouracil, through activation of Akt/PKB and Bcl-2 cell survival pathways (Ma et al., 2008). Tumorigenic $CD133^+$ colon cancer cells showed resistance to oxaliplatin and 5-fluorouracil via production of the pro-survival factor, interleukin-4 (IL-4) (Todaro et al., 2007).

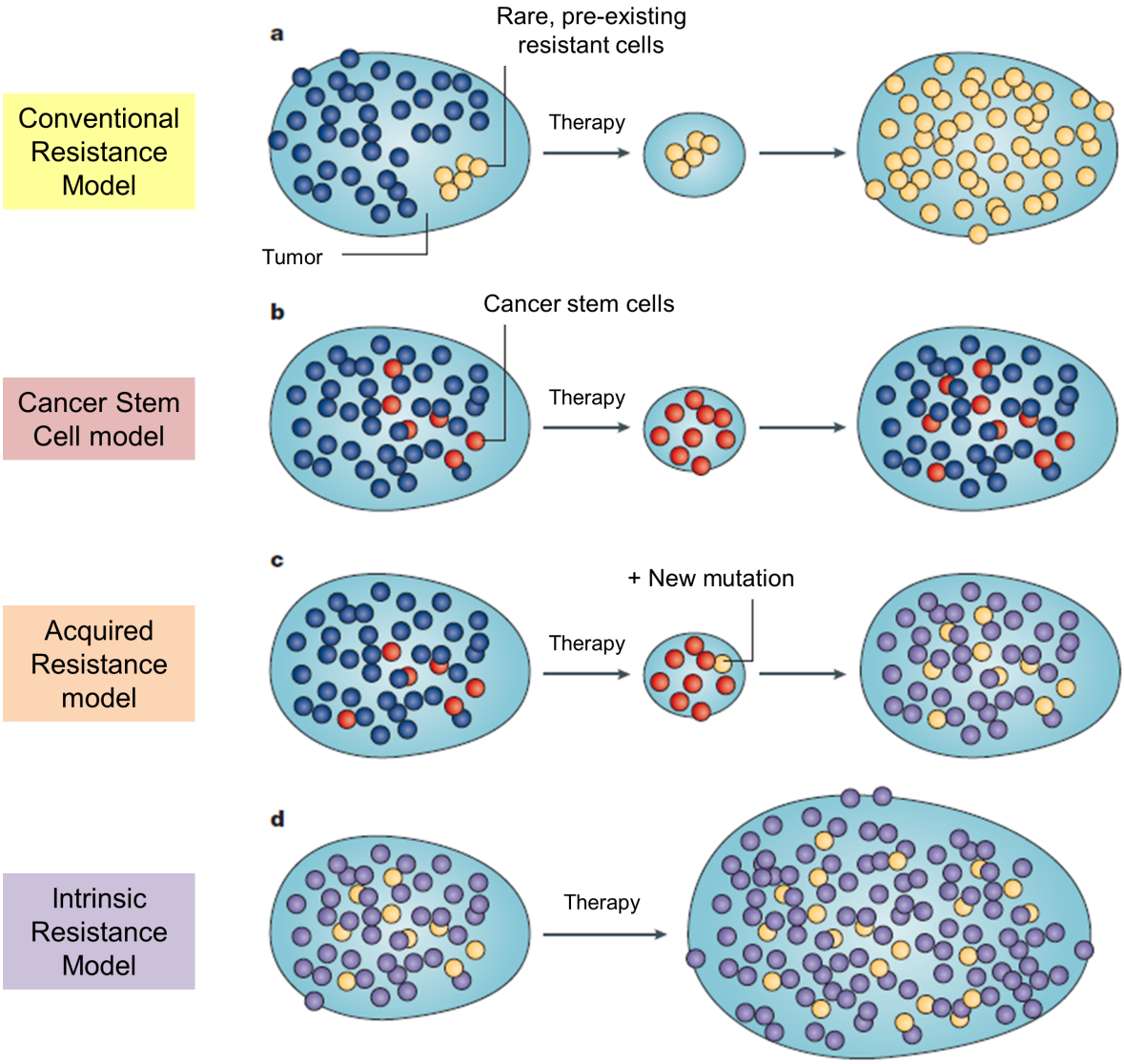

Figure 1.2 Models for Tumor Drug Resistance
(a) In the conventional model, rare tumor cells harboring pre-existing resistance-conferring alteration survive chemotherapy and give rise to a recurrent, drug refractory tumor; (b) Cancer stem cell model proposes the existence of drug resistant tumor-initiating cells that are able to repopulate the entire heterogeneous tumor post chemotherapy; (c) As per the acquired resistance model, new mutations in surviving tumor cells establish permanent resistance mechanisms; (d) Some tumors may be inherently resistant, resulting in a progressive disease even after therapy.
Modified from Dean, Fojo and Bates, Nature Reviews 2005

1.4.9 Tumor Heterogeneity and Clonal Evolution

Tumor heterogeneity is multifactorial and typically governed by genetic, epigenetic as well as environmental variations. Resistance to chemotherapy has been attributed to the existence of intra-tumor heterogeneity and the concept of Darwinian evolution that proposes the survival of biologically 'fit' cells in response to environmental selection pressure. By applying selective pressure, chemotherapy results in a transient reduction in tumor heterogeneity and creates an 'evolutionary bottleneck' with the survival of only drug resistant clones (Gerlinger and Swanton, 2010). These resistant clones gradually re-establish tumor heterogeneity with the acquisition of a new set of genetic alterations.

Genomic instability which is a hallmark of cancer can explain the existence of different pre-existing mutations in cancer cells that are positively selected under drug stress. The BCR-ABL mutations T315I and E255K that are responsible for imatinib resistance have been shown to pre-exist in rare subpopulations of chronic myelogenous leukemia cells from treatment naïve patients (Roche-Lestienne et al., 2002). Likewise, the EGFR T790M resistance mutation was also detected in a minor subpopulation of tumor cells from NSCLC patients prior to EGFR TKI treatment (Inukai et al., 2006). Presence of such rare, pre-existing tumor cells in a heterogeneous population can thus account for the observed resistance after chemotherapy.

Clinical management of drug resistance arising from tumor heterogeneity could possibly be achieved by performing serial biopsies of tumors or by liquid biopsy of circulating tumor cells (CTCs) and circulating cell-free DNA in peripheral blood during the course of chemotherapy. This might aid in the detection of enriched resistant clones during therapy. In one such study, serial plasma sampling and exome sequencing was used to track the evolution of metastatic

patient tumors in response to chemotherapy (Murtaza et al., 2013). The authors found enrichment in frequency of certain mutant alleles with emerging therapy resistance. These included activating PIK3CA mutation following treatment with paclitaxel, a truncating mutation in RB1 after cisplatin treatment, a truncating mutation in MED1 after tamoxifen, trastuzumab, and lapatinib treatment, and the resistance-conferring EGFR T790M mutation following gefitinib therapy. A clinical study called TRACERx [TRAcking non-small cell lung Cancer Evolution through therapy (Rx), NCT01888601] has been initiated for performing multi-regional and longitudinal tumor sampling to study tumor evolution from diagnosis to relapse and understand the impact of tumor clonal heterogeneity on therapeutic outcome (Jamal-Hanjani et al., 2014). In the near future, such studies provide hope for clinical detection of emerging drug resistance and consequently for guiding precision medicine based on the individual's evolving tumor profile.

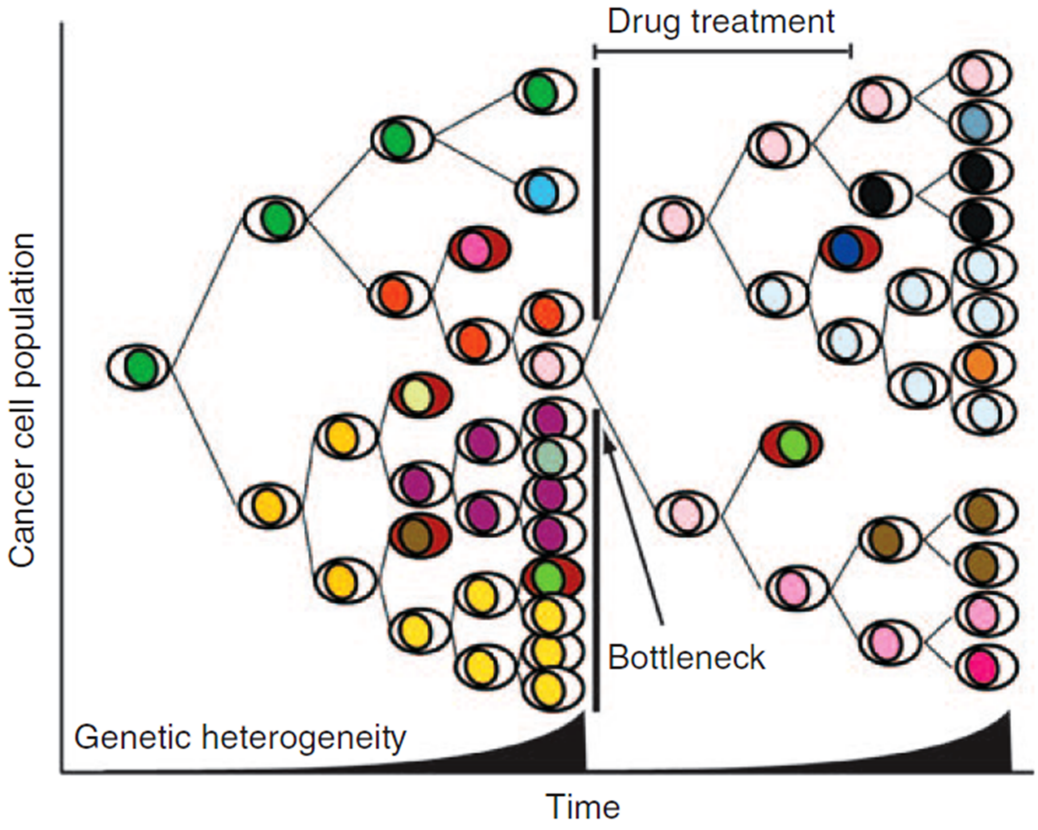

Figure 1.3 Tumor Heterogeneity and Evolution of Drug Resistance
The process of tumor initiation and progression involves natural selection of cell clones with advantageous, heritable characteristics. This evolutionary adaption also plays a major role in guiding the development of drug resistance during chemotherapy. Drug treatment leads to the selective survival of drug tolerant tumor clones (shown in pink) and creates an 'evolutionary bottleneck' with transient reduction in tumor heterogeneity. Tumor heterogeneity is re-established with the acquisition of new alterations by the daughter cells of surviving clones.
Adapted from Gerlinger and Swanton, British Journal of Cancer 2010

1.4.10 Clinical Interventions to Overcome Resistance

Majority of the efforts for overcoming drug resistance have involved inhibitors of drug efflux transporters. By inhibiting ABC transporters, these compounds can not only sensitize resistant cells but also target cancer stem cells or side population cells. Initially, first generation MDR inhibitors which were already in use for other indications, such as verapamil (Millward et al., 1993) and cyclosporine were tested in clinical trials, in combination with standard chemotherapy. Subsequent trials involved newer, more specific compounds such as PSC 833 (valspodar), VX-710 (biricodar), XR9576 (tariquidar), and LY-335979 (zosuquidar) (Dean et al., 2005). Failure of these clinical trials has been attributed to drug interactions with standard chemotherapies as well as contribution of multiple ABC transporters which were not all targeted by these new higher specificity inhibitors.

Since most of the inhibitors tested in clinical trials involved ABCB1/MDR1/Pgp inhibitors, researchers have argued that therapeutic failure could be due to lack of ABCG2 inhibition as this is the marker that more commonly defines side population cells or tumor stem cells (Dean, 2009). Fumitremorgin C (FTC) is a natural product that is an ABCG2-specific inhibitor. However, FTC was found to be generally toxic to cells and mice, and thus unsuitable for clinical studies. The synthetic derivative of FTC, called Kol43 has less toxicity related issues and studies in mice have shown its effectiveness in inhibiting ABCG2. Additionally, the compound GF120918 which is an ABCB1 inhibitor also has activity against ABCG2 and could prove more useful in inhibiting both these transporters at once.

Pan-ABC inhibitors could be developed to target multiple transporters at once; however it is necessary to keep in consideration that ABC transporters are also expressed in normal tissues

such as the GI tract, liver, kidney, brain, ovary, testes and hematopoietic stem cells. Normal stem cells depend on the expression of drug transporters to survive chemotherapy and other toxic substances. So, ABC transporter inhibition will cause increased toxicity to normal stems cells and compromise normal tissue development and regeneration.

Targeting the Notch, Hedgehog or Wnt pathways might be another way to eliminate cancer stem cells that could possibly escape killing by standard chemotherapy. While also expressed in normal stem cells, these pathways may be up-regulated in certain tumors. BMS-906024, a gamma secretase inhibitor (GSI) with anti-notch activity is being evaluated for its safety and tolerability in a phase I clinical trial for advanced metastatic tumors including NSCLCs (NCT01653470, 2012). This drug is being tested in combination with paclitaxel, 5FU + irinotecan or carboplatin + paclitaxel. The anti-Frizzled monoclonal antibody vantictumab (OMP-18R5), that targets the Wnt pathway, is being evaluated for its safety in combination with docetaxel in patients with recurrent or advanced NSCLC (NCT01957007, 2013).

Immunotherapy is also emerging as a new treatment option for advanced NSCLC patients who have failed prior chemotherapy. One of such phase I studies (NCT02298153, 2014) comprises of an anti-PD-L1 therapy called MPDL3280A, given in combination with INCB024360. MPDL3280A has been developed to improve the immune system's ability to recognize and destroy cancer cells by blocking PD-L1, while INCB024360 is designed to promote an immune response against tumor cells, through its binding to an enzyme called IDO1. Another on-going clinical trial (NCT01454102, 2011) involves nivolumab (BMS-936558) that targets PD-1, and inactivates it, thereby enhancing the body's immune response against cancer cells. This drug is being evaluated as monotherapy as well as in combination therapy with

gemcitabine + cisplatin, pemetrexed + cisplatin, paclitaxel + carboplatin, bevacizumab maintenance, erlotinib or ipilimumab.

1.5 An Overview of Epigenetic Regulation of Transcription

Epigenetic mechanisms allow for stable changes in gene expression patterns without intrinsic changes in the DNA sequence. The molecular determinants that constitute an epigenetic event are heritable through DNA replication, thereby maintaining a given 'cell state'. The new cellular gene expression pattern can be preserved even if the original stimuli that were responsible for initiation of these cell states are no longer present (Easwaran et al., 2014). This thus adds another layer of complexity in terms of intratumoral epigenetic heterogeneity and differences in therapeutic response.

Epigenetic control is mediated by a fine interplay between DNA methylation, histone modifications and nucleosome remodeling. DNA methylation involves covalent modification of DNA by a methyl group at the cytosine residues in CpG islands. CpG island methylation in gene promoters is primarily associated with transcriptional repression. Some studies have reported that CpG methylation in gene bodies has the opposite effect by enhancing gene transcription through increased transcriptional elongation or alternate promoter usage (Easwaran et al., 2014). The interaction between DNA and histone proteins is tightly regulated by histone modifications. These occur predominantly at the N-terminal tails that protrude from the nucleosome core. Histone post-translational marks can have either an activating or repressive effect depending on the type and location of modification. These modifications affect nucleosome spacing and higher-order chromatin structure, which in turn affects recruitment of other non-histone proteins.

Closely compacted nucleosomes where DNA is inaccessible for transcription are associated with silent heterochromatin while loosely packaged, "open" chromatin is typical of actively transcribed genes or euchromatin. Active transcriptional domains are separated from inactive domains by boundary elements or insulator proteins. Finally, histone-DNA contacts are altered by ATP-dependent nucleosome-remodeling complexes that can move nucleosomes to different translational positions (sliding), histone chaperones that alter histone dynamics (eviction and deposition) and their inter-woven interactions that affect DNA accessibility to transcription factors (Li et al., 2007).

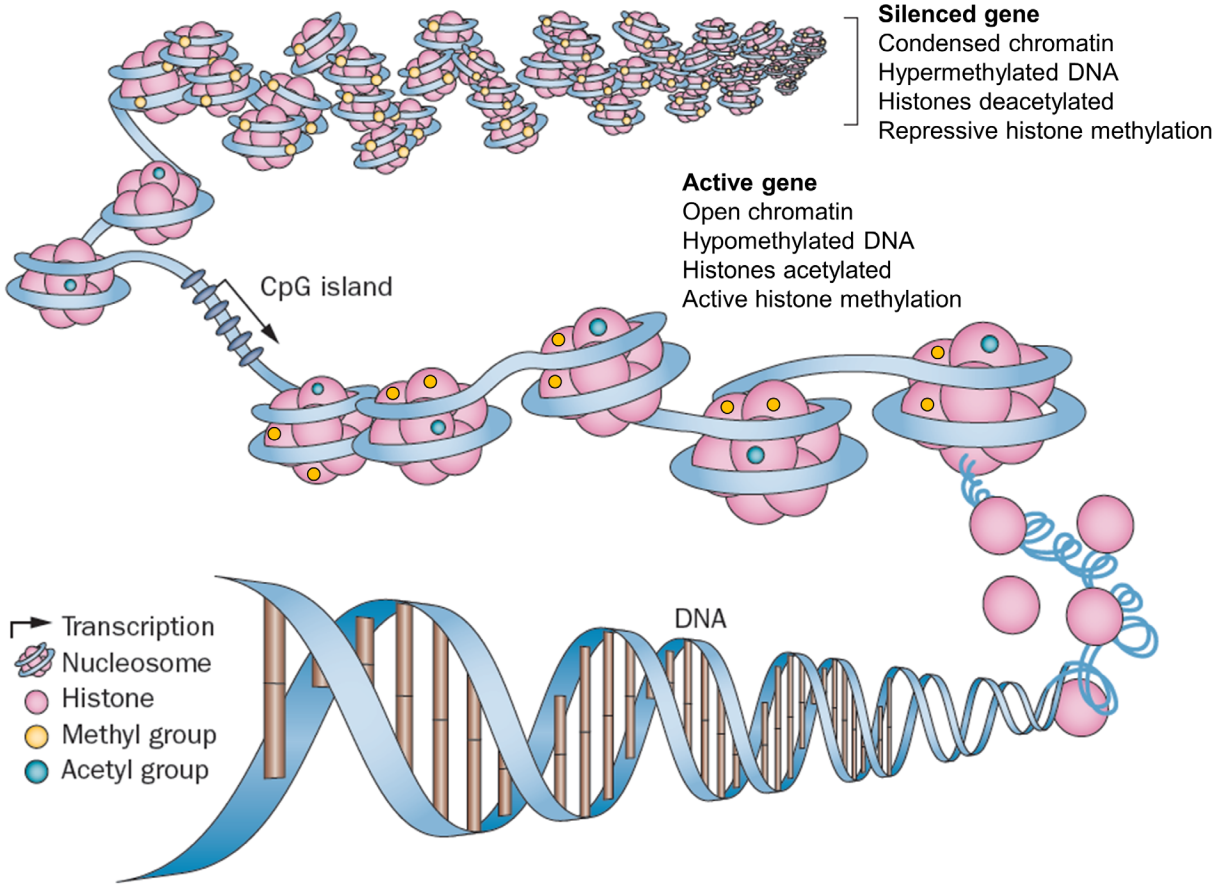

Figure 1.4 Epigenetic Regulation of Gene Expression
Gene expression is tightly regulated by interplay between DNA methylation, histone modifications and nucleosome remodeling. Silenced genes are characterized by closely compacted chromatin where DNA is inaccessible for transcription. Actively transcribed genes have an open chromatin owing to hypomethylated CpG islands, histone acetylation and activating histone methylation marks.
Adapted from Azad N. et al., Nat. Rev. Clin. Oncol. 2013

1.6 Enzymes involved in Epigenetic Regulation

Epigenetic modification of DNA occurs primarily at the 5-position of cytosine residues (5mC) in CpG dinucleotides. Histones, on the other hand, can be post-translationally modified in a variety of ways ─ lysine acetylation, lysine and arginine methylation, arginine citrullination, lysine ubiquitination, lysine sumoylation, ADP-ribosylation, proline isomerization, and serine/threonine/tyrosine phosphorylation, among several others (Rothbart and Strahl, 2014).

Enzymes that regulate DNA and histone modifications can be broadly categorized into "writers" (enzymes that establish the modifications), "erasers" (proteins that remove these marks), and "readers" (proteins that bind specific modifications and facilitate epigenetic effects). The writers encompass enzymes such as DNA methyltransferases, histone methyltransferases, histone acetyltransferases, kinases or ubiquitin ligases. The widely studied enzymes known to reverse these marks consist of the histone demethylases, histone deacetylases and phosphatases. Readers of the post-translational modifications include proteins consisting of specific domains, such as bromo-, chromo-, tudor-, MBT-, PWWP-, WD40- and PHD-domains, that bind to specific modifications (Helin and Dhanak, 2013).

DNA methylation is catalyzed by a class of enzymes called DNA methyltransferases (DNMTs) that transfer a methyl group from S-adenosylmethionine (SAM) onto cytosine. These enzymes act either as de novo methyltransferases (DNMT3a and DNMT3b), establishing the initial pattern of methylation, or as maintenance methyltransferases (DNMT1), that copy the methylation to a new DNA strand during replication (Rothbart and Strahl, 2014). Demethylation of DNA is thought to be mediated by the ten-eleven translocation (TET) family of enzymes that catalyze iterative 5mC oxidation to 5-hmC, 5-formylcytosine (5fC) and 5-carboxylcytosine

(5caC). Proteins that "read" DNA methylation include the methyl-binding domain (MBD) proteins, a family of zinc finger-containing proteins (such as Kaiso) and SET and RING-associated (SRA) domain-containing proteins (UHRF family). Interaction of the UHRF1 SRA domain with DNA is said to be required for DNMT1 chromatin targeting and subsequent maintenance of DNA methylation. On the contrary, UHRF2 has been shown to enhance oxidative demethylation by TET1. Further, it has been suggested that cysteine-rich zinc-finger CxxC-containing proteins act as readers of unmethylated CpG dinucleotides, and may serve as targeting mechanisms to direct further DNA demethylation (Rothbart and Strahl, 2014).

Histone acetylation is regulated by the opposing activities of histone acetyl transferases (HATs) and histone deacetylases (HDACs). As writer enzymes, HATs transfer acetyl groups to lysine residues of histone tails, thereby activating gene transcription. These enzymes comprise the MOZ/YBF2/SAS2/TIP60 (MYST) family, the GCN5 N-acetyltransferase (GNAT) family, and the CBP/p300 family of proteins (Ellis et al., 2009). Lysine acetylation has been found to occur on H3 (K4, K9, K14, K18, K23, K27, K36 and K56), H4 (K5, K8, K12, K16, K20 and K91), H2A (K5 and K9) and H2B (K5, K12, K15, K16, K20 and K120). The HDACs cause transcriptional silencing by catalyzing the hydrolysis and deacetylation of N-acetyl lysine residues. HDACs can be categorized into four classes ─ class I consists of HDAC 1, 2, 3, and 8, (localized to the nucleus); class II consists of HDAC 4, 5, 6, 7, 9, and 10, (present in both nucleus and cytoplasm); class III consists of sirtuins (SIRT 1-7); and class IV consists of HDAC 11. Class I, II and IV are zinc-dependent enzymes whereas the NAD+ dependent sirtuins do not rely on zinc (Ellis et al., 2009). The recognition of N-acetylation of lysine residues is primarily initiated by bromodomains that are small interaction modules found on a diverse set of proteins, including the BET family of proteins (example, BRD4), SWI/SNF-related matrix-associated

actin-dependent regulators of chromatin subfamily A (SMARCAs), ATP-dependent chromatin remodeling complexes such as BAZ1B, tripartite motif-containing proteins (TRIMs) and TBP-associated factors (TAFs) (Filippakopoulos and Knapp, 2014).

Histone methylation is catalyzed by the histone methyltransferase (HMT) family of enzymes that consist of protein arginine methyltransferases (PRMT) and lysine methyltransferases (KMTs). These enzymes sequentially transfer a methyl group from the cofactor S-adenosylmethionine (SAM) to the terminal amine of specific lysine or arginine residues. The omega nitrogen atoms of arginine can be monomethylated or dimethylated symmetrically (Rme2s) or asymmetrically (Rme2a). Lysine is methylated on its ε-amino group and can be mono-, di- or trimethylated. The catalytic domain of all KMTs (except DOT1L) consists of the SET (Su(var)3-9, Enhancer of Zeste, Trithorax) domain (McGrath and Trojer, 2015). The most widely studied KMTs are G9a, EZH2, DOT1L, SMYD2 and the KMT2/MLL family. The enzymes that erase histone methylation marks are classified into the lysine-specific demethylase (LSD) family and the JmjC domain-containing lysine demethylase family (Helin and Dhanak, 2013). The LSD family consists of LSD1 (KDM1A/AOF2) and LSD2 (KDM1B/AOF1), that act as flavin adenine dinucleotide (FAD)-dependent monooxidases and catalyze the demethylation of only mono- and di-methylated, but not tri-methylated lysines. The JmjC domain containing proteins form the largest family of histone demethylases with about 30 known human proteins, 17 of which have defined enzyme activities (Helin and Dhanak, 2013). Unlike LSD enzymes, JmjC domain containing enzymes can demethylate tri-methylated lysine in addition to the di- and mono-methyl residues. Enzymatic reaction is dependent on α-ketoglutarate (2OG) and iron, and involves an oxidative mechanism that occurs through direct hydroxylation and thus demethylation of the methyl lysine, releasing formaldehyde. Depending

on the specific residue modified, lysine methylation can be associated with either actively transcribed genes (H3K4, H3K36 or H3K79 methylation) or silenced heterochromatic genes (H3K9, H3K27 or H4K20 methylation). However, the consequence of these methylation marks is ultimately determined by effector or reader proteins. Readers of methyl lysine have been well-studied and include ADD (ATRX-DNMT3-DNMT3L), ankyrin, bromo-adjacent homology (BAH), chromo-barrel, chromodomain, double chromodomain (DCD), MBT (malignant brain tumor), PHD (plant homeodomain), PWWP (Pro-Trp-Trp-Pro), tandem Tudor domain (TTD), Tudor, WD40 and the zinc finger CW (zf-CW) proteins (Musselman et al., 2012).

Due to their vital regulatory function, many epigenetic enzymes have been found to act as important mediators in oncogenesis and were shown to be over-expressed, amplified, fused or mutated in cancers (Varier and Timmers, 2011; Wilting and Dannenberg, 2012). It should be noted that many of these epigenetic enzymes also affect non-histone proteins, further increasing the complexity of regulation and diversity of signaling pathways affected. Alterations in DNA or histone modifying enzymes, or nucleosome remodeling complexes have been reported in multiple malignancies, making them important targets for anti-tumor therapy.

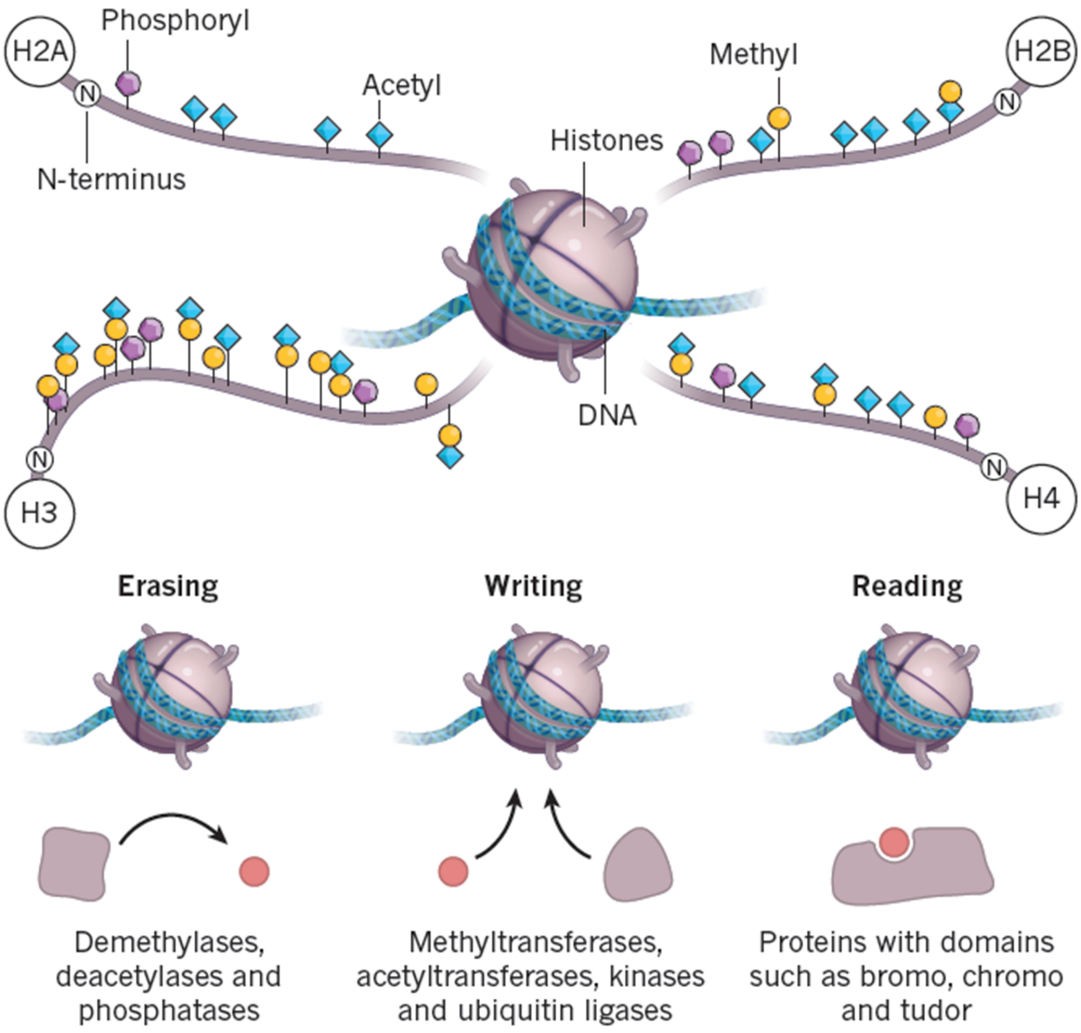

Figure 1.5 Erasers, Writers and Readers of Epigenetic Modifications
Epigenetic regulators can be broadly classified into: Erasers ─ enzymes that remove post-translational modifications, Writers ─ enzymes that catalyze addition of modifications, and Readers ─ proteins with specific domains that bind to and recognize these modifications.
Adapted from Helin and Dhanak, Nature 2013

1.7 Epigenetic Drugs in Clinical Trials

Epigenetic alterations are reversible and thus present attractive targets for anti-cancer therapy. The most well-studied and clinically implemented anti-tumor epigenetic targets are enzymes that affect DNA methylation and histone acetylation. In cancer, promoter CpG islands can become hypermethylated, resulting in silencing of tumor suppressor genes. This promoter methylation can be diminished by the use of DNA methyltransferase (DNMT) inhibitors that form covalent adducts with the enzyme, leading to its sequestration and cellular depletion, consequently leading to re-expression of the silenced genes (Zeller and Brown, 2010). Similarly, histone deacetylases (HDACs) are overexpressed in many cancers and inhibiting these enzymes promotes accumulation of the acetylated form of histone proteins, resulting in re-activation of silenced tumor suppressor genes.

DNA methyltransferase inhibitors (DNMTi) such as 5-azacytidine (Vidaza) and decitabine (5-aza-2′-deoxycytidine) were approved by the FDA in early 2000s and showed some therapeutic potential in hematological cancers (Azad et al., 2013). They have been subsequently tested in some solid tumors as well, including ovarian cancer and non-small cell lung cancer. First-generation histone deacetylase inhibitors (HDACi) like romidepsin (FK228) and vorinostat (SAHA) and subsequently newer, improved HDAC inhibitors such as panobinostat, CHR-3996, quisinostat, entinostat (MS-275) and mocetinostat (MGCD0103) have also been evaluated in the clinic either alone or in combination with other therapies (Simo-Riudalbas and Esteller, 2015). Vorinostat therapy led to significant improvement in response rates when combined with carboplatin and paclitaxel in previously untreated advanced-stage NSCLC patients (Ramalingam et al., 2010). A phase I/II trial of combined epigenetic therapy with azacytidine and entinostat in

patients with recurrent metastatic non-small cell lung cancer, reported demethylation of lung cancer-associated epigenetically silenced genes that correlated with improved progression-free and overall survival (Juergens et al., 2011). Recently, phase I/II clinical trials have been initiated for histone methyltransferase inhibitors such as EPZ-5676 (DOT1L inhibitor, Epizyme, NCT01684150) and EPZ-7438 (EZH2 inhibitor, Epizyme, NCT01897571), as well as the histone demethylase inhibitor, ORY-1001 (LSD1 inhibitor, Oryzon Genomics, EudraCT number 2013-002447-29). BET bromodomain inhibitors such as OTX015 (Oncoethix, NCT01713582) and GSK525762 (GlaxoSmithKline, NCT01943851, NCT01587703) are also being clinically evaluated for certain malignancies (Mair et al., 2014).

1.8 Role of Epigenetics in Drug Resistance

Epigenetic alterations are getting increasing attention as new approaches for anti-cancer therapies and intriguingly, for their newly-defined role in drug resistance, the major hurdle in successful treatment of malignancies. Recent studies are beginning to recognize a critical role of epigenetics in not only driving early stages of tumorigenesis but also in establishing non-genetic heterogeneity observed in tumor cell populations, and in enabling acquisition of changes that would favor cell survival under drug stress. The potential of epigenetic therapies in preventing, delaying, or reversing drug resistance is an active subject of current research.

The role of DNA hypermethylation in conferring drug resistance and cancer relapse has been extensively studied (Zeller and Brown, 2010). In platin-resistant ovarian cancer models, the DNA mismatch repair (MMR) gene MLH1 is known to be transcriptionally silenced by CpG island promoter methylation. Relapsed tumors from epithelial ovarian cancer patients after

carboplatin/taxol therapy showed increased MLH1 promoter methylation compared to matched pre-chemotherapy samples, and this was associated with poor patient survival (Gifford et al., 2004). Genome-wide DNA methylation profiling of paired diagnosis/relapse samples from childhood B-lymphoblastic leukemia patients also revealed that the chemotherapy-resistant relapse samples were DNA hypermethylated compared with matched diagnosis samples (Hogan et al., 2011).

Epigenetic inhibitors that are capable of affecting multiple downstream signaling pathways hold a potential for reversing these resistance-associated "cellular states". In agreement with this, it was shown that the DNMT inhibitor decitabine and HDAC inhibitor vorinostat were able to reverse relapse-specific gene expression signature and restore chemo-sensitivity in childhood B-lymphoblastic leukemia primary patient samples and leukemia cell lines (Bhatla et al., 2012). Likewise, another study showed that colorectal cancer cell lines exposed to increasing 5-fluorouracil concentrations developed resistance through downregulation of UMP-CMP kinase, and treatment of these cells with low dose decitabine increased UMP-CMP kinase levels and consequently reversed the resistance to 5-fluorouracil (Humeniuk et al., 2009). Previous studies have also shown that TRAIL-resistant lung cancer cell lines can be re-sensitized by DNMT inhibitors through promoter demethylation and re-expression of the pro-apoptotic calcium/calmodulin-regulated serine/threonine kinase DAPK (Tang et al., 2004).

Interestingly, the ATP-binding cassette (ABC) transporters implicated in multi-drug resistance have also been shown to be epigenetically regulated (Wilting and Dannenberg, 2012). Studies have demonstrated that bladder cancer cells usually contain a hypermethylated *MDR1*/*ABCB1* promoter which is converted into a hypomethylated state upon chemotherapy

treatment, resulting in gene overexpression (Wilting and Dannenberg, 2012). Similar epigenetic activation was also observed with the ABCG2/BCRP transporter. The exact mechanism by which *ABCB1* promoter hypomethylation occurs is unknown. Reports suggest that the transcriptional repression is maintained by recruitment of MeCP2, a Methyl-CpG-binding protein (MBP) at the hypermethylated *ABCB1* promoter which in turn provides a docking platform for nucleosome modifiers and remodelers, such as SWI/SNF, HDAC1, HDAC2 and mSIN3 (Wilting and Dannenberg, 2012). In agreement with this, HDAC inhibition or overexpression of the p300/CREB lysine acetyl transferase (KAT3B) has been shown to cause *ABCB1* gene induction (Jin and Scotto, 1998). Chemotherapy or HDAC inhibitor treatment led to hyperacetylation of histone H3 and a delayed increase in H3K4 methylation at the *ABCB1* promoter (Baker et al., 2005). Another study showed that H3K4me3 at the *ABCB1*/*MDR1* promoter is dependent on the histone methyltransferase enzyme MLL1/KMT5A. Accordingly, KMT5A knockdown decreased MDR1 expression and sensitized cancer cells to chemotherapy (Huo et al., 2010).

NSCLC cells that are intrinsically resistant to the topoisomerase II inhibitor etoposide (VP16) can benefit from HDACi therapy (Hajji et al., 2010). Treatment with HDAC inhibitors trichostatin A (TSA) or valproic acid (VPA) increased global H4K16 acetylation and sensitized cells to VP16-induced cell death. This was in fact attributed to inhibition of the class III HDAC/sirtuin called SIRT1, as TSA or VPA treatment led to a significant decrease in SIRT1 protein levels and SIRT1 overexpression abolished the sensitizing effects of TSA.

Drug-tolerant NSCLC cells that survive EGFR tyrosine kinase inhibitor (TKI) therapy can also be ablated by HDAC inhibitors (Sharma et al., 2010). Quiescent drug-tolerant persisters

(DTPs) and proliferating drug-tolerant expanded persisters (DTEPs) lacked the EGFR T790M genetic mutation or MET gene amplification, which are often associated with acquisition of EGFR TKI resistance in NSCLC patients. Instead, DTEPs regained EGFR TKI sensitivity upon prolonged drug-free passaging, indicating a reversible, epigenetic mechanism of drug resistance. The histone demethylase KMD5A (also known as JARID1A or RBP2) was found to be upregulated in both DTPs and DTEPs. These cells showed reduced H3K4me2/3 levels but also decreased H3K14 acetylation, presumably due to the association of KDM5A with HDACs. KDM5A genetic knockdown or pharmacological inhibition using HDAC inhibitors (TSA, SAHA, MS-275, and scriptaid) eliminated the emergence of DTEP clones from parental cells. Furthermore, IGF-1R signaling was also elevated in DTEPs and this was reported to be linked to KDM5A function as pharmacological inhibition of IGF-1R signaling reduced KDM5A expression, partially restored H3K4 methylation as well as prevented the emergence of DTEPs.

Intriguingly, another study identified enrichment of KDM5B (JARID1B) expressing, slow cycling cells upon treatment of melanoma cells with cisplatin, bortezomib, temozolomide or BRAFV600E-targeted vemurafenib therapy (Roesch et al., 2013). Three out of four matched pairs of patient melanomas that had relapsed under vemurafenib treatment also showed increase in JARID1B expressing cells. Cisplatin induced enrichment of JARID1B^{high} cells was fully reversible upon drug withdrawal, suggesting dynamic phenotype switching. JARID1B genetic knockdown sensitized melanoma cells to chemotherapy as was evident by the additivity with bortezomib or vemurafenib in inhibiting melanoma xenografts. The HDAC inhibitor TSA that was effective in the Sharma *et al.* study, was however unable to diminish the JARID1B^{high} cell subpopulation in this study. Instead, pharmacological targeting of the mitochondrial respiratory chain (oxidative phosphorylation, OXPHOS) using ATP-synthase inhibitor oligomycin or

complex I inhibitors rotenone and phenformin inhibited the JARID1B^{high} slow-cycling subpopulation in soft agar assays and enhanced the therapeutic efficacy of vemurafenib in xenografts.

In another recent study, chronic exposure of NOTCH1-dependent human T cell acute lymphoblastic leukemia (T-ALL) cells to a gamma-secretase inhibitor (GSI, compound E) led to the enrichment of a population of persister cells that tolerated 50-fold higher GSI concentrations compared to chemo-naïve cells (Knoechel et al., 2014). The drug-tolerant persister cells showed decreased expression of the active intracellular form of NOTCH1 (ICN1) and NOTCH1 target genes. This expression change was reversible as removal of GSI led to re-activation of NOTCH1 signaling. Persister cells exhibited an altered chromatin state with higher global levels of repressive histone modifications and chromatin compaction. The authors did not observe upregulation of KDM5A expression or sensitivity to HDAC inhibitors. However, a lentiviral short hairpin RNA (shRNA) knockdown screen for ~350 chromatin regulators identified preferential dependence of persister cells on BRD4, a BET bromodomain protein. In agreement with this, persister cells exhibited ~5-fold enhanced sensitivity to the small molecule BET inhibitor JQ1, compared to chemo-naïve T-ALL cells. Further, pre-treatment of naïve T-ALL cells with JQ1 reduced the frequency of GSI-tolerant persister cells by 20-fold. JQ1 treatment decreased protein levels of BRD4 targets BCL2 and MYC, and this was related to the loss of cell viability as BCL2 or MYC overexpression partially rescued these cells from JQ1 treatment. Combination treatment with NOTCH inhibitor DBZ and BRD4 inhibitor JQ1 was able to prolong survival of mice engrafted with primary T-ALL cells.

Such studies suggest a promising outcome with combination therapies that incorporate epigenetic modulators. The design of treatment modalities that target the epigenetic features dominant under selection pressure would eliminate tumor cell's primary defense mechanism for survival and possibly prevent the development of permanent drug resistance mechanisms. Epigenetic drugs could be used to reprogram drug-resistant cells into drug-sensitive cells by erasing their epigenetic memory responsible for drug tolerance or alternatively, in some contexts, by directly targeting the resistant cell's "addiction" or primary dependence on these epigenetic enzymes for survival. The combination of standard chemotherapy or targeted drugs that debulk the majority of the tumor with epigenetic drugs such as DNMTi, HDACi, BETi or inhibitors of pathways affected by the drug-resistant epigenome (inhibitors of IGF-1R, OXPHOS) have the potential to reform future anticancer treatment regimens to prevent multi-drug resistance and tumor relapse.

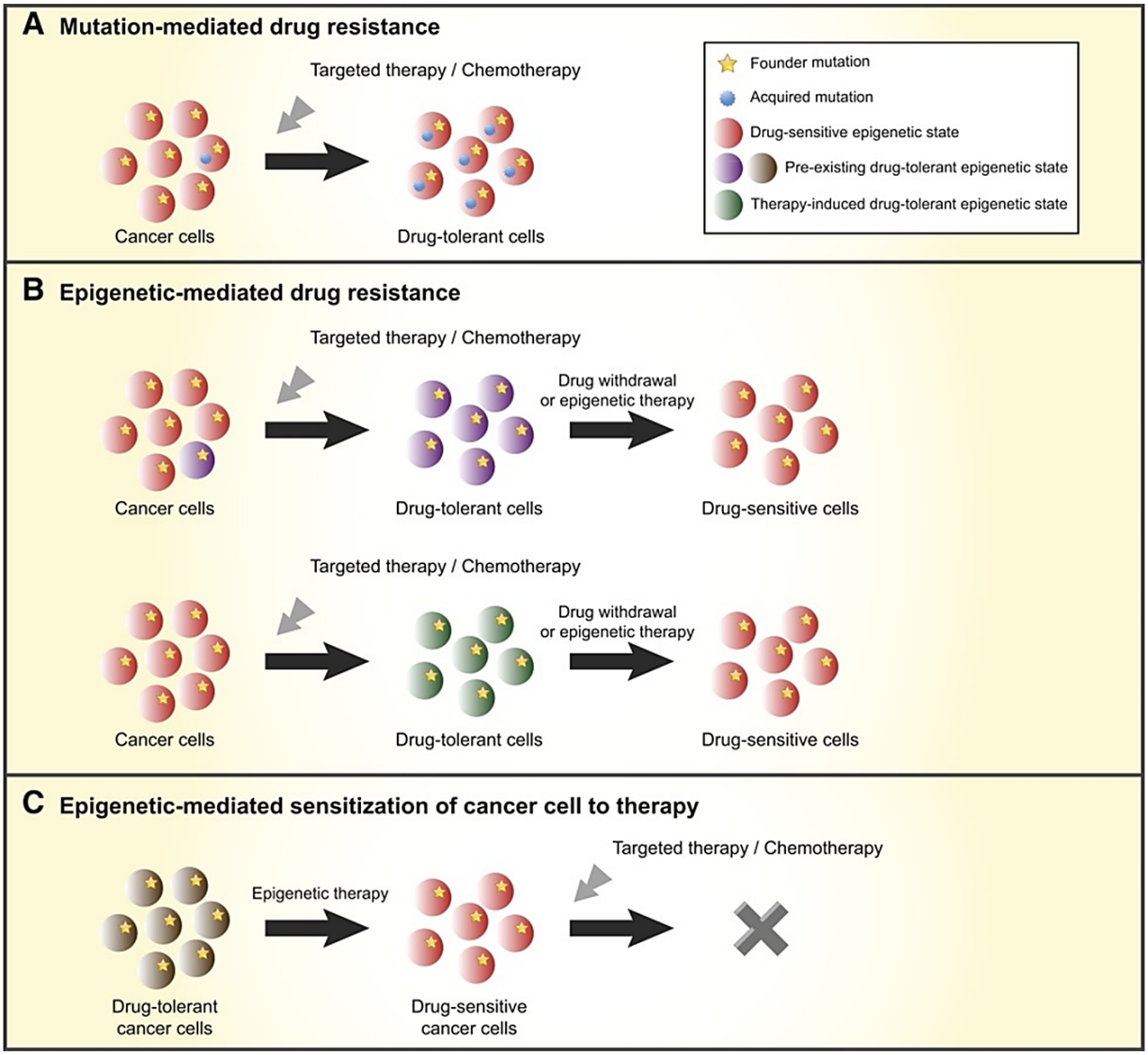

Figure 1.6 Genetic and Epigenetic Mechanisms of Drug Resistance
(A) Tumors may consist of different genetic subclones that carry the founder mutations or additional resistance-conferring mutations that enable cell survival during chemotherapy; (B) Drug resistance may be epigenetically driven, with the drug tolerant subclones either pre-existing in the tumor population or acquired as a consequence of drug treatment; (C) Entire tumor cell population may be epigenetically predisposed to be chemotherapy resistant and can be sensitized by epigenetic therapy. *Adapted from Easwaran, Tsai and Baylin, Molecular Cell 2014*

1.9 Hypothesis and Specific Aims

Drug resistance poses a major barrier in treatment of non-small cell lung cancer patients. Despite intense research in the area of chemo-resistance, mechanisms underlying resistance to standard taxane-platin chemotherapy are still not fully understood.

The goals of this work were to establish new preclinical models of resistance to taxane-platin doublet chemotherapy for NSCLC, identify clinically relevant mechanisms of resistance, and develop new rational pharmacologic approaches to overcome this resistance.

The hypothesis was that NSCLC cell lines selected for taxane-platin chemo-resistance by long-term drug treatment given in a clinically relevant dosing schedule would yield important insights into resistance-associated genes, and integration with gene expression changes detected *in vivo* in resistant xenografts and in neoadjuvant treated NSCLC patient tumors would help identify clinically relevant drug resistance biomarkers and targets for therapy.

SPECIFIC AIM ONE

To establish pre-clinical resistance models of NSCLC cell lines by long-term paclitaxel + carboplatin drug treatment, and characterize the phenotypic changes and expression profiles.

A. Develop isogenic series of progressively resistant NSCLC cell line variants by treating parental, chemo-naïve cell lines with drug ON/drug OFF cycles of paclitaxel + carboplatin doublet treatment given in clinically relevant 2:3 dose ratio.

B. Characterize drug response using cell viability and liquid colony formation assays, and validate the response in xenografts by *in vivo* treatment of tumor-bearing mice.

C. Identify any phenotypic changes such as changes in cell morphology or growth rate.

D. Characterize molecular changes by genome-wide mRNA expression profiling of parental cell lines and resistant variants.

SPECIFIC AIM TWO

To identify clinically relevant biomarkers and targets for therapy by integrating gene expression changes obtained from chemo-resistant cell lines, xenografts and neoadjuvant treated NSCLC patient tumors.

A. Identify gene expression changes that correlate with increasing resistance to paclitaxel + carboplatin therapy in isogenic resistant cell line series.

B. Filter gene expression changes that are retained *in vivo* in resistant cell line xenografts.

C. Evaluate this pre-clinical gene signature obtained from resistant cell lines and xenografts, in a clinically annotated dataset of neoadjuvant treated (mainly taxane + platin treated) NSCLC patient tumor specimens.

D. Identify important targets based on associations of gene expression with poor cancer recurrence-free outcome in neoadjuvant treated patients.

SPECIFIC AIM THREE

To identify and develop a novel pharmacologic approach for targeting taxane-platin drug resistant NSCLCs.

A. Test pharmacological inhibitors of identified gene target for their ability to selectively kill taxane-platin resistant cells over parental, chemo-sensitive cells.

B. Validate selectivity and enhanced drug sensitivity in taxane-platin resistant xenografts by *in vivo* treatment of tumor-bearing mice with these inhibitors.

C. Investigate the benefit of combining these pharmacologic inhibitors with standard paclitaxel + carboplatin chemotherapy, for targeting chemo-resistant NSCLC cells and for possibly preventing the emergence of drug resistant clones from parental cell population.

CHAPTER TWO

MATERIALS AND METHODS

2.1 Materials

2.1.1 Lung Cancer Cell Lines

Non-Small Cell Lung Cancer (NSCLC) cell lines were obtained from the National Cancer Institute (NCI) or the UT Southwestern Hamon Cancer Center (HCC) collection established by the laboratories of Drs. John D. Minna and Adi F. Gazdar. Cells were cultured in RPMI-1640 media (Life Technologies, Inc.) supplemented with 5% Fetal Bovine Serum (FBS). Cells were grown in humidified incubators with 5% CO_2 at 37°C. All cell lines were fingerprinted using a PowerPlex 1.2 kit (Promega, Madison, WI) to confirm the cell line identity. Cells were regularly tested for mycoplasma contamination using the e-Myco kit (Boca Scientific). Clinical annotations and driver oncogenotypes of NSCLC cell lines used in this study are listed in Table 2.1 and Table 2.2, respectively.

Table 2.1 Clinical Annotations of NSCLC Cell Lines

Cell Line	NSCLC Subtype	Stage	Age	Race	Gender	Smoking Pack Years (PY)
NCI-H1299	Large Cell Carcinoma	IIIA	43	Caucasian	M	50
NCI-H1355	Adenocarcinoma	IV	53	Caucasian	M	100
NCI-H1693 [a]	Adenocarcinoma	IIIB	55	Caucasian	F	80
NCI-H1819 [a]	Adenocarcinoma	IIIB	55	Caucasian	F	80
HCC4017	Large Cell Carcinoma	IA	62	Caucasian	F	Ex-smoker (76 PY)

[a] Matched cell line pair derived from the same NSCLC patient before/after chemotherapy (after etoposide + cisplatin treatment)

Table 2.2 Driver Oncogenotypes of NSCLC Cell Lines

Cell Line	TP53	KRAS	NRAS	LKB1	EGFR
NCI-H1299	Homozygous deletion	WT	Mutant	WT	WT
NCI-H1355	Mutant	Mutant	WT	Mutant	WT
NCI-H1693	Mutant	WT	WT	WT	WT
NCI-H1819	Mutant	WT	WT	WT	WT
HCC4017	Mutant	Mutant	WT	WT	WT

WT, Wild-type

2.1.2 Chemotherapeutic Drugs

Paclitaxel (Bedford Labs/Hikma Pharmaceuticals and also from Hospira, Lake Forest, IL), carboplatin (Sandoz Inc., Princeton, NJ and from Sagent Pharmaceuticals, Schaumburg, IL), cisplatin (APP Pharmaceuticals, Schaumburg, IL), doxorubicin (Teva Parenteral, Irvine, CA), vinorelbine (Pierre Fabre Company, Castres, France), gemcitabine (Eli Lilly and Company, Indianapolis, IN), pemetrexed (Eli Lilly and Company, Indianapolis, IN) and irinotecan hydrochloride (Sandoz Inc., Princeton, NJ) were purchased at the University of Texas Southwestern Medical Center Campus Pharmacy. Paclitaxel, carboplatin, cisplatin and irinotecan were stored as received at room temperature. Pemetrexed and gemcitabine were dissolved in 0.9% saline. Doxorubicin and vinorelbine were stored as received at 4°C. Verapamil (Sigma-Aldrich) was also stored at 4°C. Docetaxel (LC Laboratories, Woburn, MA), fludarabine (Selleck Chemicals, Houston, TX), PGP-4008 (Santa Cruz Biotechnology), depsipeptide/ romidepsin (ApexBio, Houston, TX), trichostatin A (Sigma-Aldrich, St. Louis, MO), GSK126 (Xcess Biosciences, San Diego, CA) and JIB-04 (Synthetic chemistry core at UT Southwestern) were stored at -20°C. PRT4165, tamoxifen citrate, NU9056, PFI3, SGC-CBP30, GSK-J5 and GSK-J4 were from Tocris Bioscience (Bristol, UK) and stored at -20°C.

2.1.3 Resected Patient Lung Tumor Samples

NSCLC patient tumor dataset was obtained from the Lung Cancer Specialized Program of Research Excellence (SPORE) Tissue Bank at The University of Texas M. D. Anderson Cancer Center (MDACC, Houston, TX), which was approved by an institutional review board. This consisted of 275 lung tumors, 66 of which were treated with neoadjuvant chemotherapy prior to surgical resection while the other 209 tumors were chemo-naïve at the time of resection. The 66 neoadjuvant treated tumors were treated with platin-based doublet chemotherapy, primarily taxane + platin combination, such as paclitaxel + carboplatin or docetaxel + cisplatin. Tumor dataset had detailed histopathological and clinical annotation including patient demographics, smoking history, tumor pathology and stage, adjuvant chemotherapy, overall survival, tumor recurrence status and cancer-free survival time. Among the neoadjuvant treated patient tumors, cancer-free survival time was unavailable for 1 of the 66 tumors. Hence clustering and survival analyses were done on 65 neoadjuvant tumors. Frozen tumor samples from the time of resection were used for Illumina gene expression profiling and formalin-fixed, paraffin-embedded tissues were used for tissue microarrays (TMA). Clinical annotations of NSCLC patient tumor dataset have been summarized in Table 2.3.

Table 2.3 Clinical Annotations for NSCLC Patient Tumor Dataset

	Chemo-treated [a] (before surgical resection; neoadjuvant)	**Chemo-naïve** (at the time of surgical resection)
Total	66	209
Platin + Taxane doublet [b]	56	-
Other platin-based doublets [c]	10	-
Diagnosis		
Adenocarcinoma	31	152
Squamous cell carcinoma	23	57
Other	12	0
Gender		
Males	36	112
Females	30	97
Stage		
I	18	115
II	15	35
III	28	58
IV	5	1
Smoking history		
Yes	58	186
No	8	20
Unknown	0	3
Race		
Caucasian	59	185
African American/ Asian/ Hispanic	7	24

[a] Cancer-free survival data was available for 65 out of 66 patients.

[b] Carboplatin + Paclitaxel (N=25), Cisplatin + Docetaxel (N=24), Carboplatin + Docetaxel (N=7)

[c] Carboplatin or Cisplatin with Etoposide/ Gemcitabine/ Pemetrexed/ Navelbine

2.1.4 NSCLC Tissue Microarray

Formalin-fixed, paraffin-embedded (FFPE) tissues from surgically resected lung cancer specimens were used to construct NSCLC tissue microarray #3 (TMA3) for immunohistochemistry (IHC). TMAs were constructed using triplicate 1-mm diameter cores per tumor; each core included central, intermediate, and peripheral tumor tissue. TMA3 consisted of 218 out of total 275 MDACC-SPORE tumor specimens, consisting of both neoadjuvant treated and chemo-naïve tumors. Cores were available from only 36 neoadjuvant treated tumors, majority of which were treated with taxane-platin combination (N = 30).

2.2 Methods

2.2.1 Long-term Drug Treatment

Non-small cell lung cancer (NSCLC) cell lines that were previously determined to be sensitive to paclitaxel + carboplatin standard chemotherapy were selected for generation of resistant variants. NCI-H1299, NCI-H1355, HCC4017, NCI-H1693 and NCI-H1819 were among a group of NSCLC cell lines that were 100-500 fold more sensitive (had lower IC50 values) in 5 day MTS assays, than the most resistant NSCLC lines, and were thus selected as "parental" cells to develop drug resistant variants. Cells were treated long-term for several months with paclitaxel + carboplatin combination given in a clinically relevant 2:3 ratio. Drug exposure was done in cycles with a drug ON/ drug OFF treatment scheme. At the start of treatment, cell lines were treated for 4-5 days (drug ON) with IC_{50} doses determined in MTS assays. Surviving cells were cultured drug-free (drug OFF) until they repopulated the plate before next treatment cycle. Drug dose was increased with each consecutive treatment cycle. Untreated parental cells were simultaneously maintained under similar culture conditions at all times for comparison with drug treated cells. Figure 2.1 describes the approach used for long-term drug treatment. Drug treated cells were characterized intermittently at different treatment cycles, with T[n] indicating cell line variant developed after 'n' cycles of doublet therapy. NCI-H1299 variant series consisted of Parental, T5, T10, T15 and T18, and NCI-H1355 isogenic cell line series comprised of Parental, T4, T8, T13 and T16 resistant variants. A schematic describing the establishment of H1299 and H1355 chemoresistant variants can be found in Figure 2.2. Table 2.4 lists all the resistant NSCLC cell lines that I have developed so far.

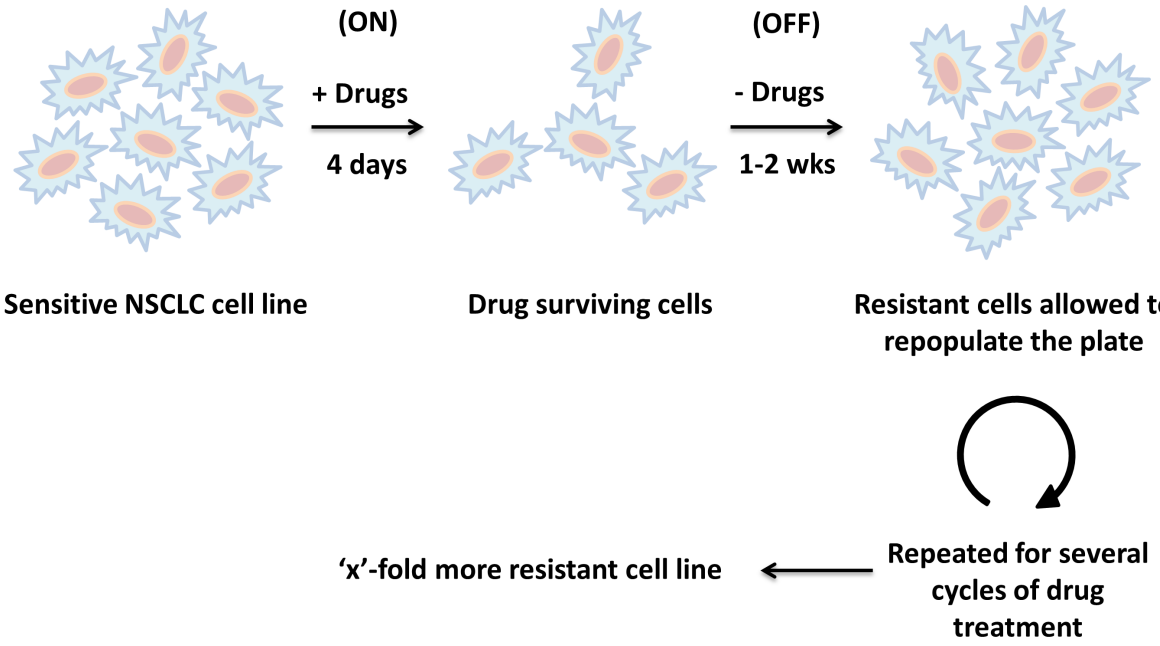

Figure 2.1 Dosing Strategy for Development of Drug Resistant Cell Lines
NSCLC cell lines that were pre-determined to be sensitive to paclitaxel + carboplatin standard doublet were selected for generation of resistant variants. Cells were treated long-term with cycles of doublet chemotherapy (drug on/drug off); such that drug treatment was given for 4 days and then surviving cells were cultured drug-free to allow them to repopulate the plate. First treatment cycle was started with IC_{50} drug dose, and chemotherapy doses were gradually incremented with increasing treatment cycles. Cells were intermittently tested for their drug response and development of resistance.

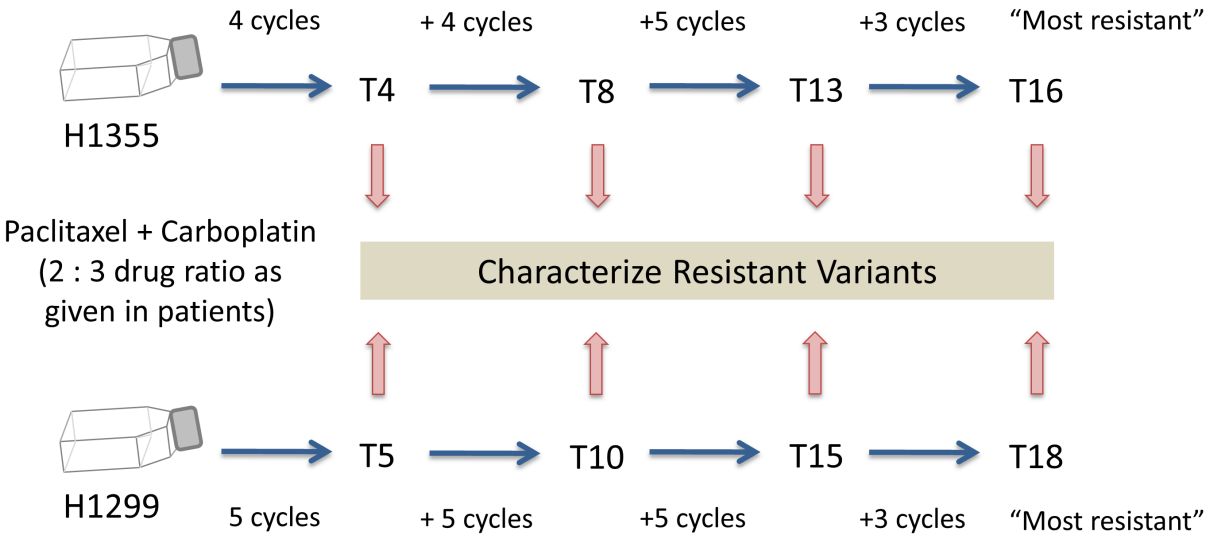

Figure 2.2 Establishment of Taxane-Platin Resistant H1355 and H1299 Cell Line Series
Taxane-platin sensitive NSCLC cell lines, NCI-H1355 and NCI-H1299, were treated long-term with increasing doses of paclitaxel + carboplatin doublet chemotherapy, given in clinically relevant 2: 3 ratio. Treatment was given in cycles (drug on/drug off). Isogenic series of cell lines were generated and resistant variants were designated with T[n] where n denotes number of treatment cycles. H1355 T16 and H1299 T18 were the most resistant time-points established. Intermediate time-points were also characterized for their drug response phenotypes.

Table 2.4 List of Taxane-platin Resistant Cell Line Variants Generated

NSCLC Cell Lines	Drugs	Length of selection	Fold Resistance
NCI-H1355	Paclitaxel + Carboplatin (2 : 3)	16 cycles	67
NCI-H1299	Paclitaxel + Carboplatin (2 : 3)	18 cycles	53
HCC4017	Paclitaxel + Carboplatin (2 : 3)	5 cycles	7
NCI-H1693	Paclitaxel + Carboplatin (2 : 3)	7 cycles	2
NCI-H1819	Paclitaxel + Carboplatin (2 : 3)	5 cycles	3
NCI-H1355	Docetaxel + Cisplatin (1 : 1)	3 cycles	8
NCI-H1299	Docetaxel + Cisplatin (1 : 1)	5 cycles	9
NCI-H1355	Pac + Carb (2 : 3) + Verapamil (5 μM)	6 cycles	178
NCI-H1355	Pac + Carb (2 : 3) without Verapamil	6 cycles	43
NCI-H1299	Pac + Carb (2 : 3) + Verapamil (5 μM)	7 cycles	12
NCI-H1299	Pac + Carb (2 : 3) without Verapamil	8 cycles	10

2.2.2 Cell Viability Assays

Cell viability was assessed by standard MTS assays using Promega's CellTiter reagents. For generating dose response curves, 1000 to 2000 cells were plated per well of a 96-well plate, depending on the cell line. Drugs were added the next day and cells were allowed to incubate for 4 days before measuring cell viability. 8 serial drug concentrations given as two- or four-fold dilutions were tested for each chemotherapeutic agent. Media-only wells and cells-only wells (no drug) were used as controls. Each experiment contained 8 replicates per concentration and the entire plate assay was repeated multiple times ($n \geq 3$). Cell viability was determined with MTS reagent (Promega, Madison, WI, final concentration 333 μg/ml), incubating for 1 to 4 hours at 37°C, and absorbance was read at 490 nm on a plate reader (Spectra Max 190, Molecular Devices, Downington, PA).

2.2.3 Colony Formation Assays

Cells were counted using a Beckman Coulter Z2 Particle Count and Size Analyzer, and plated at a density of 400 cells per well of a 6-well plate. Cells were treated the next day with serial dilutions of chemotherapeutic drug. Plates were kept in the cell culture incubator until termination of assay. After 2-3 weeks, colonies were stained with crystal violet staining solution (0.5% crystal violet, 3% formaldehyde solution), rinsed in water and imaged. Colonies were counted both manually and automatically using Quantity One image analysis software (Bio-Rad). For drug combination studies, "delta Bliss excess" was calculated as shown previously (Wilson et al., 2014). Bliss expectation was calculated as $A + B - (A \times B)$, where A and B denote fractional responses from drugs A and B given individually. The

difference between Bliss expectation and observed response from combination of drugs A and B at the same doses is the delta Bliss excess.

For testing emergence of drug resistant clones, 10,000-20,000 cells were plated per well of a 6-well plate on day 0. Cells were allowed to attach and drug treatment was given the next day. Plates were incubated for 2-3 weeks, following which they were stained with crystal violet staining solution (0.5% crystal violet, 3% formaldehyde solution), rinsed in water and imaged. Serial dilutions of chemotherapeutic drugs were tested, with duplicate wells per drug dose.

2.2.4 Cell Growth Assays

Parental or resistant cells were counted and 100,000 cells were plated on day 0 in 60 mm tissue culture treated plates. Cell counts were taken in duplicates on days 2, 3, 4 and 5. Assay was repeated to obtain biological replicates.

2.2.5 Xenograft Studies and *In Vivo* Drug Response

For tumor growth rate studies and docetaxel + cisplatin drug response comparisons, 6-8 week old female NOD/SCID mice (UTSW breeding core) were used. For all subsequent *in vivo* drug response studies, 6 week old female athymic nude mice were used (Charles River Labs or Jackson Labs). Animals were housed under standard, sterile conditions at UTSW animal facility. All experiments were carried out under approved IACUC protocols and followed UTSW animal care procedures. Cell lines were trypsinized, washed and counted

using Beckman Coulter counter. Cell viability was assessed using trypan blue to ensure >95% viability prior to injections. For studies with NCI-H1299 cell line, injections were done with 1 million cells suspended in PBS or RPMI whereas for NCI-H1355 and HCC4017 cell lines, 5 million cells were injected in PBS or matrigel. Injections were performed subcutaneously into the right flanks of mice. Tumor growth was monitored by caliper measurements and tumor volume was calculated using the equation shown below.

$$V = (l * w^2) * 0.5$$

Drug treatments were started when tumors reached ~150-200 mm^3. Chemotherapy or vehicle injections were given to tumor volume-matched pairs. Docetaxel (3 mg/kg, dissolved in DMSO, ethanol mix and diluted in saline) and cisplatin (3 mg/kg in saline) were given i.p. once a week for 3 weeks. Control mice received the injections of the appropriate vehicle. For GSK-J4 studies, mice were given 100 mg/kg GSK-J4, every day, for 10 consecutive days or DMSO vehicle control, as per a previously published study (Hashizume et al., 2014). For JIB-04 studies, nude mice were randomized to receive either of 5, 20 or 50 mg/kg drug doses or vehicle, 3x per week for 2 weeks by gavage in 12.5% cremophor EL, 12.5% DMSO, aqueous suspension. At sacrifice, tumors were harvested, weighed and portions were snap-frozen in liquid nitrogen or fixed in formalin. A schematic describing the xenograft experiments can be found in Figure 2.3.

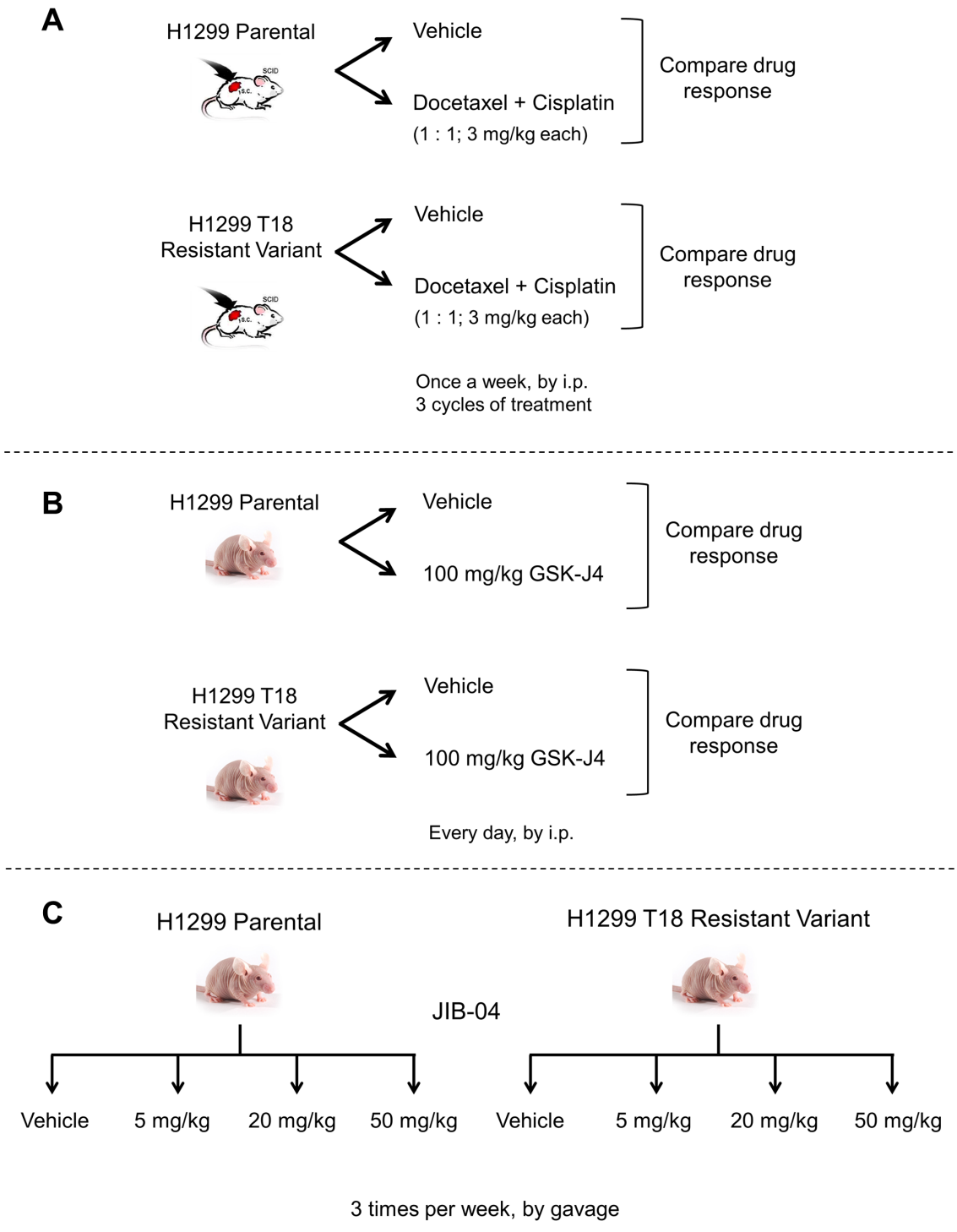

Figure 2.3 Schematic of Xenograft Experiments
(A) Docetaxel + Cisplatin, (B) GSK-J4, and (C) JIB-04 *in vivo* treatment. See text for details.

2.2.6 Flow Cytometry

Parental and resistant lung cancer cell line variants were analyzed for MDR1/Pgp and EpCAM expression by flow cytometry. MDR1 was detected using FITC mouse anti-human P-glycoprotein antibody (BD Biosciences, Catalog no. 557002). FITC Mouse IgG_{2b},κ (Catalog no. 556655) was used for isotype control. APC-conjugated antibody was used for EpCAM detection (Catalog No. 347200) along with a mouse IgG_1-APC isotype control.

Briefly, cells were detached and disaggregated using 0.05% Trypsin-EDTA (Gibco) and resuspended in HBSS+ (HBSS containing 2% FBS and 10 μM HEPES) at a concentration of 1 million cells per ml. Cells were incubated with antibody at 4°C for 30 min in dark. Cells were then washed and resuspended in fresh HBSS+ and stained with Propidium Iodide (PI) to account for non-viable cells. Flow cytometry was performed on a FACScan (Becton-Dickinson) or FACSCalibur flow cytometer (BD Biosciences) and data was analyzed using FlowJo software (Treestar).

For cell cycle analysis, cells were fixed in cold 70% EtOH, overnight at -20°C. Cells were then incubated at 37°C for 30 min in staining buffer (50 μg/ml Propidium Iodide, 50 μg/ml RNAse A, 0.05% Triton X-100, PBS). Cell cycle profiling was performed on FACScan (Becton-Dickinson) and analyzed using manual gating as well as Dean-Jett-Fox algorithm provided by the FlowJo software.

2.2.7 Immunoblotting

Cell lysates were made using RIPA lysis buffer supplemented with protease and phosphatase inhibitors. Protein content was quantified using the BioRad Protein Assay Dye Reagent Concentrate (BioRad, Hercules, CA). Lysates were diluted into loading buffer and samples were boiled for 5 minutes before loading onto a 10% Mini-PROTEAN® TGX™ precast gel (BioRad). Cellular proteins were separated by SDS-polyacrylamide gel electrophoresis and electrotransferred onto nitrocellulose membranes (Millipore, Billerica, MA). The membrane was blocked for 1 hour at room temperature (RT) in 5% milk in TBST solution, then incubated with a rabbit anti-MDR1 primary antibody overnight at 4°C, followed by incubation with a horseradish peroxidase-conjugated secondary antibody (Cell Signaling, Danvers, MA) for 1 hr at RT. HSP90 primary antibody (Santa Cruz sc-13119) was used for control. Proteins were detected by enhanced chemiluminescence (Thermo Scientific, Waltham, MA).

2.2.8 Radioactive Drug Accumulation Assay

50,000 cells were plated per well of a 12-well plate. Cells were exposed to [^{3}H]-docetaxel for different time-points (0, 4, 8 and 25 hours). Protein lysates were collected and quantified using BCA reagent. Samples were scintillated with EcolumeTM liquid scintillation cocktail. Three biological replicates were performed per cell line. Drug accumulation was calculated as CPM/ mg protein. Reagents were kindly provided by the DeBerardinis laboratory at UT Southwestern.

2.2.9 siRNA transfection

ABCB1 knockdown was achieved using three individual ABCB1 siRNAs (Qiagen) and Lipofectamine RNAiMax (Invitrogen) using standard reverse transfection protocols. Scrambled siRNA (Dharmacon) and toxic PLK1 siRNA (Sigma) were used as controls. Lipid-only controls (no siRNA) were also used for all assays. Transfections for drug response assays were performed at 20 nM final siRNA concentration in 96-well plates. All siRNAs were diluted in serum-free RPMI so as to add 20 µl volumes to appropriate wells of 96-well plates using a multi-channel pipette. RNAiMAX transfection reagent was diluted in serum-free RPMI and incubated at room temperature (RT) for 10 minutes to allow lipid complexes to form. 0.2 µl of transfection reagent in 15 µl media was used per well. Lipid and siRNA were allowed to incubate for 20 min at RT before adding cells. Cell suspension was prepared in RPMI + 10 % FBS (R10) to allow a final media constitution of RMPI + 5% FBS (R5) at the end of the assay. 2000 cells in 50 µl R10 were added per well of the 96-well plate. Final volume per well was brought up to 100 µl using RPMI. Drug treatments were performed the next day by adding 2X drug concentration in 100 µl R5 to bring the final volume to 200 µl. 8 serial drug concentrations given as four-fold dilutions were tested. Assays were terminated after 4 days of drug exposure and cell viability was determined using standard MTS reagents.

For 6-well plate transfections, 9 µl of RNAiMAX was diluted in 150 µl Opti-MEM. 3 µl of 10 µM stock siRNA was diluted in 150 µl Opti-MEM (30 pmol siRNA per well). Diluted siRNA was added to diluted RNAiMAX and incubated for 20 min. 1 x 10^6 cells

were added per well of the plate. Cells were incubated for 24 or 48 hours before harvesting. Silencing efficiency was detected using real-time PCR.

2.2.10 Gene Expression Arrays

Total RNA was extracted using QIAcube automated system and RNeasy Plus Mini kit (Qiagen, Valencia, CA). RNA quality was tested by automated electrophoresis on the Experion System (Bio-Rad). Total RNA was labeled, amplified and hybridized by the UTSW Simmons Comprehensive Cancer Center Genomics Core. Gene expression profiling was performed using Illumina HumanWG-6 V3 BeadArrays (for patient tumor samples) or Illumina HumanHT-12 V4 BeadArrays (for cell lines and xenografts). Cell line and xenograft microarrays included biological replicates (Cell lines: 5 for parental, 3 for most resistant variant, 2 for each intermediate resistance time-point; Xenografts: 3 tumors per group). Data were pre-processed using the R package mbcb for background correction (Ding et al., 2008), then log-transformed and quantile-normalized with the R package preprocessCore or using in-house MATRIX software (MicroArray TRansformation In eXcel) developed by Dr. Luc Girard in Minna lab. Genes with multiple probes were aggregated by mean.

2.2.11 Microarray Data Analysis

Log ratios, unpaired t-test p values and color-coded heat maps were obtained using in-house MATRIX software. For analyses involving multiple time-points or resistant series, analyses were performed using R package as following: Linear Regression model was fitted

on gene expression data of progressively resistant cell line series using the log transformed IC_{50} values as measures of drug response. We fitted Beta-uniform mixture model to a set of p-values using the R package ClassComparison. Genes with p-values below the FDR cutoff of 0.1 were considered statistically significant. For xenograft microarray data, differential gene expression analysis was performed by student's t-test.

Gene lists obtained from cell lines and xenografts were compared to determine overlap. Significance of overlap was determined by hypergeometric test. Overlapping genes were then represented in a color-coded heat map using MATRIX. In cases where multiple probes mapped to the same gene, we represented the best probe with largest fold changes between the parental and most resistant cell line. Using overlapping gene set (35 genes), we performed unsupervised hierarchical clustering (Eisen et al., 1998) of MDACC patients who had received neoadjuvant chemotherapy (mainly platin + taxane). The clustering was based on Euclidean distance matrix and maximum linkage method. This separated the patients into two groups which were then tested for differences in recurrence-free prognosis using Kaplan-Meier survival analysis. KM curve and multivariate cox regression analysis were performed by R survival package. Further details are provided in the SWEAVE documentation provided in Appendix A. All other single gene based KM survival plots were generated using MATRIX.

2.2.12 Quantitative RT-PCR

Total RNA was isolated using RNeasy Plus Mini kit (Qiagen, Valencia, CA) and cDNA was generated using iScript cDNA synthesis kit (BioRad, Hercules, CA). For epigenetic enzymes, transcripts were detected by SYBR Green chemistry in real time quantitative PCR assays using validated primers. TBP and GAPDH were used as endogenous controls. For H1299 T18, cyclophilin B was used since TBP and GAPDH showed DNA amplification and increased mRNA expression. For all other non-epigenetic transcripts, TaqMan probes (Life Technologies) were utilized in multiplex with GAPDH internal reference gene. Additionally, a reference sample containing pooled RNA from normal human and tumor tissues (Stratagene) was used. PCR reactions were run in triplicates using the ABI 7300 Real-time PCR System and analyzed with the included software (Applied Biosystems, Foster City, CA). The comparative C_T method was used to compute relative mRNA expression.

Table 2.5 qRT-PCR Probes used in TaqMan Assays

Gene	Probe ID	RefSeq #
ABCB1	Hs00184500_m1	NM_000927.4
ADAM22	Hs00244640_m1	NM_004194.3, NM_016351.4, NM_021721.3, NM_021722.4, NM_021723.3
DTX3	Hs01595350_m1	NM_178502.2
FUT4	Hs01106466_s1	NM_002033.3
GALNT13	Hs00287613_m1	NM_052917.2
HBE1	Hs00362216_m1	NM_005330.3
HEY2	Hs00232622_m1	NM_012259.2
JAG1	Hs00164982_m1	NM_000214.2
JAG2	Hs00171432_m1	NM_002226
KDM3B	Hs00213240_m1	NM_016604.3
MLL5	Hs01096121_m1	NM_018682.3, NM_182931.2
NAP1L3	Hs02915131_s1	NM_004538.5
NTN1	Hs00924151_m1	NM_004822.2
NXF2/ NXF2B	Hs00903817_mH	NM_022053.3, NM_001099686.2
PPARGC1B	Hs00991677_m1	NM_001172698.1, NM_001172699.1, NM_133263.3
PSMB9	Hs00160610_m1	NM_002800.4
STX11	Hs01891623_s1	NM_003764.3
TAP1	Hs00388675_m1	NM_000593.5

Table 2.6 qRT-PCR Primers used in SYBR Green Assays

Gene	Forward (QF)/ Reverse (QR) Primers	Sequence	RefSeq #
KDM1A	hAOF2-QF1	CTAATGCCACACCTCTCTCAACTC	NM_015013.2
	hAOF2-QR1	CTAATGCCACACCTCTCTCAACTC	NM_015013.2
KDM2A	hFBXL11-QF1	TCCACCGGCTGATAAACCA	NM_012308.1
	hFBXL11-QR1	AGCCGGAAGTCGGTCATGT	NM_012308.1
KDM2B	hFBXL10-QF1	GCGCTCCCACCTCACTCA	NM_001005366.1
	hFBXL10-QR1	CCGAAGAGAAGCCGTCTATGC	NM_001005366.1
KDM3A	hJMJD1A-QF1	GTGGTTTTCAGCAACCGTTATAAA	NM_018433.4
	hJMJD1A-QR1	CAGTGACGGATCAACAATTTTCA	NM_018433.4
KDM3B	hJMJD1B-QF1	TGCCCTTGTATCAGTCGACAGA	NM_016604.3
	hJMJD1B-QR1	GCACTAGGGTTTATGCTAGGAAGCT	NM_016604.3
KDM3C	hJMJD1C-QF1	TCTTCACCCGCACCATGAT	NM_004241.2
	hJMJD1C-QR1	AGACCTGCGTCGTGATGTAATG	NM_004241.2
KDM4A	hJMJD2A-QF1	TGCAGATGTGAATGGTACCCTCTA	NM_014663.2
	hJMJD2A-QR1	CACCAAGTCCAGGATTGTTCTCA	NM_014663.2
KDM4B	hJMJD2B-QF1	GGCCTCTTCACGCAGTACAATAT	NM_015015.2
	hJMJD2B-QR1	CCAGTATTTGCGTTCAAGGTCAT	NM_015015.2
KDM4C	hJMDJ2C-QF1	GAATGCTGTCTCTGCAATTTGAGA	NM_015061.2
	hJMJD2C-QR1	CAACGGCGCACATGACAT	NM_015061.2

KDM4D	hJMJD2D-QF1	CTGGGTGTATCCTCTGCATATAGAAC	NM_018039.2
	hJMJD2D-QR1	GCAGAGAATGTCCTCAGTGTTTAGAA	NM_018039.2
KDM5A	hJARID1A-QF1	TGTGTTGAGCCAGCGTATGG	NM_005056.2
	hJARID1A-QR1	CCACCCGGTTAAAAGCAGACT	NM_005056.2
KDM5B	hJARID1B-QF1	TCCATCAGCTTGTGACCATCAT	NM_006618.3
	hJARID1B-QR1	GTGGTAGGCTCTTGGAAATGTAATC	NM_006618.3
KDM5C	hKDM5C-QF2	GCCGGCAGTACCTGCG	NM_004187.3
	hKDM5C-QR2	GCAGCATGGCAGGAAGCT	NM_004187.3
	hKDM5C-QF3	GAGGAGGGCTCAGGTAAGAGAGA	NM_004187.3
	hKDM5C-QR3	TGGCAACAGCGAGGACAG	NM_004187.3
KDM5D	hSMCY-QF1	CAACCATGCAACTTCGAAAGAA	NM_001653.3
	hSMCY-QR1	CCCCACGGGAGCATACTTG	NM_001653.3
KDM6A	hUTX-QF1	CACAGTACCAGGCCTCCTCATT	NM_021140.2
	hUTX-QR1	TCACTATCTGAGTGGTCTTTATGATGACT	NM_021140.2
KDM6B	hJMJD3-QF1	CGGAGACACGGGTGATGATT	NM_001080424.1
	hJMJD3-QR1	CAGTCCTTTCACAGCCAATTCC	NM_001080424.1
KDM7A	hJHDM1D-QF1	GTCCATGGGAAGAGGACATCTT	NM_030647.1
	hJHDM1D-QR1	GATCATTATCTTTCGCTCTCCATTC	NM_030647.1
JARID2	hJARID2-QF1	TGTTCACAACGGGCATGTTT	NM_004973.2
	hJARID2-QR1	TTGTGTTTTTGAACAGGTTCCTTCT	NM_004973.2

2.2.13 Gene Set Enrichment Analysis

Ranked lists of differentially expressed genes from microarray analyses were assessed by GSEAPreranked tool through the GSEA desktop application (http://www.broadinstitute.org/gsea/downloads.jsp). All gene sets available from the Molecular Signatures Database v5.0/ MSigDB (Subramanian et al., 2005) were interrogated. After filtering out genes that were not in the expression dataset, gene sets smaller than 15 genes or larger than 3000 genes were excluded from the analysis. GSEA was run using 1000 gene set permutations to generate False Discovery Rate (FDR). Default settings were used for normalizing the enrichment scores (NES).

2.2.14 Tissue Microarray and Immunohistochemistry

Formalin-fixed, paraffin-embedded (FFPE) tissues from surgically resected lung cancer specimens in NSCLC tissue microarray #3 (TMA3) were evaluated for KDM3B staining by immunohistochemistry (IHC). IHC was kindly performed by Dr. Wistuba's group at MD Anderson Cancer Center. Staining was done using a Leica Bond autostainer, with rabbit monoclonal antibody for KDM3B (Cell Signaling Technology, clone C6D12, cat #3100, dilution 1:80). A human colon adenocarcinoma specimen was used as positive control. Stained samples were assigned an expression score by the pathologist. Expression was quantified using a four-value intensity score (0, 1, 2, and 3) and the percent of IHC+ tumor cells (0-100%). Intensity scores were defined as follows: 0 = no appreciable staining; 1 = barely detectable staining; 2 = readily appreciable staining; and 3 = dark brown staining.

An expression score was obtained by multiplying the intensity and reactivity extension values (range 0 – 300).

2.2.15 Chromatin Immunoprecipitation and Sequencing (ChIP-Seq)

H1299 Parental and T18 cells at 80% confluency (~$1x10^7$) were cross-linked with 1% formaldehyde for 10 minutes at 37°C, and quenched with 125 mM glycine at room temperature for 5 minutes. The fixed cells were washed twice with cold PBS, scraped, and transferred into 5 ml PBS containing Mini EDTA-free protease inhibitors (Roche). After centrifugation at 700 g for 4 minutes at 4°C, the cell pellets were resuspended in 1.5 ml ChIP lysis buffer (1% SDS, 10 mM EDTA, 50 mM Tris-HCl [pH 8.1] with protease inhibitors) and sonicated at 4°C with a Bioruptor (Diagenode) (30 seconds ON and 30 seconds OFF at highest power for 2 x 15 minutes). The chromatin predominantly sheared to a fragment length of ~250 – 750 bp was centrifuged at 20,000 g for 15 minutes at 4°C. 100 µl of the supernatant was used for ChIP, and DNA purified from 30 µl of sheared chromatin was used as input. A 1:10 dilution of the solubilized chromatin in ChIP dilution buffer (0.01% SDS, 1.1% Triton X-100, 1.2 mM EDTA, 167 mM NaCl 16.7 mM Tris-HCl [pH 8.1]) was incubated at 4°C overnight with 10 µg of a mouse monoclonal anti-histone H3K27me3 antibody (Abcam, cat# ab6002) or a rabbit polyclonal anti-histone H3K4me3 antibody (Millipore, cat# 07-473). Immunoprecipitation was carried out by incubating with 40 µl pre-cleared Protein G Sepharose beads (Amersham Bioscience) for 1 hour at 4°C, followed by five washes for 10 minutes with 1ml of the following buffers: Buffer I: 0.1% SDS, 1% Triton X-100, 2 mM EDTA, 20 mM Tris-HCl [pH 8.1], 150 mM NaCl, protease

inhibitors; Buffer II: 0.1% SDS, 1% Triton X-100, 2 mM EDTA, 20 mM Tris-HCl [pH 8.1], 500 mM NaCl, protease inhibitors; Buffer III: 0.25 M LiCl, 1% NP-40, 1% deoxycholate, 1 mM EDTA, 10 mM Tris-HCl [pH 8.1]; twice with TE buffer [pH 8.0]. Elution from the beads was performed twice with 100 µl ChIP elution buffer (1% SDS, 0.1 M NaHCO3) at room temperature (RT) for 15 minutes. Protein-DNA complexes were de-crosslinked by heating at 65°C in 192 mM NaCl for 16 hours. DNA fragments from immunoprecipitated chromatin and input were purified using QiaQuick PCR Purification kit (QIAGEN) and eluted into 30 µl H2O according to the manufacturer's protocol after treatment with RNase A and Proteinase K.

For ChIP-Seq, barcoded libraries of ChIP and input DNA were generated with the TruSeq® ChIP Sample Preparation Kit (Illumina), and 50-nt single-end reads were generated with the HiSeq2000 system (Illumina). Sequence reads were aligned to the human reference genome (hg19) using Bowtie2 (v.2.2.5) (Langmead et al., 2009). Uniquely mapped reads with ≤2 mismatches to the reference sequence were retained for further analysis; for H1299 parental H3K27me3 and H1299 T18 H3K27me3 we obtained 26,100,406 and 29,586,658 reads, respectively and for H1299 parental input and H1299 T18 input we obtained 26,995,155 and 25,187,823 reads, respectively. ChIP-Seq enrichment plots were generated using ngs.plot tool (Shen et al., 2014). Aligned bam files are provided as input to Ngs.plot to calculate read count per million mapped reads over all the ENSEMBL annotated gene body regions in the human genome. For each ChIP-Seq sample, the average signal in -2kb with respect to transcription start site (TSS), gene body and 2kb downstream of transcription end site (TES) regions were subtracted from respective input sample signal and visualized in the enrichment plot.

2.2.16 RNA Sequencing (RNA-Seq)

H1299 Parental and T18 cells at 80% confluency were pelleted, snap-frozen and stored at -80^{0}C. Total RNA was extracted using RNeasy Plus Mini kit (Qiagen, Valencia, CA), with a gDNA eliminator step. RNA quality check was performed using the Agilent 2100 Bioanalyzer to ensure that only high quality RNA was used (RIN Score 8 or higher). The Qubit fluorometer (Invitrogen) was used to determine RNA concentration prior to library preparation with the TruSeq Stranded Total RNA LT Sample Prep Kit (Illumina). Samples were run on the Illumina HiSeq 2500, at the McDermott Sequencing Core at UT Southwestern. For RNA-Seq analysis, TopHat was used for transcript assembly, and the Cufflinks suite was used for differential expression calling and calculation of Fragments Per Kilobase of transcript per Million mapped reads (FPKM).

2.2.17 Statistical Methods

All statistical tests such as two-way ANOVA with Sidak's multiple comparisons test, one-way ANOVA with Dunnett's multiple comparison test, post-test for linear trend and unpaired t-tests were performed using GraphPad Prism version 6.00 (GraphPad Software, La Jolla, California USA). P values are represented as * $P < 0.05$, ** $P < 0.01$, *** $P < 0.001$ and **** $P < 0.0001$. For drug assays, dose response curves and IC_{50} values were calculated using GraphPad Prism as well as in-house DIVISA software (Database of In VItro Sensitivity Assays; Dr. Luc Girard, Minna lab).

CHAPTER THREE

TAXANE-PLATIN CHEMORESISTANT PRE-CLINICAL NON-SMALL CELL LUNG CANCER MODELS

3.1 Long-term paclitaxel + carboplatin treated NSCLC cell lines develop progressive increases in chemoresistance

To establish *in vitro* models of lung cancer chemoresistance, NSCLC cell lines were treated with paclitaxel + carboplatin standard doublet chemotherapy given in a clinically relevant 2:3 taxane to platin ratio. Over 100 NSCLC lines were previously screened in a 5 day MTS assay to identify *in vitro* drug response phenotypes to paclitaxel + carboplatin. NCI-H1299 and NCI-H1355 were among a group of NSCLC cell lines that were 100-500 fold more sensitive (had lower IC_{50} values) than the most resistant cell lines, and were thus selected for this study. Clinical annotations and driver oncogenotypes for these cell lines were listed in Tables 2.1 and 2.2. NCI-H1299 and NCI-H1355 cells were treated long-term for >6 months with increasing doses of paclitaxel + carboplatin doublet. Treatment was given in cycles of drug ON (4 days)/ drug OFF (1-2 weeks). Cells were characterized intermittently for their taxane-platin drug response phenotypes after different treatment cycles, with T[n] denoting cell line variant developed after 'n' cycles of doublet therapy. I thus developed H1299 variant series consisting of T5, T10, T15 and T18, and H1355 isogenic cell line series with T4, T8, T13 and T16 resistant variants. These long-term treated variants showed progressive increase in resistance to paclitaxel

+ carboplatin with increasing treatment cycles (Figure 3.1 A, C), reaching ~53-fold and ~79-fold increases in IC_{50} in H1299 T18 and H1355 T16, respectively (Figure 3.1 B, D). Drug resistance persisted in liquid colony formation assays involving continuous exposure over 2-3 weeks to paclitaxel + carboplatin combination treatment (Figure 3.1 E-H).

Figure 3.1

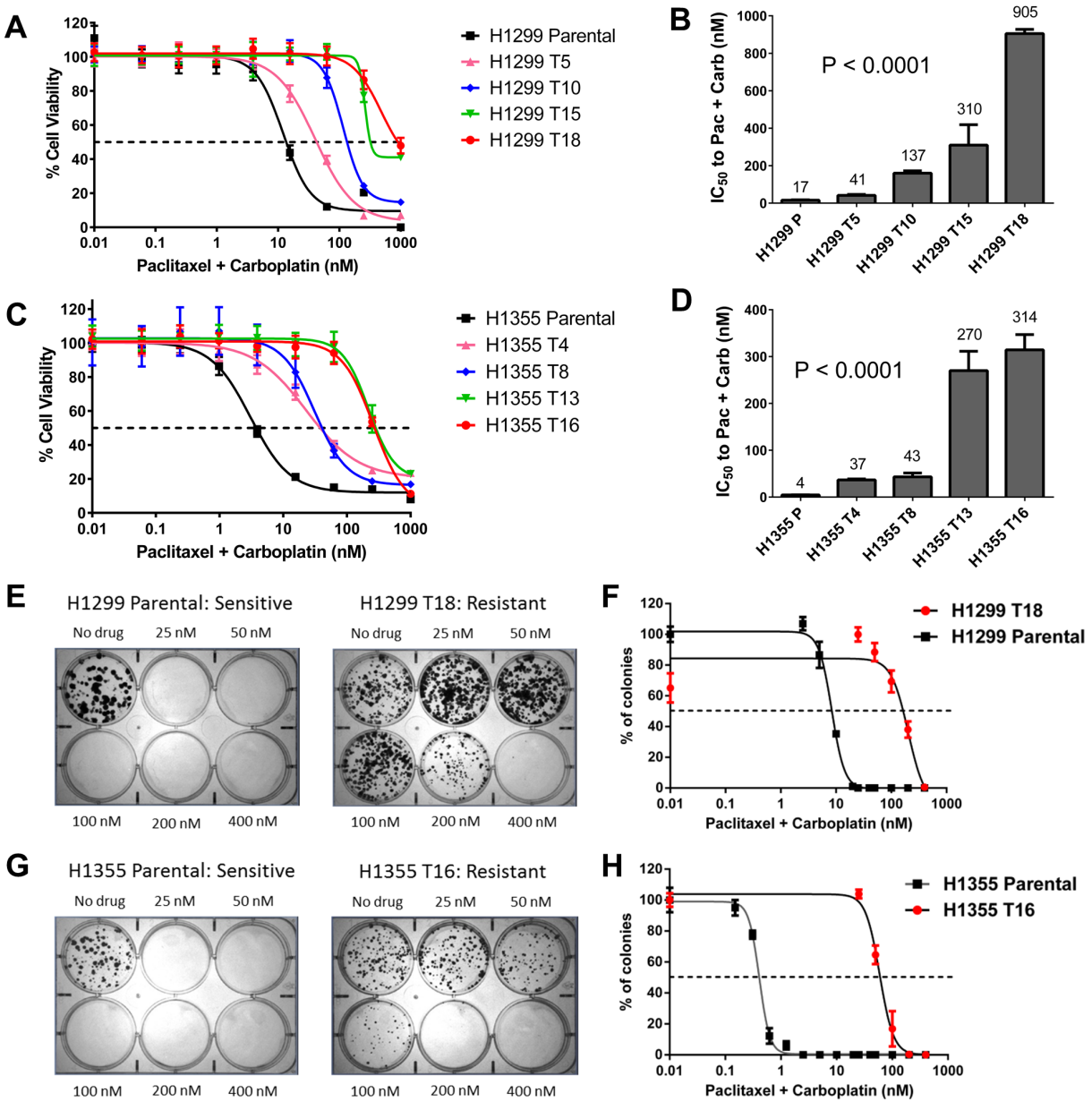
A
% Cell Viability
Paclitaxel + Carboplatin (nM)
H1299 Parental
H1299 T5
H1299 T10
H1299 T15
H1299 T18
B
IC50 to Pac + Carb (nM)
P < 0.0001
17
41
137
310
905
H1299 P
H1299 T5
H1299 T10
H1299 T15
H1299 T18
C
% Cell Viability
Paclitaxel + Carboplatin (nM)
H1355 Parental
H1355 T4
H1355 T8
H1355 T13
H1355 T16
D
IC50 to Pac + Carb (nM)
P < 0.0001
4
37
43
270
314
H1355 P
H1355 T4
H1355 T8
H1355 T13
H1355 T16
E
H1299 Parental: Sensitive
H1299 T18: Resistant
No drug
25 nM
50 nM
100 nM
200 nM
400 nM
F
% of colonies
Paclitaxel + Carboplatin (nM)
H1299 T18
H1299 Parental
G
H1355 Parental: Sensitive
H1355 T16: Resistant
No drug
25 nM
50 nM
100 nM
200 nM
400 nM
H
% of colonies
Paclitaxel + Carboplatin (nM)
H1355 Parental
H1355 T16

Figure 3.1 NSCLC cell line series develop progressively increasing resistance to paclitaxel + carboplatin standard chemotherapy.

(A, C) Dose response curves for NSCLC cell lines NCI-H1299 and NCI-H1355 cells that were treated long-term with drug on/drug off cycles of paclitaxel + carboplatin chemotherapy. P: Parental cell line, T[n]: resistant variant treated with 'n' cycles of doublet chemotherapy. Drugs were given in clinically relevant 2:3 ratio of paclitaxel: carboplatin. Values in dose response plots indicate paclitaxel concentration in the drug combination. Each assay was performed with 8 replicates per drug dose. Error bars represent mean ± SD.

(B, D) H1299 and H1355 treated cell lines showed a progressive increase in resistance to paclitaxel + carboplatin chemotherapy, reaching up to 53-fold and 79-fold increases in IC_{50} in H1299 T18 and H1355 T16 respectively. Each cell line variant had >4 assay replicates with 8 individual replicates within each assay. Data represents mean ± SD. P values are from post-test for linear trend following one-way ANOVA.

(E, G) Resistance was validated by liquid colony formation. Serial 2-fold drug dilutions from 400 nM were tested.

(F, H) Dose response curves were generated from colony formation assays. For plotting dose response of parental cell lines, additional plates were treated with lower doses of paclitaxel + carboplatin (serial 2-fold dilutions from 40 nM). Error bars represent mean ± SEM.

In all figure panels, drug values indicate concentration of paclitaxel in the 2:3 paclitaxel + carboplatin doublet.

3.2 Resistant variant shows decreased response to taxane-platin chemotherapy *in vivo*

To validate the taxane-platin resistance phenotype *in vivo*, I developed subcutaneous xenografts of H1299 Parental and H1299 T18 cells in *NOD*/*SCID* mice. Mice bearing 200 mm^3 tumors were treated with docetaxel (3 mg/kg) and cisplatin (3 mg/kg) in a 1:1 clinically relevant ratio. Doses were optimized based on previous toxicity studies and were determined to be maximum tolerated doses for the two drugs when used in combination. Treatment was administered by i.p. injections, given once a week for 3 weeks (i.e. 3 cycles of taxane + platin chemotherapy, denoted by C1, C2 and C3). While H1299 Parental xenografts treated with docetaxel + cisplatin therapy showed a dramatic reduction in tumor burden compared to the vehicle-treated group (two-way ANOVA, **P = 0.002), H1299 T18 tumors showed a non-significant response, confirming resistance (Figure 3.2).

Figure 3.2

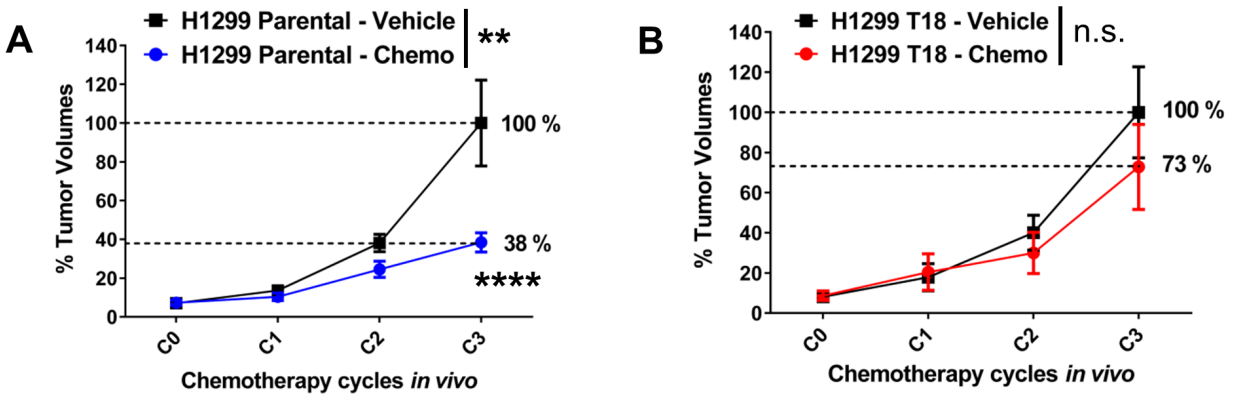

Figure 3.2 Paclitaxel + carboplatin resistant cell line variant shows reduced response to taxane-platin doublet chemotherapy *in vivo*

(A, B) H1299 Parental and H1299 T18 tumor bearing mice were randomized to receive either docetaxel + cisplatin doublet chemotherapy or vehicle. N = 8 mice per treatment group per cell line. Treatment was given once a week, for 3 weeks i.e. 3 cycles. Tumor volumes were measured after each treatment cycle (C1, C2, C3). Error bars represent mean $\pm$ SEM. Comparisons between vehicle and chemotherapy groups were done using two-way ANOVA followed by Sidak's multiple comparison tests: H1299 Parental xenografts, two-way ANOVA, **P = 0.002 and Sidak's test at C3, ****P < 0.0001; whereas H1299 T18 xenografts, two-way ANOVA P value not significant (n.s.).

3.3 Resistant cells express ABCB1/MDR1 transporter and exhibit multi-drug resistance

In vivo resistance studies confirmed my presumption that the H1299 T18 tumors were cross-resistant to docetaxel + cisplatin standard therapy (drugs that are functionally similar to paclitaxel + carboplatin). Consistent with previously published reports that suggested the involvement of MDR1 in taxane resistance (Lemontt et al., 1988; Roninson et al., 1986); I detected increased mRNA and protein expression of MDR1/Pgp/ABCB1 in both H1299 and H1355 resistant variants (Figure 3.3 A-D), and exome sequencing analysis (data not shown) revealed amplification of the MDR1 locus in H1299 T18 (but not H1355 T16). Hence, to characterize the multi-drug resistance phenotype, I tested several standard and targeted chemotherapeutic agents (Figures 3.4 and 3.5). H1299 and H1355 resistant variants were found to be cross-resistant to docetaxel, doxorubicin, vinorelbine and depsipeptide which are known MDR1 substrates (Figures 3.4 and 3.5). As expected, MDR1 expression in resistant variants corresponded with reduced intracellular docetaxel accumulation (Figure 3.6 A). However, *MDR1*/*ABCB1* siRNA knockdown in H1299 T18 cells only partially reversed taxane-platin resistance (Figure 3.6 B). Also, pharmacological inhibition of MDR transporter using verapamil or PGP4008 showed incomplete reversal of drug resistance (Figure 3.6 C, D), suggesting collateral non-MDR1 mediated resistance mechanisms. Further, long-term paclitaxel + carboplatin treatment of H1299 and H1355 parental cell lines, in the continuous presence of MDR inhibitor verapamil, was not sufficient to prevent cells from developing resistance (Figure 3.6 E, F).

Apart from MDR1 substrates, H1299 T18 and H1355 T16 resistant cell lines were both also cross-resistant to fludarabine (Figures 3.4 C and 3.5 C). Fludarabine, an antimetabolite

chemotherapeutic, is not reported to be transported by MDR1 and in fact, has been previously shown to be equally effective in non-MDR and MDR-expressing leukemia cells (Michelutti et al., 1997). Likewise, H1299 T18 cells were also cross-resistant to the nicotinamide phosphoribosyltransferase (NAMPT) targeted drug, FK866 (Figure 3.4 C). Resistance was seen only in H1299 T18 and not in H1355 T16 (Figure 3.5 C), although both variants express high levels of MDR1 (as shown previously in Figure 3.3). This suggested to me that this was a cell line-specific, MDR1-independent resistance mechanism in H1299 T18. Indeed, microarray analysis revealed that only H1299 T18 (but not H1355 T16) had increased mRNA expression of *NAMPT*, the target of FK866 (Figure 3.5 D).

Additionally, when I tested paclitaxel + carboplatin resistant variants of NCI-H1693 and HCC4017 cell lines, I found that both cell lines exhibited development of taxane-platin resistance (Figure 3.7 A-D), but HCC4017 T5 resistant variant did not show increased MDR1 mRNA or protein expression (Figure 3.7 F-H).

These findings led me to further investigate the non-MDR phenotypic and molecular changes in resistant variants.

Figure 3.3

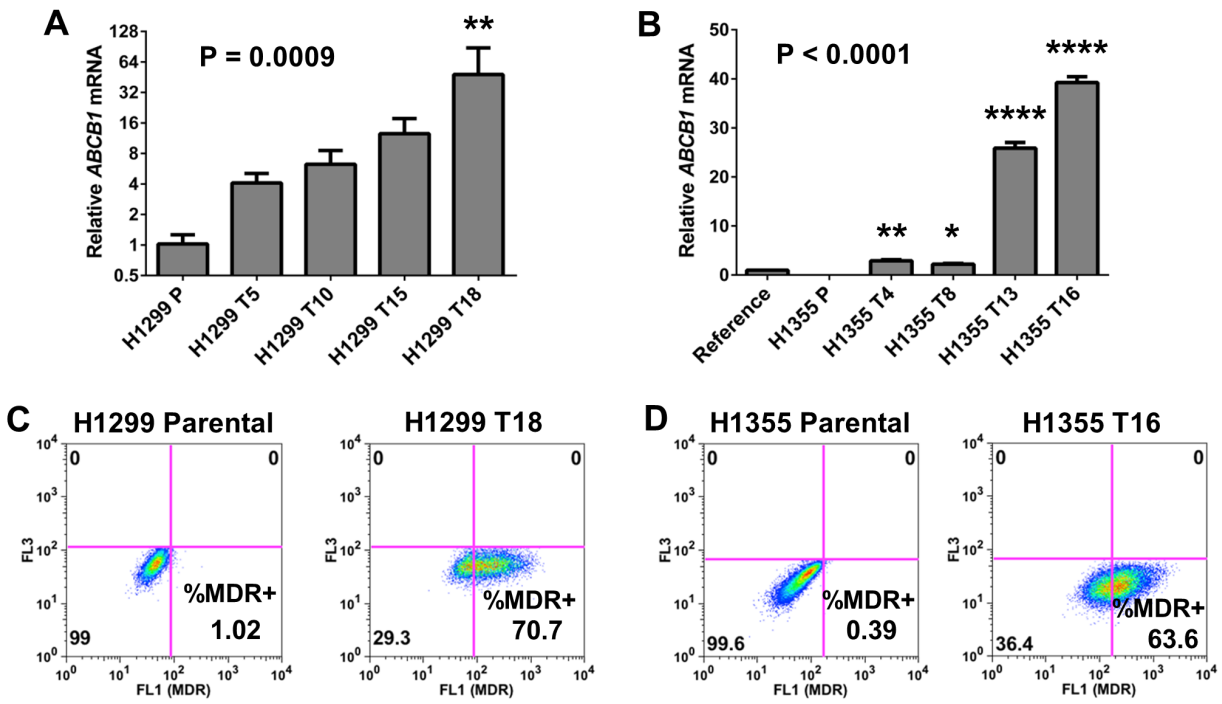

Figure 3.3 Chemoresistant cells express ABCB1/ MDR1 drug transporter
(A, B) H1299 and H1355 resistant cell line series showed increase in *ABCB1* mRNA transcripts with increasing treatment cycles. Data represents mean ± SD. Statistical significance was tested by one-way ANOVA, followed by Dunnett's multiple comparisons test of each resistant variant with the parental cell line (indicated by asterisks). P-values on graphs denote significance from post-test for linear trend.
(C, D) H1299 T18 and H1355 T16 showed enrichment in % MDR+ cells (detected by flow cytometry).

Figure 3.4

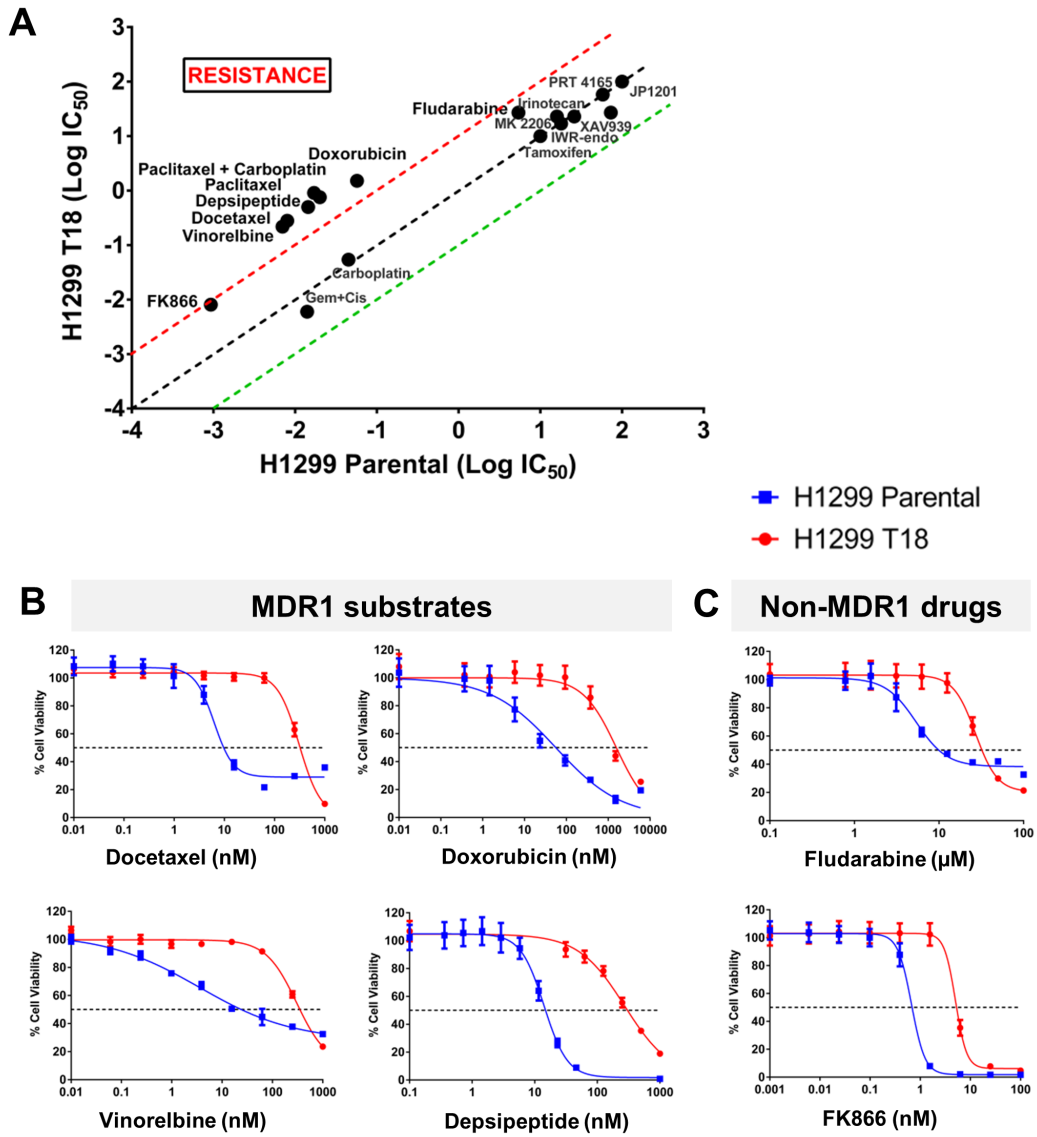

Figure 3.4 H1299 T18 cell line shows multi-drug resistance phenotype
(A) H1299 T18 resistant cells showed multi-drug resistance phenotype. Red and green dotted lines indicate 10-fold cut-offs for resistance and sensitivity respectively.
(B, C) Paclitaxel + carboplatin resistant cell line variant showed cross-resistance to substrates of MDR1 transporter (docetaxel, doxorubicin, vinorelbine, depsipeptide) as well as non-MDR1 drugs (fludarabine and FK866). Error bars represent mean ± SD.

Figure 3.5

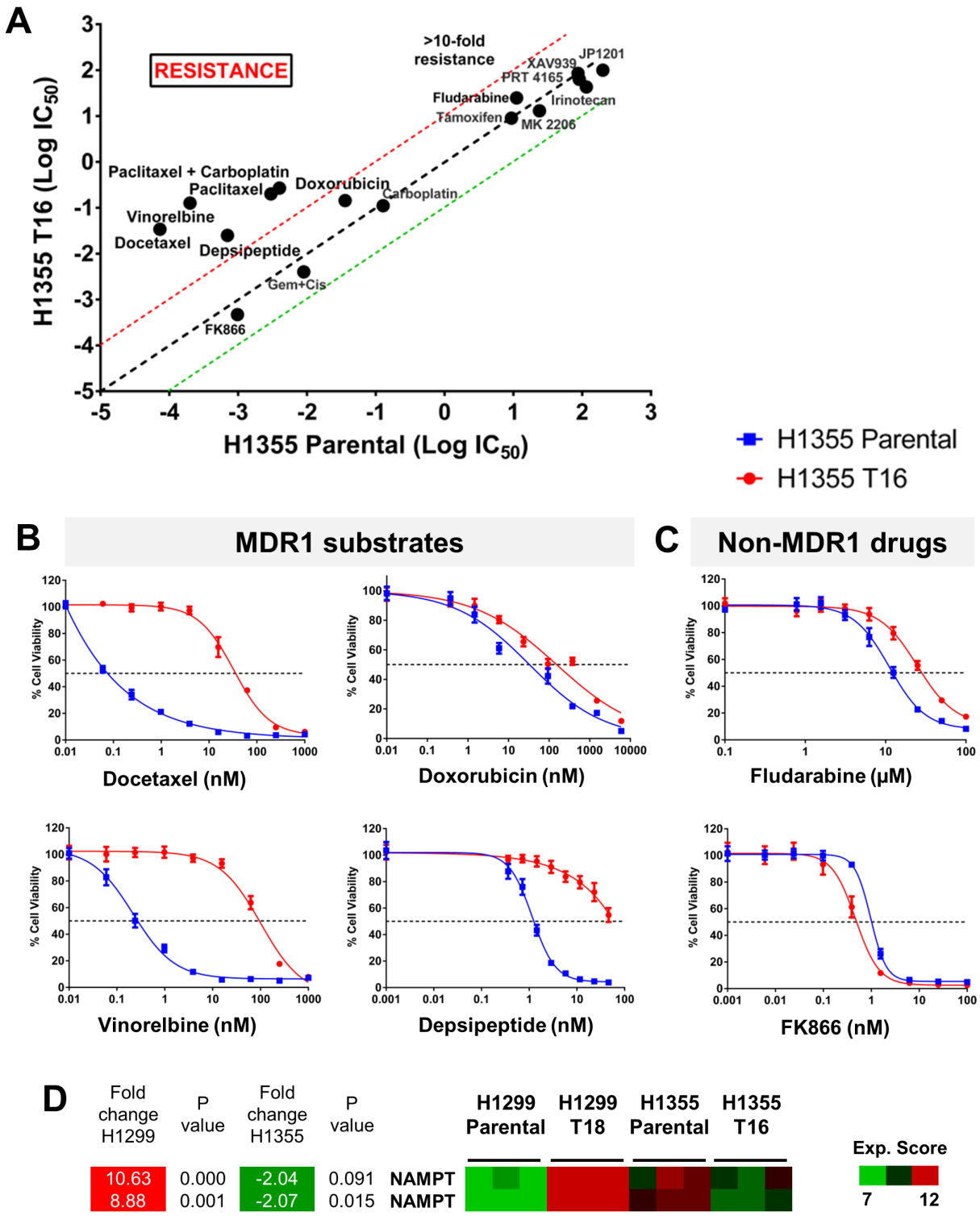
A
RESISTANCE
>10-fold resistance
JP1201
XAV939
PRT 4165
Fludarabine
Irinotecan
Tamoxifen
MK 2206
Paclitaxel + Carboplatin
Paclitaxel
Doxorubicin
Carboplatin
Vinorelbine
Docetaxel
Depsipeptide
Gem+Cis
FK866
H1355 T16 (Log IC50)
H1355 Parental (Log IC50)
H1355 Parental
H1355 T16
B
MDR1 substrates
C
Non-MDR1 drugs
% Cell Viability
Docetaxel (nM)
Doxorubicin (nM)
Fludarabine (μM)
Vinorelbine (nM)
Depsipeptide (nM)
FK866 (nM)
D
Fold change H1299
P value
Fold change H1355
P value
H1299 Parental
H1299 T18
H1355 Parental
H1355 T16
10.63
8.88
0.000
0.001
-2.04
-2.07
0.091
0.015
NAMPT
NAMPT
Exp. Score
7
12

Figure 3.5 H1355 T16 cell line shows multi-drug resistance phenotype.
(A) H1355 Parental and isogenic H1355 T16 cells were screened for differential response to several standard and targeted therapies. Red and green dotted lines indicate 10-fold cut-offs for resistance and sensitivity respectively.
(B) H1355 T16 was cross-resistant to docetaxel, doxorubicin, vinorelbine and depsipeptide, which are known substrates of MDR1 transporter. Error bars represent mean $\pm$ SD.
(C) H1355 T16 cells also showed resistance to fludarabine which is not a MDR1 substrate. These cells were however not resistant to FK866 (NAMPT inhibitor), suggesting that this was a cell line-specific response in H1299 T18 (Figure 3.4). This could be explained by differences in *NAMPT* expression detected by microarrays, as shown in panel (D).

Figure 3.6

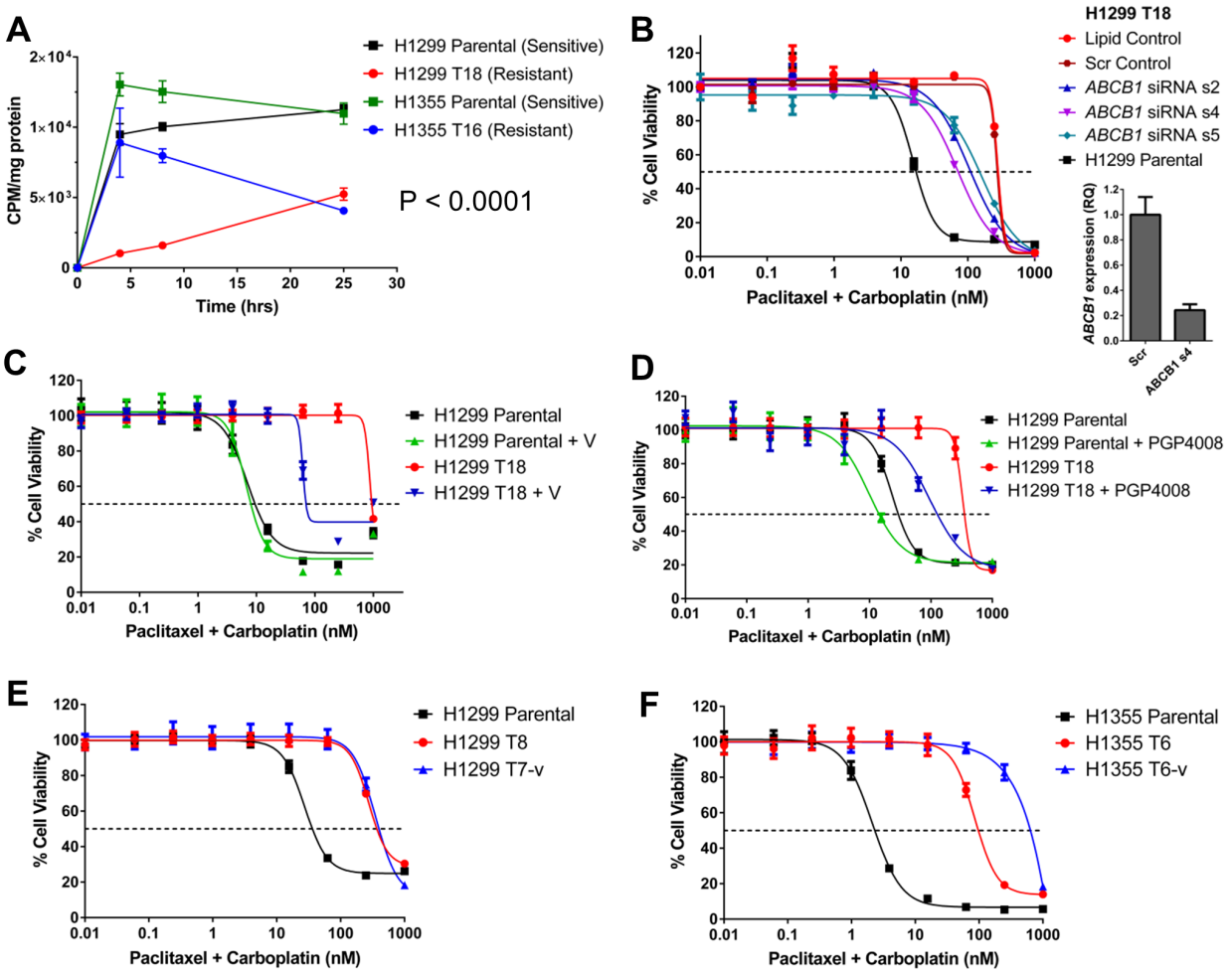
A
CPM/mg protein
Time (hrs)
H1299 Parental (Sensitive)
H1299 T18 (Resistant)
H1355 Parental (Sensitive)
H1355 T16 (Resistant)
P < 0.0001
B
% Cell Viability
Paclitaxel + Carboplatin (nM)
H1299 T18
Lipid Control
Scr Control
ABCB1 siRNA s2
ABCB1 siRNA s4
ABCB1 siRNA s5
H1299 Parental
ABCB1 expression (RQ)
Scr
ABCB1 s4
C
% Cell Viability
Paclitaxel + Carboplatin (nM)
H1299 Parental
H1299 Parental + V
H1299 T18
H1299 T18 + V
D
% Cell Viability
Paclitaxel + Carboplatin (nM)
H1299 Parental
H1299 Parental + PGP4008
H1299 T18
H1299 T18 + PGP4008
E
% Cell Viability
Paclitaxel + Carboplatin (nM)
H1299 Parental
H1299 T8
H1299 T7-v
F
% Cell Viability
Paclitaxel + Carboplatin (nM)
H1355 Parental
H1355 T6
H1355 T6-v

Figure 3.6 Chemoresistant cells that express ABCB1/ MDR1 drug transporter do not show complete reversal of resistance upon MDR1 inhibition.

(A) H1299 T18 and H1355 T16 resistant cell lines exhibited decreased intracellular accumulation of tritiated docetaxel compared to parental cells, confirming functional relevance of MDR1 expression. Data represent mean ± SEM. Two-way ANOVA, $P < 0.0001$

(B) siRNA knockdown of ABCB1 (3 individual siRNAs: s2, s4, s5) in H1299 T18 could only partially reverse resistance to paclitaxel + carboplatin. Data represents mean ± SD. Knockdown was validated by decrease in *ABCB1* mRNA (see qPCR data for s4 siRNA).

(C, D) Drug response to paclitaxel + carboplatin was tested in the presence of non-specific MDR inhibitor verapamil (V, 5 μM) or MDR1/Pgp selective inhibitor PGP4008 (10 μM). There was partial shift in drug response curves. Data represents mean ± SD.

(E, F) Repeating long term treatment of H1299 and H1355 parental cells with cycles of paclitaxel + carboplatin in the continuous presence of verapamil was not sufficient to prevent cells from becoming drug resistant. H1299 T7-v and H1355 T6-v are cell lines treated with 7 and 6 cycles respectively of paclitaxel + carboplatin, in the continuous presence of 5 μM verapamil. For comparison, H1299 T8 and H1355 T6 are cells treated simultaneously in the absence of verapamil. % Cell viability data represents mean ± SD.

Figure 3.7

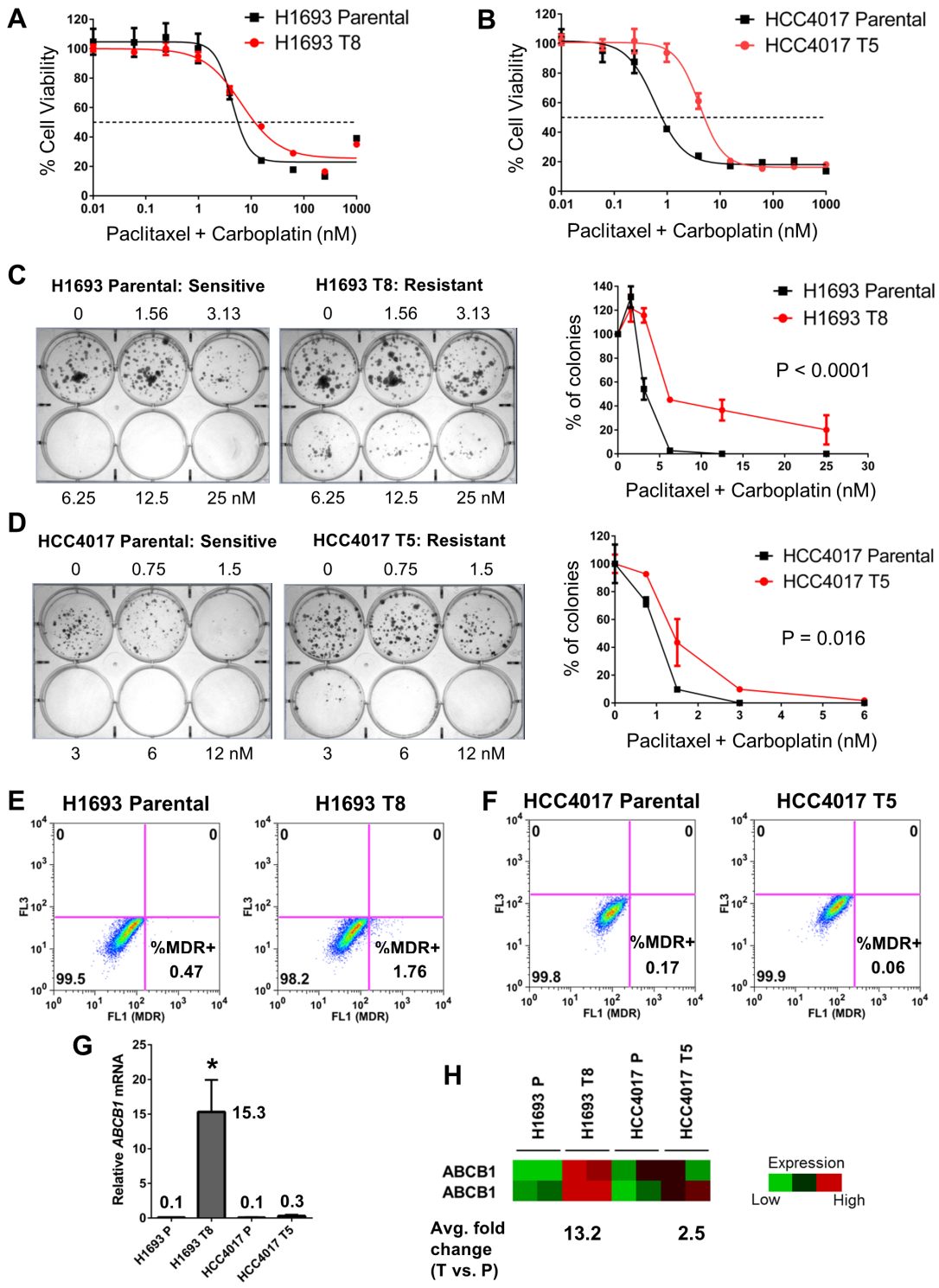
A
H1693 Parental
H1693 T8
% Cell Viability
Paclitaxel + Carboplatin (nM)
B
HCC4017 Parental
HCC4017 T5
% Cell Viability
Paclitaxel + Carboplatin (nM)
C
H1693 Parental: Sensitive
H1693 T8: Resistant
0 1.56 3.13
6.25 12.5 25 nM
H1693 Parental
H1693 T8
P < 0.0001
% of colonies
Paclitaxel + Carboplatin (nM)
D
HCC4017 Parental: Sensitive
HCC4017 T5: Resistant
0 0.75 1.5
3 6 12 nM
HCC4017 Parental
HCC4017 T5
P = 0.016
% of colonies
Paclitaxel + Carboplatin (nM)
E
H1693 Parental
H1693 T8
%MDR+
0.47
99.5
%MDR+
1.76
98.2
FL3
FL1 (MDR)
F
HCC4017 Parental
HCC4017 T5
%MDR+
0.17
99.8
%MDR+
0.06
99.9
FL3
FL1 (MDR)
G
Relative ABCB1 mRNA
15.3
0.1
0.1
0.3
H1693 P
H1693 T8
HCC4017 P
HCC4017 T5
H
H1693 P
H1693 T8
HCC4017 P
HCC4017 T5
ABCB1
ABCB1
Expression
Low
High
Avg. fold change (T vs. P)
13.2
2.5

Figure 3.7 Chemoresistant NSCLC cell line variants were generated from H1693 and HCC4017 cell lines, one of which did not express MDR1 (HCC4017 T5) but was nevertheless drug resistant.

(A, B) H1693 T8 and HCC4017 T5 cell line variants were established by long-term treatment of parental cell lines with 8 and 5 cycles respectively of paclitaxel + carboplatin (2:3) doublet. Development of resistance was tested by MTS assays. Values in dose response plots indicate paclitaxel concentration in the doublet. Each assay was performed with 8 replicates per drug dose. Data represents mean $\pm$ SD.

(C, D) Increase in drug resistance was validated by colony formation. Error bars indicate mean $\pm$ SEM. Reported P values are from two-way ANOVA comparison.

(E, F) H1693 T8 showed enrichment in % MDR+ cell subpopulation whereas HCC4017 T5 cells did not show any increase (tested by flow cytometry).

(G, H) There was significant increase in *ABCB1* mRNA expression in H1693 T8 compared to H1693 Parental, but minimal changes in *ABCB1* transcripts in HCC4017 T5 resistant cells (qRT-PCR and microarray). Error bars in qRT-PCR data represent mean $\pm$ SD. Heat map denotes expression from two *ABCB1* microarray probes and two replicates per cell line.

3.4 Taxane-platin resistant cells show slower growth *in vitro* and *in vivo*

Taxane-platin resistant variants were further characterized for their phenotypic differences from parental cell lines. Among these differences was the finding that in general, resistant variants proliferated much slower in culture. Both H1299 T18 and H1355 T16 drug resistant variants showed slower cell growth *in vitro* compared to corresponding parental cell lines (Figure 3.8 A, B). To test this difference *in vivo*, 1 million parental or resistant cells were injected subcutaneously in *NOD/SCID* mice and tumor volumes were monitored for 2 - 4 months. While there was no difference in tumor take rate or histology of these xenografts, tumors from both H1299 and H1355 resistant variants grew significantly slower compared to parental tumors (Figure 3.8 C, D). Likewise, HCC4017 T5 resistant variant also showed significantly slower tumor growth *in vivo* (Figure 3.8 E), although I did not see substantial growth rate difference *in vitro*. Slow-cycling cells have been previously linked to evasion of response to multiple chemotherapies (Roesch et al., 2013; Stewart et al., 2007).

Figure 3.8

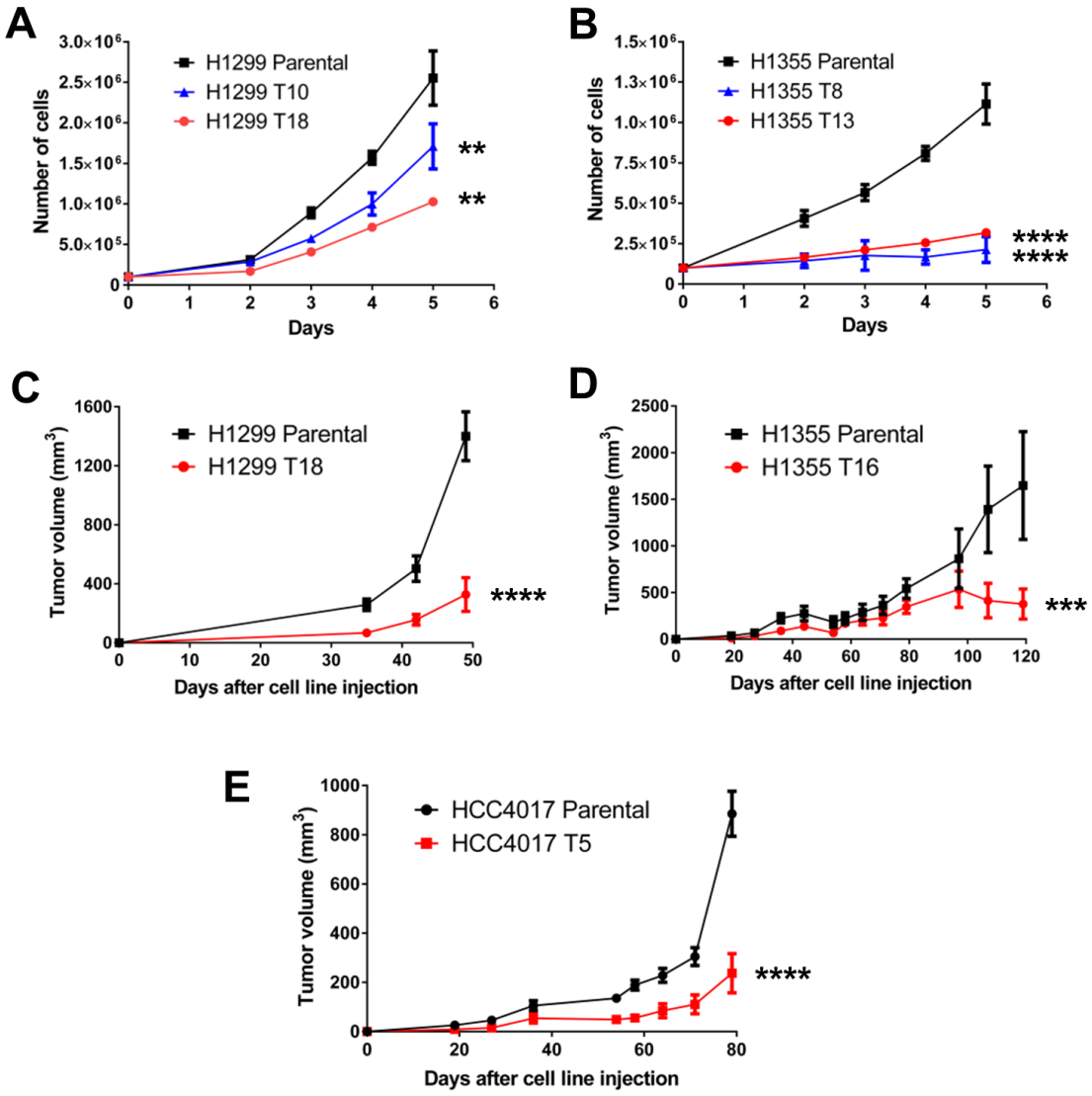

Figure 3.8 Taxane-platin resistant NSCLC cells show slower growth *in vitro* and *in vivo*
(A, B) H1299 and H1355 resistant variants showed slower cell growth rate *in vitro*. Error bars represent mean ± SEM. Statistical significance was determined by two-way ANOVA.
(C-E) Xenografts of resistant variants (H1299 T18, H1355 T16, and HCC4017 T5) showed slower tumor growth *in vivo* compared to corresponding parental xenografts. Data represents mean ± SEM. Differences in tumor growth rate were tested by two-way ANOVA.

3.5 Resistant cell line variants show epithelial-to-mesenchymal transition

Upon development of taxane-platin resistance, long-term treated H1355 T8 cells showed an epithelial-to-mesenchymal (EMT) shift in morphology (Figure 3.9 A). This was not evident in NCI-H1299, probably due to the pre-existing mesenchymal phenotype of this cell line. Regardless, I detected a significant decrease in the percentage of cells expressing the epithelial cell surface marker EpCAM, in both H1299 and H1355 resistant variants (Figure 3.9). Similarly, HCC4017 T5 resistant cells showed a dramatic reduction in %EpCAM^{High} cells (Figure 3.9). EMT has been previously described in the context of resistance to EGFR TKIs (Rho et al., 2009; Thomson et al., 2005) as well as standard chemotherapies including gemcitabine, oxaliplatin and paclitaxel (Voulgari and Pintzas, 2009). More importantly, since EMT is a reversible process, these findings suggested the possibility of transient transcriptional re-wiring during development of drug resistance.

Figure 3.9

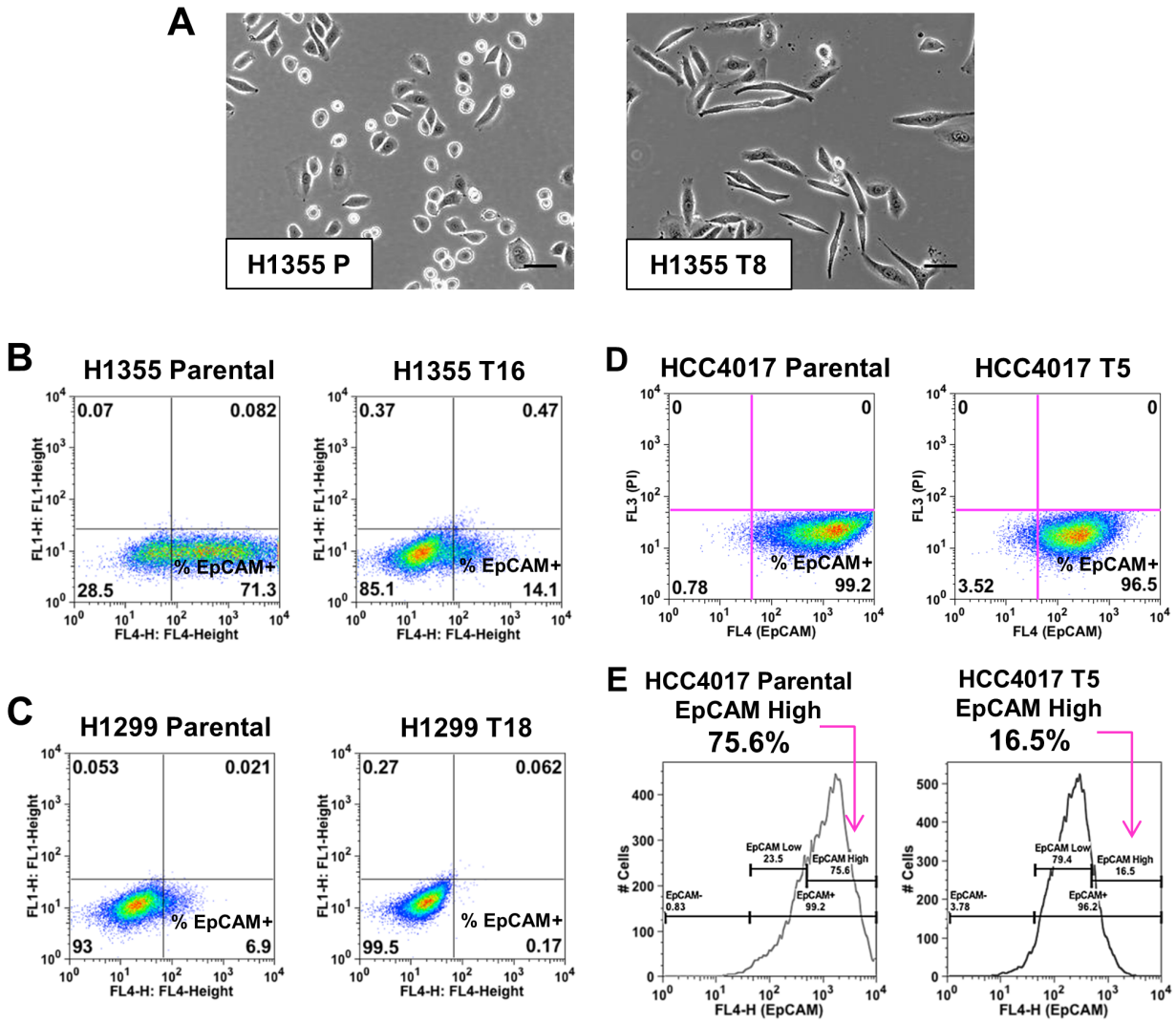

Figure 3.9 Resistant cell line variants show epithelial-to-mesenchymal transition (EMT)
(A) NCI-H1355 parental cell line (H1355 P) exhibited epithelial-to-mesenchymal shift in morphology upon development of taxane-platin resistance in H1355 T8. Scale bar, 20 µM.
(B, C) H1355 T16 and H1299 T18 resistant cells showed dramatic decreases in % EpCAM+ cells. Appropriate isotype controls were used for gating cell populations.
(D, E) HCC4017 T5 showed a substantial decrease in percentage of $EpCAM^{High}$ cell sub-population from ~76% in Parental to ~17% in T5. Note the overall shift of scatter plot (D) and histogram (E) towards the left to decreased fluorescence intensity in HCC4017 T5.

3.6 Taxane-platin resistance is partially reversible upon drug-free culturing

Upon drug-free culturing for >4 months, resistant variants showed a partial reversal in chemoresistance as indicated by decrease in drug response IC_{50} (Figure 3.10). This observation is in agreement with a previous study in EGFR-targeted therapy surviving "persister" cells that showed reversible drug tolerance (Sharma et al., 2010). In my established taxane-platin resistant NSCLC cell lines, highly resistant cells (H1299 T18, H1355 T16) as well as variants with intermediate resistance (H1299 T10, H1355 T8) showed partial (but not complete) reversibility in drug resistance. These observations suggested alterations in the epigenetic landscape of taxane-platin treated NSCLC cells, some of which could be lost in the absence of drug stress (reversed) whereas some others might be stably inherited to maintain the new altered cellular state of drug resistance.

Figure 3.10

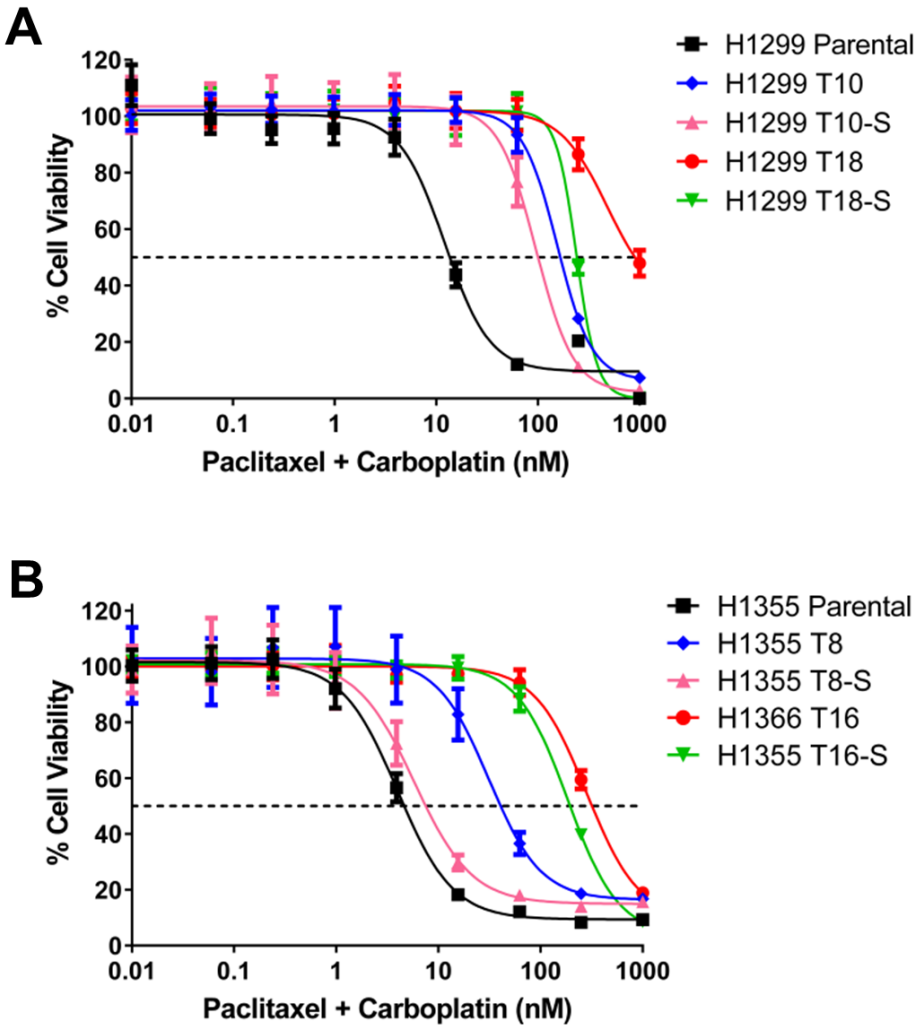

Figure 3.10 Taxane-platin resistance is partially reversible upon drug-free culturing
(A, B) H1299 and H1355 cell line variants showed "partial" reversal in paclitaxel + carboplatin resistance upon drug-free culturing for >4 months. Suffix 'S' denotes partially re-sensitized cells.

CHAPTER FOUR

PRECLINICAL RESISTANCE SIGNATURE PREDICTS RECURRENCE-FREE SURVIVAL IN NEOADJUVANT TREATED NSCLC PATIENTS

4.1 Gene expression profiles of pre-clinical cell line and xenograft models yield a resistance associated 35-gene signature

To investigate the molecular changes accompanying development of NSCLC resistance to standard taxane-platin chemotherapy, progressively resistant isogenic cell lines were subjected to genome-wide mRNA expression profiling. Microarray data was obtained for H1299 and H1355 resistant series using Illumina HumanHT-12 V4 BeadArrays. In total, five biological replicates for parental cell line, three for most resistant variant (H1299 T18/ H1355 T16) and two replicates for each intermediate resistance time-point, were used for analysis. To systematically identify genes which showed a consistent increase or decrease in expression with increasing drug resistance, a linear regression model was fitted on the gene expression data using log transformed IC_{50} values of progressively resistant series. A beta-uniform mixture model was applied to the set of p-values using R (detailed description in SWEAVE documentation in Appendix A). Genes with p-values below the false discovery rate (FDR) cutoff of 0.1 were considered statistically significant. 3752 differentially expressed genes were identified in the H1299 resistant series and 595 genes in the H1355 resistant series at FDR 0.1 (Figure 4.1 A).

To obtain the most conservative identification of differentially expressed genes, I decided to focus on gene changes (in resistant compared to parental cells) which were common between the two cell line models (H1299 and H1355 series), and between *in vitro* and *in vivo* (H1299 T18 vs. parental xenografts) grown tumor cells. 51 up-regulated and 59 down-regulated genes overlapped between H1299 and H1355 resistant cell line models (Figure 4.1 B), while intersection with xenograft tumor expression profiles (H1299 T18 versus H1299 parental xenografts, Figure 4.1 C) narrowed this list to 14 up-regulated and 21 down-regulated genes whose expression changes were sustained *in vivo* (Figure 4.1 D). These 35 genes (Figure 4.1 E) formed the pre-clinical resistance gene signature.

Figure 4.1

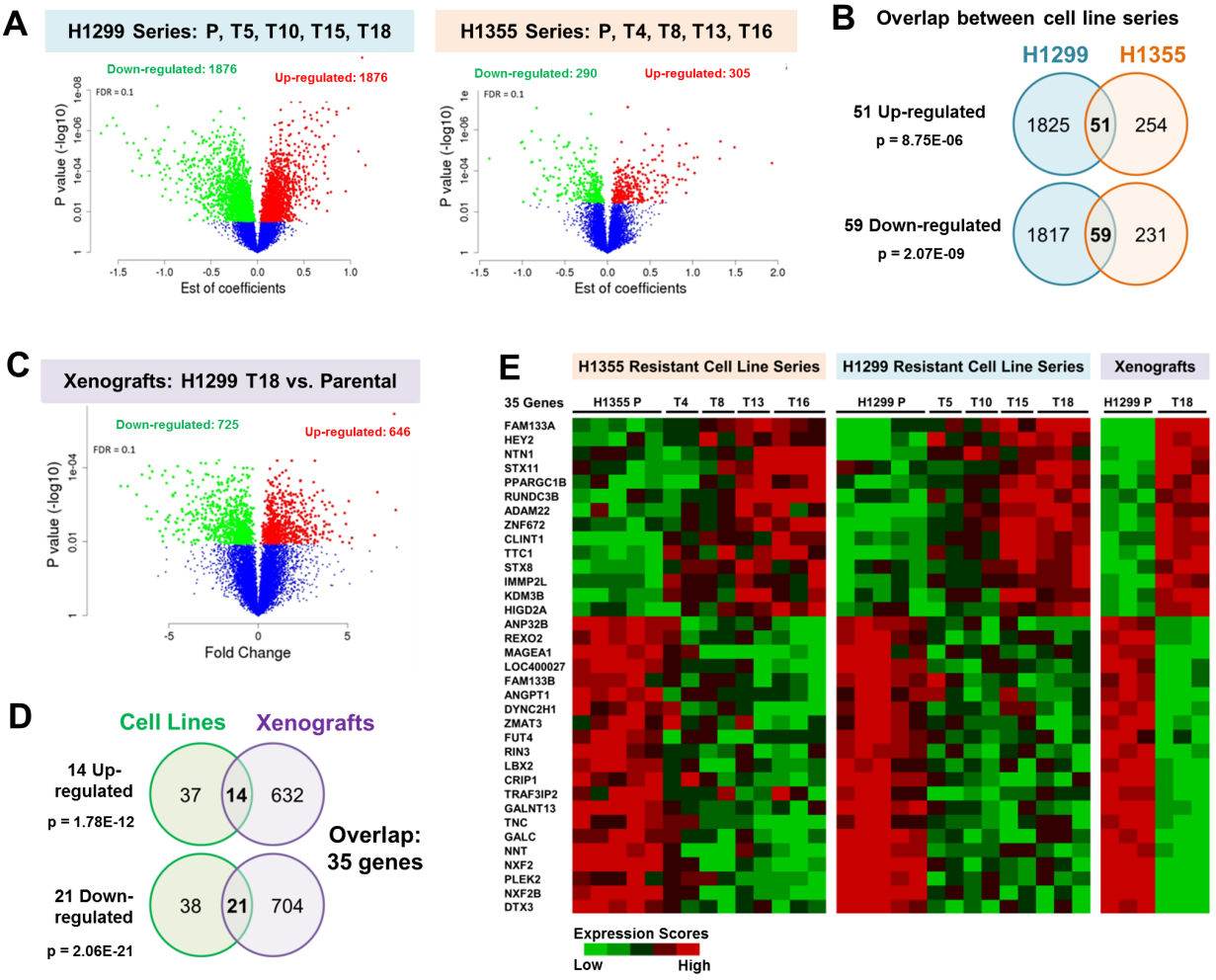
A
H1299 Series: P, T5, T10, T15, T18
Down-regulated: 1876
Up-regulated: 1876
FDR = 0.1
P value (-log10)
Est of coefficients
H1355 Series: P, T4, T8, T13, T16
Down-regulated: 290
Up-regulated: 305
FDR = 0.1
P value (-log10)
Est of coefficients
B
Overlap between cell line series
H1299
H1355
51 Up-regulated
p = 8.75E-06
1825
51
254
59 Down-regulated
p = 2.07E-09
1817
59
231
C
Xenografts: H1299 T18 vs. Parental
Down-regulated: 725
Up-regulated: 646
FDR = 0.1
P value (-log10)
Fold Change
D
Cell Lines
Xenografts
14 Up-regulated
p = 1.78E-12
37
14
632
21 Down-regulated
p = 2.06E-21
38
21
704
Overlap: 35 genes
E
H1355 Resistant Cell Line Series
H1299 Resistant Cell Line Series
Xenografts
35 Genes
H1355 P
T4
T8
T13
T16
H1299 P
T5
T10
T15
T18
H1299 P
T18
FAM133A
HEY2
NTN1
STX11
PPARGC1B
RUNDC3B
ADAM22
ZNF672
CLINT1
TTC1
STX8
IMMP2L
KDM3B
HIGD2A
ANP32B
REXO2
MAGEA1
LOC400027
FAM133B
ANGPT1
DYNC2H1
ZMAT3
FUT4
RIN3
LBX2
CRIP1
TRAF3IP2
GALNT13
TNC
GALC
NNT
NXF2
PLEK2
NXF2B
DTX3
Expression Scores
Low
High

Figure 4.1 Genome-wide mRNA expression profiling of cell lines and xenografts yields a taxane-platin resistance-associated 35-gene signature

(A) Linear regression model was fitted on microarray data of H1299 and H1355 cell line series using log transformed IC_{50} values to identify genes that were progressively up/ down-regulated with increasing drug resistance. Parental cell lines (P) and four resistant variants per cell line were analyzed. 1876 down- and 1876 up-regulated genes were identified in H1299 resistant series, while 290 down- and 305 up-regulated genes were identified in H1355 resistant series. These are represented in the volcano plots (red, up-regulated; green, down-regulated). FDR 0.1

(B) Differentially expressed gene list from H1299 and H1355 resistant cell line series was compared to identify common up/down-regulated genes. P values are from hypergeometric tests.

(C) Differential gene expression analysis was performed on xenograft microarray data (H1299 T18 resistant versus H1299 Parental) using student's t-test. FDR 0.1

(D) Gene lists obtained from cell line and xenograft microarray analyses were overlapped to identify common genes (14 up-regulated, 21 down-regulated). P values are from hypergeometric tests.

(E) Heat map representation of the expression pattern of 35 gene resistance signature in cell lines and xenografts.

4.2 Pre-clinical resistance signature predicts recurrence-free survival in NSCLC patients treated with platin-based doublet neoadjuvant chemotherapy

In order to evaluate clinical relevance, the 35-gene resistance signature was tested on NSCLC patients who had received standard chemotherapy prior to resection of their tumors (annotated in Table 2.3). This neoadjuvant treated patient group had received platin-based chemotherapy, predominantly as taxane + platin doublets (paclitaxel + carboplatin, docetaxel + cisplatin, docetaxel + carboplatin). Cancer recurrence-free survival data was available for 65 out of 66 patients. Frozen resected tumor samples were expression profiled by Illumina HumanWG-6 V3 BeadArrays.

Using the 35-gene resistance signature, unsupervised hierarchical clustering (Euclidean distance matrix and maximum linkage method) of neoadjuvant treated NSCLC tumors was performed on the 65 neoadjuvant chemotherapy-treated patients, and found to separate them into two major groups (Figure 4.2 A). Kaplan-Meier survival analysis revealed that these groups showed significant differences in recurrence-free survival (Figure 4.2 B). Group 2 showed significantly worse cancer recurrence-free prognosis than Group 1 patients ($P = 0.0012$, Hazard ratio = 2.78). Analysis was tested and adjusted for clinical covariates (Table 4.1).

Figure 4.2

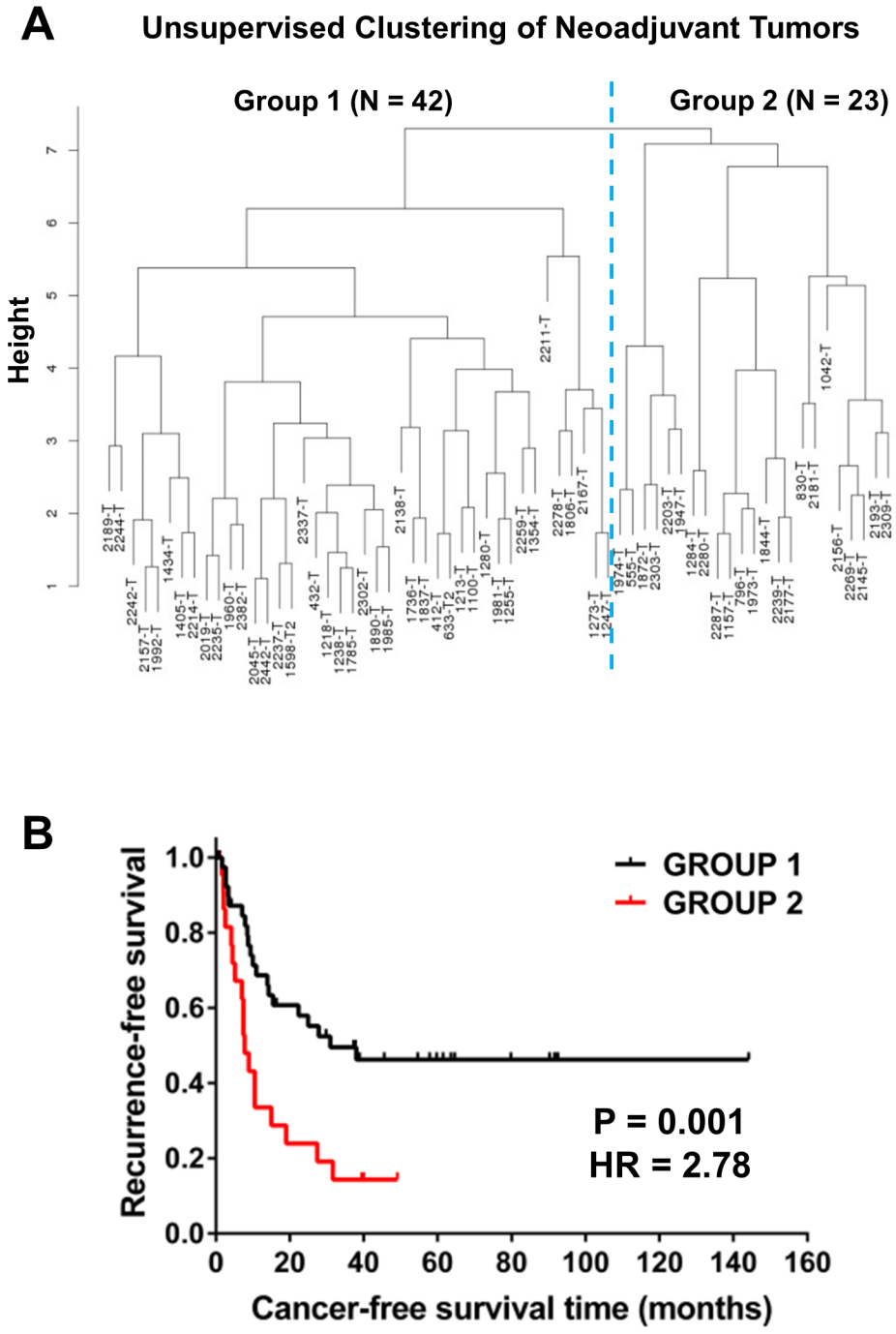
A
Unsupervised Clustering of Neoadjuvant Tumors
Group 1 (N = 42)
Group 2 (N = 23)
Height
B
GROUP 1
GROUP 2
Recurrence-free survival
P = 0.001
HR = 2.78
Cancer-free survival time (months)

Figure 4.2 35-gene pre-clinical resistance signature predicts recurrence-free survival in neoadjuvant chemotherapy treated NSCLC patients

(A) Using 35 genes, unsupervised hierarchical clustering of neoadjuvant treated NSCLC patients (N = 65, mainly taxane + platin treated) was performed and found to separate the patients into two major groups.

(B) Kaplan-Meier survival analysis of the two groups of neoadjuvant treated NSCLC patients revealed significant differences in cancer recurrence-free survival (P = 0.0012, HR = 2.78, 95% CI, 1.46 – 5.29). Survival P-value was adjusted for clinical covariates (tested by Cox multivariate regression, Table 4.1).

Table 4.1 Cox multivariate analysis on recurrence-free survival to test for bias from clinical covariates

	coef	exp(coef)	se(coef)	z	P value
Two Groups/ Clusters [a]	1.63	5.10	0.49	3.35	0.0008
Histology (Squamous)	-0.23	0.80	0.50	-0.46	0.64
Histology (Non Squamous)	0.37	1.45	0.47	0.78	0.43
Age	0.02	1.02	0.03	0.88	0.38
Smoking history (Y)	-0.93	0.40	0.67	-1.39	0.16
Gender (M)	-0.21	0.81	0.43	-0.49	0.62
Race (Asian or Pacific Islander)	-0.28	0.76	1.52	-0.18	0.85
Race (Caucasian)	-0.87	0.42	0.80	-1.09	0.28
Race (Hispanic)	-0.13	0.88	1.29	-0.10	0.92
Adjuvant therapy (Y)	-1.03	0.36	0.50	-2.07	0.04
Neoadjuvant (Pac + Carb)	0.53	1.69	0.52	1.01	0.31
Stage (II)	-0.24	0.79	0.59	-0.40	0.69
Stage (III)	1.00	2.73	0.50	2.02	0.04
Stage (IV)	0.95	2.59	0.67	1.43	0.15

[a] Clustering of patients into two major groups was the most significant contributor to the cancer recurrence-free survival difference (P = 0.0008).

CHAPTER FIVE

HISTONE LYSINE DEMETHYLASES CORRELATED WITH POOR RECURRENCE-FREE PATIENT SURVIVAL AND SHOWED INCREASED EXPRESSION IN TAXANE-PLATIN RESISTANT CELLS

5.1 Multivariate analysis of 35-gene resistance signature identifies *KDM3B* as a significant contributor to poor recurrence-free survival in NSCLC patients

The 35-gene resistance signature derived from preclinical taxane-platin resistant cell lines and xenografts was shown to be clinically relevant in predicting poor recurrence-free survival outcome in neoadjuvant treated NSCLC patients. To identify a significant gene candidate for potential therapeutic targeting of taxane-platin resistant, relapsing NSCLC tumors, Cox multivariate regression was performed to dissect the individual contribution of the 35 genes in the signature (Table 5.1). Among the 14 genes that were up-regulated in pre-clinical resistance models, the gene that showed the largest hazard risk for poor recurrence-free survival in chemotherapy treated NSCLC patients was the histone lysine demethylase, *KDM3B* (P value = 0.025, hazard ratio = 10.28, Figure 5.1 A).

To verify increased expression of KDM3B in Group 2 of neoadjuvant chemotherapy treated patients who showed poor recurrence-free outcome, immunohistochemistry (IHC) of formalin-fixed tumor samples was performed in a tissue microarray (TMA). Based on the extent

and intensity of KDM3B staining, tumor samples were assigned an expression score by a pathologist who was study-blind with respect to classification of tumors into the two clustering groups. Indeed, Group 2 patients were found to exhibit higher overall KDM3B IHC scores compared to Group 1 patients (Figure 5.1 B). Representative KDM3B IHC images and the corresponding tumor H&E images are shown in Figure 5.1 C.

Table 5.1 Multivariate analysis of 35-gene signature towards cancer recurrence-free survival of 65 neoadjuvant treated NSCLC patients

Genes	coef	exp(coef)	se(coef)	z	P value
KDM3B [a]	2.33	10.28	1.04	2.24	0.025
ADAM22	1.81	6.10	1.22	1.48	0.14
IMMP2L	0.64	1.89	0.76	0.84	0.40
NTN1	0.42	1.52	0.48	0.87	0.38
FAM133A	0.19	1.20	0.24	0.76	0.44
STX11	-0.06	0.94	0.41	-0.15	0.88
HEY2	-0.11	0.89	0.23	-0.50	0.62
HIGD2A	-0.15	0.86	1.15	-0.13	0.89
RUNDC3B	-0.17	0.84	0.37	-0.47	0.64
PPARGC1B	-0.34	0.71	0.39	-0.86	0.39
TTC1	-0.75	0.47	0.88	-0.85	0.40
ZNF672	-1.72	0.18	1.03	-1.67	0.094
STX8	-2.12	0.12	0.86	-2.47	0.014
CLINT1	-2.99	0.05	1.37	-2.18	0.029
NNT [b]	3.02	20.41	0.89	3.40	0.001
NXF2B	2.71	14.96	1.65	1.64	0.10
TRAF3IP2	1.36	3.89	0.90	1.52	0.13
DTX3	0.88	2.41	0.32	2.73	0.006
REXO2	0.82	2.28	1.08	0.76	0.44
LBX2	0.69	2.00	0.35	2.00	0.046
FUT4	0.70	2.00	0.85	0.82	0.41
GALNT13	0.52	1.68	0.38	1.37	0.17
CRIP1	0.48	1.62	0.41	1.18	0.24
TNC	0.45	1.58	0.27	1.68	0.092
MAGEA1	0.39	1.47	0.22	1.78	0.075
ANGPT1	0.21	1.23	0.35	0.59	0.55
RIN3	0.18	1.19	0.41	0.43	0.67
GALC	0.10	1.11	0.65	0.16	0.88
PLEK2	-0.09	0.92	0.27	-0.32	0.75
ZMAT3	-0.24	0.78	0.89	-0.27	0.79
LOC400027	-0.32	0.73	0.51	-0.62	0.54
DYNC2H1	-0.72	0.48	0.45	-1.61	0.11
ANP32B	-0.80	0.45	0.76	-1.06	0.29
FAM133B	-1.68	0.19	1.32	-1.27	0.20
NXF2	-1.96	0.14	1.31	-1.50	0.13

Table 5.1

[a] KDM3B was up-regulated in resistant cell lines and xenografts, and showed the most significant, positive correlation with poor cancer recurrence-free survival (exp coeff/ Hazard ratio = 10.28, P value = 0.025)

[b] Though NNT expression had a high positive correlation in this multivariate analysis, it was actually down-regulated in our pre-clinical resistant models and was hence not selected as a top priority for therapeutic targeting.

Figure 5.1

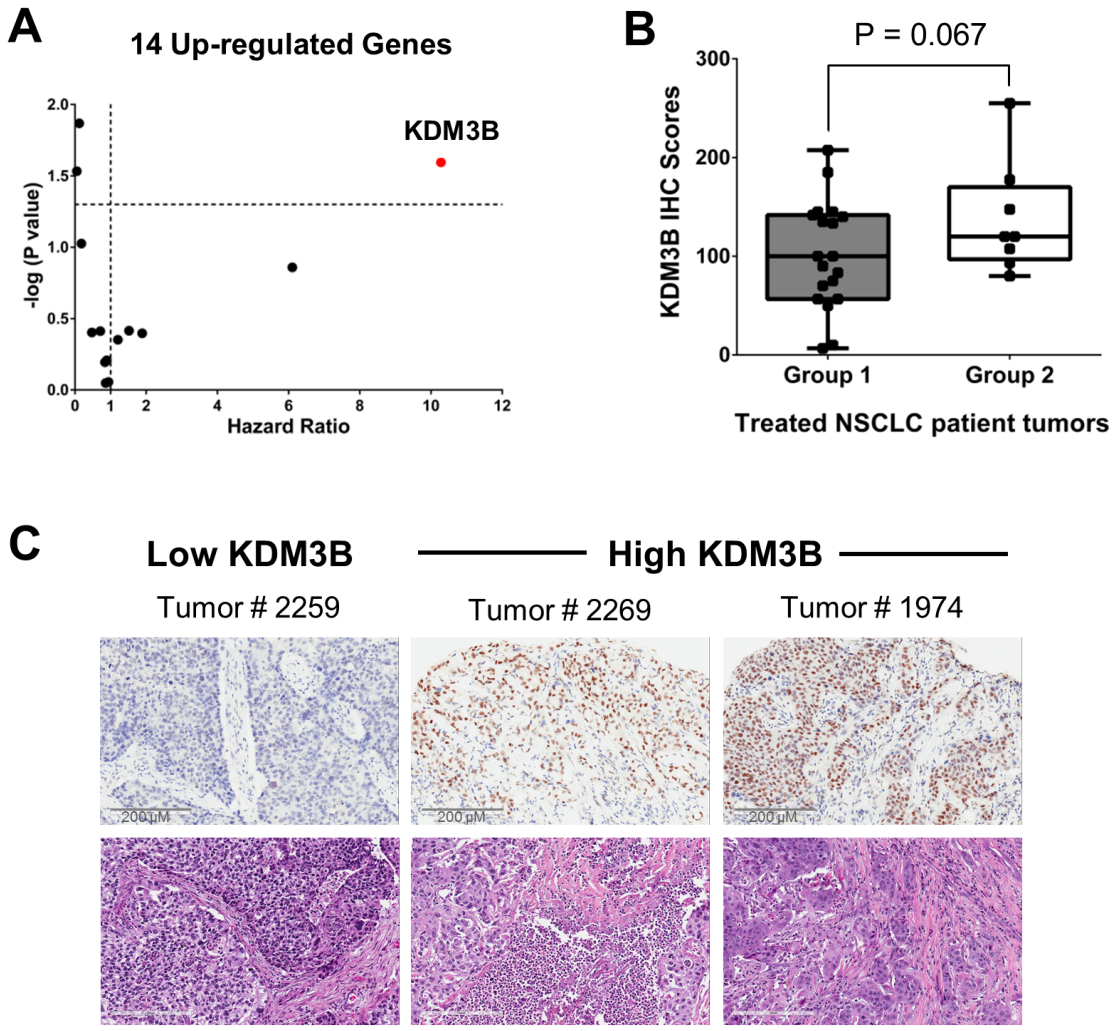

Figure 5.1 KDM3B was identified as a significant contributor to poor recurrence-free survival and showed higher expression in Group 2 of neoadjuvant treated NSCLC patients
(A) Cox multivariate regression hazard ratios i.e. exp (regression coefficient) and –log (P values) for the 14 up-regulated genes from 35-gene signature, showing *KDM3B* as a major contributor.
(B) IHC-TMA verified that Group 2 of neoadjuvant treated patients (poor recurrence-free survival) showed higher KDM3B protein expression compared to Group 1 patients.
(C) Representative images of KDM3B IHC and corresponding tumor H&E staining.

5.2 KDMs show higher expression in treated NSCLC patient tumors than chemo-naïve tumors, and high expression correlates with poor recurrence-free survival

The epigenetic enzyme *KDM3B* (also known as *JMJD1B*) was identified through the clinical evaluation of 35-gene preclinical resistance signature. There are however ~20 known human proteins that function as histone lysine demethylases/ KDMs (Hojfeldt et al., 2013). So we further evaluated the expression of other members of the KDM family.

Residual NSCLC patient tumor cells surviving standard platin-based neoadjuvant chemotherapy showed higher overall *KDM3A, KDM4A and KDM6B* mRNA expression compared to chemo-naïve patient tumors (Figure 5.2). To investigate whether increased expression of these family members correlated with cancer relapse, we compared the recurrence-free survival of high and low expressers, segregated by median expression value. Indeed, high *KDM3A*, *KDM4A* or *KDM6B* mRNA expression correlated with significantly worse recurrence-free prognosis (Figure 5.2) in the cohort of 275 NSCLC patients (neoadjuvant treated + chemo-naïve, annotated in Table 2.3).

Figure 5.2

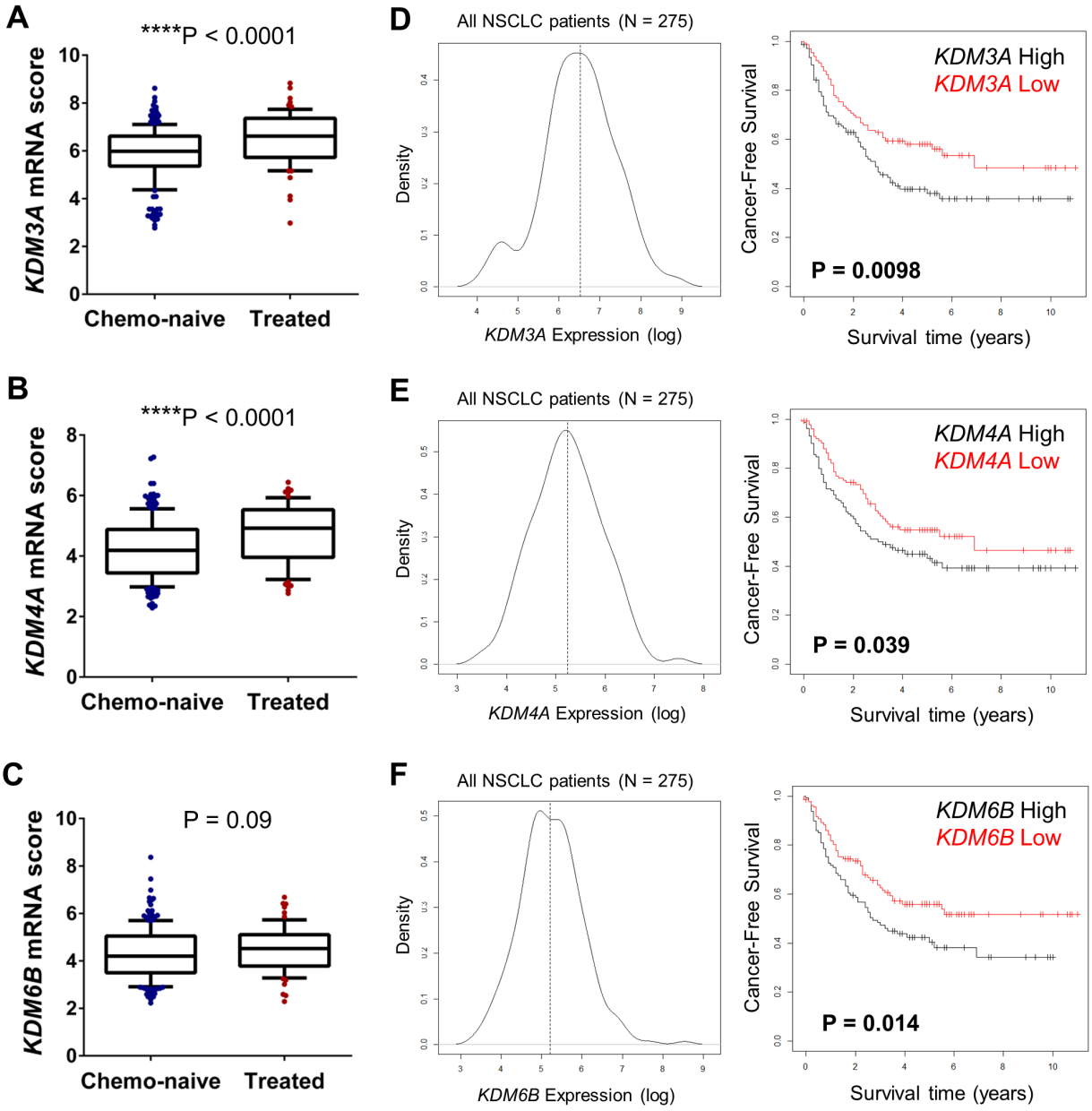
A
****P < 0.0001
KDM3A mRNA score
Chemo-naive
Treated
B
****P < 0.0001
KDM4A mRNA score
Chemo-naive
Treated
C
P = 0.09
KDM6B mRNA score
Chemo-naive
Treated
D
All NSCLC patients (N = 275)
Density
KDM3A Expression (log)
KDM3A High
KDM3A Low
Cancer-Free Survival
P = 0.0098
Survival time (years)
E
All NSCLC patients (N = 275)
Density
KDM4A Expression (log)
KDM4A High
KDM4A Low
Cancer-Free Survival
P = 0.039
Survival time (years)
F
All NSCLC patients (N = 275)
Density
KDM6B Expression (log)
KDM6B High
KDM6B Low
Cancer-Free Survival
P = 0.014
Survival time (years)

Figure 5.2 Neoadjuvant treated NSCLC patient tumors show higher KDM3A, KDM4A and KDM6B expression than chemo-naïve tumors, and high expression correlates with poor cancer recurrence-free survival

(A-C) Within a cohort of 275 NSCLC patients, residual tumors from neoadjuvant chemotherapy-treated patients (N = 66) showed higher *KDM3A*, *KDM4A* and *KDM6B* mRNA log expression compared to tumors that were chemo-naïve at the time of resection (N = 209). P values are from one-tailed unpaired t-test.

(D-F) High *KDM3A*, *KDM4A* and *KDM6B* mRNA expression correlated with poor cancer-free survival in NSCLC patient tumor dataset (275 tumors). High/Low groups were separated by median log expression value.

5.3 Taxane-platin resistant cell line variants show increased expression of several histone lysine demethylases, compared to chemo-sensitive parental cell lines

Expression of histone lysine demethylases in chemoresistant/parental cell line pairs was compared by quantitative real time-PCR. This mini-screen included LSD1 demethylase (KDM1A/ AOF2), JumonjiC (JmjC) domain-containing histone demethylases (KDMs 2-7) and some other JmjC family members (JARID2 and KDM8/ JMJD5) which do not have "defined" demethylase activity (Hojfeldt et al., 2013).

H1299 T18 taxane-platin resistant cells showed increased expression of several JmjC histone lysine demethylases compared to H1299 parental cells (Figure 5.3 A). Other than *KDM3B* (*JMJD1B*) which is an H3K9me1/2 demethylase, chemoresistant cells also showed higher expression of *KDM6A* (*UTX*) and predominantly *KDM6B* (*JMJD3*), both of which are H3K27me2/3 demethylases. Taxane-platin resistant H1355 T16 variant developed from NCI-H1355 cell line also showed increased expression of *KDM6A* and *KDM6B*, in addition to *KDM3B* (Figure 5.3 B).

Additionally, H1299 T18 cells (but not H1355 T16) had elevated levels of *JARID2*, which has been suggested to indirectly regulate H2K27me3 modification via its interaction with the PRC2 complex (Peng et al., 2009; Sanulli et al., 2015; Shen et al., 2009). *KDM7A* (JHDM1D) which is an H3K9me1/2 and H3K27me1/2 demethylase was also overexpressed in H1299 T18 (Figure 5.3 A).

Apart from histone demethylases that erase repressive K9 and K27 methylation marks, chemoresistant H1299 T18 showed modest up-regulation of *KDM5A* (*JARID1A*) and *KDM5B*

(*JARID1B*) which are both H3K4me2/3 demethylases. Interestingly, these two KDMs have been previously reported in drug-tolerant "persister" cells, with KDM5A overexpression in erlotinib/gefitinib-tolerant EGFR-mutant NSCLC cells (Sharma et al., 2010) and KDM5B in vemurafenib resistant BRAFV600E-mutated melanoma cells (Roesch et al., 2013). H1355 T16 did not exhibit *KDM5A*/*5B* up-regulation (Figure 5.3 B).

Figure 5.3

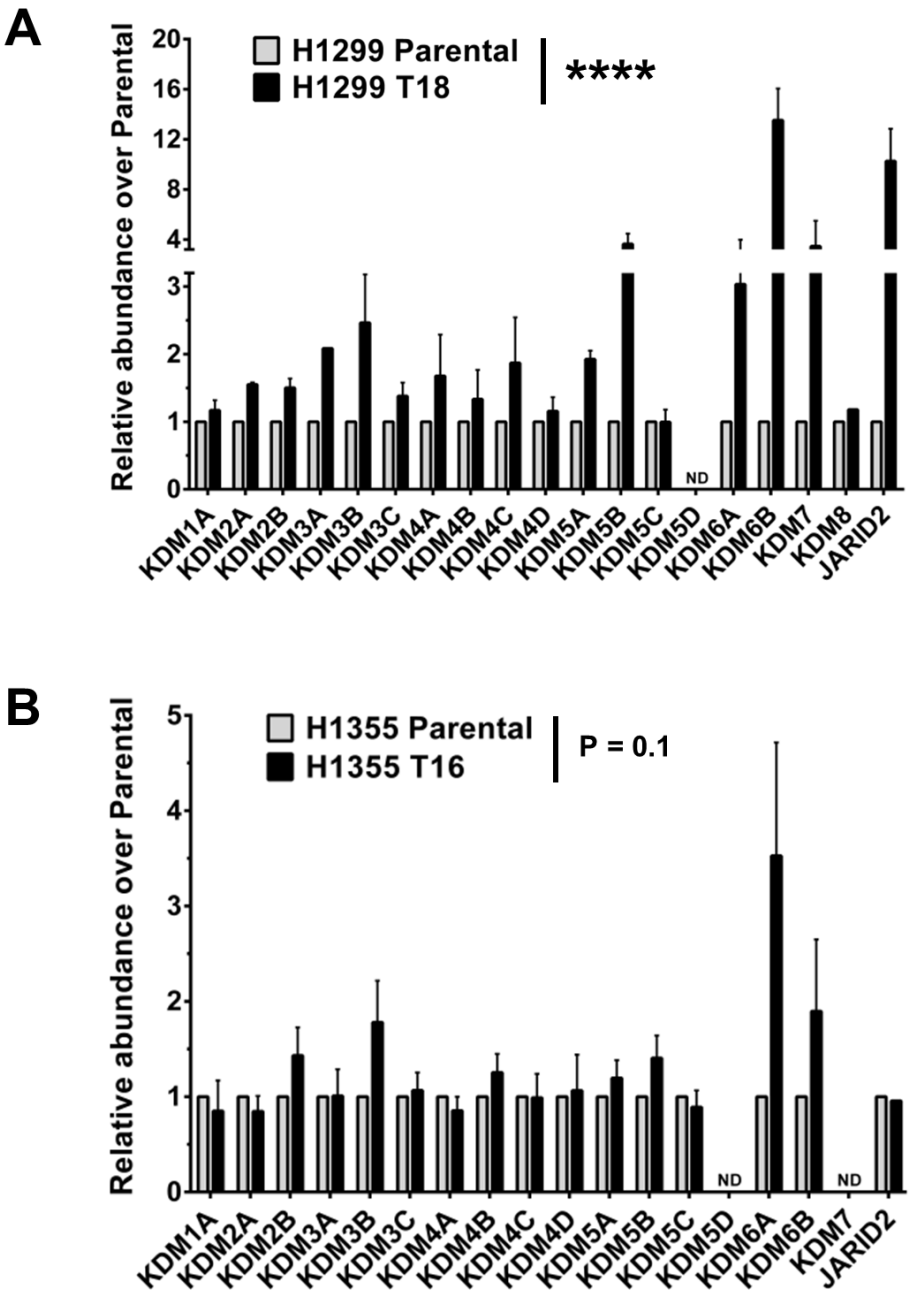

Figure 5.3 Taxane-platin resistant cell lines show up-regulation of several histone lysine demethylases, compared to chemo-sensitive parental cell lines

H1299 T18 (A) and H1355 T16 (B) showed increased mRNA expression of several members of histone lysine demethylase (KDM) family, by qRT-PCR. Error bars represent mean $\pm$ SEM. Significance was tested by two-way ANOVA. H1299 T18 vs. H1299 Parental, ****P = 0.0003

5.4 H1299 T18 chemoresistant cells exhibit overall global reduction of H3K27me3 across the genome, and reciprocal H3K4me3/H3K27me3 marks on differentially expressed gene promoters

Given the strong up-regulation of H3K27me3 demethylases (*KDM6A*/*6B*) in H1299 T18 cells, I decided to investigate global changes in this histone methylation mark by chromatin immunoprecipitation followed by next-generation sequencing (ChIP-Seq). Concomitant with increased expression of H3K27me3 demethylases, H1299 T18 resistant cells showed globally reduced levels of H3K27 trimethylation across the genome (transcriptional start site/TSS, gene body, etc.), compared to H1299 parental cell line (Figure 5.4).

This overall decrease in repressive H3K27me3 mark across the genomic regions persisted in the subset of genes that were significantly 'up-regulated' in H1299 T18 over H1299 parental cells (Figure 5.5 A), and as expected, there was an increase in histone H3K4me3 activating mark at the TSS of these genes (Figure 5.5 B). Genes that were significantly 'down-regulated' in H1299 T18 exhibited focal gain of H3K27me3 selectively at the TSS (Figure 5.5 C), and this was accompanied by reciprocal decrease in histone H3K4me3 activating mark at the TSS (Figure 5.5 D).

Figure 5.4

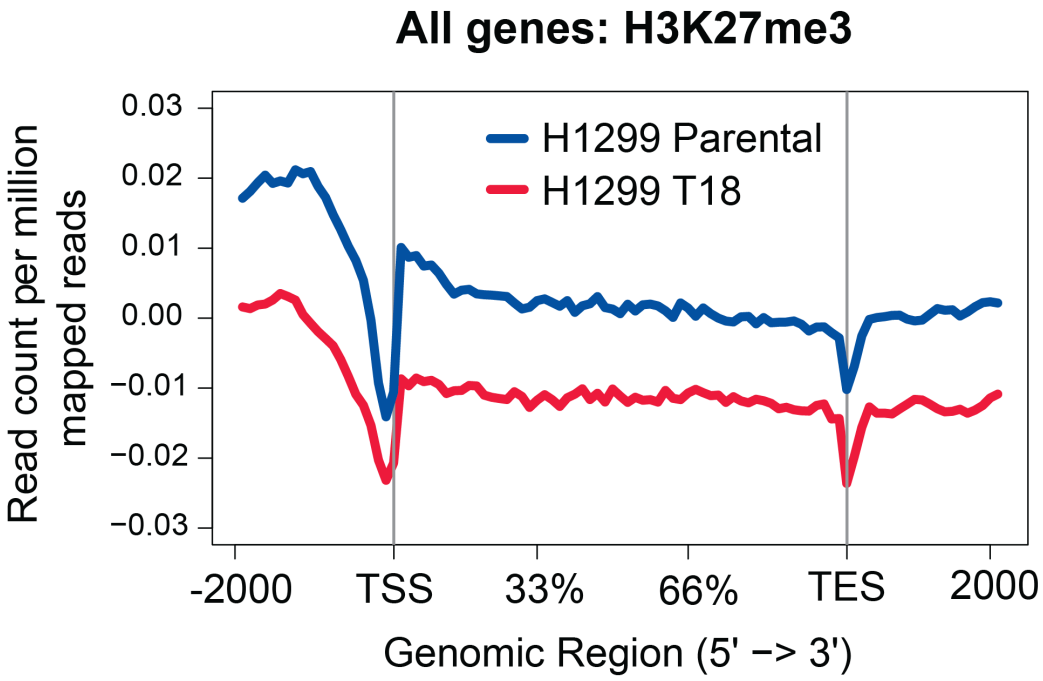

Figure 5.4 H3K27me3 enrichment plots for H1299 parental and T18 cells by ChIP-Seq showing overall global decrease in T18

Average H3K27me3 ChIP read depth in the gene body regions and 2kb 5' and 3' to the gene body regions was subtracted from respective input read depth and plotted. The x axis represents the genomic regions for all human gene body regions from 5' to 3' and the y axis represents read depth. TSS, transcription start site; TES, transcription end site.

Figure 5.5

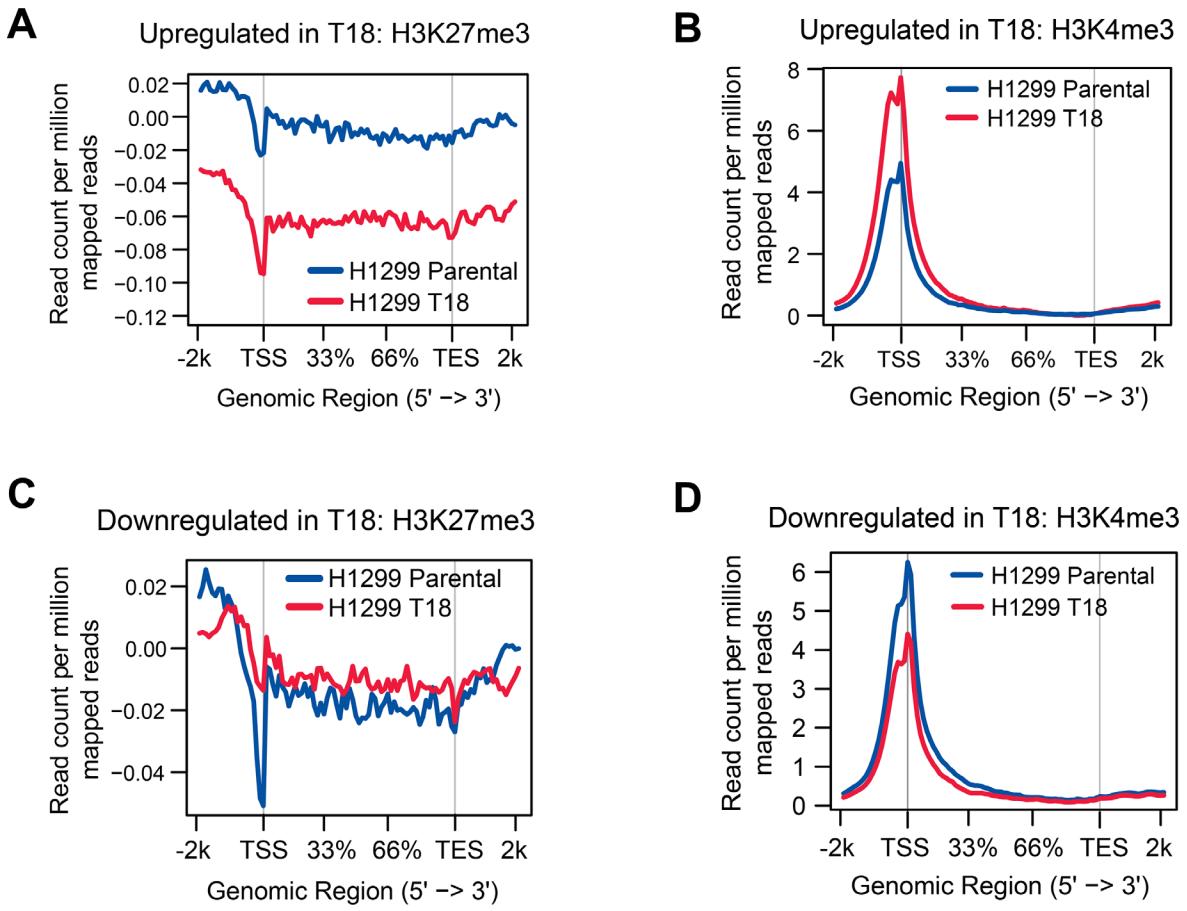

Figure 5.5 H3K27me3 and H3K4me3 enrichment plots by ChIP-Seq for differentially expressed genes in H1299 T18 over H1299 Parental cells

The x axis represents the genomic regions from 5' to 3' for genes that were significantly up-regulated (panels A and B, 960 genes) or down-regulated (panels C and D, 1173 genes) in H1299 T18 over H1299 Parental, as determined by RNA-Seq analysis at FDR 0.05 and FPKM cutoff of 1 in parental or T18 cells. Average H3K27me3 and H3K4me3 ChIP read depth in the gene body regions and 2kb 5' and 3' to the gene body regions was subtracted from respective input read depth and plotted. The y axis represents ChIP read depth. TSS, transcription start site; TES, transcription end site.

5.5 Isogenic series of H1299 chemoresistant cells show progressive increase in histone lysine demethylase expression with increasing taxane-platin resistance

Since H1299 resistant variants showed increasing resistance to paclitaxel + carboplatin doublet therapy with increasing treatment cycles, I next sought to investigate whether this progressive development of resistance correlated with consistent increase in expression of histone lysine demethylases. This was obvious for *KDM3B* as this gene was identified through linear regression of microarray data for H1299 and H1355 resistant series using log transformed IC_{50} values (Figure 4.1). This was verified in qRT-PCR data (Figure 5.6). In addition, *KDM6A* and *KDM6B* were also found to exhibit a significant linear trend for increased mRNA expression as cells progressed from H1299 Parental to H1299 T18 (Figure 5.6). These results suggested a clear association between KDM up-regulation and increasing taxane-platin resistance.

Figure 5.6

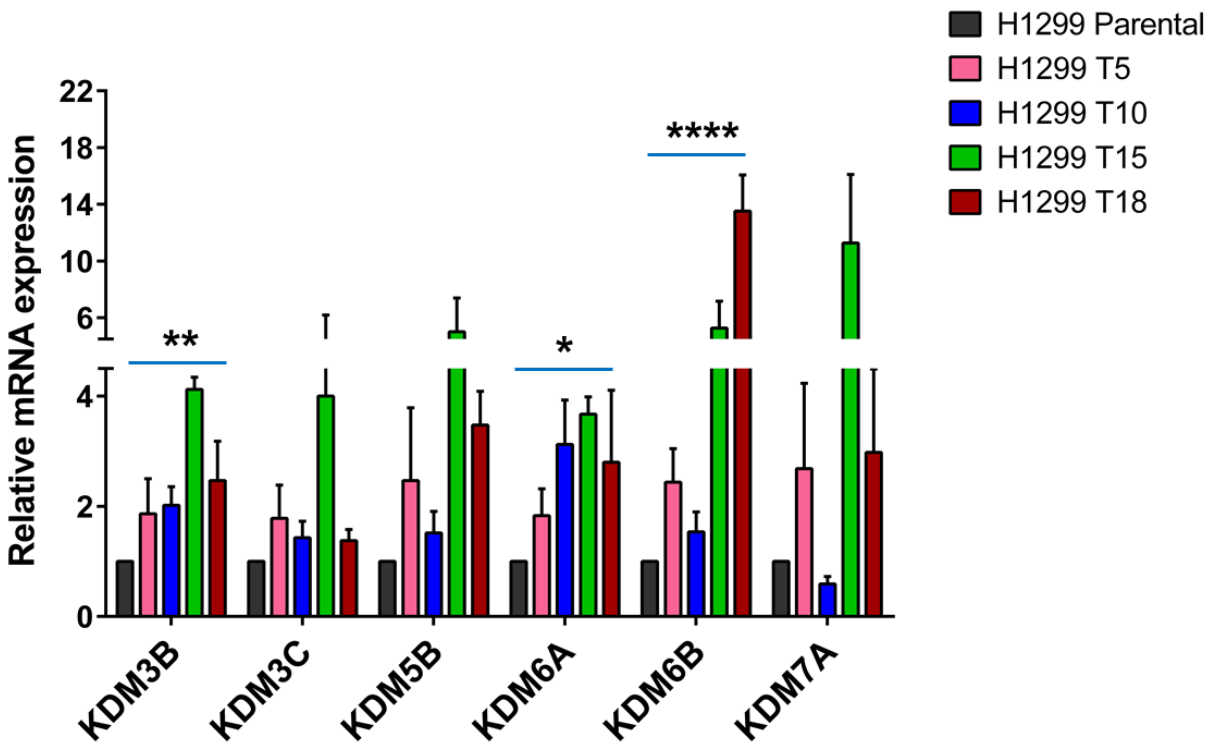

Figure 5.6 Isogenic series of H1299 chemoresistant cells show progressive increase in histone lysine demethylase expression with increasing taxane-platin resistance

H1299 isogenic resistant cells showed progressive increase in expression of several histone lysine demethylases with increasing drug resistance. P values are from one-way ANOVA post-test for linear trend: KDM3B, **P = 0.009; KDM6A, *P = 0.016; KDM6B, P < 0.0001

CHAPTER SIX

TAXANE-PLATIN RESISTANT NSCLC CELLS ARE HYPER-SENSITIZED TO JMJC KDM INHIBITORS *IN VITRO* AND *IN VIVO*

6.1 H1299 T18 taxane-platin resistant NSCLC cells are hyper-sensitized to JumonjiC lysine demethylase inhibitors compared to corresponding parental cell line

Since taxane-platin resistant cells showed increased expression of several members of JumonjiC (JmjC) histone lysine demethylase family, I investigated their survival dependence on KDMs by employing a pan-JmjC histone lysine demethylase inhibitor, JIB-04 (Wang et al., 2013). H1299 T18 chemo-resistant cell line was hyper-sensitized to JIB-04 compared to H1299 parental cells (active E isomer in Figure 6.1 A). There was no viability loss in drug resistant or parental cells with the epigenetically inactive Z isomer of JIB-04.

Since *KDM6* subfamily was one of the most significantly altered in resistant cells (as shown in Figure 5.3), I also tested the KDM6A/KDM6B (UTX/JMJD3) inhibitor, GSK-J4 (Kruidenier et al., 2012). Again, H1299 T18 showed higher sensitivity to GSK-J4 compared to H1299 parental cells and there was no effect on cell viability with the inactive GSK-J5 isomer (Figure 6.1 B).

Figure 6.1

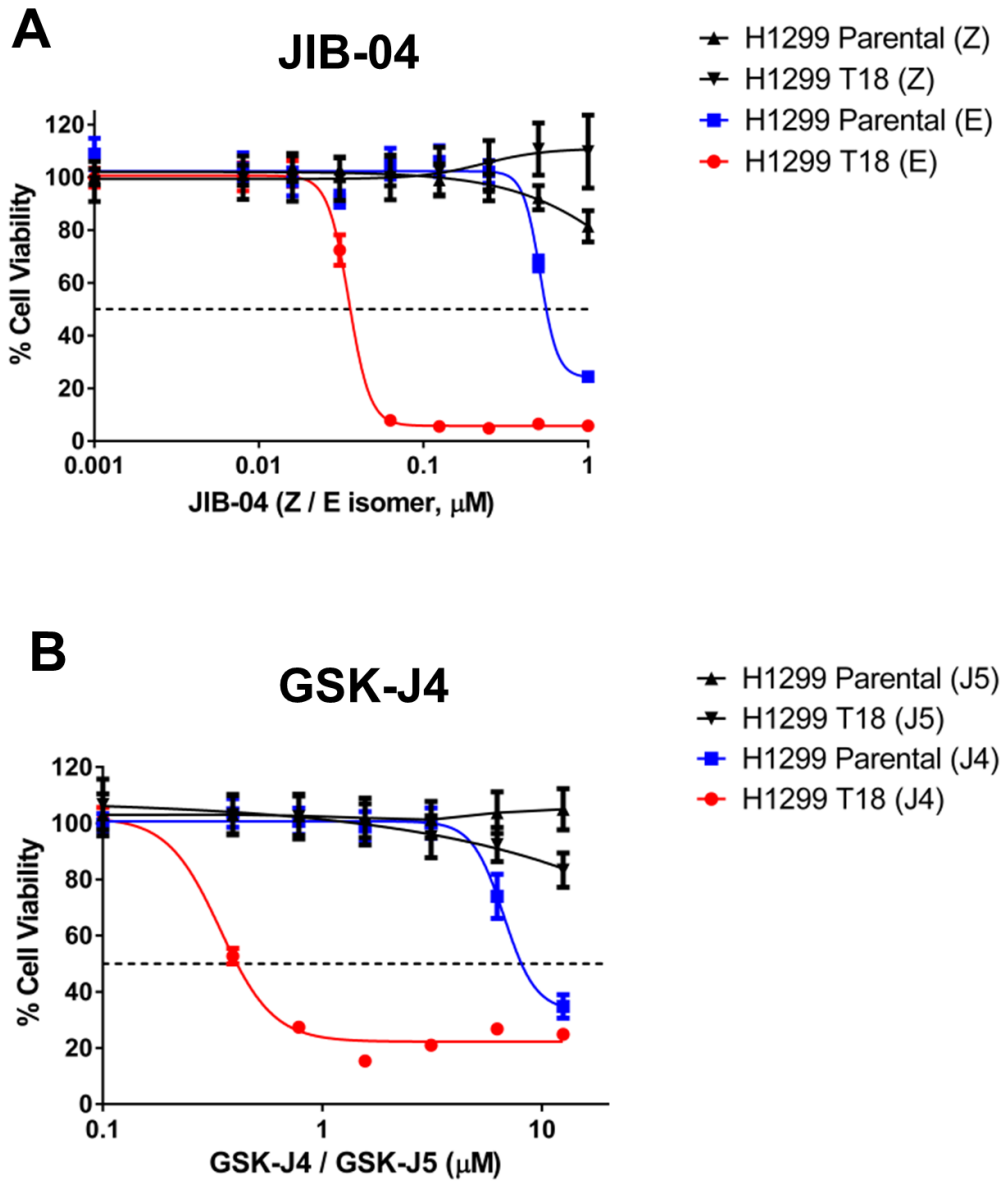

Figure 6.1 H1299 T18 taxane-platin resistant cells are hyper-sensitized to JIB-04 and GSK-J4, compared to H1299 parental cell line

H1299 T18 showed increased sensitivity to (A) JIB-04 as well as (B) GSK-J4, compared to H1299 parental cell line. There was no viability difference with the inactive isomers (JIB-04 Z isomer/ GSK-J5). Each assay was performed with 8 replicates per drug dose. Error bars indicate mean $\pm$ SD. Average IC_{50} values from multiple assays/replicates are indicated in Figure 6.3 E.

6.2 Isogenic series of H1299 resistant cells show progressively increasing sensitization to JmjC lysine demethylase inhibitors with increasing taxane-platin resistance

To investigate whether increased KDM expression and pharmacological sensitivity was directly correlated with increase in drug resistance, I queried the entire H1299 isogenic resistant series. H1299 resistant series that showed a progressive increase in KDM mRNA expression (shown previously in Figure 5.4), exhibited a consistent shift in JIB-04 dose response curves, illustrating increased sensitivity to JIB-04 with increasing taxane-platin drug resistance (Figure 6.2 A). Cells showed progressive sensitization to both JmjC inhibitors (JIB-04 and GSK-J4), as shown by consistent decrease in IC_{50} values from H1299 Parental to H1299 T18 resistant variant (Figures 6.2 B and C).

Figure 6.2

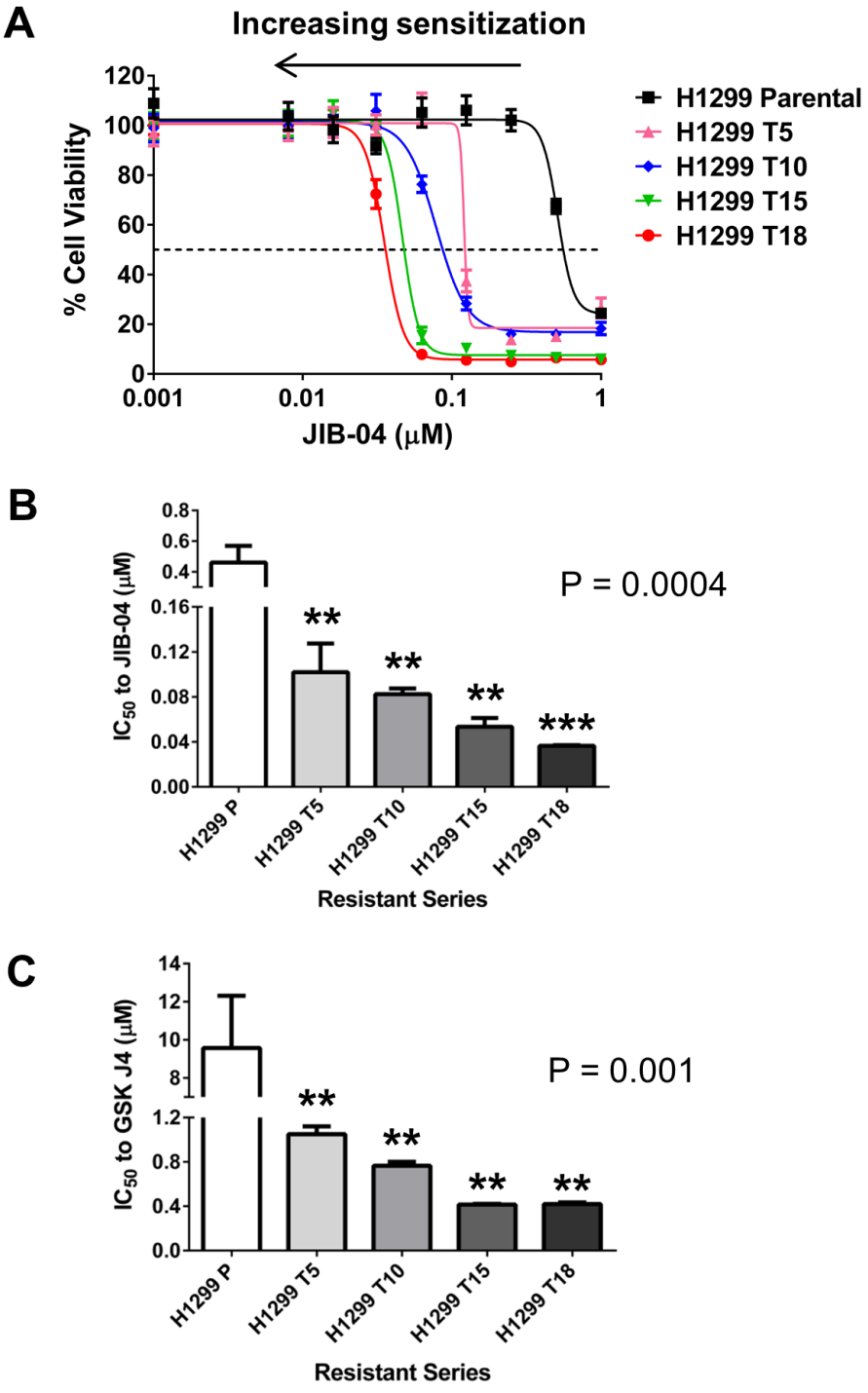
A
Increasing sensitization
% Cell Viability
JIB-04 (μM)
H1299 Parental
H1299 T5
H1299 T10
H1299 T15
H1299 T18
B
IC50 to JIB-04 (μM)
P = 0.0004
H1299 P
H1299 T5
H1299 T10
H1299 T15
H1299 T18
Resistant Series
C
IC50 to GSK J4 (μM)
P = 0.001
Resistant Series

Figure 6.2 Isogenic series of H1299 chemoresistant cells show progressively increasing sensitization to JIB-04 and GSK-J4 with increasing taxane-platin resistance

(A) Dose response curves for H1299 chemoresistant series showing progressive JIB-04 sensitization with increasing resistance to paclitaxel + carboplatin.

(B, C) IC_{50} plots for H1299 resistant series showing increasing sensitivity to JIB-04 and GSK-J4 with increasing resistance to standard chemotherapy. Data represents mean $\pm$ SD. Statistical significance was tested by one-way ANOVA, followed by Dunnett's multiple comparisons tests with H1299 Parental (H1299 P). P values on graphs denote significance from post-test for linear trend.

6.3 Taxane-platin resistant variants from other NSCLC cell lines (H1355, HCC4017 and H1693) also show increased sensitivity to JIB-04

To explore the universality of increased sensitivity of taxane + platin chemo-resistant NSCLC cells to JmjC KDM inhibitors, I tested other resistant cell line variants. H1355 T16 that had up-regulation of KDM genes (shown previously in Figure 5.3 B) showed higher sensitivity to GSK-J4 (Figure 6.3 A) and JIB-04 (Figure 6.3 B), compared to H1355 parental.

HCC4017 T5 and H1693 T8 resistant variants that were ~2-7 fold more resistant to paclitaxel + carboplatin than corresponding parental cell lines (Table 2.4 and Figure 3.7), were now ~2-3 fold more sensitive to JIB-04 (Figures 6.3 C-E). Interestingly, H1819 "parental" cell line was found to be originally very sensitive to JIB-04 (IC_{50} ~1 nM). Of note, H1693/H1819 is a matched cell line pair (before/after chemotherapy) derived from the same NSCLC patient. H1819 obtained after etoposide + cisplatin chemotherapy was more sensitive to JIB-04 compared to H1693 (Figure 6.3 D). Additionally, a cell line (HCC4047) derived from a NSCLC patient who was treated with paclitaxel + carboplatin chemotherapy in the clinic was found to be resistant to this standard doublet but sensitive to JIB-04 (Figure 6.3 F).

Figure 6.3

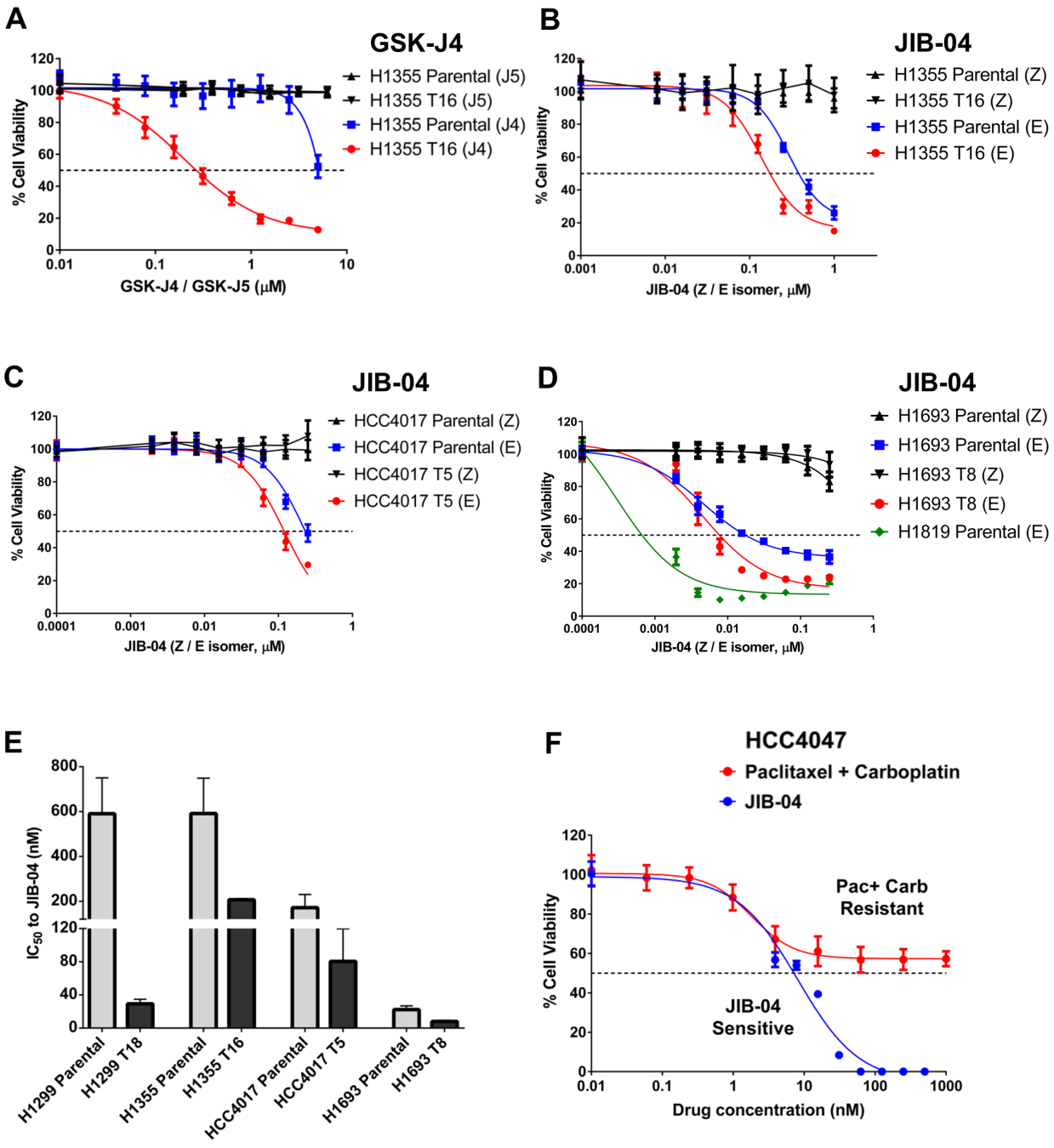
A
GSK-J4
H1355 Parental (J5)
H1355 T16 (J5)
H1355 Parental (J4)
H1355 T16 (J4)
% Cell Viability
GSK-J4 / GSK-J5 (μM)
B
JIB-04
H1355 Parental (Z)
H1355 T16 (Z)
H1355 Parental (E)
H1355 T16 (E)
% Cell Viability
JIB-04 (Z / E isomer, μM)
C
JIB-04
HCC4017 Parental (Z)
HCC4017 Parental (E)
HCC4017 T5 (Z)
HCC4017 T5 (E)
% Cell Viability
JIB-04 (Z / E isomer, μM)
D
JIB-04
H1693 Parental (Z)
H1693 Parental (E)
H1693 T8 (Z)
H1693 T8 (E)
H1819 Parental (E)
% Cell Viability
JIB-04 (Z / E isomer, μM)
E
IC50 to JIB-04 (nM)
H1299 Parental
H1299 T18
H1355 Parental
H1355 T16
HCC4017 Parental
HCC4017 T5
H1693 Parental
H1693 T8
F
HCC4047
Paclitaxel + Carboplatin
JIB-04
Pac+ Carb Resistant
JIB-04 Sensitive
% Cell Viability
Drug concentration (nM)

Figure 6.3 All NSCLC taxane-platin resistant variants show increased sensitivity to JIB-04, compared to parental cells

(A, B) H1355 T16 resistant variant was hyper-sensitized to GSK-J4 and JIB-04, compared to H1355 Parental cell line. Drug response was specific to the epigenetically active E or J4 isomers. No loss in cell viability was seen with the inactive Z or J5 controls. Error bars indicate mean ± SD.

(C) HCC5017 T5 resistant cell line was more sensitive to JIB-04, compared to HCC4017 Parental cell line. Error bars indicate mean ± SD.

(D) H1693 T8 taxane-platin resistant variant that was generated *in vitro* showed increased sensitivity to JIB-04, compared to H1693 Parental cell line. Matched cell line derived from the same NSCLC patient after etoposide + cisplatin chemotherapy in the clinic (H1819 Parental) also showed increased response to JIB-04 than H1693 Parental. Error bars indicate mean ± SD.

(E) JIB-04 IC_{50} values for parental/resistant NSCLC cell line pairs established *in vitro* (H1299, H1355, HCC4017 and H1693). IC_{50} values are from multiple independent assays. Data represents mean ± SEM. Two-way ANOVA, P value = 0.003

(F) HCC4047, a stage IIIA lung adenocarcinoma cell line derived from a patient who had received paclitaxel + carboplatin chemotherapy in the clinic, was found to be extremely resistant to this drug doublet in *in vitro* MTS assays (IC_{50} > 1000 nM) but very sensitive to JIB-04 (IC_{50} = 8.1 nM).

6.4 Hyper-sensitization of taxane-platin resistant cells is specific to JmjC KDM inhibitors over other classes of epigenetic drugs

In order to investigate whether the epigenetic vulnerability in taxane + platin chemo-resistant cells was specific to JmjC histone demethylase inhibitors, I evaluated compounds that target histone methyltransferases (HMT), LSD1 demethylase, histone acetyltransferases (HAT), histone deacetylases (HDAC), DNA methyltransferases (DNMT) as well as bromodomain inhibitors. H1299 T18 resistant variant was not hyper-sensitized to any of these drugs over H1299 parental cell line (Figure 6.4). H1299 T18 showed modest (< 4-fold) sensitization to some drugs (Figure 6.5). Selectivity ratios indicating fold change in IC_{50} values for H1299 and H1355 parental/resistant cell line pairs for all tested drugs are listed in Table 6.1.

My studies with JIB-04 and GSK-J4 have thus uncovered a specific, targetable epigenetic vulnerability that can be exploited therapeutically to treat NSCLCs that develop resistance to standard taxane + platin chemotherapy.

Figure 6.4

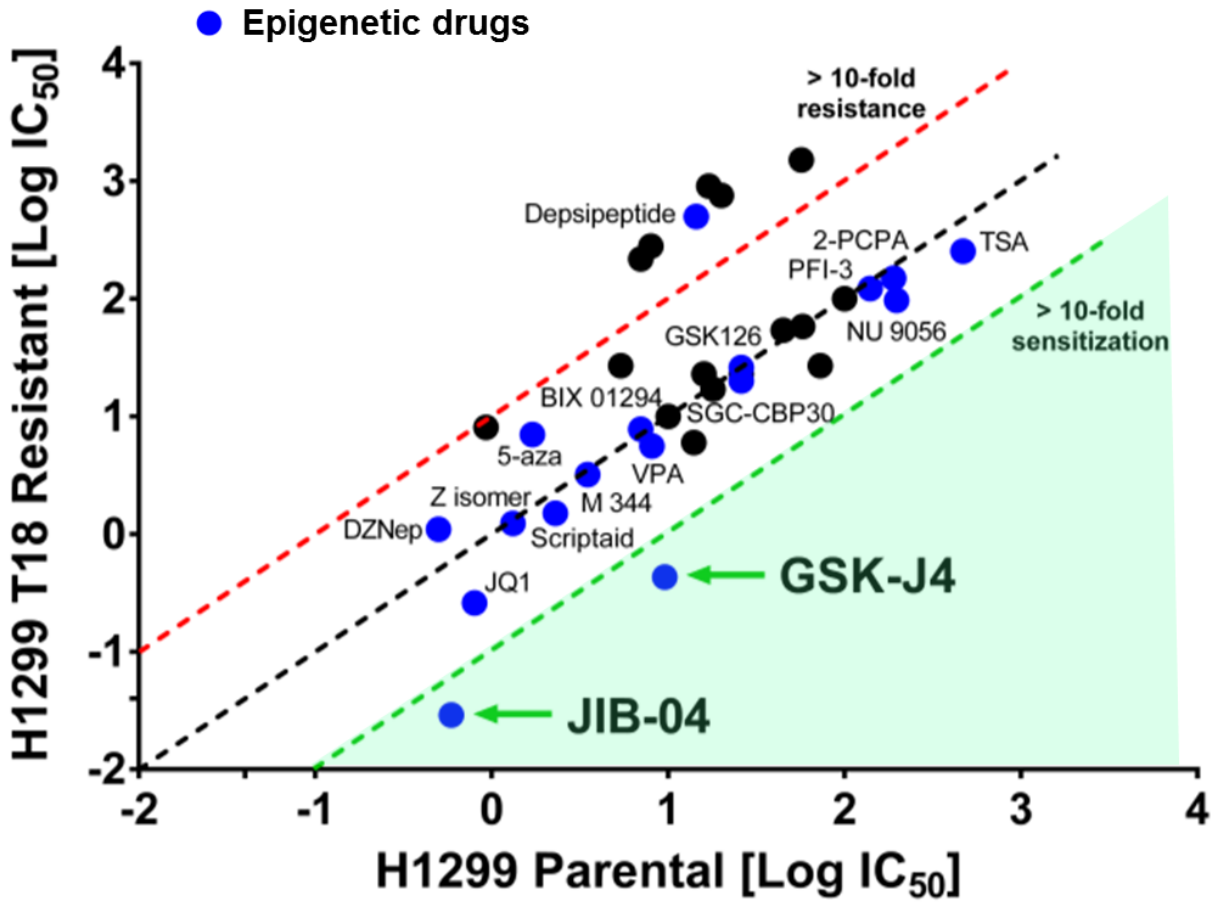

Figure 6.4 Hyper-sensitization of H1299 T18 taxane-platin resistant cells is specific to JmjC KDM inhibitors over other classes of epigenetic drugs

A comparison plot of IC_{50} values for standard, targeted and epigenetic drugs for H1299 T18 chemoresistant versus H1299 parental cells. Blue circles represent epigenetic drugs. Red dotted line denotes the 10-fold cut-off for cross-resistance and green dotted line is the 10-fold cut-off for sensitization of taxane + platin resistant cells. Only JIB-04 and GSK-J4 fall below the sensitivity threshold, illustrating specificity of response.

Figure 6.5

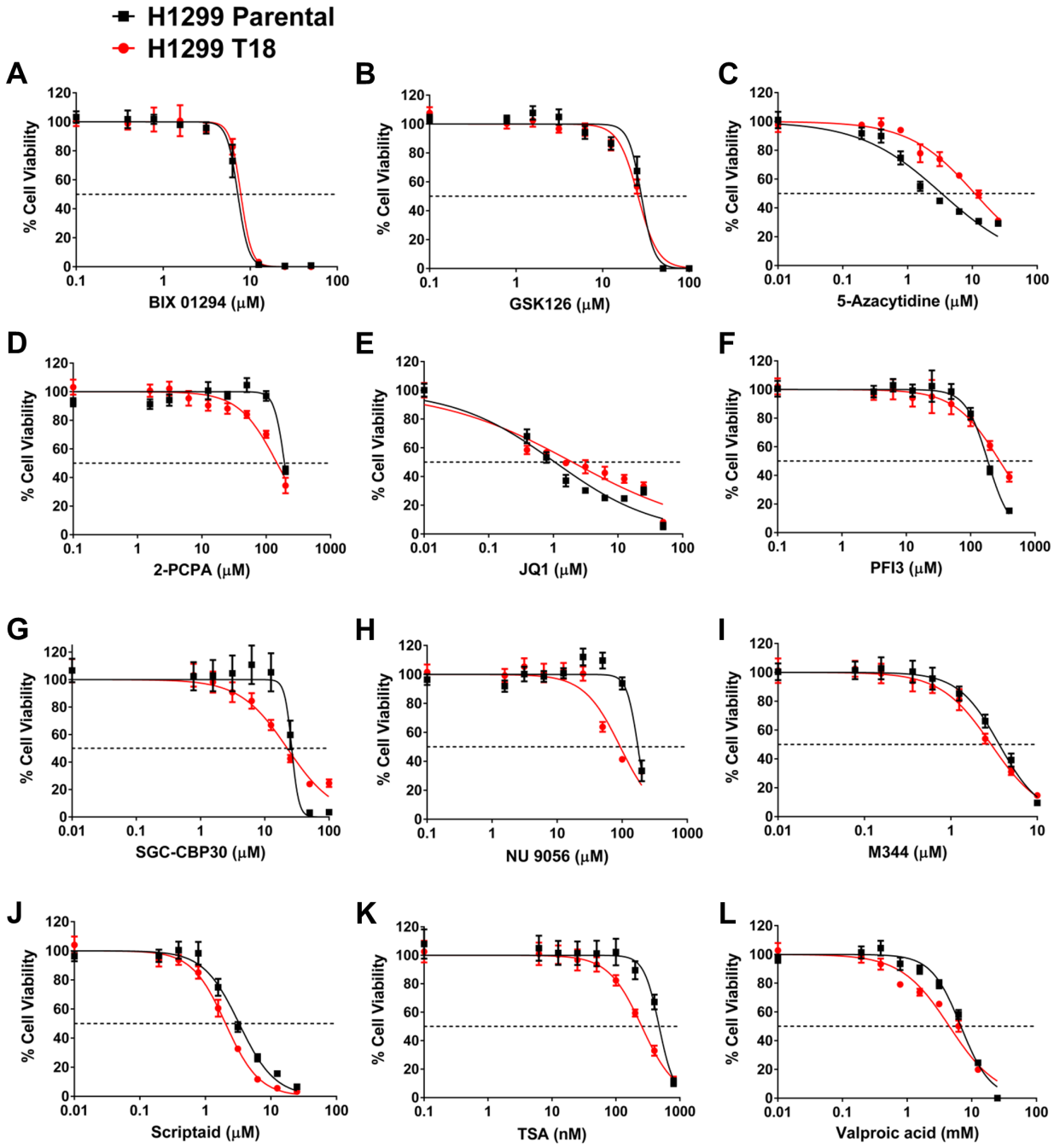

Figure 6.5 Dose response curves of H1299 Parental/ H1299 T18 pair to epigenetic inhibitors H1299 T18 cells did not show hyper-sensitization to other classes of epigenetic drugs: Inhibitors of HMTs (A─C), LSD1 (D), BRD (E-G), HATs (H) or HDACs (I─L).

Table 6.1 Selectivity Ratios of resistant cells to standard, targeted and epigenetic therapies

	Drug Class	Drugs	H1299 T18 SR	H1355 T16 SR
MDR1 substrates	Taxanes	Paclitaxel+Carboplatin	0.02	0.01
		Paclitaxel	0.03	0.02
		Docetaxel	0.03	0.002
	Anthracycline	Doxorubicin	0.04	0.25
	Vinca alkaloid	Vinorelbine	0.03	0.002
	HDAC	Depsipeptide	0.05	0.03
Other standard and targeted chemotherapies	NAMPT	FK866	0.1	2.1
	Platinum drug	Carboplatin	0.8	1.2
	Nucleoside metabolic + platin	Gemcitabine+Cisplatin	2.3	2.3
	Akt	MK-2206	0.7	1.8
	SMAC mimetic	JP1201	1.0	2.0
	Estrogen receptor agonist/antagonist	Tamoxifen	1.0	1.0
	Wnt	XAV939	2.7	1.0
	Topoisomerase	Irinotecan	1.1	2.7
	Bmi1/Ring1A	PRT 4165	1.0	1.4
Epigenetic drugs	DNMT	5-azacytidine	0.2	2.6
	Bromodomain	SGC-CBP30	1.3	0.9
		JQ1	0.6	6.6
		PFI 3	1.1	2.5
	HAT	NU 9056	2.0	1.0
	HDAC	M 344	1.1	1.8
		Valproic acid	1.4	1.3
		Scriptaid	1.5	1.4
		Trichostatin A	1.8	2.6
	HMT	BIX 01294	0.9	1.9
		DZNep	0.5	1.7
		GSK 126	1.0	0.8
	LSD1	2-PCPA	1.3	1.8
	JIB 04 Control	Z isomer (Inactive)	1.1	1.0
	JmjC KDMs	JIB-04 (E; Active)	20.3	2.8
		GSK J4	22.3	10.4

Selectivity Ratio 'SR' = [IC_{50} of Parental] / [IC_{50} of Resistant]

SR < 1 implies that variant cell lines (H1299 T18 and H1355 T16) are cross-resistant to these drugs

SR = 1 indicates no change in drug response between parental and variant cell lines

SR > 1 implies sensitization of chemo-resistant variants to these drugs; values denote fold reduction in IC_{50} values

6.5 Chemoresistant tumors show increased response to GSK-J4 and JIB-04 *in vivo*

To test the response of taxane-platin chemoresistant NSCLC cells to JIB-04 and GSK-J4 *in vivo*, subcutaneous xenografts of H1299 Parental and H1299 T18 cell lines were established. JmjC inhibitor treatment was given to tumor volume matched pairs, and mice were administered either vehicle or drug treatment once tumors reached ~150-200 mm3.

GSK-J4 was administered as a 100 mg/kg dose, by i.p. injections given every day for 10 days. GSK-J4 treatment caused a significant reduction in tumor volumes selectively in H1299 T18 xenografts ($P < 0.0001$) and not in H1299 parental tumors (Figure 6.6 A). Treated T18 tumors also showed a significant decrease in final tumor weights ($P = 0.007$) whereas there was no decrease in H1299 parental tumors (Figure 6.6 B).

For the JIB-04 study, tumor bearing mice were randomized to receive 5 mg/kg, 20 mg/kg or 50 mg/kg treatment or vehicle, given by gavage three times a week, for 2 weeks. At all tested doses, JIB-04 resulted in greater percent reduction in final tumor volumes of H1299 T18 xenografts compared to H1299 Parental (Figure 6.7 A). JIB-04 treatment preferentially slowed T18 tumor growth and decreased tumor growth rate as seen by increased tumor doubling times (Figure 6.7 B). There was also a significant decrease in final tumor weights of 50 mg/kg JIB-04-treated H1299 T18 xenografts ($P = 0.045$, Figure 6.7 C).

These pre-clinical studies confirm the enhanced sensitivity of taxane + platin chemoresistant tumors to JIB-04 and GSK-J4 *in vivo*, and provide proof-of-principle for potential use of JmjC demethylase inhibitors for targeting drug resistant NSCLCs in the clinic.

Figure 6.6

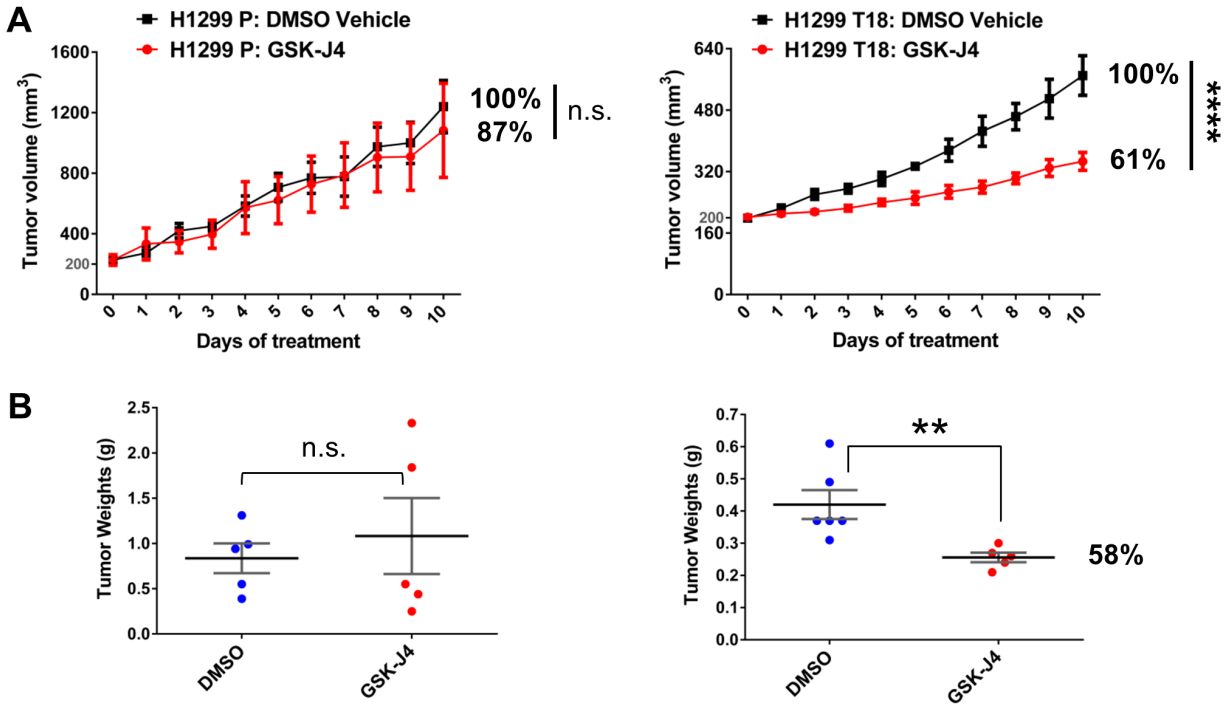

Figure 6.6 H1299 T18 taxane-platin resistant tumors show increased response to GSK-J4 treatment *in vivo*, than the chemo-sensitive parental tumors

(A) GSK-J4 treatment (100 mg/kg, every day, for 10 days) caused a significant decrease in final tumor volumes of H1299 T18 tumors and no response in H1299 parental tumors. Data represent mean ± SEM. Two-way ANOVA P value for H1299 T18 treatment response, ****P < 0.0001

(B) GSK-J4 treatment dramatically reduced final tumor weights in H1299 T18 xenografts (**P = 0.007), without significantly affecting H1299 Parental tumors (P = 0.6). Tumor weights were compared using two-tailed unpaired t-test.

Figure 6.7

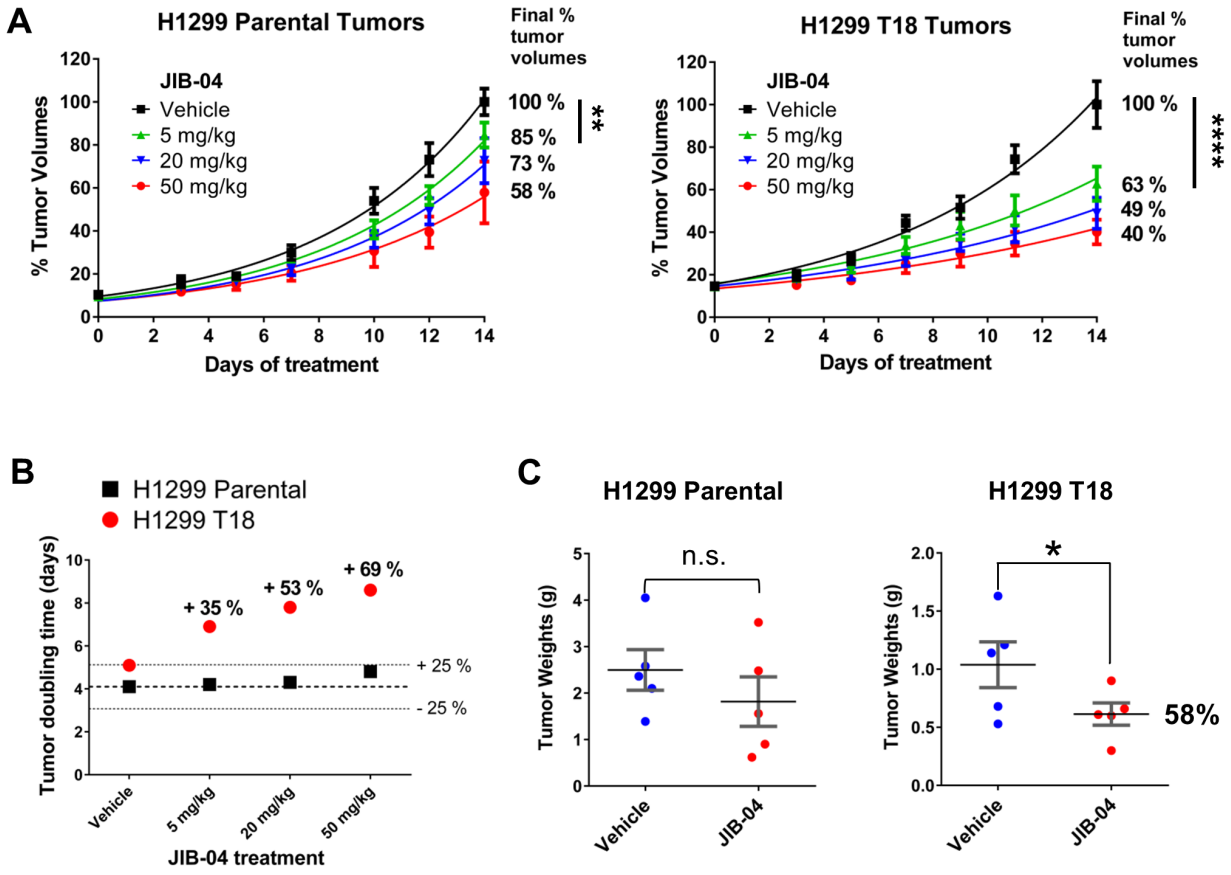

Figure 6.7 H1299 T18 chemoresistant tumors show increased response to JIB-04 *in vivo*, compared to H1299 parental tumors

(A) At all tested doses, JIB-04 significantly reduced tumor burden and caused a greater percent reduction in H1299 T18 tumor volumes when compared to H1299 Parental tumors. Data represent mean ± SEM. Exponential growth curves were fitted using non-linear regression. Drug response was compared using two-way ANOVA (5 mg/kg vs. vehicle group: H1299 Parental, **P = 0.0013 and H1299 T18, ****P < 0.0001).

(B) JIB-04 treatment slowed tumor growth and substantially increased doubling time of treated H1299 T18 tumors. Doubling time was derived from non-linear regression (exponential growth curves).

(C) Mice bearing H1299 T18 tumors, upon treatment with 50 mg/kg JIB-04, showed a greater decrease in final tumor weights at sacrifice. Data represents matched vehicle and treated tumors that were harvested on the same day (14-17 days after start of treatment). One-tailed unpaired t-test revealed a significant change in H1299 T18 treated tumors (*P = 0.045) compared to non-significant response in H1299 Parental tumors (P = 0.2).

CHAPTER SEVEN

JMJC KDM INHIBITORS CAUSE PARTIAL TRANSCRIPTIONAL REPROGRAMMING OF TAXANE-PLATIN RESISTANT CELLS

7.1 JIB-04 or GSK-J4 treatment led to several gene expression changes, selectively in H1299 T18 over H1299 parental cells

My findings show that taxane-platin resistant NSCLC cells are selectively sensitized to JmjC demethylase inhibitors over parental cells, both *in vitro* and *in vivo*. So, in order to explore the transcriptional changes induced by JIB-04 or GSK-J4 treatment in chemoresistant cells, drug treated H1299 T18 or H1299 parental cells were profiled by Illumina gene expression arrays. I determined mRNA expression changes that are caused by 24 h treatment with 0.2 μM JIB-04 or 1 μM GSK-J4 over DMSO treated controls in H1299 Parental and T18 cell lines (≥ 2-fold change, P value ≤ 0.05). In agreement with the enhanced sensitivity of T18 cells to JmjC KDM inhibitors, I observed that JIB-04 and GSK-J4 led to several gene expression changes selectively in H1299 T18 resistant cells (Figure 7.1 A, C) and minimal transcriptomic changes in H1299 parental cells (Figure 7.1 B, D). Roughly, about 5-6 times greater mRNA expression changes were detected in JIB-04 or GSK-J4 treated H1299 T18 cells compared to H1299 parental cells (corresponding to 523 versus 106 Illumina probes in JIB-04 treated, and 190 versus only 34 probes in GSK-J4 treated T18 versus parental cells).

Figure 7.1

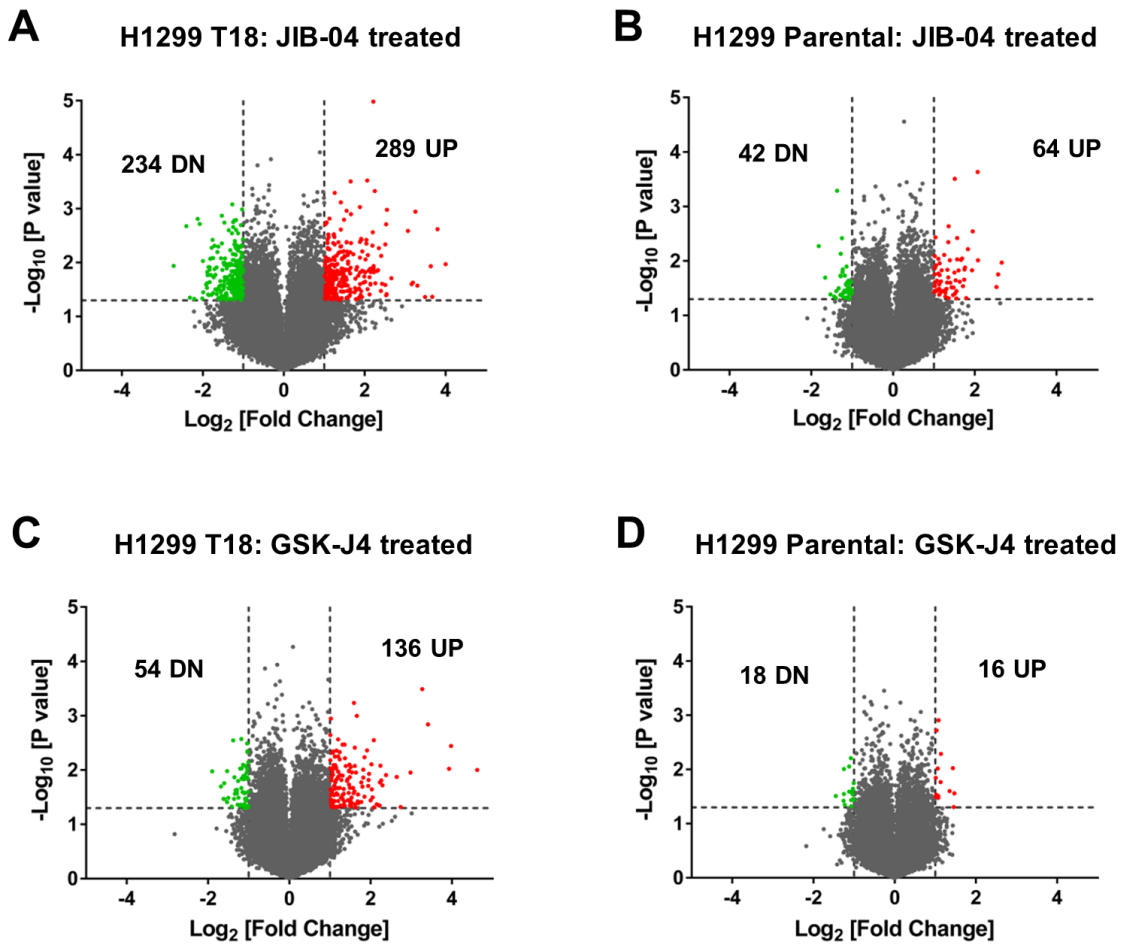

Figure 7.1 JIB-04 or GSK-J4 treatment led to several transcriptional changes, selectively in H1299 T18 cells over H1299 parental cells

(A, B) There were ~5-times more JIB-04 induced gene expression changes in H1299 T18, compared to treated H1299 Parental cells. Cells were treated for 24 h with 0.2 μM JIB-04.

(C, D) H1299 T18 cells showed ~6-times more GSK-J4 induced gene expression changes than parental cells, after 24 h of 1 μM drug treatment.

Analysis represents two biological replicates per treatment condition per cell line. Differentially expressed genes were filtered by ≥ 2-fold change and t-test P value ≤ 0.05

7.2 Transcriptional changes caused by JIB-04 and GSK-J4 in H1299 T18 cells show a significant overlap

Since I was studying gene expression changes after only a short 24 h drug exposure, I decided to expand the list of differentially expressed genes using a more liberal 1.5 fold change cutoff. Upon JIB-04 treatment, 1189 annotated genes (total 1469 Illumina probes) were found to be significantly altered in H1299 T18 cells, at t-test P value ≤ 0.05. Similarly, 552 annotated genes (total 710 Illumina probes) were differentially expressed in GSK-J4 treated H1299 T18 cells over DMSO controls, at $P \leq 0.05$. About 33% of GSK-J4 altered genes (181 genes) overlapped with JIB-04 altered transcripts (Figure 7.2), suggesting convergence of mechanisms.

Figure 7.2

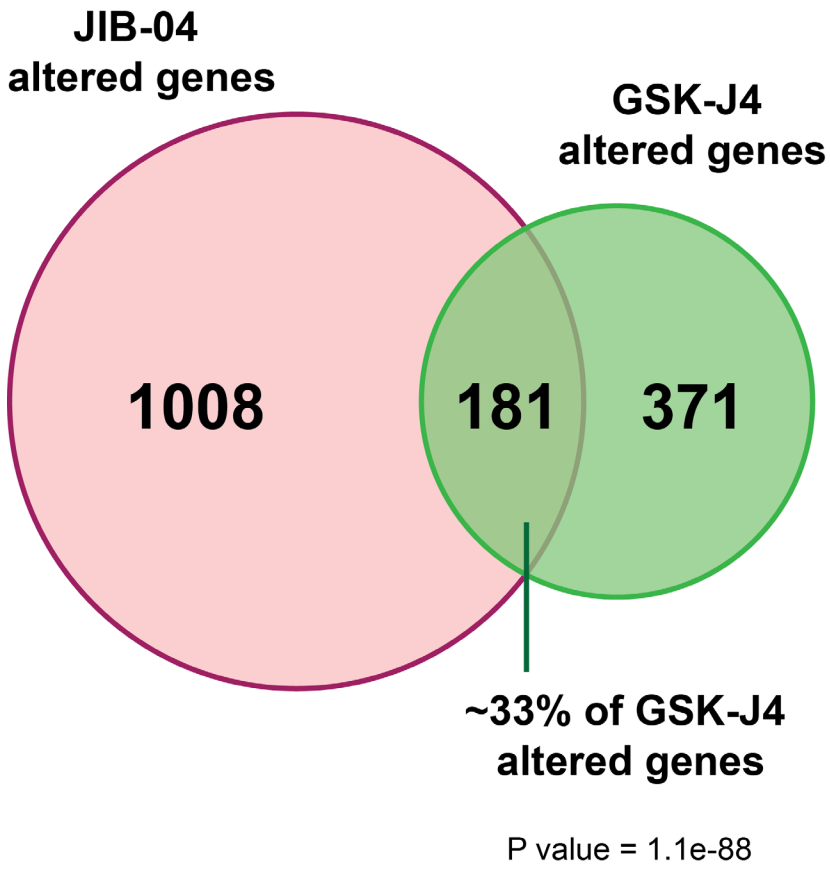

Figure 7.2 Transcriptional changes caused by JIB-04 and GSK-J4 in H1299 T18 cells show a significant overlap

Venn diagram illustrating extent of overlap between genes that were differentially expressed in H1299 T18 cells following 24 h of JIB-04 (0.2 μM) or GSK-J4 (1 μM) treatment. Plot represents differentially expressed genes that showed at least 1.5 fold changes and t-test P value ≤ 0.05. Significance of overlap was determined by hypergeometric test (P value = 1.1e-88). ~33% of GSK-J4 altered genes overlapped with JIB-04 altered gene set.

7.3 Expression changes seen in H1299 T18 after JIB-04 or GSK-J4 treatment represent 'partial reversal' of mRNA changes acquired after development of taxane-platin resistance

Since the targets of JIB-04 and GSK-J4 are epigenetic enzymes that have broad regulatory roles in activating/repressing gene transcription, it is likely that inhibition of these enzymes can alter expression of multiple genes, including those that are associated with response to drug stress or development of drug resistance. I asked whether such genes that were 'deregulated' in chemoresistant cells, were now reversed back to 'parental', drug-sensitive cellular state. I compared transcriptional changes induced by JmjC inhibitor treatment in H1299 T18 cells against gene expression changes in H1299 T18 over parental cell line. Indeed, after short 24 h exposure to 0.2 μM JIB-04 or 1 μM GSK-J4, I found a partial reversal of mRNA expression changes in H1299 T18 that had been acquired upon development of taxane-platin resistance (Figure 7.3 and Appendix B, C). ~200 genes were reversed after JIB-04 treatment and over 100 genes were reversed by GSK-J4. These epigenetic drugs were thus found to cause partial transcriptional reprogramming of chemoresistant cells.

Figure 7.3

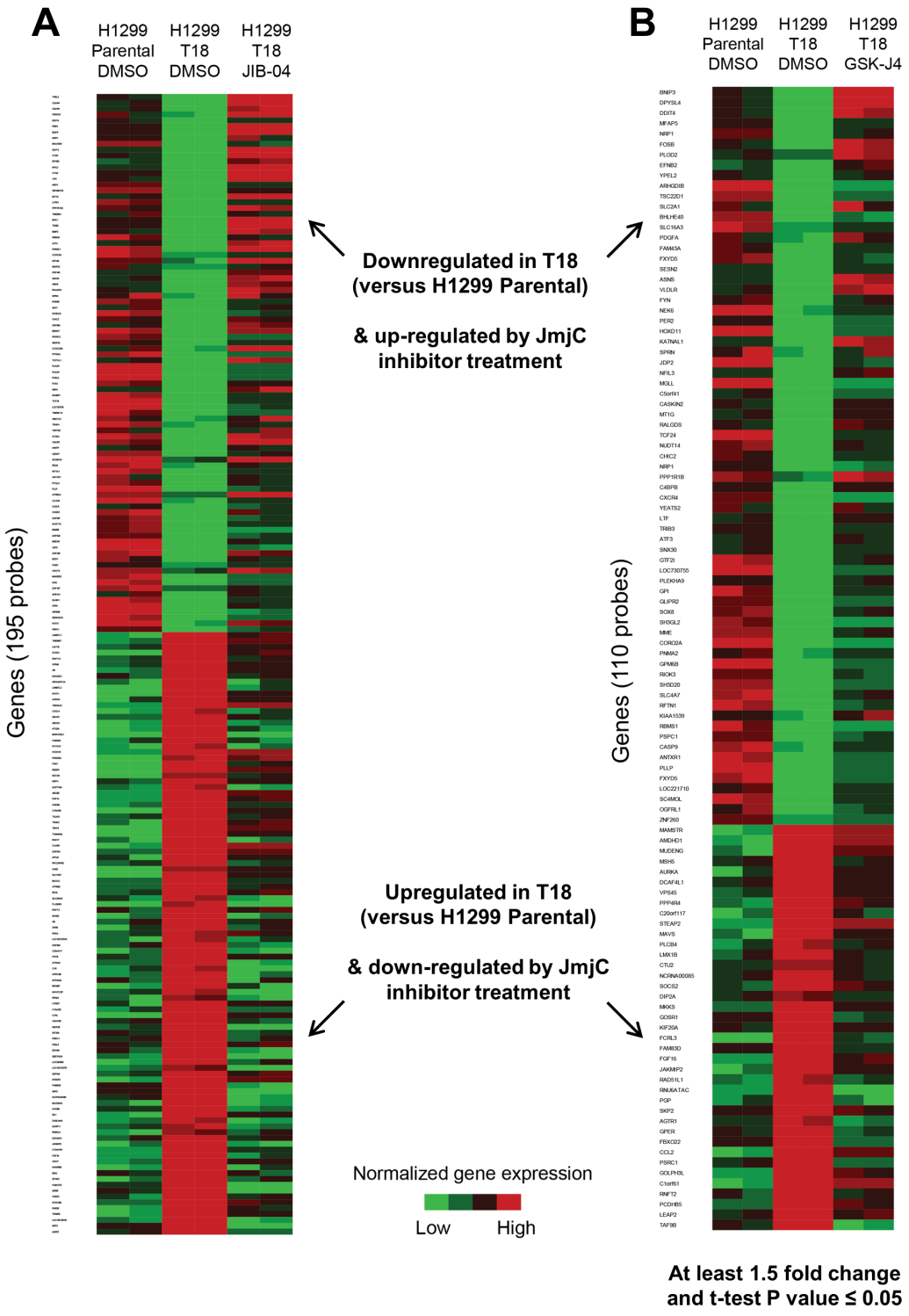
A
H1299 Parental DMSO
H1299 T18 DMSO
H1299 T18 JIB-04
Genes (195 probes)
B
H1299 Parental DMSO
H1299 T18 DMSO
H1299 T18 GSK-J4
Genes (110 probes)
Downregulated in T18 (versus H1299 Parental)
& up-regulated by JmjC inhibitor treatment
Upregulated in T18 (versus H1299 Parental)
& down-regulated by JmjC inhibitor treatment
Normalized gene expression
Low
High
At least 1.5 fold change and t-test P value ≤ 0.05

Figure 7.3 Short-term JIB-04 or GSK-J4 treatment leads to partial reversal of gene expression changes acquired in H1299 T18 taxane-platin resistant cells

H1299 T18 cells at low confluency (1 million cells in 15 cm dish) were treated with DMSO, JIB-04 (0.2 μM) or GSK-J4 (1 μM) for 24 h. DMSO treated H1299 parental cells were used as control. Heat maps represent subset of genes that showed significant expression changes in H1299 T18 (DMSO) over H1299 Parental (DMSO), and were reversed after short-term (A) JIB-04 or (B) GSK-J4 treatment. Data represents two biological replicates per sample. Differentially expressed genes showed at least 1.5 fold changes and t-test P value ≤ 0.05.

(A) 187 genes (represented by 195 Illumina v4 probes) whose expression in H1299 T18 was reversed after short-term JIB-04 treatment. Genes are ordered by fold change in H1299 T18 JIB-04 versus H1299 T18 DMSO. Gene at the top of the list showed 16-fold up-regulation, whereas the bottom-most gene was 5-fold down-regulated in JIB-04 treated H1299 T18 cells.

(B) 108 differentially expressed genes (represented by 110 illumina v4 probes) in H1299 T18 over parental cell line, which showed reversed expression after short-term GSK-J4 treatment. Genes are in descending order of fold change in H1299 T18 GSK-J4 versus H1299 T18 DMSO. Gene at the top of the list was 10-fold up-regulated, and the bottom-most gene was 3-fold down-regulated after GSK-J4 treatment.

List of genes can be found in Appendix B (for JIB-04) and Appendix C (for GSK-J4).

7.4 Gene set enrichment analysis reveals reversal of altered transcriptional programs in H1299 T18 cells after JIB-04 or GSK-J4 treatment

As JIB-04 and GSK-J4 caused partial reversal of gene expression in H1299 T18, I interrogated whether this represented reversal of specific transcriptional programs. I performed gene set enrichment analysis (GSEA) on differentially expressed gene lists representing JIB-04 and GSK-J4 induced mRNA changes in H1299 T18 cells (genes with at least 1.5 fold change, t-test P value ≤ 0.05). These pre-ranked gene lists were queried against curated gene sets (C2) from the molecular signatures database (MSigDB), and significantly enriched gene sets (FDR $\leq$ 0.25) between different datasets were further evaluated.

Firstly, I found a significant overlap between JIB-04 and GSK-J4 altered gene sets (116 common enrichments, Figure 7.4 A and Appendix D). Secondly, there was also a 'reversal' of certain transcriptional programs that were altered in taxane-platin resistant H1299 T18, compared to H1299 parental cells. Out of the 214 gene sets that were depleted in H1299 T18 over parental cells, 43 and 73 gene sets, respectively, were enriched by short-term GSK-J4 and JIB-04 treatment. Further, many of these T18 reversed gene sets in fact overlapped between JIB-04 and GSK-J4 drug treatments (38 common reversed, Figure 7.4 A and Appendix D). In agreement with my studies, this overlap included epigenetic gene sets representing genes with H3K4me3 and H3K27me3 marks (Meissner et al., 2008), as well as SUZ12 ChIP on chip targets (Ben-Porath et al., 2008), indicative of genes regulated by H3K27me3 (Figure 7.4 B).

Figure 7.4

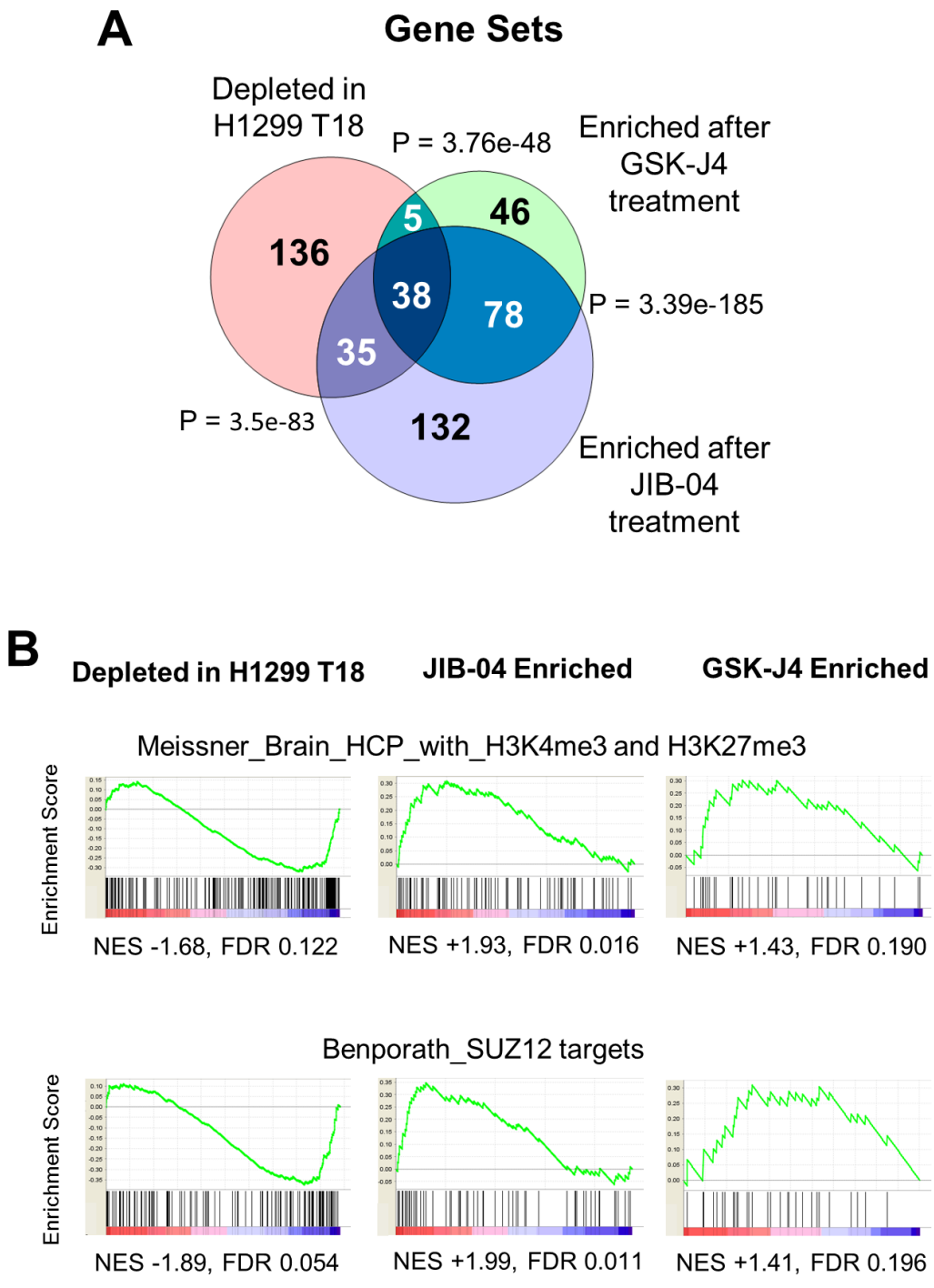
A
Gene Sets
Depleted in H1299 T18
P = 3.76e-48
Enriched after GSK-J4 treatment
136
5
46
38
78
P = 3.39e-185
35
P = 3.5e-83
132
Enriched after JIB-04 treatment
B
Depleted in H1299 T18
JIB-04 Enriched
GSK-J4 Enriched
Meissner_Brain_HCP_with_H3K4me3 and H3K27me3
Enrichment Score
NES -1.68, FDR 0.122
NES +1.93, FDR 0.016
NES +1.43, FDR 0.190
Benporath_SUZ12 targets
Enrichment Score
NES -1.89, FDR 0.054
NES +1.99, FDR 0.011
NES +1.41, FDR 0.196

Figure 7.4 Gene set enrichment analysis reveals reversal of certain transcriptional programs by JIB-04 or GSK-J4 treatment in H1299 T18 cells

(A) GSEA against curated gene sets from MSigDB revealed that several of the transcriptional programs that were altered in H1299 T18 drug resistant cells (depleted gene sets) were reversed/enriched by short-term JIB-04 or GSK-J4 treatment. FDR for gene set significance ≤ 0.25. P values for overlap are from hypergeometric tests.

(B) Reversed gene sets representing genes with H3K4me3 and H3K27me3 marks in the brain (top panel, Meissner et al.) and SUZ12 targets (bottom panel, Ben-Porath et al.).

NES, Normalized Enrichment Score.

CHAPTER EIGHT

JMJC KDM INHIBITORS SYNERGIZE WITH TAXANE-PLATIN CHEMOTHERAPY IN ELIMINATING AND PREVENTING EMERGENCE OF DRUG RESISTANT NSCLC COLONIES

8.1 JIB-04/GSK-J4 caused synergistic growth inhibition of chemoresistant colonies when combined with paclitaxel + carboplatin standard chemotherapy

Given the hypersensitivity of chemoresistant cells to JmjC KDM inhibitors, and the transcriptional reprogramming caused by these epigenetic drugs in resistant cells, I next asked whether JIB-04 or GSK-J4 would synergize with standard taxane + platin chemotherapy in killing chemoresistant lung cancer cells. Using JIB-04 or GSK-J4 doses that were pre-determined to not cause complete growth inhibition as single agents, I assessed the effect of combining these with paclitaxel + carboplatin doublet. Delta Bliss excess was calculated as the difference between expected and observed viability response from combination of these drugs (described in Methods section 2.2.3). I found that both JIB-04 and GSK-J4 caused synergistic growth inhibition of chemoresistant colonies from H1299 T18 treated with paclitaxel + carboplatin (synergy indicated by positive delta Bliss, Figure 8.1 A-B).

Figure 8.1

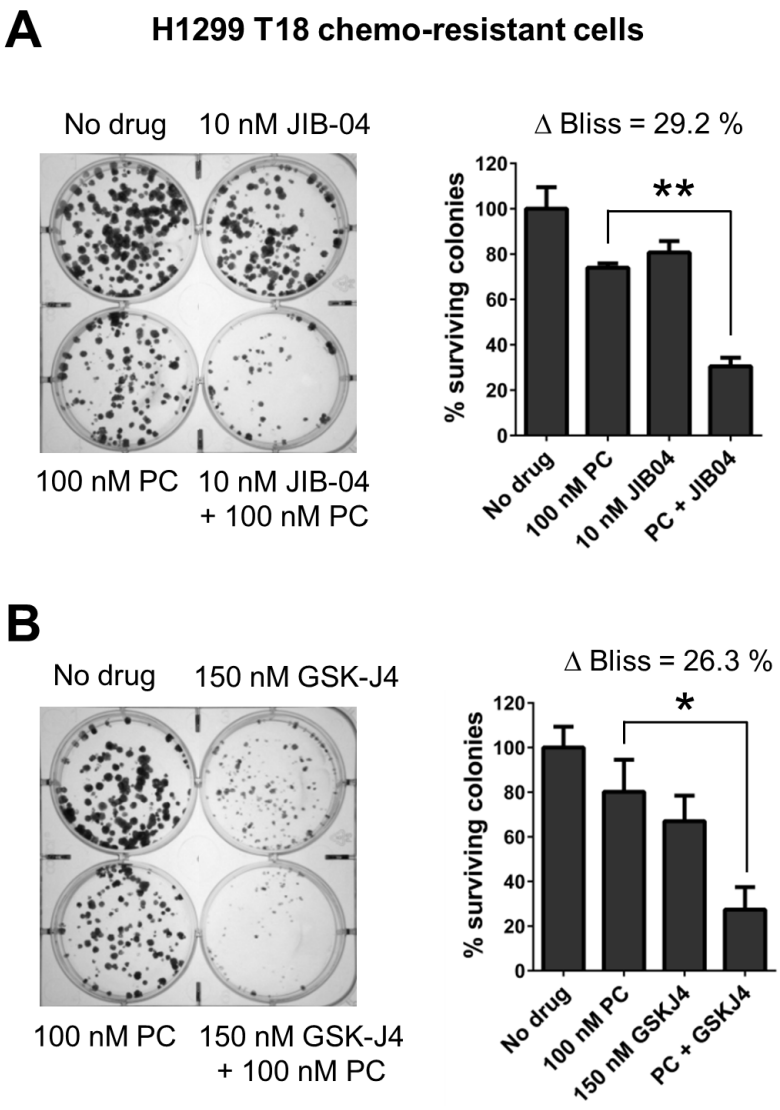

Figure 8.1 JIB-04 and GSK-J4 showed synergy with paclitaxel + carboplatin standard chemotherapy in inhibiting chemoresistant colonies

(A, B) Combination of JIB-04 (A) or GSK-J4 (B) with standard paclitaxel + carboplatin chemotherapy resulted in synergistic inhibition of colony formation of H1299 T18 chemoresistant cells. Response was greater than additive (indicated by positive delta Bliss). Error bars represent mean $\pm$ SD. P values are from unpaired t test (**P = 0.008 and *P = 0.05).

8.2 GSK-J4 prevented the emergence of taxane-platin drug-tolerant persister colonies from parental, chemo-sensitive NSCLC cell lines

Since JmjC KDM inhibitors synergized with paclitaxel + carboplatin standard treatment in abrogating drug resistant cells, I next tested whether this could be employed in blocking the emergence of drug resistance in the first place. I investigated this possibility by designing an assay that mimicked emergence of drug tolerant, surviving clones from chemo-sensitive mass cell population seeded in high density (10,000 – 20,000 cells) and exposed to doublet chemotherapy over 3-5 weeks. Drug concentration for paclitaxel + carboplatin doublet treatment for each cell line was determined based on individual drug response curves from standard 5 day MTS assays. Chemo-sensitive parental cells were exposed to taxane-platin drug doses that allowed for a surviving subpopulation. I evaluated the effect of sub-lethal doses of GSK-J4 (1-2 μM) in inhibiting survival and colony forming ability of these taxane-platin 'persister' cells. When used in combination, GSK-J4 prevented the emergence of paclitaxel + carboplatin drug-tolerant persister colonies from taxane-platin sensitive NSCLC cell lines (Figure 8.2).

Figure 8.2

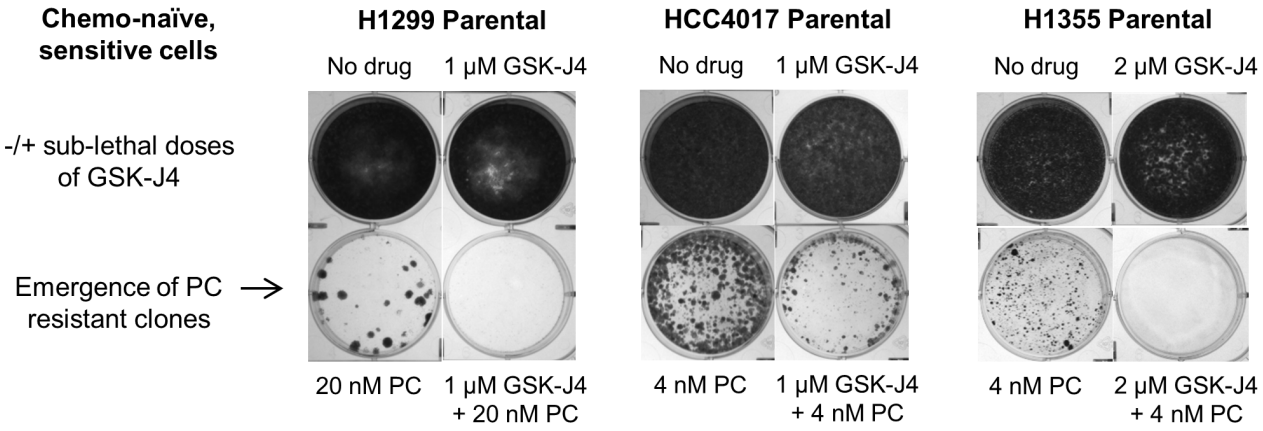

Figure 8.2 GSK-J4 prevented the emergence of taxane-platin drug-tolerant persister colonies from parental, chemo-sensitive NSCLC cell lines
Sub-lethal doses of GSK-J4 (1-2 μM) blocked the outgrowth of paclitaxel + carboplatin drug tolerant persister clones from parental NCI-H1299, HCC4017 and NCI-H1355 non-small cell lung cancer cell lines exposed to combination therapy over 3-5 weeks.

CHAPTER NINE

CONCLUSIONS AND FUTURE DIRECTIONS

9.1 Main Findings

My work using newly developed preclinical models of non-small cell lung cancer (NSCLC) resistance to standard taxane-platin doublet chemotherapy has identified upregulation of JumonjiC (JmjC) histone lysine demethylases (KDM) as an underlying epigenetic mechanism for drug resistance. Concomitant with increased KDM expression, taxane-platin resistant cells exhibited overall global reduction in H3K27me3 levels across the genome, compared to parental cell line. Chemoresistant NSCLC cell lines show increased sensitivity to JmjC KDM inhibitors, JIB-04 and GSK-J4, *in vitro* and *in vivo*. Using progressively resistant cell line series, my studies have established a connection between increased resistance to taxane-platin chemotherapy and progressive sensitization to JIB-04 and GSK-J4. JmjC KDM inhibitors synergistically inhibited taxane-platin resistant colonies from chemoresistant cell lines, and also blocked the outgrowth of drug-tolerant colonies from chemo-naïve, parental cell lines. My findings thus define JmjC KDMs as new therapeutic targets not only for the treatment of drug resistant NSCLCs, but also for preventing the emergence of taxane-platin drug-tolerant clones from chemo-sensitive tumors.

Figure 9.1

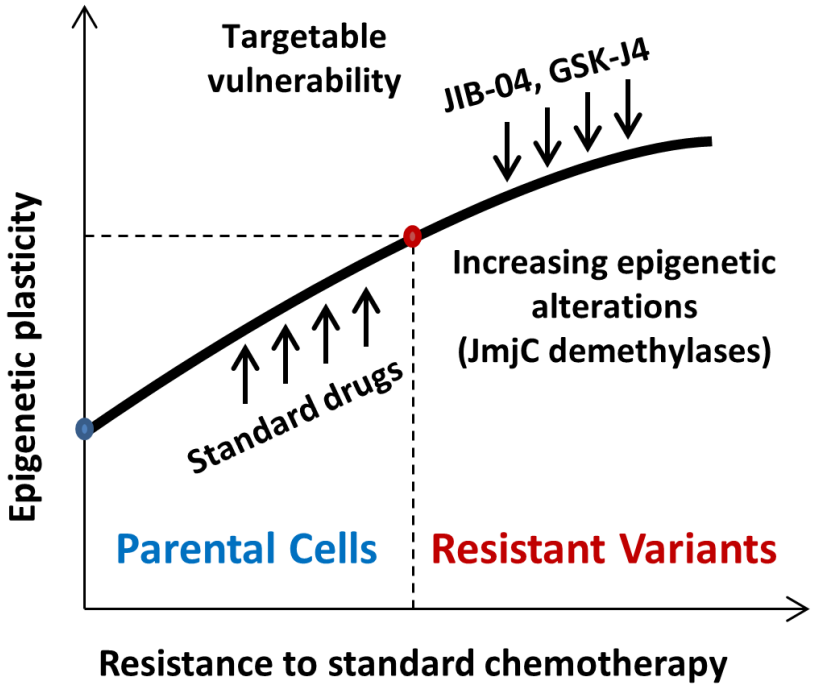

Figure 9.1 Model for increasing epigenetic plasticity during the development of resistance to standard chemotherapy

My studies reveal that upon treatment with standard paclitaxel + carboplatin chemotherapy, drug-surviving NSCLC parental cells accumulate increasing epigenetic alterations in the form of up-regulated JmjC histone lysine demethylases. This offers an opportunity for therapeutic targeting of resistant tumor cells with the pharmacological inhibitors, JIB-04 and GSK-J4.

Figure 9.2

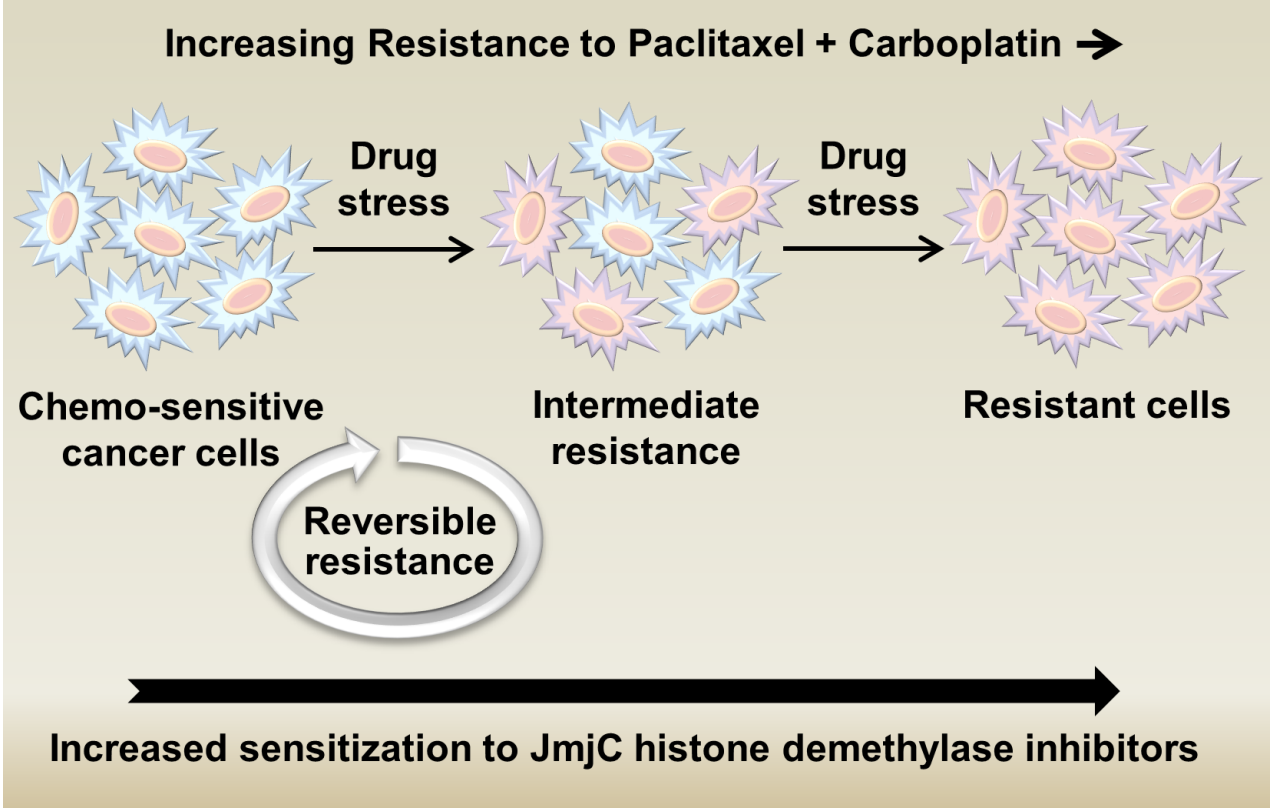

Figure 9.2 Graphical representation of increasing taxane-platin resistance in NSCLC and progressive sensitization to JmjC histone demethylase inhibitors
Upon long-term treatment with cycles of paclitaxel + carboplatin therapy, chemo-sensitive NSCLC cell lines developed increasing resistance to this standard chemotherapy doublet. Drug resistance was partially reversible upon drug-free culturing, suggesting epigenetic mechanisms. Correspondingly, resistant cells were progressively sensitized to JmjC histone lysine demethylase inhibitors (JIB-04 and GSK-J4).

9.2 Discussion

Previous studies have reported reversible, slow-cycling and dynamically evolving drug-tolerant subpopulations in cancer cells exposed to targeted therapy, such as “persister” populations expressing KDM5A in EGFR TKI drug tolerance (Sharma et al., 2010) or KDM5B in BRAFV600E inhibitor-resistant melanoma cells (Roesch et al., 2013). My work suggests that cancer cells may dynamically express these KDMs not only to survive the first contact with chemotherapeutic drugs as has been previously demonstrated, but that these persisters continue to accumulate increasing levels of epigenetic alterations during the progression of drug resistance. Chemoresistant cells continue to depend on KDMs for survival and appear to be epigenetically “addicted”, even after resistance has partially locked in, after several cycles of chemotherapy treatment. In addition, I found concurrent alterations in several KDMs in NSCLC cells resistant to taxane-platin standard chemotherapy although H3K27me3 demethylases were the more strongly upregulated. It is possible that different tumors may up-regulate different subsets of histone lysine demethylases during the progression of drug resistance. Also within the same tumor, it is likely that there exist distinct drug-tolerant subpopulations overexpressing different KDMs, a possibility that needs to be further explored. But because many of these enzymes are known to have overlapping functions, I propose that a viable strategy would be simultaneous inhibition of several of these JmjC demethylases. Clearly, taxane-platin drug resistant tumors depend on these KDMs for survival, given their hyper-sensitivity to JIB-04 and GSK-J4. Since epigenetic mechanisms are tightly inter-linked, I also tested other classes of epigenetic drugs for their differential response towards chemoresistant cells. This led to the discovery that the hyper-sensitization of taxane-platin resistant cells is specific to JmjC KDM class of epigenetic inhibitors.

Due to their ability to regulate multiple transcriptional programs at once, epigenetic mechanisms might serve to restore the cellular signaling balance or homeostasis (Mair et al., 2014) that is perturbed by chemotherapy stress and possibly "compensate" for gene expression changes induced by drug treatment. By doing so, these epigenetic modulators might act as a cellular defense mechanism to protect cells from further drug insults. My studies show that chemoresistant cells develop a dependence on histone lysine demethylases for their survival, and pharmacological KDM inhibition results in cell death in culture and *in vivo*. Furthermore, while utilizing this epigenetic "protective shield", drug surviving cells may in turn switch on multiple other resistance mechanisms such as expression of MDR drug efflux transporters, slow-cycling phenotype and EMT, as was seen in the developed chemo-resistant cell lines. The JmjC KDM inhibitor GSK-J4 prevented the emergence of taxane-platin drug tolerant clones from chemo-naive parental cell lines, thereby offering an epigenetic strategy for eliminating and preventing the outgrowth of drug-tolerant tumor subpopulations.

The presence of MDR drug efflux phenotype in chemoresistant cell lines also raises the question of whether these cells exhibit any other molecular or phenotypical features of cancer stem cells, knowing that tumor-initiating side-population cells overexpress ABC transporters (Ho et al., 2007). Some past studies have demonstrated elevation of ALDH+ or CD133+ cell subpopulation in drug treated cancer cells (Bertolini et al., 2009; Liu et al., 2013; Shien et al., 2013). While I did not see any enrichment in ALDH+ or CD133+ cell subpopulation in chemoresistant variants, microarray data revealed up-regulation of *ALDH1A3* isoform in H1299 T18 and gene expression changes in several members of Notch, Wnt and TGF-β pathways that have been widely implicated in stem-ness (Takebe et al., 2011). Moreover, the slow-cycling nature and EMT-like phenotypes of resistant cell lines also concur with some previous findings

on stem cell-like characteristics of drug resistant cells (Kemper et al., 2014; Roesch et al., 2010; Voulgari and Pintzas, 2009) and suggest phenotypic switching.

Given the differential response of chemoresistant cells to JmjC KDM inhibitors, it was interesting to see that JIB-04 or GSK-J4 treatment induced several transcriptional changes selectively in the taxane-platin resistant variant, with minimal changes in parental cells. Further, these mRNA changes reflected partial reversal of the gene expression profile acquired upon development of taxane-platin resistance. These molecular insights into transcriptional reprogramming and the hyper-sensitization phenotype of chemoresistant cells to JIB-04 and GSK-J4 pave a rational way towards developing JmjC KDM inhibitor therapy to target taxane-platin resistant lung cancers in the clinic. Also, since previous studies from our laboratory have shown that normal human bronchial epithelial cells are not sensitive to JIB-04 (Wang et al., 2013), this offers a wide therapeutic window for cancer therapy and raises the possibility of extending the utility of JmjC histone lysine demethylase inhibitors in other drug resistant solid tumors.

Finally, the 35-gene preclinical resistance signature and its ability to predict cancer recurrence in neoadjuvant chemotherapy treated NSCLC patients, presents a clear clinical translational path for biomarker development in future studies. Such biomarkers could potentially aid in identifying which patients are responding well to standard chemotherapy and which patient tumors would eventually develop recurrence. JmjC KDM targeting of the tumors that show signs of emerging drug-tolerant clones could help in preventing development of chemoresistance and cancer relapses.

9.3 Ongoing or Future Studies

My studies thus far have uncovered increased expression of several members of JmjC histone lysine demethylase family in taxane-platin drug resistant NSCLCs. However, it remains unanswered whether drug-tolerant persister cells survive and outgrow due to simultaneous up-regulation of multiple KDMs on a "single-cell level" or alternatively, distinct persister clones exist within the surviving population, each overexpressing a different KDM that confers that clone with the ability to survive under chemotherapy stress. This question could be potentially addressed in future studies by performing single cell quantitative PCR or single-cell RNA-Seq (Wu et al., 2014) on resistant cells to determine variation in KDM expression pattern between different cells within a resistant population. Further, single cell ChIP-Seq analyses (Rotem et al., 2015) may reveal alterations in histone methylation in individual cells. Such studies on parental cells might also help in understanding whether there are pre-existing drug-tolerant or "resistance-primed" cells in the parental tumor cell population that are likely to adapt more easily under drug stress. After uncovering the extent of involvement of different KDMs in causing drug resistance, a systematic genetic knockdown approach (using shRNAs or CRISPRs) could also be undertaken in different oncogenotypes of NSCLC cell lines to test if knocking down one or more of such KDMs at once can recapitulate the effect of pharmacological inhibition in targeting or preventing drug resistance.

Availability of more standard chemotherapy-treated NSCLC patient tumor specimens would aid biomarker development in future studies. Analyses of such tumors by immunohistochemistry or customized quantitative PCR array for 35 genes in my resistance signature as well as KDM gene family will enable better understanding of the prognostic power

of these resistance markers. Further, if matched chemotherapy-responsive and recurrent tumors from the same patient are made available, this would greatly expedite such studies in establishing a direct correlation between biomarker expression post chemotherapy and development of drug resistance and tumor relapse. Predicting which patients are responding to chemotherapy and which are likely to develop resistant, recurrent tumors would help in informing therapeutic decisions in the future.

Apart from taxane-platin doublet therapy, other standard chemotherapy agents that are administered to NSCLC patients include vinorelbine, gemcitabine and pemetrexed. Whether JmjC KDMs are also up-regulated in development of resistance to these agents remains undefined. It would be necessary to investigate whether combination treatment with JmjC KDM inhibitors can also prevent the outgrowth of persister clones that are tolerant to vinorelbine, gemcitabine or pemetrexed. Knowing the connection between KDM5A and resistance to EGFR targeted therapy (Sharma et al., 2010) and KDM5B in BRAFV600E targeted vemurafenib resistance (Roesch et al., 2013), it appears that histone demethylase driven drug tolerance might be more generalized and not restricted to any one chemotherapy. If this is proven to be the case, then special attention needs to be invested in developing new drugs to expand the small molecule repertoire of available JmjC KDM inhibitors. Such inhibitors could be incorporated into standard and targeted combination treatment regimens, to overcome drug resistance in the clinic.

Finally, it would be important to study genetic mutations acquired upon development of taxane-platin drug resistance in my cell line models and uncover any link between such mutations and KDM up-regulation. Recent studies have revealed the existence of oncogenic K27M mutation of histone H3.3 (*H3F3A* gene) in pediatric brainstem gliomas that causes

reduction in H3K27 methylation and consequently, increases susceptibility to the H3K27 demethylase inhibitor GSK-J4 (Hashizume et al., 2014). Whether taxane-platin resistant NSCLC cells develop any such mutations in histones or epigenetic enzymes remains undetermined. My taxane-platin resistant NSCLC cell lines (H1299 T18 and H1355 T16) were recently subjected to whole exome sequencing. Comparative analysis of exome-seq data with parental H1299 and H1355 cell lines is in progress and once available, should reveal interesting insights into the acquired mutations in resistant cell lines, and connection (if any) between genetic mutations and epigenetic mechanisms in NSCLC drug resistance.

APPENDICES

APPENDIX A. SWEAVE DOCUMENTATION FOR MICROARRAY ANALYSES

Introduction

This section includes R documentation for microarray analysis in Chapter 4 and Chapter 5, Section 5.1. Significantly altered genes were identified at a false discovery rate (FDR) of 0.1, from taxane-platin resistant cell line series (H1299 and H1355) by fitting linear regression model on gene expression data using log transformed IC_{50} values. For xenograft microarray data, student's t test was used for differential gene expression analysis at FDR of 0.1. After intersection of gene lists from cell lines and xenografts, 35 genes (14 up regulated and 21 down regulated) were obtained. The 35 gene pre-clinical signature was tested on 65 NSCLC patients who had received neoadjuvant chemotherapy. Unsupervised clustering using 35 genes separated the 65 patients into two groups. Kaplan-Meier (K-M) survival curve for recurrence-free survival analysis showed that group 2 has significantly worse prognosis. Multivariate Cox regression model for the 35 genes showed that the up-regulated gene ***KDM3B*** has the largest hazard ratio for poor cancer recurrence-free survival.

Microarray data were pre-processed by R package mbcb for background correction, then log-transformed and quantile-normalized with the R package preprocessCore. The gene-level expression was obtained by averaging the normalized probes intensity value if multiple probes mapped to the same gene.

Before running the code, put the data in the same folder with the code.

Statistics Analysis

H1299 and H1355 linear regression model

1. Set the working environment and call the library package

```
setwd("~/Documents/YY_Project/Maithili/SWEAVE/")
#library(preprocessCore)
library(ClassComparison)

## Loading required package: oompaBase

library(survival)
library(VennDiagram)

## Loading required package: grid

library(siggenes)

## Loading required package: Biobase
## Loading required package: BiocGenerics
## Loading required package: parallel
##
## Attaching package: 'BiocGenerics'
##
## The following objects are masked from 'package:parallel':
##
##     clusterApply, clusterApplyLB, clusterCall, clusterEvalQ,
##     clusterExport, clusterMap, parApply, parCapply, parLapply,
##     parLapplyLB, parRapply, parSapply, parSapplyLB
##
## The following object is masked from 'package:ClassComparison':
##
##     as.data.frame
##
## The following object is masked from 'package:oompaBase':
##
##     as.data.frame
##
## The following object is masked from 'package:stats':
##
##     xtabs
##
## The following objects are masked from 'package:base':
##
##     anyDuplicated, append, as.data.frame, as.vector, cbind,
##     colnames, duplicated, eval, evalq, Filter, Find, get,
##     intersect, is.unsorted, lapply, Map, mapply, match, mget,
##     order, paste, pmax, pmax.int, pmin, pmin.int, Position, rank,
##     rbind, Reduce, rep.int, rownames, sapply, setdiff, sort,
##     table, tapply, union, unique, unlist
```

```
##
## Welcome to Bioconductor
##
##     Vignettes contain introductory material; view with
##     'browseVignettes()'. To cite Bioconductor, see
##     'citation("Biobase")', and for packages 'citation("pkgname")'.
##
## Loading required package: multtest
## Loading required package: splines
```

```
library(gplots)
```

```
##
## Attaching package: 'gplots'
##
## The following object is masked from 'package:multtest':
##
##     wapply
##
## The following object is masked from 'package:oompaBase':
##
##     redgreen
##
## The following object is masked from 'package:stats':
##
##     lowess
```

2. Load normalized gene level expression data (preprocess procedure described in the method)

```
load("cell_line.RData")
```

3. Run core function/analysis for H1299 Linear regression model for microarray at different time series with log transformed drug response IC50.

```
# IC 50
ic50=c(rep(9.2, 5), rep(53, 2), rep(190, 2), rep(490, 2), rep(943, 3))
ic50=log(ic50) # log transform, otherwise est is too big.

# linear function
lm.ic=function(x){
  x=as.numeric(x)
  lm.x=lm(x~ic50)
  lm.co=summary(lm.x)$coefficients
  return(t(c(lm.co[2, 1], lm.co[2, 4])))
}

dim(df.1299)
```

```
## [1] 20549    19
```

```
head(df.1299[,1:5])
```

```
##   gene.id n gene.symbol H1299.Parental.1 H1299.Parental.2
## 1       1 2        A1BG         3.538114         3.530899
## 2       2 1         A2M         2.623364         3.244314
## 3       9 3        NAT1         3.791201         3.896611
## 4      10 1        NAT2         2.965261         3.086720
## 5      12 1    SERPINA3         2.933633         3.332563
## 6      13 1       AADAC         2.845070         3.086720
```

```
colnames(df.1299)
```

```
##  [1] "gene.id"          "n"                "gene.symbol"
##  [4] "H1299.Parental.1" "H1299.Parental.2" "H1299.Parental.3"
##  [7] "H1299.Untr.1"     "H1299.Untr.2"     "H1299.T5.1"
## [10] "H1299.T5.2"       "H1299.T10.1"      "H1299.T10.2"
## [13] "H1299.T15.1"      "H1299.T15.2"      "H1299.T18.1"
## [16] "H1299.T18.2"      "H1299.T18.3"      "est"
## [19] "p.value"
```

```
apply(df.1299[1:5, cell.1299], 1, lm.ic)
```

```
##                 1           2            3           4          5
## [1,] -0.005878157 -0.04970737 -0.166829025 0.008405362 0.79070808
## [2,]  0.884844954  0.20710959  0.003930657 0.826502466 0.00106438
```

```
est=apply(df.1299[, cell.1299], 1, lm.ic)
est=t(est)
est=data.frame(est)
head(est)
```

```
##             X1          X2
## 1 -0.005878157 0.884844954
## 2 -0.049707375 0.207109593
## 3 -0.166829025 0.003930657
## 4  0.008405362 0.826502466
## 5  0.790708076 0.001064380
## 6  0.057528835 0.283359856
```

```
names(est)=c("est", "p.value")
head(est)
```

```
##            est     p.value
## 1 -0.005878157 0.884844954
## 2 -0.049707375 0.207109593
## 3 -0.166829025 0.003930657
## 4  0.008405362 0.826502466
## 5  0.790708076 0.001064380
## 6  0.057528835 0.283359856
```

```
df.1299=cbind(df.1299, est)
```

```
p.1299=cutoffSignificant(Bum(df.1299$p.value), fdr)
p.1299

## [1] 0.02927903

table(df.1299$p.value < p.1299)

##
## FALSE  TRUE
## 16797  3752

table(df.1299$p.value < p.1299 & df.1299$est < 0)

##
## FALSE  TRUE
## 18673  1876

table(df.1299$p.value < p.1299 & df.1299$est > 0)

##
## FALSE  TRUE
## 18673  1876

id.up.1299=df.1299$gene.id[df.1299$p.value < p.1299 & df.1299$est > 0]
id.down.1299=df.1299$gene.id[df.1299$p.value < p.1299 & df.1299$est < 0]


# volcano plot: p valu only
par(mar=c(5, 5, 2, 1))
plot(df.1299$est, -log10(df.1299$p.value), xlab="Est of coefficients", cex=0.
5,
     ylab="P value (-log10)", cex.lab=2, cex.axis=1.5, bty="n", col="blue", p
ch=20,
     yaxt="n")
axis(2, at=c(0, 2, 4, 6, 8), labels=c(1, 0.01, 0.0001, 0.000001, 0.00000001),
cex.axis=1.5)
points(df.1299$est[df.1299$p.value < p.1299 & df.1299$est > 0],
       -log10(df.1299$p.value[df.1299$p.value < p.1299 & df.1299$est > 0]), c
ol="red",
       pch=20)
points(df.1299$est[df.1299$p.value < p.1299 & df.1299$est < 0],
       -log10(df.1299$p.value[df.1299$p.value < p.1299 & df.1299$est < 0]), c
ol="green",
       pch=20)
table(df.1299$p.value < p.1299 & df.1299$est > 0)

##
## FALSE  TRUE
## 18673  1876

table(df.1299$p.value < p.1299 & df.1299$est < 0)
```

```
##
## FALSE  TRUE
## 18673  1876

legend("topleft", c("Upregulated:      1876", "Downregulated: 1876"),
       col=c("red", "green"), pch=20, bty="n")
```

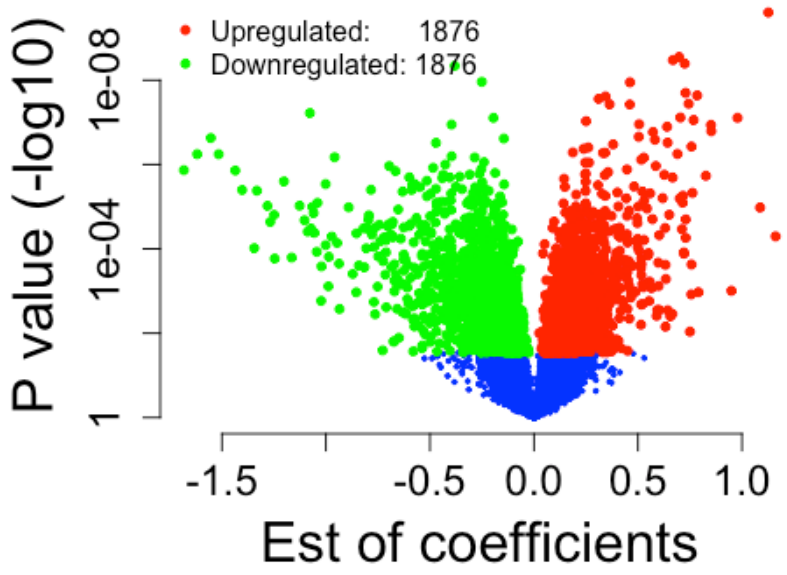

4. Run core function/analysis for H1355

```
# IC 50
ic50=c(rep(2.2, 5), rep(15, 2), rep(25, 2), rep(245, 2), rep(315, 3))
ic50=log(ic50) # log transform, otherwise est is too big.
# significant p values will enrich.
ic50

##  [1] 0.7884574 0.7884574 0.7884574 0.7884574 0.7884574 2.7080502 2.7080502
##  [8] 3.2188758 3.2188758 5.5012582 5.5012582 5.7525726 5.7525726 5.7525726

# linear function
dim(df.1355)

## [1] 20549    19

head(df.1355[,1:5])

##   gene.id n gene.symbol H1355.Parental.1 H1355.Parental.2
## 1       1 2        A1BG         3.980461         3.570940
## 2       2 1         A2M         2.705274         2.888426
## 3       9 3        NAT1         4.303963         3.966284
## 4      10 1        NAT2         3.796795         3.593245
```

```
## 5      12 1    SERPINA3         3.229223         3.493975
## 6      13 1       AADAC         4.967962         5.713092
```

```
colnames(df.1355)
```

```
##  [1] "gene.id"          "n"                "gene.symbol"
##  [4] "H1355.Parental.1" "H1355.Parental.2" "H1355.Parental.3"
##  [7] "H1355.Untr.1"     "H1355.Untr.2"     "H1355.T4.1"
## [10] "H1355.T4.2"       "H1355.T8.1"       "H1355.T8.2"
## [13] "H1355.T13.1"      "H1355.T13.2"      "H1355.T16.1"
## [16] "H1355.T16.2"      "H1355.T16.3"      "est"
## [19] "p.value"
```

```
est=apply(df.1355[, cell.1355], 1, lm.ic)
est=t(est)
est=data.frame(est)
head(est)
```

```
##            X1           X2
## 1  0.02633836 0.4573952245
## 2 -0.03237285 0.1441376047
## 3  0.28051951 0.0004062189
## 4 -0.13380885 0.0753998578
## 5 -0.05697809 0.2763634625
## 6  0.14990967 0.2601679463
```

```
names(est)=c("est", "p.value")
head(est)
```

```
##           est      p.value
## 1  0.02633836 0.4573952245
## 2 -0.03237285 0.1441376047
## 3  0.28051951 0.0004062189
## 4 -0.13380885 0.0753998578
## 5 -0.05697809 0.2763634625
## 6  0.14990967 0.2601679463
```

```
df.1355=cbind(df.1355, est)
```

```
p.1355=cutoffSignificant(Bum(df.1355$p.value), fdr)
p.1355
```

```
## [1] 0.003536239
```

```
table(df.1355$p.value < p.1355)
```

```
##
## FALSE  TRUE
## 19954   595
```

```r
table(df.1355$p.value < p.1355 & df.1355$est <0)
```

```
##
## FALSE  TRUE
## 20259   290
```

```r
table(df.1355$p.value < p.1355 & df.1355$est > 0)
```

```
##
## FALSE  TRUE
## 20244   305
```

```r
id.up.1355=df.1355$gene.id[df.1355$p.value < p.1355 & df.1355$est > 0]
id.down.1355=df.1355$gene.id[df.1355$p.value < p.1355 & df.1355$est < 0]
sum(id.up.1355 %in% id.up.1299)
```

```
## [1] 51
```

```r
sum(id.down.1355 %in% id.down.1299)
```

```
## [1] 59
```

```r
# volcano plot:
par(mar=c(5, 5, 2, 1))
plot(df.1355$est, -log10(df.1355$p.value), xlab="Est of coefficients", cex=0.
5,
     ylab="P value (-log10)", cex.lab=2, cex.axis=1.5, bty="n", col="blue", p
ch=20,
     yaxt="n")
axis(2, at=c(0, 2, 4, 6, 8), labels=c(1, 0.01, 0.0001, 0.000001, 0.00000001),
cex.axis=1.5)
points(df.1355$est[df.1355$p.value < p.1355 & df.1355$est > 0],
       -log10(df.1355$p.value[df.1355$p.value < p.1355 & df.1355$est > 0]), c
ol="red",
       pch=20)
points(df.1355$est[df.1355$p.value < p.1355 & df.1355$est < 0],
       -log10(df.1355$p.value[df.1355$p.value < p.1355 & df.1355$est < 0]), c
ol="green",
       pch=20)
table(df.1355$p.value < p.1355 & df.1355$est > 0)
```

```
##
## FALSE  TRUE
## 20244   305
```

```r
table(df.1355$p.value < p.1355 & df.1355$est < 0)
```

```
##
## FALSE  TRUE
## 20259   290
```

```
legend("topleft", c("Upregulated:      305", "Downregulated: 290"),
       col=c("red", "green"), pch=20, bty="n")
```

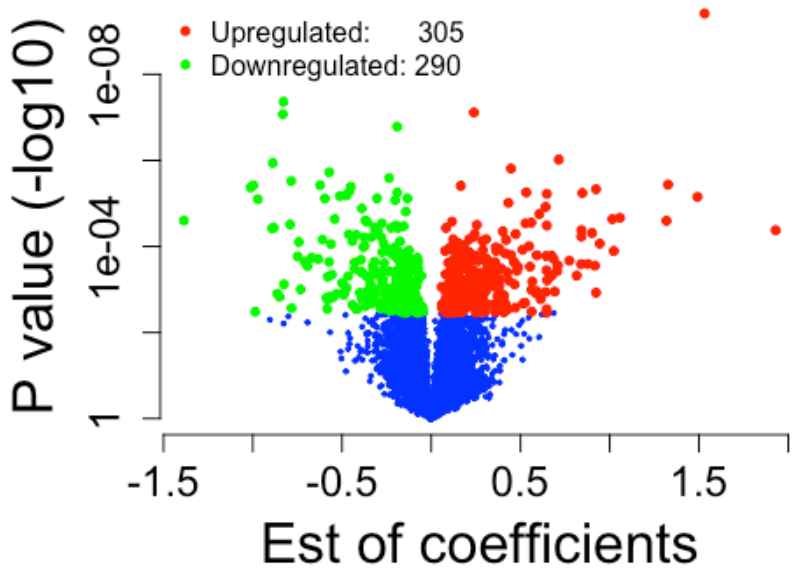

5. Venn diagram for H1299 and H1355 intersected up and down regulated genes.

```
# upregulated
sum(df.1299$p.value < p.1299 & df.1299$est > 0)

## [1] 1876

sum(df.1355$p.value < p.1355 & df.1355$est > 0)

## [1] 305

sum((df.1299$p.value < p.1299 & df.1299$est > 0) &
      (df.1355$p.value < p.1355 & df.1355$est > 0))

## [1] 51

plot.new()
draw.pairwise.venn(1876, 305, 51, cex=3,
                   fill=c("purple", "blue"), lty="blank")
```

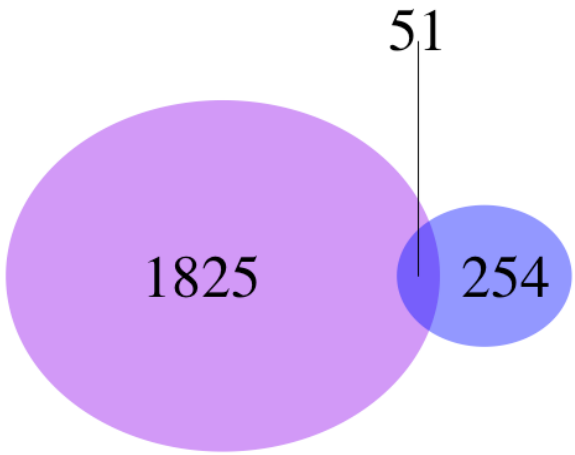


```
## (polygon[GRID.polygon.1], polygon[GRID.polygon.2], polygon[GRID.polygon.3]
, polygon[GRID.polygon.4], text[GRID.text.5], text[GRID.text.6], text[GRID.te
xt.7], lines[GRID.lines.8], text[GRID.text.9], text[GRID.text.10])

# down regulated
sum(df.1299$p.value < p.1299 & df.1299$est < 0)

## [1] 1876

sum(df.1355$p.value < p.1355 & df.1355$est < 0)

## [1] 290

sum((df.1299$p.value < p.1299 & df.1299$est < 0) &
      (df.1355$p.value < p.1355 & df.1355$est < 0))

## [1] 59

plot.new()
draw.pairwise.venn(1876, 290, 59, cex=3,
                   fill=c("purple", "blue"), lty="blank")
```

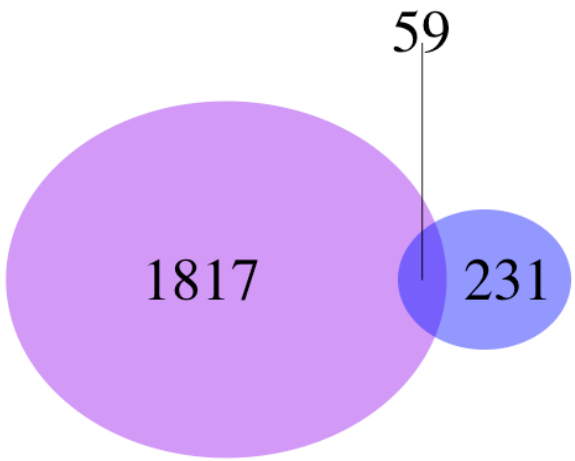

```
## (polygon[GRID.polygon.11], polygon[GRID.polygon.12], polygon[GRID.polygon.
13], polygon[GRID.polygon.14], text[GRID.text.15], text[GRID.text.16], text[G
RID.text.17], lines[GRID.lines.18], text[GRID.text.19], text[GRID.text.20])
```

Xenografts

2. Load the xenograft data

```
load("xeno.RData")
head(df.xeno[,1:5])
```

```
##   gene.id n gene.symbol H1299.Parental.Cis+Doc.871
## 1       1 2        A1BG                   3.633839
## 2       2 1         A2M                   2.229475
## 3       9 3        NAT1                   3.012080
## 4      10 1        NAT2                   2.419627
## 5      12 1    SERPINA3                   5.481228
## 6      13 1       AADAC                   2.488485
##   H1299.Parental.Cis+Doc.873
## 1                   3.136163
## 2                   1.674401
## 3                   3.092054
## 4                   2.585305
## 5                   7.112472
## 6                   2.548242
```

```
dim(df.xeno)
```

```
## [1] 20549    15
```

```
colnames(df.xeno)
```

```
##  [1] "gene.id"                   "n"
##  [3] "gene.symbol"               "H1299.Parental.Cis+Doc.871"
##  [5] "H1299.Parental.Cis+Doc.873" "H1299.Parental.Cis+Doc.878"
##  [7] "H1299.Parental.Saline.872"  "H1299.Parental.Saline.877"
##  [9] "H1299.Parental.Saline.891"  "H1299.T18.Cis+Doc.868"
## [11] "H1299.T18.Cis+Doc.882"      "H1299.T18.Cis+Doc.889"
## [13] "H1299.T18.Saline.862"       "H1299.T18.Saline.870"
## [15] "H1299.T18.Saline.886"
```

```
xeno.line
```

```
##  [1] "H1299.Parental.Cis+Doc.871" "H1299.Parental.Cis+Doc.873"
##  [3] "H1299.Parental.Cis+Doc.878" "H1299.Parental.Saline.872"
##  [5] "H1299.Parental.Saline.877"  "H1299.Parental.Saline.891"
##  [7] "H1299.T18.Cis+Doc.868"      "H1299.T18.Cis+Doc.882"
##  [9] "H1299.T18.Cis+Doc.889"      "H1299.T18.Saline.862"
## [11] "H1299.T18.Saline.870"       "H1299.T18.Saline.886"
```

```
id.up=df.1299$gene.id[df.1299$p.value < p.1299 & df.1299$est > 0 &
                        df.1355$p.value < p.1355 & df.1355$est > 0]
id.down=df.1299$gene.id[df.1299$p.value < p.1299 & df.1299$est < 0 &
                          df.1355$p.value < p.1355 & df.1355$est < 0]
```

3. Significant differential expression gene analysis **(FDR 0.1)**

```
xeno.untr=xeno.line[c(4:6, 10:12)]
xeno.untr
```

```
## [1] "H1299.Parental.Saline.872" "H1299.Parental.Saline.877"
## [3] "H1299.Parental.Saline.891" "H1299.T18.Saline.862"
## [5] "H1299.T18.Saline.870"      "H1299.T18.Saline.886"
```

```
head(df.xeno)
```

```
##   gene.id n gene.symbol H1299.Parental.Cis+Doc.871
## 1       1 2        A1BG                   3.633839
## 2       2 1         A2M                   2.229475
## 3       9 3        NAT1                   3.012080
## 4      10 1        NAT2                   2.419627
## 5      12 1    SERPINA3                   5.481228
## 6      13 1       AADAC                   2.488485
##   H1299.Parental.Cis+Doc.873 H1299.Parental.Cis+Doc.878
## 1                   3.136163                   2.745621
## 2                   1.674401                   1.610231
## 3                   3.092054                   2.863332
## 4                   2.585305                   2.481384
## 5                   7.112472                   5.059355
## 6                   2.548242                   3.361560
```

```
dat.validate=df.xeno[, c("gene.id", "n", "gene.symbol", xeno.untr)]
head(dat.validate)
```

```
##   gene.id n gene.symbol H1299.Parental.Saline.872
## 1       1 2        A1BG                   3.536566
## 2       2 1         A2M                   2.307369
## 3       9 3        NAT1                   3.045042
## 4      10 1        NAT2                   2.596068
## 5      12 1    SERPINA3                   2.822787
## 6      13 1       AADAC                   3.526960
```

```
dat.validate$fold.change=apply(dat.validate[,7:9], 1, mean)-apply(dat.validat
e[, 4:6], 1, mean)

xeno.p=function(x){
  x=as.numeric(x)
  return(t.test(x[1:3], x[4:6], alternative="two.sided")$p.value)
```

```
}
xeno.p(dat.validate[1, 4:9])

## [1] 0.2900682

dat.validate$p.value=apply(dat.validate[, 4:9], 1, xeno.p)
```

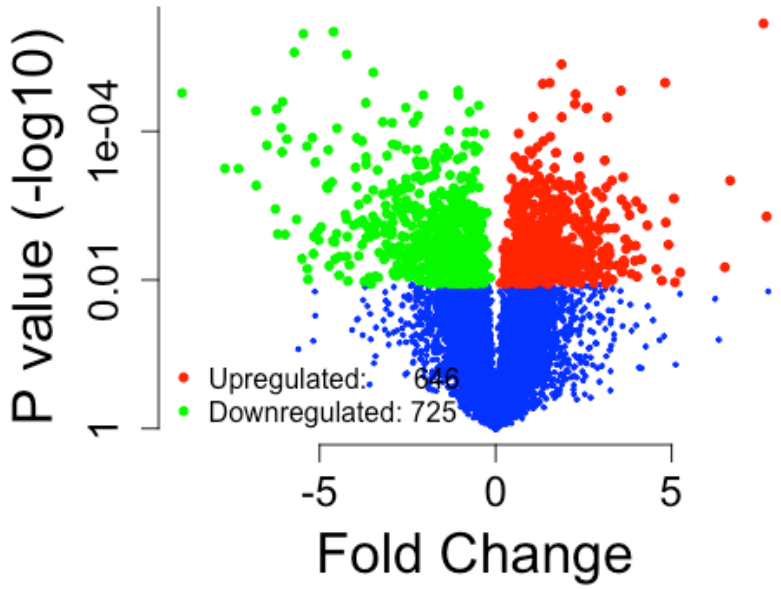

Gene signatures

3. Venn diagram for up and down regulated genes for both cell lines and xenografts

```
#venn diagram
p.xeno=cutoffSignificant(Bum(dat.validate$p.value), 0.1)
p.xeno

## [1] 0.01136179

table(dat.validate$p.value < p.xeno)

##
## FALSE  TRUE
## 19178  1371

id.up.xeno=dat.validate$gene.id[dat.validate$p.value < p.xeno &
                                  dat.validate$fold.change > 0]
length(id.up)

## [1] 51

length(id.up.xeno)
```

```
## [1] 646

sum(id.up %in% id.up.xeno)

## [1] 14

plot.new()
draw.pairwise.venn(646, 51, 14, cex=3,
                   fill=c("light blue", "light green"), lty="blank")
```

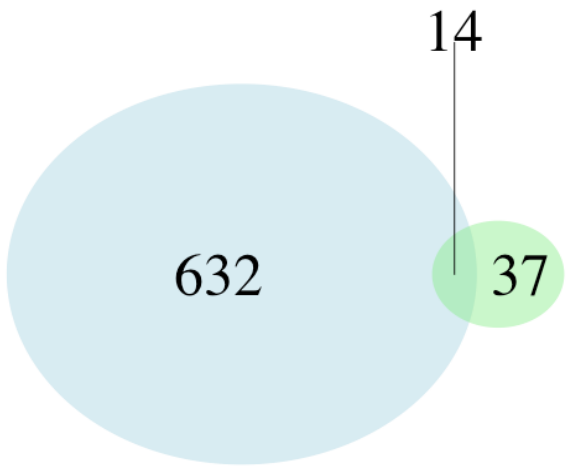


```
## (polygon[GRID.polygon.21], polygon[GRID.polygon.22], polygon[GRID.polygon.
23], polygon[GRID.polygon.24], text[GRID.text.25], text[GRID.text.26], text[G
RID.text.27], lines[GRID.lines.28], text[GRID.text.29], text[GRID.text.30])

id.down.xeno=dat.validate$gene.id[dat.validate$p.value < p.xeno &
                                  dat.validate$fold.change < 0]
length(id.down)

## [1] 59

length(id.down.xeno)

## [1] 725

sum(id.down %in% id.down.xeno)

## [1] 21

plot.new()
draw.pairwise.venn(725, 59, 21, cex=3,
                   fill=c("light blue", "light green"), lty="blank")
```

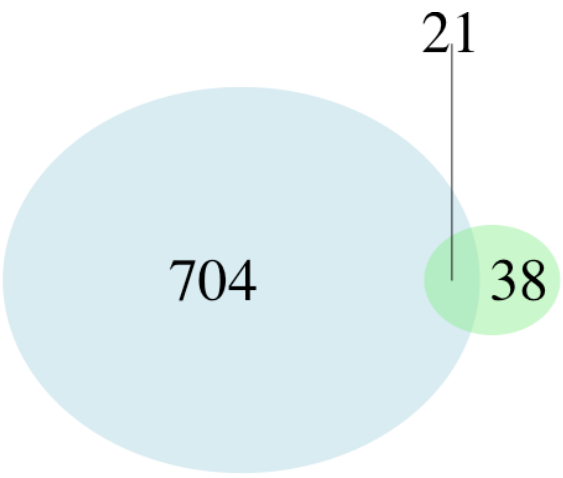


```
## (polygon[GRID.polygon.31], polygon[GRID.polygon.32], polygon[GRID.polygon.
33], polygon[GRID.polygon.34], text[GRID.text.35], text[GRID.text.36], text[G
RID.text.37], lines[GRID.lines.38], text[GRID.text.39], text[GRID.text.40])

id.up.regulate=id.up[id.up %in% id.up.xeno]
id.down.regulate=id.down[id.down %in% id.down.xeno]
sig.gene=dat.validate[dat.validate$gene.id %in% c(id.up.regulate,id.down.regu
late),c("gene.id", "gene.symbol")]
gene35=as.character(sig.gene$gene.symbol)
```

4. Xenografts volcano plot

```
par(mar=c(5, 5, 2, 1))
plot(dat.validate$fold.change, -log10(dat.validate$p.value), xlab="Fold Chang
e", cex=0.5,
     ylab="P value (-log10)", cex.lab=2, cex.axis=1.5, bty="n", col="blue", p
ch=20,
     yaxt="n")
axis(2, at=c(0, 2, 4, 6, 8), labels=c(1, 0.01, 0.0001, 0.000001, 0.00000001),
cex.axis=1.5)
points(dat.validate$fold.change[dat.validate$p.value < p.xeno & dat.validate$
fold.change > 0],
       -log10(dat.validate$p.value[dat.validate$p.value < p.xeno & dat.valida
te$fold.change > 0]), col="red",
       pch=20)
points(dat.validate$fold.change[dat.validate$p.value < p.xeno & dat.validate$
fold.change < 0],
       -log10(dat.validate$p.value[dat.validate$p.value < p.xeno & dat.valida
te$fold.change < 0]), col="green",
       pch=20)
table(dat.validate$p.value < p.xeno & dat.validate$fold.change > 0)

##
## FALSE  TRUE
## 19903   646
```

```
table(dat.validate$p.value < p.xeno & dat.validate$fold.change < 0)

##
## FALSE  TRUE
## 19824   725

legend("bottomleft", c("Upregulated:      646", "Downregulated: 725"),
       col=c("red", "green"), pch=20, bty="n")
```

4. Heat maps for 35 gene signature in Cell lines H1355,H1299 and Xenografts

```
# load 35 genes signature

xeno <- read.table("xenografts.txt",sep="\t",head=TRUE)
CL <- read.table("cellLines.txt",sep="\t",head=TRUE)


# In xenografts, select probes with largest absolute Fold change to represent
the genes expression
xeno35 <- xeno[xeno$Symbol %in% gene35,]
dat <- NULL

for (id in unique(xeno35$Symbol)){
  tmp <- xeno35[xeno35$Symbol %in% id,]
  if (nrow(tmp)>1){

    mm = tmp[tmp$H1299.T18.vs.H1299.P==max(abs(tmp$H1299.T18.vs.H1299.P))|tmp
$H1299.T18.vs.H1299.P==-max(abs(tmp$H1299.T18.vs.H1299.P)) ,]
    dat <- rbind(dat,mm)

  } else {
    dat=rbind(dat,tmp)

  }
}
xe <- dat[,10:21]
rownames(xe) <- dat$Symbol
xe=as.matrix(xe)
xe=xe[,c(1,2,3,7,8,9)]


################################################################
# In cell lines, select probes with largest absolute Fold change to represent
the genes expression

# cell lines
CL35 <- CL[CL$Symbol %in% gene35,]
CL35.H1355 <- data.frame(Symbol=CL35$Symbol,ProbeID=CL35$Probe.ID,CL35[,grep(
"H1355",colnames(CL35))])
```

```
CL35.H1299 <- data.frame(Symbol=CL35$Symbol,ProbeID=CL35$Probe.ID,CL35[,grep(
"H1299",colnames(CL35))])
H1355.dat <- NULL

for (id in unique(CL35.H1355$Symbol)){
  tmp <- CL35.H1355[CL35.H1355$Symbol %in% id,]
  if (nrow(tmp)>1){

    mm = tmp[tmp$H1355.T16.vs.H1355.P==max(abs(tmp$H1355.T16.vs.H1355.P))|tmp
$H1355.T16.vs.H1355.P==-max(abs(tmp$H1355.T16.vs.H1355.P)) ,]
    H1355.dat <- rbind(H1355.dat,mm)

  } else {
    H1355.dat=rbind(H1355.dat,tmp)

  }
}

H1355.cb <- as.matrix(H1355.dat[,4:17])
rownames(H1355.cb) <- as.character(H1355.dat$Symbol)


H1299.dat <- NULL

for (id in unique(CL35.H1299$Symbol)){
  tmp <- CL35.H1299[CL35.H1299$Symbol %in% id,]
  if (nrow(tmp)>1){

    mm = tmp[tmp$H1299.T18.vs.H1299.P==max(abs(tmp$H1299.T18.vs.H1299.P))|tmp
$H1299.T18.vs.H1299.P==-max(abs(tmp$H1299.T18.vs.H1299.P)) ,]
    H1299.dat <- rbind(H1299.dat,mm)

  } else {
    H1299.dat=rbind(H1299.dat,tmp)

  }
}
H1299.cb <- as.matrix(H1299.dat[,4:17])
rownames(H1299.cb) <- H1299.dat$Symbol


# heatmaps

mm=heatmap.2(xe, col=greenred, scale="row",distfun=function(x) {as.dist(1-cor
(t(x)))},tracecol=NULL,,Colv=FALSE,key=FALSE)

## Warning in heatmap.2(xe, col = greenred, scale = "row", distfun =
## function(x) {: Discrepancy: Colv is FALSE, while dendrogram is `row'.
## Omitting column dendogram.
```

```
go=rownames(xe)[mm$rowInd] # keep the gene rows in the same order as xenografts

heatmap.2(H1355.cb[go,], col=greenred, margin=c(3,3),scale="row",Rowv=FALSE,Colv=FALSE,tracecol=NULL,key=FALSE,labRow="")

## Warning in heatmap.2(H1355.cb[go, ], col = greenred, margin = c(3, 3),
## scale = "row", : Discrepancy: Rowv is FALSE, while dendrogram is `none'.
## Omitting row dendogram.
```

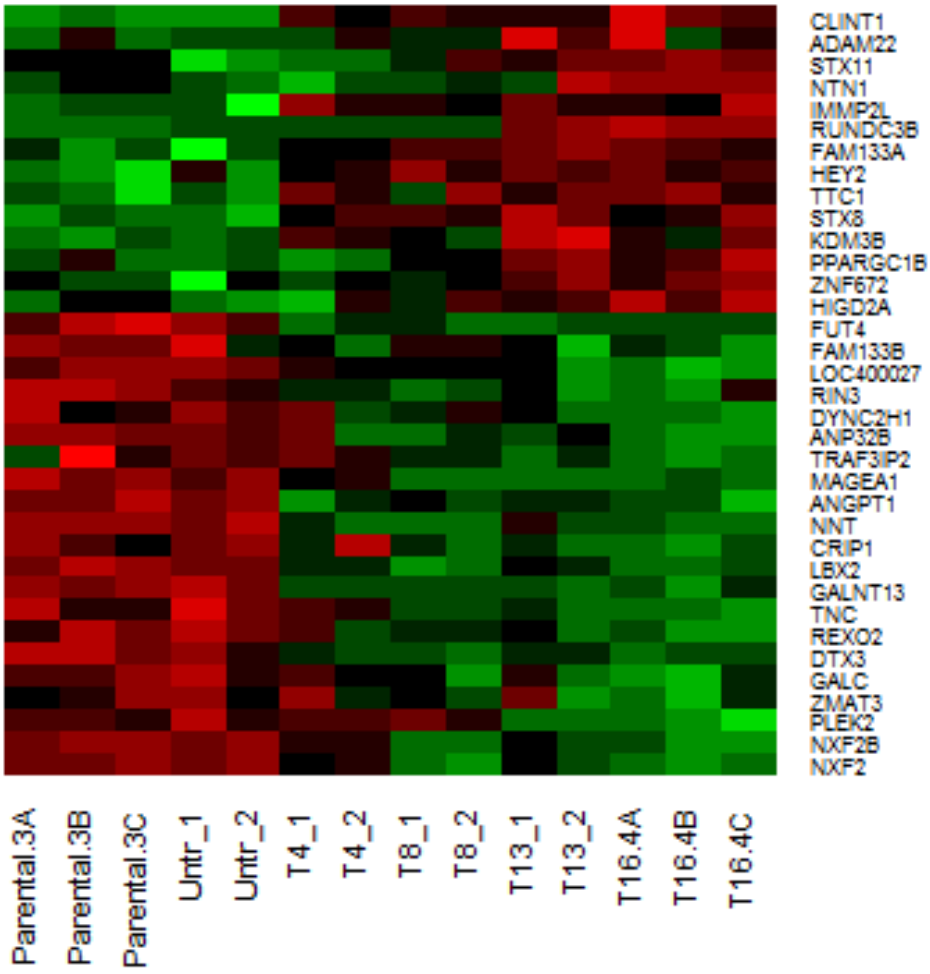


```
heatmap.2(H1299.cb[go,], col=greenred, margin=c(3,3),scale="row",Rowv=FALSE,Colv=FALSE,tracecol=NULL,key=FALSE,labRow="")
```

```
## Warning in heatmap.2(H1299.cb[go, ], col = greenred, margin = c(3, 3),
## scale = "row", : Discrepancy: Rowv is FALSE, while dendrogram is `none'.
## Omitting row dendogram.
```

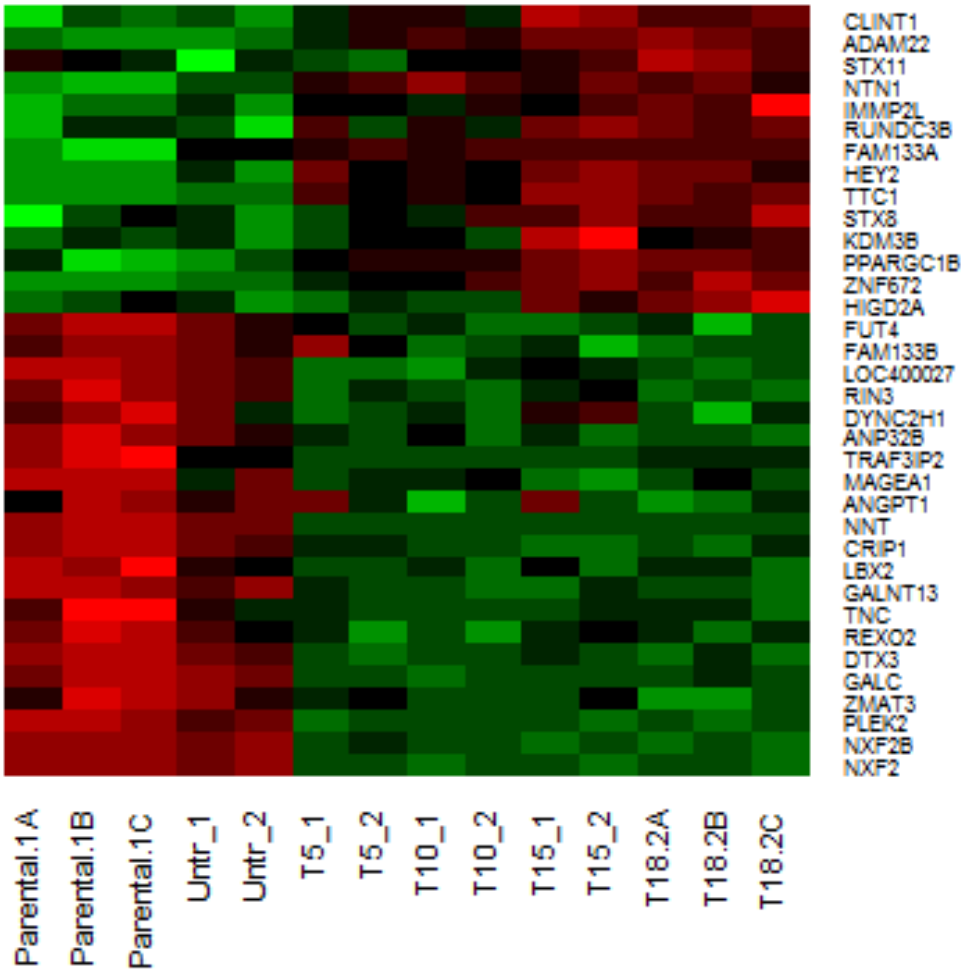


```
heatmap.2(xe[go,], col=greenred, scale="row",distfun=function(x) {as.dist(1-c
or(t(x)))},tracecol=NULL,Colv=FALSE,Rowv=FALSE,key=FALSE)

## Warning in heatmap.2(xe[go, ], col = greenred, scale = "row", distfun =
## function(x) {: Discrepancy: Rowv is FALSE, while dendrogram is `none'.
## Omitting row dendogram.
```

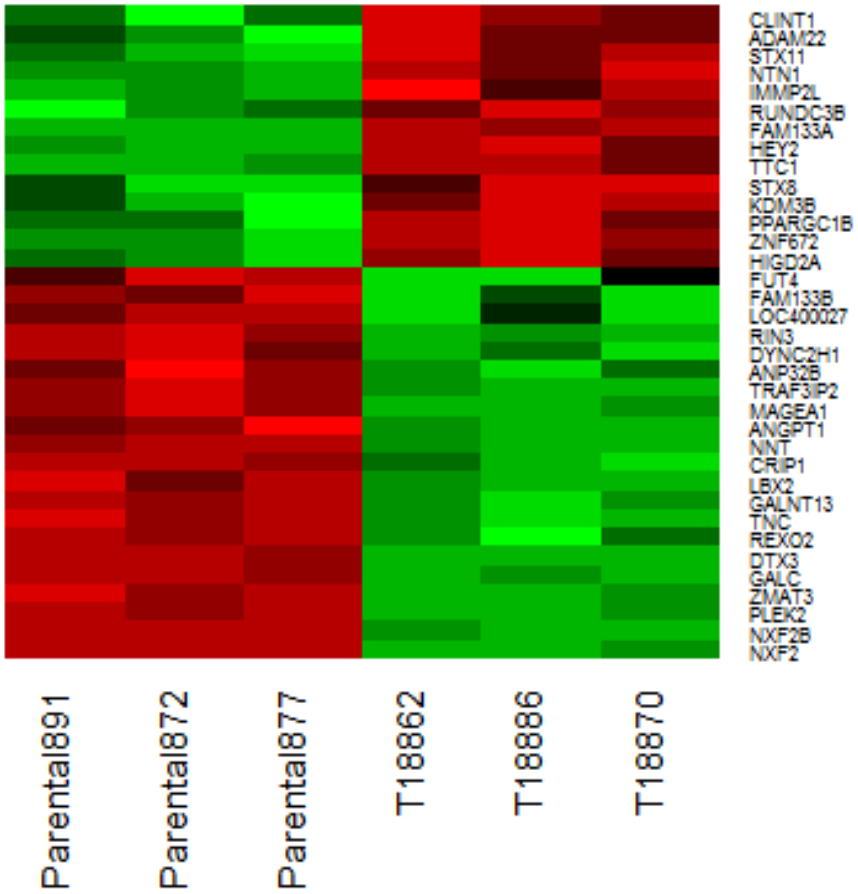

Evaluate gene signature in patient dataset

Unsupervised learning for 35 gene signatures on 65 patients who got the neoadjuvant therapy.

5. Load the data

```
load("patient expr.RData")

names(dat.pati)[4:278] <- sub("\\.", "-", names(dat.pati[4:278]))


# load clinical data
dat.clin <- read.csv("03-28-2014_Dalvi M_65 Neoadjuvant patients with UPDATED
annotation.csv", as.is=T)
dat.clin$id %in% names(dat.pati)

##  [1] TRUE TRUE TRUE TRUE TRUE TRUE TRUE TRUE TRUE TRUE TRUE TRUE TRUE TRUE
## [15] TRUE TRUE TRUE TRUE TRUE TRUE TRUE TRUE TRUE TRUE TRUE TRUE TRUE TRUE
## [29] TRUE TRUE TRUE TRUE TRUE TRUE TRUE TRUE TRUE TRUE TRUE TRUE TRUE TRUE
```

```
## [43] TRUE TRUE TRUE TRUE TRUE TRUE TRUE TRUE TRUE TRUE TRUE TRUE TRUE TRUE
## [57] TRUE TRUE TRUE TRUE TRUE TRUE TRUE TRUE TRUE

dat.neoa <- dat.pati[, c(names(dat.pati[1:3]), dat.clin$id)]
id <- c(id.up.regulate, id.down.regulate)

dat.neoa <- dat.neoa[dat.neoa$gene.id %in% id, ]
row.names(dat.neoa) <- dat.neoa$gene.id
row.names(dat.neoa)

##  [1] "284"    "1396"   "2526"   "2581"   "3371"   "4100"   "7265"
##  [8] "8676"   "9423"   "9482"   "9685"   "10541"  "10758"  "23493"
## [15] "23530"  "25996"  "26499"  "51780"  "53616"  "56001"  "64393"
## [22] "79659"  "79890"  "79894"  "83943"  "85474"  "114805" "133522"
## [29] "154661" "192286" "196403" "257415" "286499" "400027" "728343"

dat.neoa <- dat.neoa[, 4:68]
```

4. Cluster plot and K-M curve recurrence free survival analysis

```
# cluster plot
hc.cell=hclust(dist(t(dat.neoa), method="maximum"))
plot(hc.cell)
```

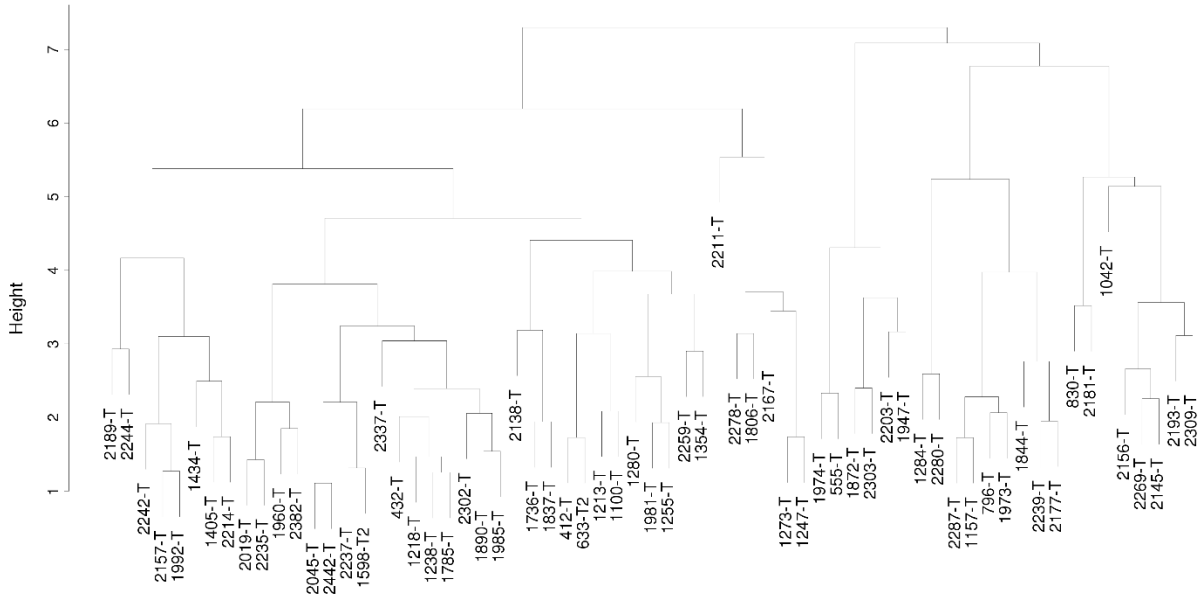


```
hc.cell$order

##  [1] 30 52 32  3 50 12 15 29 37 38 10 22  4 19  5  8 53 18 21  2 45  1  7
## [24] 44 14 11 17 16 20 43 46 39 34 36  6  9 49 13 33 47 48 51 57 65 28 54
## [47] 42 55 27 61 25 58 40 63 56 59 64 31 41 62 60 26 35 23 24

dat.surv <- data.frame(id=hc.cell$labels[hc.cell$order], group=c(rep(1, 42),
rep(2, 23)))
```

```
dat.surv <- merge(dat.surv, dat.clin, by="id")

# K-M plot
kmplot <- function(survival,groups, title.lab="",xlab="",ylab="",
               survivallimit=c(60, 120), display=TRUE, cex.axis=1.5, cex.lab=
1.4, cex.main=1.5,
               mar=c(5.1 , 5.3, 4.1, 1.1), sig=NULL, ...)
{
  require(survival)
  survival<-survival[!is.na(groups),]
  groups<-groups[!is.na(groups)]
  if(length(levels(factor(groups)))<2)
  { cat("error in kmplot\n"); return() }
  logrank<-survdiff(survival ~ groups,  ...)
  pv <- pchisq(logrank$chisq,1, lower.tail=F)

  summary_coxph <- summary(coxph(survival ~ groups, ...))
  ci <-summary_coxph$conf.int


  col=c("black", "red")
  if (display) {
      sfit= survfit(survival ~ groups, ...)

      plot(sfit, col=col, lty=1:2, main=title.lab, xlab=xlab,ylab=ylab, mark.
time=TRUE,mark=19,
         cex.axis=cex.axis, cex.lab=cex.lab, cex.main=cex.main, mar=mar, ...)

      ### add two vertical line represent 5 year and 10 year
#      sapply(survivallimit, function(x) abline(v=x, col="grey"))

       ### add results on plot
      stat=paste("n = ",length(groups),", ",pv.expr(pv) , "\n HR=",format(ci[
1],digits=3),
                 " (95%CI,",format(ci[3],digits=3),"-",
                 format(ci[4],digits=3),")",sep="")
      x=min(survival[,1])+0.5*(max(survival[,1])-min(survival[,1]))
      text(x, 0.15 ,stat , cex=cex.lab)
  }
  return(list(group_table=table(groups),logrank.p=pv,
              hr=ci[1],hr.5=ci[3],hr.95=ci[4], n=length(groups),
              ebeta=summary_coxph$coef[1], z=summary_coxph$coef[4],pr.z=summa
ry_coxph$coef[5],
              groups=groups))
}

         ##Function to format pvalues in K-M plot
pv.expr <- function(x, digits = 2) {
    if (!x) return(0)
```

```
    exponent <- floor(log10(x))
    base <- round(x / 10^exponent, digits)
    ifelse(x > 0.0001,
        paste("p = ", base*(10^exponent), sep=""),
        paste("p = ", base, "E", exponent, sep=""))
}


survival <- Surv(time=as.numeric(as.character(dat.surv$cancer.free.survival.m
onth)),
              event=dat.surv$recurrence == 'Y')
survdiff(survival ~ dat.surv$group)
```

```
## Call:
## survdiff(formula = survival ~ dat.surv$group)
##
##                      N Observed Expected (O-E)^2/E (O-E)^2/V
## dat.surv$group=1 42       20    28.56      2.56      10.5
## dat.surv$group=2 23       18     9.44      7.75      10.5
##
##  Chisq= 10.5  on 1 degrees of freedom, p= 0.0012
```

```
kmplot(survival, dat.surv$group)
```

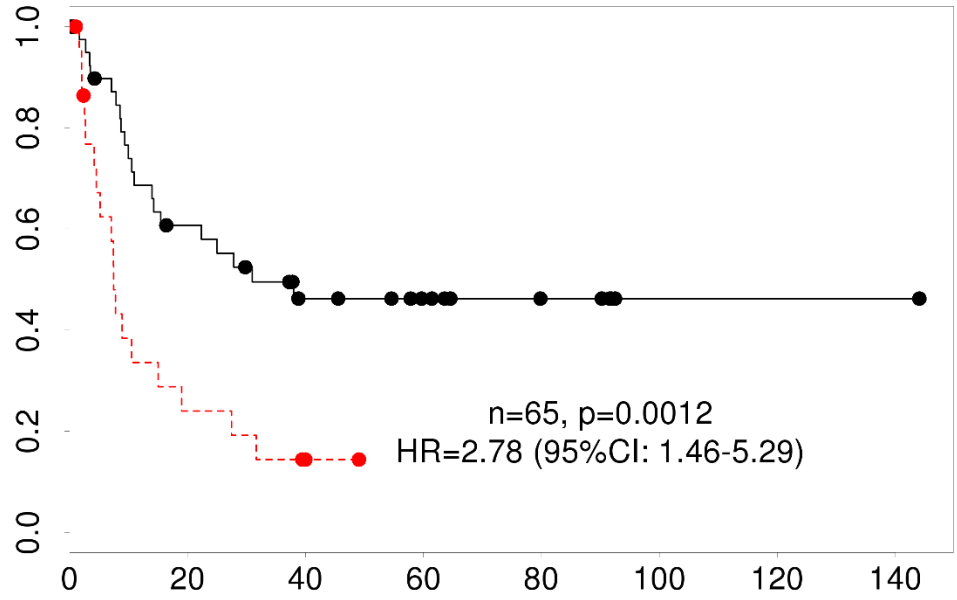


```
## $group_table
## groups
##  1  2
## 42 23
##
```

```
## $logrank.p
## [1] 0.001200184
##
## $hr
## [1] 2.776687
##
## $hr.5
## [1] 1.458712
##
## $hr.95
## [1] 5.28548
##
## $n
## [1] 65
##
## $ebeta
## [1] 1.021258
##
## $z
## [1] 3.109546
##
## $pr.z
## [1] 0.001873753
##
## $groups
##  [1] 2 1 2 1 1 1 1 1 1 2 1 1 1 1 1 1 1 2 2 1 2 1 2 2 1 1 1 1 1 2 2 1
## [36] 1 2 2 1 2 2 1 1 1 1 2 1 1 1 2 1 2 2 1 2 2 1 1 1 1 2 1 2 2
```

5. Multivariate Cox regression model

```
# data for 65 neoajuvant patients
load("dat65.RData")
head(dat65[,1:5])
```

```
##   gene.id n gene.symbol    2302-T    1238-T
## 1       1 2        A1BG  3.638638  2.605372
## 2       2 1         A2M 10.282485 11.270556
## 3       9 3        NAT1  3.201879  3.562783
## 4      10 1        NAT2  2.183924  2.484070
## 5      12 1    SERPINA3 10.435610  9.637462
## 6      13 1       AADAC  8.201044  3.566616
```

```
dim(dat65)
```

```
## [1] 19579    68
```

```
cli65=dat.clin
sig.id <- c(id.up.regulate, id.down.regulate)
sur65 <- dat65[dat65$gene.id %in% sig.id,]
row.names(sur65) <- sur65$gene.symbol
sur65 <- sur65[, -c(1:3)]
```

```
sur65 <- data.frame(t(sur65))
head(sur65)
```

```
##          ANGPT1    CRIP1     FUT4     GALC      TNC   MAGEA1     TTC1
## 2302-T 8.235965 10.73370 5.422461 7.486111 8.190325 2.634824 8.216957
## 1238-T 7.010597 11.35512 5.125421 7.166048 8.693179 2.708898 7.949370
## 2157-T 5.381803 10.67481 4.150018 6.272858 7.075845 2.896832 8.054993
## 2045-T 7.963517 11.84460 4.616963 6.794380 7.304523 2.662581 7.866941
## 2237-T 7.489364 12.19631 5.336181 7.265428 7.057829 2.768827 8.055649
## 2259-T 6.587808 12.08331 4.885976 6.528196 8.851127 3.828562 8.342618
##           STX11     NTN1     STX8   CLINT1   ANP32B TRAF3IP2     HEY2
## 2302-T 8.806033 3.866315 7.807953 9.964402 11.97116 5.748529 4.538813
## 1238-T 8.990390 3.934511 8.164496 9.348762 11.80851 5.224289 6.463278
## 2157-T 7.266282 4.691052 7.932429 8.789924 12.60085 5.632375 4.672881
## 2045-T 9.024002 3.782765 7.853039 9.588817 11.81897 4.804227 5.344224
## 2237-T 8.642615 3.650787 7.420597 9.801010 11.90997 5.340369 6.014473
## 2259-T 6.644821 3.998293 7.765663 9.865428 11.74342 5.591911 8.132118
```

```
sur65$id <- row.names(sur65)
sur65 <- merge(sur65, cli65, by="id")
sur65$event <- ifelse(sur65$recurrence == "Y", 1, 0)
paste(names(sur65)[2:36], collapse = " + ")
```

```
## [1] "ANGPT1 + CRIP1 + FUT4 + GALC + TNC + MAGEA1 + TTC1 + STX11 + NTN1 + S
TX8 + CLINT1 + ANP32B + TRAF3IP2 + HEY2 + NNT + REXO2 + PLEK2 + KDM3B + ADAM2
2 + NXF2 + ZMAT3 + DYNC2H1 + RIN3 + ZNF672 + IMMP2L + LBX2 + GALNT13 + PPARGC
1B + RUNDC3B + HIGD2A + DTX3 + FAM133B + FAM133A + LOC400027 + NXF2B"
```

```
# multivariate cox regression model
fit65 <- coxph(Surv(cancer.free.survival.month, event)~ ANGPT1 + CRIP1 + FUT4
+ GALC + TNC + MAGEA1 + TTC1 + STX11 + NTN1 + STX8 + CLINT1 + ANP32B + TRAF3I
P2 + HEY2 + NNT + REXO2 + PLEK2 + KDM3B + ADAM22 + NXF2 + ZMAT3 + DYNC2H1 + R
IN3 + ZNF672 + IMMP2L + LBX2 + GALNT13 + PPARGC1B + RUNDC3B + HIGD2A + DTX3 +
FAM133B + FAM133A + LOC400027 + NXF2B, data=sur65)
sum65 <- summary(fit65)
coe65=sum65$coefficients
coe65
```

```
##                coef   exp(coef)  se(coef)          z     Pr(>|z|)
## ANGPT1     0.2091745  1.23266002 0.3522183  0.5938772 0.5525942229
## CRIP1      0.4827728  1.62056161 0.4083533  1.1822427 0.2371093988
## FUT4       0.6953699  2.00445029 0.8489477  0.8190962 0.4127315352
## GALC       0.1018298  1.10719499 0.6486271  0.1569928 0.8752505211
## TNC        0.4542830  1.57504372 0.2696067  1.6849841 0.0919916316
## MAGEA1     0.3877544  1.47366785 0.2178626  1.7798117 0.0751067903
## TTC1      -0.7462477  0.47414233 0.8774816 -0.8504426 0.3950790600
## STX11     -0.0624412  0.93946831 0.4083143 -0.1529243 0.8784579357
## NTN1       0.4174976  1.51815770 0.4800938  0.8696166 0.3845099402
## STX8      -2.1243707  0.11950815 0.8603591 -2.4691674 0.0135427840
```

```
## CLINT1    -2.9858164  0.05049826 1.3702253 -2.1790697 0.0293264880
## ANP32B    -0.8004983  0.44910512 0.7571715 -1.0572219 0.2904103310
## TRAF3IP2   1.3593645  3.89371789 0.8955198  1.5179613 0.1290241587
## HEY2      -0.1132994  0.89288327 0.2281820 -0.4965310 0.6195198115
## NNT        3.0160368 20.41024063 0.8867630  3.4011757 0.0006709668
## REXO2      0.8232530  2.27789773 1.0772530  0.7642150 0.4447391043
## PLEK2     -0.0854132  0.91813283 0.2689104 -0.3176270 0.7507679273
## KDM3B      2.3300661 10.27862073 1.0422492  2.2356132 0.0253771209
## ADAM22     1.8088556  6.10345840 1.2200918  1.4825569 0.1381921728
## NXF2      -1.9577895  0.14117013 1.3088808 -1.4957738 0.1347126236
## ZMAT3     -0.2423971  0.78474446 0.8924421 -0.2716111 0.7859210966
## DYNC2H1   -0.7245371  0.48454882 0.4513348 -1.6053205 0.1084232849
## RIN3       0.1752646  1.19156148 0.4063743  0.4312886 0.6662585233
## ZNF672    -1.7224168  0.17863391 1.0290374 -1.6738135 0.0941672569
## IMMP2L     0.6351963  1.88739254 0.7552601  0.8410299 0.4003311966
## LBX2       0.6945857  2.00287903 0.3475644  1.9984375 0.0456692455
## GALNT13    0.5186821  1.67981236 0.3777974  1.3729106 0.1697801307
## PPARGC1B  -0.3403402  0.71152822 0.3936462 -0.8645839 0.3872672093
## RUNDC3B   -0.1737039  0.84054572 0.3701324 -0.4693021 0.6388537108
## HIGD2A    -0.1515406  0.85938303 1.1451527 -0.1323322 0.8947215570
## DTX3       0.8800273  2.41096560 0.3218440  2.7343286 0.0062507638
## FAM133B   -1.6762593  0.18707245 1.3213149 -1.2686297 0.2045731611
## FAM133A    0.1851519  1.20340119 0.2420717  0.7648639 0.4443526181
## LOC400027 -0.3161092  0.72897986 0.5113653 -0.6181670 0.5364652793
## NXF2B      2.7053611 14.95971778 1.6524065  1.6372249 0.1015834781
```

```
dm=coe65[as.character(up$gene.symbol),]
dim(dm)
```

```
## [1] 14  5
```

14 up regulated genes

```
plot(dm[,2],-log(dm[,5]),type="p",pch=19,xlab="Hazard Ratio",ylab="-log(p.val
ue)")
abline(h=1.25,v=0,lty=2)
```

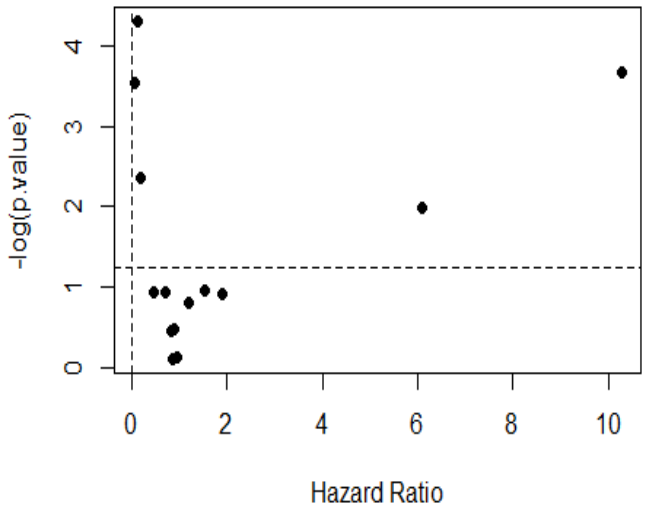


```
dat.surv$neoadj <- ifelse(dat.surv$Neoadjuvant.Drugs %in% c("Cisplatin Doceta
xel", "Carboplatin Paclitaxel", "Carboplatin Docetaxel", "Cisplatin"), 1, 0)


table(dat.surv$neoadj)

##
##  0  1
## 10 55

dat.surv$path[grep("IA", dat.surv$pathology)] <- "I"
dat.surv$path[grep("IB", dat.surv$pathology)] <- "I"
dat.surv$path[grep("IIA", dat.surv$pathology)] <- "II"
dat.surv$path[grep("IIB", dat.surv$pathology)] <- "II"
dat.surv$path[grep("IIIA", dat.surv$pathology)] <- "III"
dat.surv$path[grep("IIIB", dat.surv$pathology)] <- "III"
dat.surv$path[grep("IV", dat.surv$pathology)] <- "IV"

coxph(Surv(cancer.free.survival.month, recurrence == 'Y') ~ group, data=dat.s
urv)

## Call:
## coxph(formula = Surv(cancer.free.survival.month, recurrence ==
##     "Y") ~ group, data = dat.surv)
##
##
##       coef exp(coef) se(coef)    z      p
## group 1.02      2.78    0.328 3.11 0.0019
##
## Likelihood ratio test=9.15  on 1 df, p=0.00249  n= 65, number of events= 3
8
```

```
cox.fit <- coxph(Surv(cancer.free.survival.month, recurrence == 'Y') ~ group
+ histology + age + smoke + Gender + Race + Adjuvant.Therapy + neoadj + path,
data=dat.surv)

cox.fit

## Call:
## coxph(formula = Surv(cancer.free.survival.month, recurrence ==
##     "Y") ~ group + histology + age + smoke + Gender + Race +
##     Adjuvant.Therapy + neoadj + path, data = dat.surv)
##
##
##                                   coef exp(coef) se(coef)      z      p
## group                           1.6292     5.100   0.4858  3.354 0.0008
## histologyOther                  0.3710     1.449   0.4745  0.782 0.4300
## histologySquamous              -0.2292     0.795   0.4969 -0.461 0.6400
## age                             0.0222     1.022   0.0251  0.884 0.3800
## smokeY                         -0.9275     0.396   0.6676 -1.389 0.1600
## GenderM                        -0.2108     0.810   0.4312 -0.489 0.6200
## RaceAsian or Pacific Islander -0.2788     0.757   1.5221 -0.183 0.8500
## RaceCaucasian                  -0.8713     0.418   0.8005 -1.088 0.2800
## RaceHispanic                   -0.1321     0.876   1.2877 -0.103 0.9200
## Adjuvant.TherapyY              -1.0292     0.357   0.4962 -2.074 0.0380
## neoadj                          0.5252     1.691   0.5182  1.014 0.3100
## pathII                         -0.2370     0.789   0.5893 -0.402 0.6900
## pathIII                         1.0031     2.727   0.4973  2.017 0.0440
## pathIV                          0.9530     2.594   0.6674  1.428 0.1500
##
## Likelihood ratio test=23.2  on 14 df, p=0.0566  n= 65, number of events=38
```

APPENDIX B. GENES REVERSED IN H1299 T18 BY JIB-04 TREATMENT

(Supplemental to Figure 7.3; D, Down-regulated and U, Up-regulated; Fold change ≥ 1.5)

Gene	H1299 T18 DMSO vs H1299 Parental DMSO	Log_2 [Fold Change]	T-test P value	H1299 T18 JIB04 vs H1299 T18 DMSO	Log_2 [Fold Change]	T-test P value
YPEL2	D	-1.73	0.040	U	4.00	0.011
C5orf41	D	-1.73	0.003	U	3.30	0.027
C5orf41	D	-1.55	0.019	U	3.19	0.024
FBXO32	D	-1.37	0.046	U	2.51	0.026
DDIT4	D	-2.27	0.022	U	2.22	0.012
PER2	D	-1.82	0.001	U	2.19	0.005
EGFR	D	-1.05	0.020	U	2.19	0.013
NRP1	D	-2.08	0.008	U	2.15	0.015
BHLHE40	D	-3.76	0.025	U	2.14	0.026
DDIT3	D	-0.95	0.035	U	2.13	0.013
CTGF	D	-1.03	0.029	U	2.07	0.031
EFNB2	D	-1.14	0.035	U	2.04	0.004
NFIL3	D	-0.72	0.011	U	1.94	0.006
CTGF	D	-0.89	0.018	U	1.88	0.001
JUN	D	-1.46	0.034	U	1.88	0.008
NRP1	D	-2.27	0.029	U	1.82	0.048
GRAMD1B	D	-2.01	0.014	U	1.65	0.000
MT1G	D	-0.89	0.027	U	1.63	0.041
LYPD1	D	-2.28	0.032	U	1.58	0.007
PPP1R15A	D	-1.37	0.032	U	1.57	0.033
TMEM91	D	-1.67	0.019	U	1.55	0.004
BNC1	D	-0.97	0.035	U	1.54	0.019
TRIB3	D	-1.04	0.004	U	1.50	0.008
BMP2	D	-0.92	0.031	U	1.48	0.017
RBMS1	D	-1.83	0.039	U	1.48	0.006
ATF3	D	-0.89	0.028	U	1.46	0.019
RAB3IL1	D	-1.37	0.025	U	1.45	0.015
CCDC93	D	-2.37	0.000	U	1.45	0.006
KRT86	D	-0.73	0.039	U	1.44	0.034
WDR33	D	-1.50	0.005	U	1.42	0.005
ZNF442	D	-0.93	0.048	U	1.41	0.034
SNX30	D	-0.97	0.007	U	1.26	0.005
ASNS	D	-0.90	0.003	U	1.26	0.001
RALGDS	D	-0.77	0.041	U	1.22	0.015

SPRN	D	-1.17	0.033	U	1.21	0.031
RAB4B	D	-1.69	0.009	U	1.20	0.026
SAT1	D	-1.39	0.018	U	1.20	0.032
DCBLD2	D	-2.43	0.015	U	1.18	0.035
CHIC2	D	-1.15	0.015	U	1.17	0.015
ZMYM5	D	-0.84	0.028	U	1.15	0.031
BEND7	D	-1.15	0.045	U	1.13	0.006
SH3GL2	D	-2.72	0.038	U	1.13	0.012
WDR33	D	-1.36	0.016	U	1.08	0.004
CCDC28A	D	-0.70	0.032	U	1.05	0.038
PTP4A3	D	-2.32	0.030	U	1.03	0.048
TCP11L1	D	-0.87	0.003	U	1.02	0.002
PLAUR	D	-3.00	0.014	U	1.01	0.018
PLAUR	D	-2.73	0.001	U	1.00	0.007
PVRL2	D	-3.20	0.004	U	1.00	0.007
PLAU	D	-1.12	0.011	U	0.97	0.000
WIPI1	D	-0.80	0.045	U	0.97	0.006
SH3BP1	D	-1.83	0.009	U	0.96	0.047
TCF24	D	-1.61	0.013	U	0.96	0.023
LOC730755	D	-2.89	0.018	U	0.95	0.019
TMEM114	D	-1.75	0.048	U	0.93	0.045
AMOTL2	D	-0.85	0.033	U	0.89	0.038
TRAF4	D	-1.55	0.015	U	0.89	0.043
YEATS2	D	-0.84	0.023	U	0.88	0.018
ATXN3	D	-0.88	0.026	U	0.86	0.012
C9orf21	D	-0.65	0.010	U	0.86	0.003
HINFP	D	-0.85	0.001	U	0.84	0.001
UBXN7	D	-1.40	0.008	U	0.84	0.031
SCGB1A1	D	-0.81	0.004	U	0.83	0.005
RELB	D	-1.19	0.017	U	0.82	0.034
RFTN1	D	-1.35	0.014	U	0.81	0.003
ANTXR1	D	-1.06	0.026	U	0.81	0.040
PTHLH	D	-1.13	0.008	U	0.80	0.019
PLLP	D	-1.63	0.003	U	0.80	0.043
ATPBD4	D	-0.65	0.004	U	0.77	0.016
CLCN6	D	-1.83	0.001	U	0.77	0.020
VLDLR	D	-1.00	0.022	U	0.76	0.009
CHEK2	D	-0.96	0.006	U	0.75	0.040
ZNF567	D	-1.20	0.029	U	0.74	0.044
NUDT14	D	-1.11	0.008	U	0.74	0.001
BAMBI	D	-3.02	0.024	U	0.74	0.012
ZNF529	D	-1.30	0.022	U	0.74	0.039
MED30	D	-0.99	0.040	U	0.73	0.023

JDP2	D	-2.00	0.002	U	0.73	0.014
ZNF259	D	-0.80	0.037	U	0.72	0.017
BOD1	D	-0.76	0.003	U	0.71	0.025
FGGY	D	-0.82	0.021	U	0.68	0.011
CNOT4	D	-0.61	0.047	U	0.66	0.025
MAGED2	D	-1.96	0.011	U	0.65	0.026
NXN	D	-1.49	0.034	U	0.64	0.015
ZNF197	D	-0.83	0.027	U	0.62	0.020
AKR1A1	D	-0.69	0.031	U	0.62	0.033
SLAIN1	D	-1.30	0.038	U	0.61	0.017
HPS1	D	-0.86	0.002	U	0.61	0.004
GPM6B	D	-2.33	0.002	U	0.61	0.012
DENND1A	D	-1.46	0.008	U	0.60	0.041
KLK13	D	-0.78	0.050	U	0.60	0.040
PSPC1	D	-1.36	0.018	U	0.60	0.036
L3MBTL1	U	1.71	0.046	D	-0.61	0.040
TMEM67	U	1.17	0.034	D	-0.61	0.007
LACTB	U	0.85	0.023	D	-0.61	0.028
ZC4H2	U	1.31	0.000	D	-0.62	0.047
RNF114	U	0.71	0.008	D	-0.63	0.004
VPS45	U	0.80	0.007	D	-0.63	0.016
GK	U	0.97	0.029	D	-0.64	0.046
D2HGDH	U	0.69	0.020	D	-0.64	0.040
ARHGAP11A	U	0.67	0.017	D	-0.64	0.041
L3MBTL2	U	0.80	0.024	D	-0.65	0.014
PHTF1	U	1.07	0.004	D	-0.65	0.022
AURKA	U	0.82	0.036	D	-0.65	0.011
TSPAN12	U	3.41	0.015	D	-0.66	0.011
CXXC4	U	0.78	0.035	D	-0.66	0.040
GNA15	U	1.10	0.011	D	-0.67	0.007
ABCD3	U	0.81	0.027	D	-0.67	0.015
ATG2A	U	0.80	0.010	D	-0.67	0.013
MARCKSL1	U	0.70	0.005	D	-0.67	0.007
FAM36A	U	0.68	0.023	D	-0.67	0.015
PCYOX1	U	0.71	0.010	D	-0.67	0.011
HOXA10	U	3.43	0.010	D	-0.69	0.036
PARD6G	U	3.44	0.002	D	-0.69	0.021
FAN1	U	1.14	0.035	D	-0.70	0.041
REEP5	U	1.25	0.004	D	-0.71	0.003
SOCS4	U	1.30	0.035	D	-0.71	0.039
NEFH	U	1.16	0.035	D	-0.72	0.017
SUPT16H	U	0.60	0.022	D	-0.72	0.029
ABCB6	U	1.68	0.018	D	-0.73	0.022

PHF10	U	1.36	0.014	D	-0.73	0.041
FARSB	U	1.05	0.040	D	-0.73	0.033
C18orf55	U	1.38	0.015	D	-0.75	0.032
TXLNG	U	0.88	0.050	D	-0.77	0.049
TRAK2	U	1.42	0.030	D	-0.77	0.024
TBX18	U	2.23	0.011	D	-0.78	0.043
TOMM40L	U	1.34	0.001	D	-0.78	0.019
RAD17	U	0.77	0.018	D	-0.78	0.024
C1orf61	U	3.73	0.004	D	-0.78	0.039
ZNF618	U	1.98	0.004	D	-0.79	0.027
AP1G1	U	0.97	0.013	D	-0.79	0.029
RPL23AP82	U	0.81	0.049	D	-0.79	0.048
HAS3	U	2.01	0.011	D	-0.80	0.020
SLC10A7	U	1.57	0.001	D	-0.80	0.007
BACH2	U	0.94	0.009	D	-0.81	0.014
ATP8B2	U	0.93	0.042	D	-0.82	0.013
MLKL	U	1.44	0.027	D	-0.82	0.029
SLC25A44	U	0.70	0.027	D	-0.82	0.020
FLJ39061	U	0.88	0.001	D	-0.83	0.004
RNFT2	U	1.41	0.049	D	-0.86	0.048
SATB2	U	0.83	0.013	D	-0.87	0.044
GK	U	0.93	0.039	D	-0.87	0.015
GAS8	U	1.01	0.033	D	-0.88	0.028
PRKX	U	1.42	0.017	D	-0.88	0.034
LOC100127910	U	1.08	0.043	D	-0.90	0.049
ZNF839	U	0.73	0.044	D	-0.91	0.004
C20orf117	U	0.92	0.032	D	-0.91	0.011
FNTB	U	1.01	0.005	D	-0.93	0.026
ATP2A2	U	0.74	0.005	D	-0.93	0.049
C1R	U	0.60	0.044	D	-0.94	0.037
LRRC8B	U	0.91	0.027	D	-0.94	0.006
STRADB	U	0.86	0.024	D	-0.96	0.023
BRI3BP	U	1.02	0.008	D	-0.97	0.040
NFATC2IP	U	0.60	0.021	D	-0.97	0.008
RRM2	U	0.90	0.037	D	-0.98	0.016
LYRM7	U	1.31	0.027	D	-0.98	0.044
C15orf52	U	0.94	0.042	D	-0.99	0.010
C1RL	U	2.47	0.002	D	-1.00	0.011
C6orf168	U	0.80	0.036	D	-1.00	0.029
WDR36	U	0.69	0.029	D	-1.00	0.004
KIF20A	U	0.94	0.016	D	-1.00	0.015
PSRC1	U	0.87	0.016	D	-1.00	0.045
FBXL5	U	1.32	0.014	D	-1.05	0.038

DDX46	U	0.82	0.017	D	-1.05	0.008
SERTAD4	U	0.88	0.010	D	-1.06	0.002
LOC283683	U	1.35	0.033	D	-1.08	0.024
LOC100132707	U	0.81	0.030	D	-1.10	0.014
GSTM4	U	1.84	0.033	D	-1.13	0.038
STEAP2	U	3.37	0.046	D	-1.19	0.031
FAM83D	U	0.66	0.023	D	-1.19	0.007
SKP2	U	0.62	0.021	D	-1.21	0.004
NCRNA00085	U	0.72	0.011	D	-1.21	0.042
MUDENG	U	1.18	0.024	D	-1.22	0.002
HOXB5	U	1.18	0.002	D	-1.26	0.007
ISL1	U	2.30	0.009	D	-1.27	0.026
ZKSCAN5	U	0.81	0.019	D	-1.28	0.036
NLRP11	U	1.14	0.029	D	-1.32	0.017
RIMKLA	U	1.76	0.027	D	-1.33	0.047
D2HGDH	U	1.47	0.017	D	-1.33	0.026
JAKMIP2	U	1.33	0.040	D	-1.35	0.024
C10orf140	U	1.92	0.005	D	-1.37	0.011
FGF16	U	1.56	0.020	D	-1.38	0.024
CROT	U	1.77	0.027	D	-1.40	0.020
KIAA0895	U	1.57	0.009	D	-1.46	0.010
ERI2	U	1.47	0.049	D	-1.46	0.019
SFXN5	U	1.89	0.026	D	-1.66	0.032
FAM127C	U	0.69	0.010	D	-1.71	0.005
GPER	U	0.71	0.025	D	-1.78	0.005
VASH2	U	2.01	0.016	D	-1.80	0.017
PCDHB5	U	3.01	0.010	D	-1.83	0.023
RAB36	U	2.85	0.007	D	-1.88	0.017
TRIM55	U	3.06	0.011	D	-1.90	0.029
LOC100128191	U	1.49	0.022	D	-1.99	0.035
SKP2	U	0.96	0.017	D	-2.08	0.002
LEAP2	U	1.84	0.026	D	-2.21	0.047

APPENDIX C. GENES REVERSED IN H1299 T18 BY GSK-J4 TREATMENT

(Supplemental to Figure 7.3; D, Down-regulated and U, Up-regulated; Fold change ≥ 1.5)

Gene	H1299 T18 DMSO vs H1299 Parental DMSO	Log_2 [Fold Change]	T-test P value	H1299 T18 GSKJ4 vs H1299 T18 DMSO	Log_2 [Fold Change]	T-test P value
BNIP3	D	-0.86	0.002	U	3.27	0.000
DPYSL4	D	-2.03	0.046	U	2.74	0.048
DDIT4	D	-2.27	0.022	U	2.64	0.013
MFAP5	D	-2.63	0.000	U	2.05	0.032
NRP1	D	-2.27	0.029	U	1.95	0.015
FOSB	D	-1.06	0.041	U	1.85	0.006
PLOD2	D	-0.86	0.021	U	1.85	0.031
EFNB2	D	-1.14	0.035	U	1.77	0.017
YPEL2	D	-1.73	0.040	U	1.77	0.039
ARHGDIB	D	-7.55	0.007	U	1.58	0.027
TSC22D1	D	-3.70	0.020	U	1.57	0.021
SLC2A1	D	-1.43	0.026	U	1.52	0.046
BHLHE40	D	-3.76	0.025	U	1.49	0.021
SLC16A3	D	-2.37	0.004	U	1.46	0.027
PDGFA	D	-1.31	0.035	U	1.44	0.036
FAM43A	D	-2.06	0.024	U	1.43	0.015
FXYD5	D	-2.28	0.008	U	1.42	0.016
ASNS	D	-0.90	0.003	U	1.31	0.003
SESN2	D	-1.48	0.011	U	1.31	0.034
VLDLR	D	-1.00	0.022	U	1.24	0.006
NEK6	D	-1.77	0.007	U	1.20	0.006
FYN	D	-1.35	0.018	U	1.20	0.022
PER2	D	-1.82	0.001	U	1.18	0.048
HOXD11	D	-2.67	0.008	U	1.16	0.027
KATNAL1	D	-0.88	0.003	U	1.10	0.020
SPRN	D	-1.17	0.033	U	1.07	0.040
JDP2	D	-2.00	0.002	U	1.05	0.036
NFIL3	D	-0.72	0.011	U	1.04	0.023
MGLL	D	-5.61	0.012	U	1.02	0.001
C5orf41	D	-1.55	0.019	U	1.02	0.039
CASKIN2	D	-0.89	0.029	U	1.01	0.007
MT1G	D	-0.89	0.027	U	1.01	0.023
RALGDS	D	-0.77	0.041	U	0.97	0.022
TCF24	D	-1.61	0.013	U	0.96	0.020

NUDT14	D	-1.11	0.008	U	0.95	0.001
CHIC2	D	-1.15	0.015	U	0.94	0.039
NRP1	D	-2.08	0.008	U	0.94	0.011
PPP1R1B	D	-0.72	0.006	U	0.92	0.018
C4BPB	D	-0.82	0.017	U	0.91	0.004
CXCR4	D	-3.85	0.003	U	0.89	0.034
YEATS2	D	-0.84	0.023	U	0.88	0.027
LTF	D	-0.77	0.024	U	0.88	0.012
TRIB3	D	-1.04	0.004	U	0.87	0.004
ATF3	D	-0.89	0.028	U	0.87	0.020
SNX30	D	-0.97	0.007	U	0.80	0.010
GTF2I	D	-1.33	0.014	U	0.78	0.029
LOC730755	D	-2.89	0.018	U	0.77	0.005
PLEKHA9	D	-0.77	0.004	U	0.76	0.007
GLIPR2	D	-1.76	0.009	U	0.76	0.019
GPI	D	-1.05	0.035	U	0.76	0.039
SOX8	D	-1.24	0.014	U	0.74	0.034
SH3GL2	D	-2.72	0.038	U	0.73	0.050
MME	D	-1.02	0.018	U	0.73	0.015
CORO2A	D	-3.45	0.005	U	0.71	0.027
PNMA2	D	-1.16	0.008	U	0.71	0.020
GPM6B	D	-2.33	0.002	U	0.70	0.038
RIOK3	D	-1.28	0.005	U	0.69	0.008
SH3D20	D	-1.98	0.015	U	0.69	0.028
SLC4A7	D	-0.99	0.008	U	0.68	0.032
RFTN1	D	-1.35	0.014	U	0.68	0.040
RBMS1	D	-1.83	0.039	U	0.67	0.010
KIAA1539	D	-0.61	0.032	U	0.67	0.032
PSPC1	D	-1.36	0.018	U	0.66	0.048
CASP9	D	-1.40	0.027	U	0.65	0.043
ANTXR1	D	-1.32	0.006	U	0.65	0.029
PLLP	D	-1.63	0.003	U	0.63	0.024
FXYD5	D	-1.33	0.011	U	0.61	0.022
LOC221710	D	-0.79	0.021	U	0.61	0.009
SC4MOL	D	-1.29	0.014	U	0.61	0.043
OGFRL1	D	-1.03	0.036	U	0.61	0.032
ZNF260	D	-1.58	0.008	U	0.60	0.017
MAMSTR	U	2.43	0.026	D	-0.61	0.003
AMDHD1	U	2.35	0.014	D	-0.61	0.006
MUDENG	U	1.18	0.024	D	-0.61	0.027
MSH5	U	0.61	0.031	D	-0.62	0.024
AURKA	U	0.82	0.036	D	-0.63	0.017
DCAF4L1	U	0.60	0.009	D	-0.63	0.036

VPS45	U	0.80	0.007	D	-0.63	0.019
PPP4R4	U	1.69	0.007	D	-0.64	0.022
C20orf117	U	0.92	0.032	D	-0.64	0.046
STEAP2	U	3.34	0.027	D	-0.65	0.039
MAVS	U	1.13	0.020	D	-0.66	0.014
PLCB4	U	0.97	0.027	D	-0.66	0.038
LMX1B	U	0.71	0.044	D	-0.67	0.044
CTU2	U	0.70	0.026	D	-0.68	0.007
NCRNA00085	U	0.72	0.011	D	-0.69	0.015
SOCS2	U	1.22	0.016	D	-0.70	0.026
DIP2A	U	0.64	0.033	D	-0.72	0.036
MKKS	U	1.17	0.008	D	-0.73	0.026
GOSR1	U	0.62	0.014	D	-0.76	0.006
KIF20A	U	0.94	0.016	D	-0.78	0.007
FCRL3	U	0.96	0.015	D	-0.80	0.004
FAM83D	U	0.66	0.023	D	-0.80	0.036
FGF16	U	1.56	0.020	D	-0.81	0.045
JAKMIP2	U	1.33	0.040	D	-0.83	0.048
RNU6ATAC	U	0.75	0.048	D	-0.88	0.028
RAD51L1	U	1.12	0.018	D	-0.88	0.028
PGP	U	0.84	0.012	D	-0.90	0.012
SKP2	U	0.96	0.017	D	-0.90	0.032
GPER	U	0.71	0.025	D	-0.97	0.007
AGTR1	U	0.73	0.033	D	-0.97	0.011
FBXO22	U	0.62	0.015	D	-0.98	0.005
CCL2	U	3.70	0.020	D	-1.04	0.003
PSRC1	U	0.87	0.016	D	-1.05	0.011
GOLPH3L	U	1.97	0.028	D	-1.07	0.037
C1orf61	U	3.73	0.004	D	-1.10	0.013
RNFT2	U	1.41	0.049	D	-1.21	0.009
PCDHB5	U	3.01	0.010	D	-1.50	0.033
LEAP2	U	1.84	0.026	D	-1.53	0.039
TAF9B	U	0.60	0.041	D	-1.60	0.017

APPENDIX D. GENE SET OVERLAP BETWEEN JIB-04/GSK-J4 TREATED T18

(Supplemental to Figure 7.4 A; GSEA; 38+78 overlapping curated gene sets; 1000 permutations; FDR ≤ 0.25)

38 gene sets depleted in H1299 T18 and enriched (reversed) by both JIB-04 and GSK-J4:

Elvidge_Hypoxia_Up
Elvidge_Hypoxia_By_DMOG_Up
Martoriati_MDM4_Targets_Fetal_Liver_Up
Jiang_Hypoxia_Normal
Manalo_Hypoxia_Up
Martoriati_MDM4_Targets_Neuroepithelium_Up
Boquest_Stem_Cell_Cultured_Vs_Fresh_Up
Monnier_Postradiation_Tumor_Escape_Dn
Sweet_Lung_Cancer_KRAS_Dn
Rozanov_MMP14_Targets_Up
Dazard_Response_To_UV_NHEK_Up
Acevedo_Liver_Cancer_Dn
Gozgit_ESR1_Targets_Dn
Acevedo_Liver_Tumor_Vs_Normal_Adjacent_Tissue_Dn
Pedersen_Metastasis_By_ERBB2_Isoform_7
Martens_Bound_By_PML_RARA_Fusion
Schaeffer_Prostate_Development_48hr_Dn
Wong_Adult_Tissue_Stem_Module
Koyama_SEMA3B_Targets_Up
Lim_Mammary_Stem_Cell_Up
Sweet_Lung_Cancer_KRAS_Up
Onder_CDH1_Targets_2_Dn
Fulcher_Inflammatory_Response_Lectin_Vs_Lps_Up
Plasari_TGFB1_Targets_10hr_Up
Perez_TP63_Targets
Bruins_UVC_Response_Via_TP53_Group_B
Enk_UV_Response_Keratinocyte_Up
Schuetz_Breast_Cancer_Ductal_Invasive_Up
West_Adrenocortical_Tumor_Dn
Delys_Thyroid_Cancer_Up
Martens_Tretinoin_Response_Up
Chicas_RB1_Targets_Senescent
Lei_MYB_Targets
Meissner_Brain_HCP_With_H3K4me3_And_H3K27me3
Naba_Matrisome
Benporath_SUZ12_Targets
Lindgren_Bladder_Cancer_Cluster_2b
Pasini_SUZ12_Targets_Dn

78 other common gene sets enriched by both JIB-04 and GSK-J4:

Mense_Hypoxia_Up
Krieg_Hypoxia_Not_Via_KDM3A
Winter_Hypoxia_Metagene
Gross_Hypoxia_Via_ELK3_And_HIF1A_Up
Qi_Hypoxia
Graessmann_Apoptosis_By_Serum_Deprivation_Dn
Wierenga_STAT5A_Targets_Up
Nuytten_EZH2_Targets_Up
Basaki_YBX1_Targets_Dn
Smirnov_Response_To_IR_6hr_Dn
Gary_CD5_Targets_Up
Gross_Hypoxia_Via_HIF1A_Dn
Gross_Hypoxia_Via_ELK3_Dn
Odonnell_TFRC_Targets_Up
Enk_UV_Response_Keratinocyte_Dn
Krige_Response_To_Tosedostat_24hr_Up
Krige_Response_To_Tosedostat_6hr_Up
Rutella_Response_To_HGF_Dn
Oswald_Hematopoietic_Stem_Cell_In_Collagen_Gel_Dn
Creighton_Endocrine_Therapy_Resistance_3
Bild_HRAS_Oncogenic_Signature
Dutertre_Estradiol_Response_24hr_Dn
Wierenga_STAT5A_Targets_Group1
Nagashima_NRG1_Signaling_Up
Rutella_Response_To_CSF2RB_And_IL4_Dn
Johnstone_PARVB_Targets_3_Up
Kan_Response_To_Arsenic_Trioxide
Gobert_Oligodendrocyte_Differentiation_Dn
Dodd_Nasopharyngeal_Carcinoma_Up
Martinez_RB1_And_TP53_Targets_Up
Zwang_Class_3_Transiently_Induced_By_EGF
Zwang_Class_1_Transiently_Induced_By_EGF
Rutella_Response_To_HGF_Vs_CSF2RB_And_IL4_Up
Hirsch_Cellular_Transformation_Signature_Up
Zhang_TLX_Targets_60hr_Up
Smid_Breast_Cancer_Basal_Up
Buytaert_Photodynamic_Therapy_Stress_Up
Blum_Response_To_Salirasib_Up
Smid_Breast_Cancer_Luminal_B_Dn
Han_SATB1_Targets_Up
Cui_TCF21_Targets_2_Dn
Chen_HOXA5_Targets_9hr_Up
Fulcher_Inflammatory_Response_Lectin_Vs_Lps_Dn
Nuytten_NIPP1_Targets_Up

Mitsiades_Response_To_Aplidin_Up
Gruetzmann_Pancreatic_Cancer_Up
Debiasi_Apoptosis_By_Reovirus_Infection_Up
Fevr_CTNNB1_Targets_Up
Heller_Hdac_Targets_Silenced_By_Methylation_Up
Fortschegger_PHF8_Targets_Up
Charafe_Breast_Cancer_Luminal_Vs_Mesenchymal_Dn
Charafe_Breast_Cancer_Luminal_Vs_Basal_Dn
Smid_Breast_Cancer_Relapse_In_Bone_Dn
Rutella_Response_To_CSF2RB_And_IL4_Up
Senese_HDAC3_Targets_Up
Creighton_Endocrine_Therapy_Resistance_5
Koinuma_Targets_Of_SMAD2_Or_SMAD3
Zhang_TLX_Targets_36hr_Up
Johnstone_PARVB_Targets_2_Dn
Bystrykh_Hematopoiesis_Stem_Cell_Qtl_Trans
Winzen_Degraded_Via_KHSRP
Miyagawa_Targets_Of_EWSR1_ETS_Fusions_Dn
Martinez_RB1_Targets_Up
Phong_TNF_Response_Via_P38_Partial
Foster_Tolerant_Macrophage_Dn
Berenjeno_Transformed_By_RHOA_Up
Riggi_Ewing_Sarcoma_Progenitor_Dn
Udayakumar_MED1_Targets_Dn
Lopez_MBD_Targets
Zheng_Bound_By_FOXP3
Mcbryan_Pubertal_TGFB1_Targets_Up
Enk_UV_Response_Epidermis_Dn
Graessmann_Apoptosis_By_Serum_Deprivation_Up
Rutella_Response_To_HGF_Up
Delys_Thyroid_Cancer_Dn
Zwang_Transiently_Up_By_1st_EGF_Pulse_Only
Goldrath_Antigen_Response
Haddad_B_Lymphocyte_Progenitor

BIBLIOGRAPHY

American Cancer Society (2015). Cancer Facts & Figures.

Allikmets, R., Schriml, L. M., Hutchinson, A., Romano-Spica, V., and Dean, M. (1998). A human placenta-specific ATP-binding cassette gene (ABCP) on chromosome 4q22 that is involved in multidrug resistance. Cancer research *58*, 5337-5339.

Annereau, J. P., Szakacs, G., Tucker, C. J., Arciello, A., Cardarelli, C., Collins, J., Grissom, S., Zeeberg, B. R., Reinhold, W., Weinstein, J. N.*, et al.* (2004). Analysis of ATP-binding cassette transporter expression in drug-selected cell lines by a microarray dedicated to multidrug resistance. Molecular pharmacology *66*, 1397-1405.

Azad, N., Zahnow, C. A., Rudin, C. M., and Baylin, S. B. (2013). The future of epigenetic therapy in solid tumours--lessons from the past. Nature reviews Clinical oncology *10*, 256-266.

Bai, F., Nakanishi, Y., Kawasaki, M., Takayama, K., Yatsunami, J., Pei, X. H., Tsuruta, N., Wakamatsu, K., and Hara, N. (1996). Immunohistochemical expression of glutathione S-transferase-Pi can predict chemotherapy response in patients with nonsmall cell lung carcinoma. Cancer *78*, 416-421.

Baker, E. K., Johnstone, R. W., Zalcberg, J. R., and El-Osta, A. (2005). Epigenetic changes to the MDR1 locus in response to chemotherapeutic drugs. Oncogene *24*, 8061-8075.

Ben-Porath, I., Thomson, M. W., Carey, V. J., Ge, R., Bell, G. W., Regev, A., and Weinberg, R. A. (2008). An embryonic stem cell-like gene expression signature in poorly differentiated aggressive human tumors. Nature genetics *40*, 499-507.

Bertolini, G., Roz, L., Perego, P., Tortoreto, M., Fontanella, E., Gatti, L., Pratesi, G., Fabbri, A., Andriani, F., Tinelli, S.*, et al.* (2009). Highly tumorigenic lung cancer CD133+ cells display stem-like features and are spared by cisplatin treatment. Proceedings of the National Academy of Sciences of the United States of America *106*, 16281-16286.

Bhatia, R., Holtz, M., Niu, N., Gray, R., Snyder, D. S., Sawyers, C. L., Arber, D. A., Slovak, M. L., and Forman, S. J. (2003). Persistence of malignant hematopoietic progenitors in chronic myelogenous leukemia patients in complete cytogenetic remission following imatinib mesylate treatment. Blood *101*, 4701-4707.

Bhatla, T., Wang, J., Morrison, D. J., Raetz, E. A., Burke, M. J., Brown, P., and Carroll, W. L. (2012). Epigenetic reprogramming reverses the relapse-specific gene expression signature and restores chemosensitivity in childhood B-lymphoblastic leukemia. Blood *119*, 5201-5210.

Brockman, R. W. (1963). Mechanisms of Resistance to Anticancer Agents. Advances in cancer research *7*, 129-234.

Burkhart, C. A., Kavallaris, M., and Band Horwitz, S. (2001). The role of beta-tubulin isotypes in resistance to antimitotic drugs. Biochimica et biophysica acta *1471*, O1-9.

Byers, L. A., Diao, L., Wang, J., Saintigny, P., Girard, L., Peyton, M., Shen, L., Fan, Y., Giri, U., Tumula, P. K.*, et al.* (2013). An epithelial-mesenchymal transition gene signature predicts resistance to EGFR and PI3K inhibitors and identifies Axl as a therapeutic target for overcoming EGFR inhibitor resistance. Clinical cancer research : an official journal of the American Association for Cancer Research *19*, 279-290.

Canino, C., Luo, Y., Marcato, P., Blandino, G., Pass, H. I., and Cioce, M. (2015). A STAT3-NFkB/DDIT3/CEBPbeta axis modulates ALDH1A3 expression in chemoresistant cell subpopulations. Oncotarget *6*, 12637-12653.

Chen, C. J., Chin, J. E., Ueda, K., Clark, D. P., Pastan, I., Gottesman, M. M., and Roninson, I. B. (1986). Internal duplication and homology with bacterial transport proteins in the mdr1 (P-glycoprotein) gene from multidrug-resistant human cells. Cell *47*, 381-389.

Childs, S., Yeh, R. L., Hui, D., and Ling, V. (1998). Taxol resistance mediated by transfection of the liver-specific sister gene of P-glycoprotein. Cancer research *58*, 4160-4167.

Cole, S. P., Bhardwaj, G., Gerlach, J. H., Mackie, J. E., Grant, C. E., Almquist, K. C., Stewart, A. J., Kurz, E. U., Duncan, A. M., and Deeley, R. G. (1992). Overexpression of a transporter gene in a multidrug-resistant human lung cancer cell line. Science *258*, 1650-1654.

d'Amato, T. A., Landreneau, R. J., Ricketts, W., Huang, W., Parker, R., Mechetner, E., Yu, I. R., and Luketich, J. D. (2007). Chemotherapy resistance and oncogene expression in non-small cell lung cancer. The Journal of thoracic and cardiovascular surgery *133*, 352-363.

Dean, M. (2009). ABC transporters, drug resistance, and cancer stem cells. Journal of mammary gland biology and neoplasia *14*, 3-9.

Dean, M., Fojo, T., and Bates, S. (2005). Tumour stem cells and drug resistance. Nature reviews Cancer *5*, 275-284.

Denis, M. G., Vallee, A., and Theoleyre, S. (2015). EGFR T790M resistance mutation in non small-cell lung carcinoma. Clinica chimica acta; international journal of clinical chemistry *444*, 81-85.

Deriano, L., Guipaud, O., Merle-Beral, H., Binet, J. L., Ricoul, M., Potocki-Veronese, G., Favaudon, V., Maciorowski, Z., Muller, C., Salles, B.*, et al.* (2005). Human chronic lymphocytic leukemia B cells can escape DNA damage-induced apoptosis through the nonhomologous end-joining DNA repair pathway. Blood *105*, 4776-4783.

Ding, L. H., Xie, Y., Park, S., Xiao, G., and Story, M. D. (2008). Enhanced identification and biological validation of differential gene expression via Illumina whole-genome expression arrays through the use of the model-based background correction methodology. Nucleic acids research *36*, e58.

Doyle, L. A., Yang, W., Abruzzo, L. V., Krogmann, T., Gao, Y., Rishi, A. K., and Ross, D. D. (1998). A multidrug resistance transporter from human MCF-7 breast cancer cells. Proceedings of the National Academy of Sciences of the United States of America *95*, 15665-15670.

Easwaran, H., Tsai, H. C., and Baylin, S. B. (2014). Cancer epigenetics: tumor heterogeneity, plasticity of stem-like states, and drug resistance. Molecular cell *54*, 716-727.

Eisen, M. B., Spellman, P. T., Brown, P. O., and Botstein, D. (1998). Cluster analysis and display of genome-wide expression patterns. Proceedings of the National Academy of Sciences of the United States of America *95*, 14863-14868.

Ellis, L., Atadja, P. W., and Johnstone, R. W. (2009). Epigenetics in cancer: targeting chromatin modifications. Molecular cancer therapeutics *8*, 1409-1420.

Filippakopoulos, P., and Knapp, S. (2014). Targeting bromodomains: epigenetic readers of lysine acetylation. Nature reviews Drug discovery *13*, 337-356.

Gately, D. P., and Howell, S. B. (1993). Cellular accumulation of the anticancer agent cisplatin: a review. British journal of cancer *67*, 1171-1176.

Gerlinger, M., and Swanton, C. (2010). How Darwinian models inform therapeutic failure initiated by clonal heterogeneity in cancer medicine. British journal of cancer *103*, 1139-1143.

Gifford, G., Paul, J., Vasey, P. A., Kaye, S. B., and Brown, R. (2004). The acquisition of hMLH1 methylation in plasma DNA after chemotherapy predicts poor survival for ovarian cancer patients. Clinical cancer research : an official journal of the American Association for Cancer Research *10*, 4420-4426.

Goldstein, L. J., Galski, H., Fojo, A., Willingham, M., Lai, S. L., Gazdar, A., Pirker, R., Green, A., Crist, W., Brodeur, G. M., and et al. (1989). Expression of a multidrug resistance gene in human cancers. Journal of the National Cancer Institute *81*, 116-124.

Gottesman, M. M. (2002). Mechanisms of cancer drug resistance. Annual review of medicine *53*, 615-627.

Gottesman, M. M., Fojo, T., and Bates, S. E. (2002). Multidrug resistance in cancer: role of ATP-dependent transporters. Nature reviews Cancer *2*, 48-58.

Greer, R. M., Peyton, M., Larsen, J. E., Girard, L., Xie, Y., Gazdar, A. F., Harran, P., Wang, L., Brekken, R. A., Wang, X., and Minna, J. D. (2011). SMAC mimetic (JP1201) sensitizes non-small cell lung cancers to multiple chemotherapy agents in an IAP-dependent but TNF-alpha-independent manner. Cancer research *71*, 7640-7648.

Hajji, N., Wallenborg, K., Vlachos, P., Fullgrabe, J., Hermanson, O., and Joseph, B. (2010). Opposing effects of hMOF and SIRT1 on H4K16 acetylation and the sensitivity to the topoisomerase II inhibitor etoposide. Oncogene *29*, 2192-2204.

Hansen, L. T., Lundin, C., Spang-Thomsen, M., Petersen, L. N., and Helleday, T. (2003). The role of RAD51 in etoposide (VP16) resistance in small cell lung cancer. International journal of cancer Journal international du cancer *105*, 472-479.

Hardt, O., Wild, S., Oerlecke, I., Hofmann, K., Luo, S., Wiencek, Y., Kantelhardt, E., Vess, C., Smith, G. P., Schroth, G. P.*, et al.* (2012). Highly sensitive profiling of CD44+/CD24- breast cancer stem cells by combining global mRNA amplification and next generation sequencing: evidence for a hyperactive PI3K pathway. Cancer letters *325*, 165-174.

Hashizume, R., Andor, N., Ihara, Y., Lerner, R., Gan, H., Chen, X., Fang, D., Huang, X., Tom, M. W., Ngo, V.*, et al.* (2014). Pharmacologic inhibition of histone demethylation as a therapy for pediatric brainstem glioma. Nature medicine *20*, 1394-1396.

Heidel, F. H., Bullinger, L., Feng, Z., Wang, Z., Neff, T. A., Stein, L., Kalaitzidis, D., Lane, S. W., and Armstrong, S. A. (2012). Genetic and pharmacologic inhibition of beta-catenin targets imatinib-resistant leukemia stem cells in CML. Cell stem cell *10*, 412-424.

Helin, K., and Dhanak, D. (2013). Chromatin proteins and modifications as drug targets. Nature *502*, 480-488.

Hirschmann-Jax, C., Foster, A. E., Wulf, G. G., Nuchtern, J. G., Jax, T. W., Gobel, U., Goodell, M. A., and Brenner, M. K. (2004). A distinct "side population" of cells with high drug efflux capacity in human tumor cells. Proceedings of the National Academy of Sciences of the United States of America *101*, 14228-14233.

Ho, M. M., Ng, A. V., Lam, S., and Hung, J. Y. (2007). Side population in human lung cancer cell lines and tumors is enriched with stem-like cancer cells. Cancer research *67*, 4827-4833.

Hogan, L. E., Meyer, J. A., Yang, J., Wang, J., Wong, N., Yang, W., Condos, G., Hunger, S. P., Raetz, E., Saffery, R.*, et al.* (2011). Integrated genomic analysis of relapsed childhood acute lymphoblastic leukemia reveals therapeutic strategies. Blood *118*, 5218-5226.

Hojfeldt, J. W., Agger, K., and Helin, K. (2013). Histone lysine demethylases as targets for anticancer therapy. Nature reviews Drug discovery *12*, 917-930.

Howie, A. F., Forrester, L. M., Glancey, M. J., Schlager, J. J., Powis, G., Beckett, G. J., Hayes, J. D., and Wolf, C. R. (1990). Glutathione S-transferase and glutathione peroxidase expression in normal and tumour human tissues. Carcinogenesis *11*, 451-458.

Howlader N, N. A., Krapcho M, Garshell J, Miller D, Altekruse SF, Kosary CL, Yu M, Ruhl J, Tatalovich Z,Mariotto A, Lewis DR, Chen HS, Feuer EJ, Cronin KA (eds) (1975-2012). SEER Cancer Statistics Review. In, (Bethesda, MD: National Cancer Institute).

Huang, S., Holzel, M., Knijnenburg, T., Schlicker, A., Roepman, P., McDermott, U., Garnett, M., Grernrum, W., Sun, C., Prahallad, A.*, et al.* (2012). MED12 controls the response to multiple cancer drugs through regulation of TGF-beta receptor signaling. Cell *151*, 937-950.

Humeniuk, R., Mishra, P. J., Bertino, J. R., and Banerjee, D. (2009). Epigenetic reversal of acquired resistance to 5-fluorouracil treatment. Molecular cancer therapeutics *8*, 1045-1054.

Huo, H., Magro, P. G., Pietsch, E. C., Patel, B. B., and Scotto, K. W. (2010). Histone methyltransferase MLL1 regulates MDR1 transcription and chemoresistance. Cancer research *70*, 8726-8735.

Inukai, M., Toyooka, S., Ito, S., Asano, H., Ichihara, S., Soh, J., Suehisa, H., Ouchida, M., Aoe, K., Aoe, M.*, et al.* (2006). Presence of epidermal growth factor receptor gene T790M mutation as a minor clone in non-small cell lung cancer. Cancer research *66*, 7854-7858.

Isla, D., Sarries, C., Rosell, R., Alonso, G., Domine, M., Taron, M., Lopez-Vivanco, G., Camps, C., Botia, M., Nunez, L.*, et al.* (2004). Single nucleotide polymorphisms and outcome in docetaxel-cisplatin-treated advanced non-small-cell lung cancer. Annals of oncology : official journal of the European Society for Medical Oncology / ESMO *15*, 1194-1203.

Islam, F., Gopalan, V., Smith, R. A., and Lam, A. K. (2015). Translational potential of cancer stem cells: A review of the detection of cancer stem cells and their roles in cancer recurrence and cancer treatment. Experimental cell research *335*, 135-147.

Jamal-Hanjani, M., Hackshaw, A., Ngai, Y., Shaw, J., Dive, C., Quezada, S., Middleton, G., de Bruin, E., Le Quesne, J., Shafi, S.*, et al.* (2014). Tracking genomic cancer evolution for precision medicine: the lung TRACERx study. PLoS biology *12*, e1001906.

Jin, S., and Scotto, K. W. (1998). Transcriptional regulation of the MDR1 gene by histone acetyltransferase and deacetylase is mediated by NF-Y. Molecular and cellular biology *18*, 4377-4384.

Jordan, M. A., and Wilson, L. (2004). Microtubules as a target for anticancer drugs. Nature reviews Cancer *4*, 253-265.

Juergens, R. A., Wrangle, J., Vendetti, F. P., Murphy, S. C., Zhao, M., Coleman, B., Sebree, R., Rodgers, K., Hooker, C. M., Franco, N.*, et al.* (2011). Combination epigenetic therapy has efficacy in patients with refractory advanced non-small cell lung cancer. Cancer discovery *1*, 598-607.

Kajiyama, H., Shibata, K., Terauchi, M., Yamashita, M., Ino, K., Nawa, A., and Kikkawa, F. (2007). Chemoresistance to paclitaxel induces epithelial-mesenchymal transition and enhances metastatic potential for epithelial ovarian carcinoma cells. International journal of oncology *31*, 277-283.

Karczmarek-Borowska, B., Filip, A., Wojcierowski, J., Smolen, A., Korobowicz, E., Korszen-Pilecka, I., and Zdunek, M. (2006). Estimation of prognostic value of Bcl-xL gene expression in non-small cell lung cancer. Lung cancer *51*, 61-69.

Kartner, N., Riordan, J. R., and Ling, V. (1983a). Cell surface P-glycoprotein associated with multidrug resistance in mammalian cell lines. Science *221*, 1285-1288.

Kartner, N., Shales, M., Riordan, J. R., and Ling, V. (1983b). Daunorubicin-resistant Chinese hamster ovary cells expressing multidrug resistance and a cell-surface P-glycoprotein. Cancer research *43*, 4413-4419.

Kawabata, S., Oka, M., Shiozawa, K., Tsukamoto, K., Nakatomi, K., Soda, H., Fukuda, M., Ikegami, Y., Sugahara, K., Yamada, Y.*, et al.* (2001). Breast cancer resistance protein directly confers SN-38 resistance of lung cancer cells. Biochemical and biophysical research communications *280*, 1216-1223.

Kemper, K., de Goeje, P. L., Peeper, D. S., and van Amerongen, R. (2014). Phenotype switching: tumor cell plasticity as a resistance mechanism and target for therapy. Cancer research *74*, 5937-5941.

Kim, A. Y., Kwak, J. H., Je, N. K., Lee, Y. H., and Jung, Y. S. (2015). Epithelial-mesenchymal Transition is Associated with Acquired Resistance to 5-Fluorocuracil in HT-29 Colon Cancer Cells. Toxicological research *31*, 151-156.

Klastersky, J., and Awada, A. (2012). Milestones in the use of chemotherapy for the management of non-small cell lung cancer (NSCLC). Critical reviews in oncology/hematology *81*, 49-57.

Knoechel, B., Roderick, J. E., Williamson, K. E., Zhu, J., Lohr, J. G., Cotton, M. J., Gillespie, S. M., Fernandez, D., Ku, M., Wang, H.*, et al.* (2014). An epigenetic mechanism of resistance to targeted therapy in T cell acute lymphoblastic leukemia. Nature genetics *46*, 364-370.

Kruidenier, L., Chung, C. W., Cheng, Z., Liddle, J., Che, K., Joberty, G., Bantscheff, M., Bountra, C., Bridges, A., Diallo, H.*, et al.* (2012). A selective jumonji H3K27 demethylase inhibitor modulates the proinflammatory macrophage response. Nature *488*, 404-408.

Lai, S. L., Goldstein, L. J., Gottesman, M. M., Pastan, I., Tsai, C. M., Johnson, B. E., Mulshine, J. L., Ihde, D. C., Kayser, K., and Gazdar, A. F. (1989). MDR1 gene expression in lung cancer. Journal of the National Cancer Institute *81*, 1144-1150.

Langmead, B., Trapnell, C., Pop, M., and Salzberg, S. L. (2009). Ultrafast and memory-efficient alignment of short DNA sequences to the human genome. Genome biology *10*, R25.

Lemontt, J. F., Azzaria, M., and Gros, P. (1988). Increased mdr gene expression and decreased drug accumulation in multidrug-resistant human melanoma cells. Cancer research *48*, 6348-6353.

Li, B., Carey, M., and Workman, J. L. (2007). The role of chromatin during transcription. Cell *128*, 707-719.

Liedert, B., Materna, V., Schadendorf, D., Thomale, J., and Lage, H. (2003). Overexpression of cMOAT (MRP2/ABCC2) is associated with decreased formation of platinum-DNA adducts and decreased G2-arrest in melanoma cells resistant to cisplatin. The Journal of investigative dermatology *121*, 172-176.

Liu, G., Yuan, X., Zeng, Z., Tunici, P., Ng, H., Abdulkadir, I. R., Lu, L., Irvin, D., Black, K. L., and Yu, J. S. (2006). Analysis of gene expression and chemoresistance of CD133+ cancer stem cells in glioblastoma. Molecular cancer *5*, 67.

Liu, J., Chen, H., Miller, D. S., Saavedra, J. E., Keefer, L. K., Johnson, D. R., Klaassen, C. D., and Waalkes, M. P. (2001). Overexpression of glutathione S-transferase II and multidrug resistance transport proteins is associated with acquired tolerance to inorganic arsenic. Molecular pharmacology *60*, 302-309.

Liu, Y. P., Yang, C. J., Huang, M. S., Yeh, C. T., Wu, A. T., Lee, Y. C., Lai, T. C., Lee, C. H., Hsiao, Y. W., Lu, J.*, et al.* (2013). Cisplatin selects for multidrug-resistant CD133+ cells in lung adenocarcinoma by activating Notch signaling. Cancer research *73*, 406-416.

Lopes, R. B., Gangeswaran, R., McNeish, I. A., Wang, Y., and Lemoine, N. R. (2007). Expression of the IAP protein family is dysregulated in pancreatic cancer cells and is important for resistance to chemotherapy. International journal of cancer Journal international du cancer *120*, 2344-2352.

Lord, R. V., Brabender, J., Gandara, D., Alberola, V., Camps, C., Domine, M., Cardenal, F., Sanchez, J. M., Gumerlock, P. H., Taron, M.*, et al.* (2002). Low ERCC1 expression correlates with prolonged survival after cisplatin plus gemcitabine chemotherapy in non-small cell lung cancer. Clinical cancer research : an official journal of the American Association for Cancer Research *8*, 2286-2291.

Ma, S., Lee, T. K., Zheng, B. J., Chan, K. W., and Guan, X. Y. (2008). CD133+ HCC cancer stem cells confer chemoresistance by preferential expression of the Akt/PKB survival pathway. Oncogene *27*, 1749-1758.

Mair, B., Kubicek, S., and Nijman, S. M. (2014). Exploiting epigenetic vulnerabilities for cancer therapeutics. Trends in pharmacological sciences *35*, 136-145.

Martello, L. A., Verdier-Pinard, P., Shen, H. J., He, L., Torres, K., Orr, G. A., and Horwitz, S. B. (2003). Elevated levels of microtubule destabilizing factors in a Taxol-resistant/dependent A549 cell line with an alpha-tubulin mutation. Cancer research *63*, 1207-1213.

Martin, J., Ginsberg, R. J., Venkatraman, E. S., Bains, M. S., Downey, R. J., Korst, R. J., Kris, M. G., and Rusch, V. W. (2002). Long-term results of combined-modality therapy in resectable non-small-cell lung cancer. Journal of clinical oncology : official journal of the American Society of Clinical Oncology *20*, 1989-1995.

Massarelli, E., Andre, F., Liu, D. D., Lee, J. J., Wolf, M., Fandi, A., Ochs, J., Le Chevalier, T., Fossella, F., and Herbst, R. S. (2003). A retrospective analysis of the outcome of patients who have received two prior chemotherapy regimens including platinum and docetaxel for recurrent non-small-cell lung cancer. Lung cancer *39*, 55-61.

Matsumoto, Y., Oka, M., Sakamoto, A., Narasaki, F., Fukuda, M., Takatani, H., Terashi, K., Ikeda, K., Tsurutani, J., Nagashima, S.*, et al.* (1997). Enhanced expression of metallothionein in

human non-small-cell lung carcinomas following chemotherapy. Anticancer research *17*, 3777-3780.

McGrath, J., and Trojer, P. (2015). Targeting histone lysine methylation in cancer. Pharmacology & therapeutics *150*, 1-22.

Meissner, A., Mikkelsen, T. S., Gu, H., Wernig, M., Hanna, J., Sivachenko, A., Zhang, X., Bernstein, B. E., Nusbaum, C., Jaffe, D. B.*, et al.* (2008). Genome-scale DNA methylation maps of pluripotent and differentiated cells. Nature *454*, 766-770.

Michelutti, A., Michieli, M., Damiani, D., Melli, C., Ermacora, A., Grimaz, S., Candoni, A., Russo, D., Fanin, R., and Baccarani, M. (1997). Effect of fludarabine and arabinosylcytosine on multidrug resistant cells. Haematologica *82*, 143-147.

Millward, M. J., Cantwell, B. M., Munro, N. C., Robinson, A., Corris, P. A., and Harris, A. L. (1993). Oral verapamil with chemotherapy for advanced non-small cell lung cancer: a randomised study. British journal of cancer *67*, 1031-1035.

Mini, E., Nobili, S., Caciagli, B., Landini, I., and Mazzei, T. (2006). Cellular pharmacology of gemcitabine. Annals of oncology : official journal of the European Society for Medical Oncology / ESMO *17 Suppl 5*, v7-12.

Murtaza, M., Dawson, S. J., Tsui, D. W., Gale, D., Forshew, T., Piskorz, A. M., Parkinson, C., Chin, S. F., Kingsbury, Z., Wong, A. S.*, et al.* (2013). Non-invasive analysis of acquired resistance to cancer therapy by sequencing of plasma DNA. Nature *497*, 108-112.

Musselman, C. A., Lalonde, M. E., Cote, J., and Kutateladze, T. G. (2012). Perceiving the epigenetic landscape through histone readers. Nature structural & molecular biology *19*, 1218-1227.

NCT01454102 (2011). A Multi-arm Phase I Safety Study of Nivolumab in Combination With Gemcitabine/Cisplatin, Pemetrexed/Cisplatin, Carboplatin/Paclitaxel, Bevacizumab Maintenance, Erlotinib, Ipilimumab or as Monotherapy in Subjects With Stage IIIB/IV Non-small Cell Lung Cancer (NSCLC). In, (Bristol-Myers Squibb).

NCT01653470 (2012). Study to Evaluate Safety & Tolerability of BMS-906024 in Combination With Chemotherapy & to Define DLTs & MTD of BMS-906024 in Combination With One of the Following Chemotherapy Regimens; Weekly Paclitaxel, 5FU+Irinotecan or Carboplatin+Paclitaxel in Subjects With Advanced / Metastatic Solid Tumors. In, (Bristol-Myers Squibb).

NCT01957007 (2013). A Study of Vantictumab (OMP-18R5) in Combination With Docetaxel in Patients With Previously Treated NSCLC. In, (OncoMed Pharmaceuticals, Inc.).

NCT02298153 (2014). A Study of MPDL3280A in Combination With INCB024360 in Subjects With Previously Treated Stage IIIB or Stage IV Non-Small Cell Lung Cancer. In, (Incyte Corporation, collaboration with Hoffmann-La Roche, Genentech, Inc.).

Nguyen, K. S., Kobayashi, S., and Costa, D. B. (2009). Acquired resistance to epidermal growth factor receptor tyrosine kinase inhibitors in non-small-cell lung cancers dependent on the epidermal growth factor receptor pathway. Clinical lung cancer *10*, 281-289.

Ogawa, J., Iwazaki, M., Inoue, H., Koide, S., and Shohtsu, A. (1993). Immunohistochemical study of glutathione-related enzymes and proliferative antigens in lung cancer. Relation to cisplatin sensitivity. Cancer *71*, 2204-2209.

Oka, M., Fukuda, M., Sakamoto, A., Takatani, H., Fukuda, M., Soda, H., and Kohno, S. (1997). The clinical role of MDR1 gene expression in human lung cancer. Anticancer research *17*, 721-724.

Oliveras-Ferraros, C., Corominas-Faja, B., Cufi, S., Vazquez-Martin, A., Martin-Castillo, B., Iglesias, J. M., Lopez-Bonet, E., Martin, A. G., and Menendez, J. A. (2012). Epithelial-to-mesenchymal transition (EMT) confers primary resistance to trastuzumab (Herceptin). Cell cycle *11*, 4020-4032.

Ozvegy-Laczka, C., Cserepes, J., Elkind, N. B., and Sarkadi, B. (2005). Tyrosine kinase inhibitor resistance in cancer: role of ABC multidrug transporters. Drug resistance updates : reviews and commentaries in antimicrobial and anticancer chemotherapy *8*, 15-26.

Pang, B., Qiao, X., Janssen, L., Velds, A., Groothuis, T., Kerkhoven, R., Nieuwland, M., Ovaa, H., Rottenberg, S., van Tellingen, O*., et al.* (2013). Drug-induced histone eviction from open chromatin contributes to the chemotherapeutic effects of doxorubicin. Nature communications *4*, 1908.

Peng, J. C., Valouev, A., Swigut, T., Zhang, J., Zhao, Y., Sidow, A., and Wysocka, J. (2009). Jarid2/Jumonji coordinates control of PRC2 enzymatic activity and target gene occupancy in pluripotent cells. Cell *139*, 1290-1302.

Ramalingam, S. S., Maitland, M. L., Frankel, P., Argiris, A. E., Koczywas, M., Gitlitz, B., Thomas, S., Espinoza-Delgado, I., Vokes, E. E., Gandara, D. R., and Belani, C. P. (2010). Carboplatin and Paclitaxel in combination with either vorinostat or placebo for first-line therapy of advanced non-small-cell lung cancer. Journal of clinical oncology : official journal of the American Society of Clinical Oncology *28*, 56-62.

Redmond, K. M., Wilson, T. R., Johnston, P. G., and Longley, D. B. (2008). Resistance mechanisms to cancer chemotherapy. Frontiers in bioscience : a journal and virtual library *13*, 5138-5154.

Ren, S., Su, C., Wang, Z., Li, J., Fan, L., Li, B., Li, X., Zhao, C., Wu, C., Hou, L*., et al.* (2014). Epithelial phenotype as a predictive marker for response to EGFR-TKIs in non-small cell lung cancer patients with wild-type EGFR. International journal of cancer Journal international du cancer *135*, 2962-2971.

Rho, J. K., Choi, Y. J., Lee, J. K., Ryoo, B. Y., Na, II, Yang, S. H., Kim, C. H., and Lee, J. C. (2009). Epithelial to mesenchymal transition derived from repeated exposure to gefitinib

determines the sensitivity to EGFR inhibitors in A549, a non-small cell lung cancer cell line. Lung cancer *63*, 219-226.

Rigas, J. R. (2004). Taxane-platinum combinations in advanced non-small cell lung cancer: a review. The oncologist *9 Suppl 2*, 16-23.

Roche-Lestienne, C., Soenen-Cornu, V., Grardel-Duflos, N., Lai, J. L., Philippe, N., Facon, T., Fenaux, P., and Preudhomme, C. (2002). Several types of mutations of the Abl gene can be found in chronic myeloid leukemia patients resistant to STI571, and they can pre-exist to the onset of treatment. Blood *100*, 1014-1018.

Roesch, A., Fukunaga-Kalabis, M., Schmidt, E. C., Zabierowski, S. E., Brafford, P. A., Vultur, A., Basu, D., Gimotty, P., Vogt, T., and Herlyn, M. (2010). A temporarily distinct subpopulation of slow-cycling melanoma cells is required for continuous tumor growth. Cell *141*, 583-594.

Roesch, A., Vultur, A., Bogeski, I., Wang, H., Zimmermann, K. M., Speicher, D., Korbel, C., Laschke, M. W., Gimotty, P. A., Philipp, S. E*., et al.* (2013). Overcoming intrinsic multidrug resistance in melanoma by blocking the mitochondrial respiratory chain of slow-cycling JARID1B(high) cells. Cancer cell *23*, 811-825.

Rollins, K. D., and Lindley, C. (2005). Pemetrexed: a multitargeted antifolate. Clinical therapeutics *27*, 1343-1382.

Roninson, I. B., Chin, J. E., Choi, K. G., Gros, P., Housman, D. E., Fojo, A., Shen, D. W., Gottesman, M. M., and Pastan, I. (1986). Isolation of human mdr DNA sequences amplified in multidrug-resistant KB carcinoma cells. Proceedings of the National Academy of Sciences of the United States of America *83*, 4538-4542.

Rosano, L., Cianfrocca, R., Spinella, F., Di Castro, V., Nicotra, M. R., Lucidi, A., Ferrandina, G., Natali, P. G., and Bagnato, A. (2011). Acquisition of chemoresistance and EMT phenotype is linked with activation of the endothelin A receptor pathway in ovarian carcinoma cells. Clinical cancer research : an official journal of the American Association for Cancer Research *17*, 2350-2360.

Rotem, A., Ram, O., Shoresh, N., Sperling, R. A., Goren, A., Weitz, D. A., and Bernstein, B. E. (2015). Single-cell ChIP-seq reveals cell subpopulations defined by chromatin state. Nature biotechnology.

Rothbart, S. B., and Strahl, B. D. (2014). Interpreting the language of histone and DNA modifications. Biochimica et biophysica acta *1839*, 627-643.

Salnikov, A. V., Gladkich, J., Moldenhauer, G., Volm, M., Mattern, J., and Herr, I. (2010). CD133 is indicative for a resistance phenotype but does not represent a prognostic marker for survival of non-small cell lung cancer patients. International journal of cancer Journal international du cancer *126*, 950-958.

Salonga, D., Danenberg, K. D., Johnson, M., Metzger, R., Groshen, S., Tsao-Wei, D. D., Lenz, H. J., Leichman, C. G., Leichman, L., Diasio, R. B., and Danenberg, P. V. (2000). Colorectal tumors responding to 5-fluorouracil have low gene expression levels of dihydropyrimidine dehydrogenase, thymidylate synthase, and thymidine phosphorylase. Clinical cancer research : an official journal of the American Association for Cancer Research *6*, 1322-1327.

Sanulli, S., Justin, N., Teissandier, A., Ancelin, K., Portoso, M., Caron, M., Michaud, A., Lombard, B., da Rocha, S. T., Offer, J.*, et al.* (2015). Jarid2 Methylation via the PRC2 Complex Regulates H3K27me3 Deposition during Cell Differentiation. Molecular cell *57*, 769-783.

Sauna, Z. E., and Ambudkar, S. V. (2000). Evidence for a requirement for ATP hydrolysis at two distinct steps during a single turnover of the catalytic cycle of human P-glycoprotein. Proceedings of the National Academy of Sciences of the United States of America *97*, 2515-2520.

Seve, P., and Dumontet, C. (2005). Chemoresistance in non-small cell lung cancer. Current medicinal chemistry Anti-cancer agents *5*, 73-88.

Shao, C., Sullivan, J. P., Girard, L., Augustyn, A., Yenerall, P., Rodriguez-Canales, J., Liu, H., Behrens, C., Shay, J. W., Wistuba, II, and Minna, J. D. (2014). Essential role of aldehyde dehydrogenase 1A3 for the maintenance of non-small cell lung cancer stem cells is associated with the STAT3 pathway. Clinical cancer research : an official journal of the American Association for Cancer Research *20*, 4154-4166.

Sharma, S. V., Lee, D. Y., Li, B., Quinlan, M. P., Takahashi, F., Maheswaran, S., McDermott, U., Azizian, N., Zou, L., Fischbach, M. A.*, et al.* (2010). A chromatin-mediated reversible drug-tolerant state in cancer cell subpopulations. Cell *141*, 69-80.

Shen, D., Pastan, I., and Gottesman, M. M. (1998). Cross-resistance to methotrexate and metals in human cisplatin-resistant cell lines results from a pleiotropic defect in accumulation of these compounds associated with reduced plasma membrane binding proteins. Cancer research *58*, 268-275.

Shen, L., Shao, N., Liu, X., and Nestler, E. (2014). ngs.plot: Quick mining and visualization of next-generation sequencing data by integrating genomic databases. BMC genomics *15*, 284.

Shen, X., Kim, W., Fujiwara, Y., Simon, M. D., Liu, Y., Mysliwiec, M. R., Yuan, G. C., Lee, Y., and Orkin, S. H. (2009). Jumonji modulates polycomb activity and self-renewal versus differentiation of stem cells. Cell *139*, 1303-1314.

Shien, K., Toyooka, S., Yamamoto, H., Soh, J., Jida, M., Thu, K. L., Hashida, S., Maki, Y., Ichihara, E., Asano, H.*, et al.* (2013). Acquired resistance to EGFR inhibitors is associated with a manifestation of stem cell-like properties in cancer cells. Cancer research *73*, 3051-3061.

Simo-Riudalbas, L., and Esteller, M. (2015). Targeting the histone orthography of cancer: drugs for writers, erasers and readers. British journal of pharmacology *172*, 2716-2732.

Smith, A. J., van Helvoort, A., van Meer, G., Szabo, K., Welker, E., Szakacs, G., Varadi, A., Sarkadi, B., and Borst, P. (2000). MDR3 P-glycoprotein, a phosphatidylcholine translocase, transports several cytotoxic drugs and directly interacts with drugs as judged by interference with nucleotide trapping. The Journal of biological chemistry *275*, 23530-23539.

Stewart, D. J., Chiritescu, G., Dahrouge, S., Banerjee, S., and Tomiak, E. M. (2007). Chemotherapy dose--response relationships in non-small cell lung cancer and implied resistance mechanisms. Cancer treatment reviews *33*, 101-137.

Stewart, E. L., Tan, S. Z., Liu, G., and Tsao, M. S. (2015). Known and putative mechanisms of resistance to EGFR targeted therapies in NSCLC patients with EGFR mutations-a review. Translational lung cancer research *4*, 67-81.

Subramanian, A., Tamayo, P., Mootha, V. K., Mukherjee, S., Ebert, B. L., Gillette, M. A., Paulovich, A., Pomeroy, S. L., Golub, T. R., Lander, E. S., and Mesirov, J. P. (2005). Gene set enrichment analysis: a knowledge-based approach for interpreting genome-wide expression profiles. Proceedings of the National Academy of Sciences of the United States of America *102*, 15545-15550.

Sugimura, H., Nichols, F. C., Yang, P., Allen, M. S., Cassivi, S. D., Deschamps, C., Williams, B. A., and Pairolero, P. C. (2007). Survival after recurrent nonsmall-cell lung cancer after complete pulmonary resection. The Annals of thoracic surgery *83*, 409-417; discussioin 417-408.

Sun, F. F., Hu, Y. H., Xiong, L. P., Tu, X. Y., Zhao, J. H., Chen, S. S., Song, J., and Ye, X. Q. (2015). Enhanced expression of stem cell markers and drug resistance in sphere-forming non-small cell lung cancer cells. International journal of clinical and experimental pathology *8*, 6287-6300.

Szakacs, G., Annereau, J. P., Lababidi, S., Shankavaram, U., Arciello, A., Bussey, K. J., Reinhold, W., Guo, Y., Kruh, G. D., Reimers, M.*, et al.* (2004). Predicting drug sensitivity and resistance: profiling ABC transporter genes in cancer cells. Cancer cell *6*, 129-137.

Takebe, N., Harris, P. J., Warren, R. Q., and Ivy, S. P. (2011). Targeting cancer stem cells by inhibiting Wnt, Notch, and Hedgehog pathways. Nature reviews Clinical oncology *8*, 97-106.

Tang, X., Khuri, F. R., Lee, J. J., Kemp, B. L., Liu, D., Hong, W. K., and Mao, L. (2000). Hypermethylation of the death-associated protein (DAP) kinase promoter and aggressiveness in stage I non-small-cell lung cancer. Journal of the National Cancer Institute *92*, 1511-1516.

Tang, X., Wu, W., Sun, S. Y., Wistuba, II, Hong, W. K., and Mao, L. (2004). Hypermethylation of the death-associated protein kinase promoter attenuates the sensitivity to TRAIL-induced apoptosis in human non-small cell lung cancer cells. Molecular cancer research : MCR *2*, 685-691.

Thomson, S., Buck, E., Petti, F., Griffin, G., Brown, E., Ramnarine, N., Iwata, K. K., Gibson, N., and Haley, J. D. (2005). Epithelial to mesenchymal transition is a determinant of sensitivity of

non-small-cell lung carcinoma cell lines and xenografts to epidermal growth factor receptor inhibition. Cancer research *65*, 9455-9462.

Todaro, M., Alea, M. P., Di Stefano, A. B., Cammareri, P., Vermeulen, L., Iovino, F., Tripodo, C., Russo, A., Gulotta, G., Medema, J. P., and Stassi, G. (2007). Colon cancer stem cells dictate tumor growth and resist cell death by production of interleukin-4. Cell stem cell *1*, 389-402.

Tourneur, L., Delluc, S., Levy, V., Valensi, F., Radford-Weiss, I., Legrand, O., Vargaftig, J., Boix, C., Macintyre, E. A., Varet, B.*, et al.* (2004). Absence or low expression of fas-associated protein with death domain in acute myeloid leukemia cells predicts resistance to chemotherapy and poor outcome. Cancer research *64*, 8101-8108.

Ulasov, I. V., Nandi, S., Dey, M., Sonabend, A. M., and Lesniak, M. S. (2011). Inhibition of Sonic hedgehog and Notch pathways enhances sensitivity of CD133(+) glioma stem cells to temozolomide therapy. Molecular medicine *17*, 103-112.

Varier, R. A., and Timmers, H. T. (2011). Histone lysine methylation and demethylation pathways in cancer. Biochimica et biophysica acta *1815*, 75-89.

Voulgari, A., and Pintzas, A. (2009). Epithelial-mesenchymal transition in cancer metastasis: mechanisms, markers and strategies to overcome drug resistance in the clinic. Biochimica et biophysica acta *1796*, 75-90.

Wang, L., Chang, J., Varghese, D., Dellinger, M., Kumar, S., Best, A. M., Ruiz, J., Bruick, R., Pena-Llopis, S., Xu, J.*, et al.* (2013). A small molecule modulates Jumonji histone demethylase activity and selectively inhibits cancer growth. Nature communications *4*, 2035.

Williams, J., Lucas, P. C., Griffith, K. A., Choi, M., Fogoros, S., Hu, Y. Y., and Liu, J. R. (2005). Expression of Bcl-xL in ovarian carcinoma is associated with chemoresistance and recurrent disease. Gynecologic oncology *96*, 287-295.

Wilting, R. H., and Dannenberg, J. H. (2012). Epigenetic mechanisms in tumorigenesis, tumor cell heterogeneity and drug resistance. Drug resistance updates : reviews and commentaries in antimicrobial and anticancer chemotherapy *15*, 21-38.

Wu, A. R., Neff, N. F., Kalisky, T., Dalerba, P., Treutlein, B., Rothenberg, M. E., Mburu, F. M., Mantalas, G. L., Sim, S., Clarke, M. F., and Quake, S. R. (2014). Quantitative assessment of single-cell RNA-sequencing methods. Nature methods *11*, 41-46.

Yang, A. D., Fan, F., Camp, E. R., van Buren, G., Liu, W., Somcio, R., Gray, M. J., Cheng, H., Hoff, P. M., and Ellis, L. M. (2006). Chronic oxaliplatin resistance induces epithelial-to-mesenchymal transition in colorectal cancer cell lines. Clinical cancer research : an official journal of the American Association for Cancer Research *12*, 4147-4153.

Yauch, R. L., Januario, T., Eberhard, D. A., Cavet, G., Zhu, W., Fu, L., Pham, T. Q., Soriano, R., Stinson, J., Seshagiri, S.*, et al.* (2005). Epithelial versus mesenchymal phenotype determines in

vitro sensitivity and predicts clinical activity of erlotinib in lung cancer patients. Clinical cancer research : an official journal of the American Association for Cancer Research *11*, 8686-8698.

Young, L. C., Campling, B. G., Voskoglou-Nomikos, T., Cole, S. P., Deeley, R. G., and Gerlach, J. H. (1999). Expression of multidrug resistance protein-related genes in lung cancer: correlation with drug response. Clinical cancer research : an official journal of the American Association for Cancer Research *5*, 673-680.

Zeller, C., and Brown, R. (2010). Therapeutic modulation of epigenetic drivers of drug resistance in ovarian cancer. Therapeutic advances in medical oncology *2*, 319-329.

Zhang, W., Feng, M., Zheng, G., Chen, Y., Wang, X., Pen, B., Yin, J., Yu, Y., and He, Z. (2012a). Chemoresistance to 5-fluorouracil induces epithelial-mesenchymal transition via up-regulation of Snail in MCF7 human breast cancer cells. Biochemical and biophysical research communications *417*, 679-685.

Zhang, Z., Lee, J. C., Lin, L., Olivas, V., Au, V., LaFramboise, T., Abdel-Rahman, M., Wang, X., Levine, A. D., Rho, J. K.*, et al.* (2012b). Activation of the AXL kinase causes resistance to EGFR-targeted therapy in lung cancer. Nature genetics *44*, 852-860.

Zhao, R., and Goldman, I. D. (2003). Resistance to antifolates. Oncogene *22*, 7431-7457.

Zhou, J., Wulfkuhle, J., Zhang, H., Gu, P., Yang, Y., Deng, J., Margolick, J. B., Liotta, L. A., Petricoin, E., 3rd, and Zhang, Y. (2007). Activation of the PTEN/mTOR/STAT3 pathway in breast cancer stem-like cells is required for viability and maintenance. Proceedings of the National Academy of Sciences of the United States of America *104*, 16158-16163.

VITAE

Maithili was born in Pune, India, on April 16, 1987, daughter of Dr. Prafulla and Dr. Mrs. Manik Dalvi. She has one sister, Vaishnavi Dalvi. She is married to Aditya Paranjape. Maithili developed her interest in biological sciences research during her high school years, when she presented her very first research project in January 2003 at the Intel Science Talent Discovery Fair at the Indian Institute of Technology (IIT), Mumbai, India. She was presented the Best Project award and selected to participate in the Intel International Science and Engineering Fair (ISEF), Cleveland, OH, in May 2003, where she won two other awards. Maithili filed a patent on this project in 2004. To continue her passion in biological sciences, she joined the Institute of Bioinformatics and Biotechnology (IBB), Savitribai Phule Pune University, and graduated with a Master's degree in 2009 with an 'Outstanding' final grade, 'O'. During this integrated Master's in Biotechnology five-year program, she did two short research projects under the guidance of Dr. Shridhar Gejji, in the Department of Chemistry. She was also awarded the IASc-INSA-NASI fellowship to pursue a summer research project in molecular biology in the laboratory of Dr. Ghanshyam Swarup at the Centre for Cellular and Molecular Biology (CCMB), Hyderabad, India. Maithili did her Master's thesis work in the Stem Cells and Diabetes section of National Centre for Cell Science (NCCS), Pune, India, under the mentorship of Dr. Anandwardhan Hardikar. In 2009, Maithili joined the Graduate School for Biomedical Sciences at the University of Texas Southwestern Medical Center, Dallas, TX. She joined the Cancer Biology graduate program and was presented with the HHMI Med-into-Grad fellowship to gain experience in clinical and translational research under the Mechanisms of Disease training track. Maithili began her dissertation research in 2010 under the guidance of Dr. John D. Minna, and was subsequently co-mentored by Dr. Elisabeth D. Martinez starting in 2014. During her graduate research, Maithili was presented the Best Poster award in Cancer Research by Convergence and the Harold C. Simmons Comprehensive Cancer at UT Southwestern (2010), Top Abstract Honor at the 44th annual abstract competition by Sigma Xi scientific research society at UT Southwestern (2012), and the Scholars Abstract award at the Translational Science meeting in Washington D.C. (2013). Maithili defended her Ph.D. dissertation on November 17, 2015.